BEST AVAILABLE IMAGES

Defective images within this document are accurate representations of the original documents submitted by the applicant.

Defects in the images may include (but are not limited to):

- BLACK BORDERS
- TEXT CUT OFF AT TOP, BOTTOM OR SIDES
- FADED TEXT
- ILLEGIBLE TEXT
- SKEWED/SLANTED IMAGES
- COLORED PHOTOS
- BLACK OR VERY BLACK AND WHITE DARK PHOTOS
- GRAY SCALE DOCUMENTS

IMAGES ARE BEST AVAILABLE COPY.

As rescanning documents *will not* correct images, please do not report the images to the Image Problem Mailbox.

Prespore-specific gene expression in *Bacillus subtilis* is driven by sequestration of SpoIIE phosphatase to the prespore side of the asymmetric septum

Ling Juan Wu, Andrea Feucht, and Jeffery Errington[1]

Sir William Dunn School of Pathology, University of Oxford, Oxford OX1 3RE, UK

The *spoIIE* gene is essential for the compartment-specific activation of transcription factor σ^F during sporulation in *Bacillus subtilis*. SpoIIE is a membrane protein that is targeted to the potential sites of asymmetric septation near each pole of the sporulating cell. The cytoplasmic carboxy-terminal domain of SpoIIE contains a serine phosphatase that triggers the release of σ^F in the prespore compartment after septation. To understand how septum-located SpoIIE is activated selectively in the prespore, we examined the distribution of a SpoIIE-GFP fusion protein. We show that the polar bands of SpoIIE protein actually form sequentially and that the most prominent band develops at the pole where the prespore forms. We also show that the protein is sequestered to the prespore side of the asymmetric septum. Sequestration of SpoIIE into the prespore compartment provides a mechanism that could explain the cell specificity of σ^F activation.

[*Key Words: Bacillus subtilis;* sporulation; transcriptional regulation; SpoIIE protein; σ^F; differentiation]

Received December 8, 1997; revised version accepted February 16, 1998.

The onset of sporulation of *Bacillus subtilis* is marked by the formation of the asymmetric septum, which divides the sporulating cell into a small prespore and a large mother cell. Soon after formation of the asymmetric septum, new transcriptional activities directed by σ factors σ^F and σ^E appear (for review, see Errington 1993; Stragier and Losick 1996). σ^F becomes active specifically in the prespore and initiates the prespore program of developmental gene expression. It also directs a signal across the septum, which leads to activation of σ^E in the mother cell. Mutations in several genes affect the morphology of sporulation in ways that can be used to probe the regulation of σ^F and σ^E. Thus, mutations in the *spoIIG* operon (encoding σ^E and its regulator) lead to sequential formation of two prespore-like cells, at opposite poles of the parent cell, in both of which σ^F becomes activated (Piggot and Coote 1976; Lewis et al. 1994). Mutations in the *spoIIIE* gene interfere with segregation of the prespore chromosome (Wu and Errington 1994). In the absence of SpoIIIE protein, only a segment comprising about one-third of the chromosome, centered approximately on *oriC*, enters the prespore compartment, leaving the remaining two-thirds of the chromosome in the mother cell. Therefore, mutations in *spoIIIE* affect σ^F-directed gene expression in a manner dependent on chromosome position (Wu and Errington 1994, 1998). Also, null mutations in *spoIIIE* result in aberrant release of σ^F activity in the mother cell, for reasons that are not yet understood (Wu and Errington 1994).

σ^F is made before asymmetric septation, together with two coordinately expressed regulatory proteins, SpoIIAA and SpoIIAB (for review, see Errington 1996; Stragier and Losick 1996). At first, σ^F is held in an inactive complex by the anti-σ factor SpoIIAB (Duncan and Losick 1993; Min et al. 1993; Alper et al. 1994). The anti-anti-σ factor SpoIIAA is also maintained in an inactive state by the kinase activity of SpoIIAB, which phosphorylates it on a specific serine residue (Min et al. 1993; Diederich et al. 1994; Najafi et al. 1995; Magnin et al. 1996). After asymmetric septation, σ^F remains inactive in the mother cell, as in the preseptational cell, but in the prespore it is released from SpoIIAB (Margolis et al. 1991; Lewis et al. 1996). This release is triggered by SpoIIE, a membrane-bound phosphatase, which dephosphorylates SpoIIAA-P and allows it to bind SpoIIAB, thereby releasing σ^F (Duncan et al. 1995; Arigoni et al. 1996; Feucht et al. 1996; Magnin et al. 1997). Thus, SpoIIE plays a critical role in the regulation of σ^F.

SpoIIE protein is synthesized soon after the initiation of sporulation, before asymmetric septation (Guzman et

[1]Corresponding author.
E-MAIL erring@molbiol.ox.ac.uk; FAX 44-1865-275556.

al. 1988). Arigoni et al. (1995) reported that the protein is localized initially in a bipolar pattern, with bands (probably corresponding to circumferential rings of protein) located close to but not at both poles of the predivisional cell. Asymmetric septation then takes place at the site of one of the bands. Subsequently, the prespore-distal band disappears and the prespore-proximal SpoIIE protein, which presumably triggers activation of σ^F in the prespore, is retained. Eventually the prespore-proximal SpoIIE band also disappears. A crucial question that remains, however, concerns how the septum-located SpoIIE phosphatase selectively dephosphorylates SpoIIAA-P in the prespore but not in the mother cell. The asymmetric septum consists of two membranes flanking a thin layer of wall material (Illing and Errington 1991). As the septum forms, the SpoIIE protein, which is anchored to the membrane through its amino-terminal hydrophobic domain (Barak et al. 1996), could become equally distributed on both faces of the septum. Localized activation of σ^F could then occur as a result of the relatively higher concentration of the phosphatase in the small prespore compared with the much larger mother cell compartment (Duncan et al. 1995). Alternatively, there could be selective inactivation or degradation of the SpoIIE protein on the mother cell face of the septum. A third possiblility is that the SpoIIE protein is sequestered specifically onto the prespore side of the asymmetric septum as it forms (Feucht et al. 1996). Biochemical fractionation experiments (Barak et al. 1996) have shown that most of the SpoIIE protein eventually associates with the prespore, but these experiments can only address the localization of the protein in completely engulfed prespores, long after the protein acts on septation and σ^F activation.

To better understand the mechanism by which the compartmentalization of σ^F activity and, therefore, cellular asymmetry is established, we have re-examined the distribution of the SpoIIE protein tagged with green fluorescent protein (GFP). Previous studies have established that GFP fusions provide a convenient and accurate means of determining the subcellular localization of proteins in bacteria (see, e.g., Glaser et al. 1997), although it is important to establish that the fusion protein functions normally. With a fully functional SpoIIE-GFP fusion we show first that the two polar SpoIIE bands (rings) form sequentially, suggesting that the limited availability of a component of the machinery required for septation could be responsible for the formation of only one asymmetric septum. We also show directly that the SpoIIE phosphatase is sequestered to the prespore side of the septum when it forms. This sequestration could explain the localized activation of σ^F in the prespore compartment.

Results

Construction and characterization of a spoIIE-gfp *fusion strain*

To examine the distribution of the SpoIIE protein, we constructed a plasmid carrying an in-frame *spoIIE-gfp* fusion, which would allow easy introduction of the fusion onto the *B. subtilis* chromosome by Campell-like recombination. A previously described SpoIIE-GFP strain (Arigoni et al. 1995) showed reduced sporulation efficiency, suggesting that the fusion protein is not fully functional. Cormack et al. (1996) have reported the derivation of mutant forms of GFP with improved folding properties and brightness. Therefore, we fused the SpoIIE protein to such a mutant GFP. Sporulating cells of the wild-type strain SG38 and the *spoIIE-gfp* derivative (strain 1305) showed similar frequencies of asymmetric septation at 80 min after initiation of sporulation (t_{80}) (46% and 45%, respectively) and spore formation at t_{420} (84% and 82%, respectively), suggesting that the fusion protein is fully functional. We also examined the fusion protein by Western blot analysis using both anti-SpoIIE and anti-GFP antibodies. Figure 1 shows that the time courses for production of SpoIIE or SpoIIE-GFP proteins were similar for both strains. In some experiments a faint fast migrating band that cross-reacted with anti-SpoIIE but not anti-GFP antibody could be detected from cultures of strain 1305. This band migrated at the same position as untagged SpoIIE protein and seemed to appear as early as t_{60} (broken arrow in Fig. 1). Because no free GFP protein was detected at this time (see below and Fig. 2A), this fast migrating band could be SpoIIE without the GFP tag, formed by a low level of translational arrest before the *gfp* coding sequence. Alternatively, it could be attributable to a low level of cleavage of the fusion protein, in which case the free GFP protein must either have been degraded or be present in quantities too low to be detected by Western blot analysis.

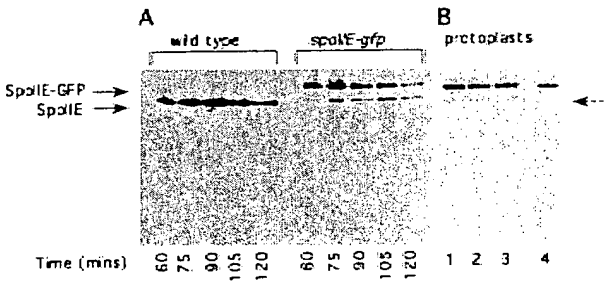

Figure 1. Accumulation and stability of SpoIIE and SpoIIE-GFP in sporulating cells and protoplasts. (*A*) Whole cell extracts of sporulating wild-type strain SG38 and the *spoIIE-gfp*-carrying strain 1305, taken at the times indicated, were analyzed by Western blot using anti-SpoIIE antibodies. (*B*) To demonstrate that protoplasting does not change the degradation pattern of SpoIIE-GFP, cells of strain 1305 were collected and protoplasted at t_{90}, then treated in various ways before being subjected to Western blot analysis using anti-SpoIIE antibodies (lanes *1–3*) or monoclonal anti-GFP antibody (lane *4*). The protoplasts were treated as follows: (lane *1*) pelleted and frozen immediately; left for 30 min (lanes *2,4*) at room temperature or (lane *3*) on ice, then pelleted and frozen. The positions of SpoIIE and SpoIIE-GFP are indicated by solid arrows. The broken arrow indicates the position of a faster migrating band that cross-reacted with anti-SpoIIE, possibly representing near full-length SpoIIE without the GFP tag.

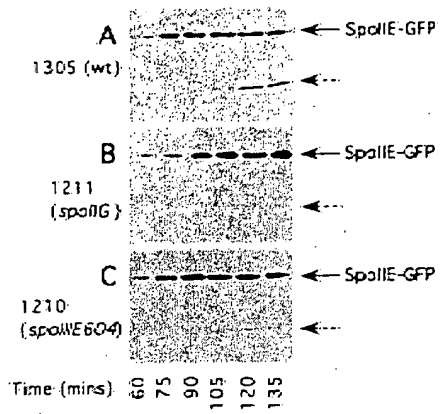

Figure 2. Time course of SpoIIE/SpoIIE-GFP degradation during sporulation. Whole cell extracts from sporulating cells were loaded on a 10% SDS-polyacrylamide gel and analyzed by Western blot using monoclonal anti-GFP antibody. Samples were prepared from the following strains: (*A*) 1305 (*spoIIE-gfp*); (*B*) 1211(*spoIIE-gfp spoIIGA::aph-A3*); (*C*) 1210 (*spoIIE-gfp spoIIIE604*). Samples were taken and prepared as described in the legend to Fig. 1. The positions of full-length SpoIIE-GFP and the major SpoIIE-GFP degradation product are indicated by solid and broken arrows, respectively.

When the cultures of strain 1305 were probed with anti-GFP antibody, a small band of expected size for the GFP protein alone began to be detected from about t_{105} (Fig. 2A). Formation of this band was greatly reduced in *spoIIG* and *spoIIIE* mutants (Fig. 2B,C). This proteolytic cleavage probably corresponds to developmentally regulated degradation of SpoIIE. Pogliano et al. (1997) showed that disappearance of the prespore-distal SpoIIE band was blocked by mutations in these genes. Although this developmental degradation of SpoIIE generates free, and thus untargeted, GFP, this should not affect interpretation of the results described below because it is not formed until well after σ^F and σ^E become active.

Kinetics of SpoIIE ring formation

Previous observations based on immunofluorescence microscopy suggested that SpoIIE bands form initially at both poles of the sporulating cell and that later they break down sequentially, first at the prespore-distal pole (Arigoni et al. 1995). When we looked at early sporulating cells containing the new *spoIIE-gfp* fusion, we were surprised to find that many cells had a single SpoIIE band (90% of the cells with localized SpoIIE at t_{70}, and 67% at t_{90}), or a bipolar pattern with one bright and one weaker band. Similar results were obtained with immunofluorescence microscopy (data not shown). At such an early stage of sporulation, it seemed unlikely that this was attributable to developmental degradation (i.e., loss of one band). Therefore, we examined the kinetics of the SpoIIE band formation in greater detail, using both live and fixed sporulating cells. Figure 3 shows examples of fields of cells of the wild type at different times of sporulation and illustrating different patterns of SpoIIE-GFP localization. Cells with "1 band" were further divided into those exhibiting a weak straight band and those with a curving band. The curved bands were only observed at later time points, and we assume that they represent cells at a much later stage of development, either undergoing or having completed engulfment. The developmental stages of the cells were defined more precisely by staining the cells with DAPI to reveal their nucleoid morphology (Fig. 3B,D,F). It is clear from the images that in early samples (t_{70}), probably before or dur-

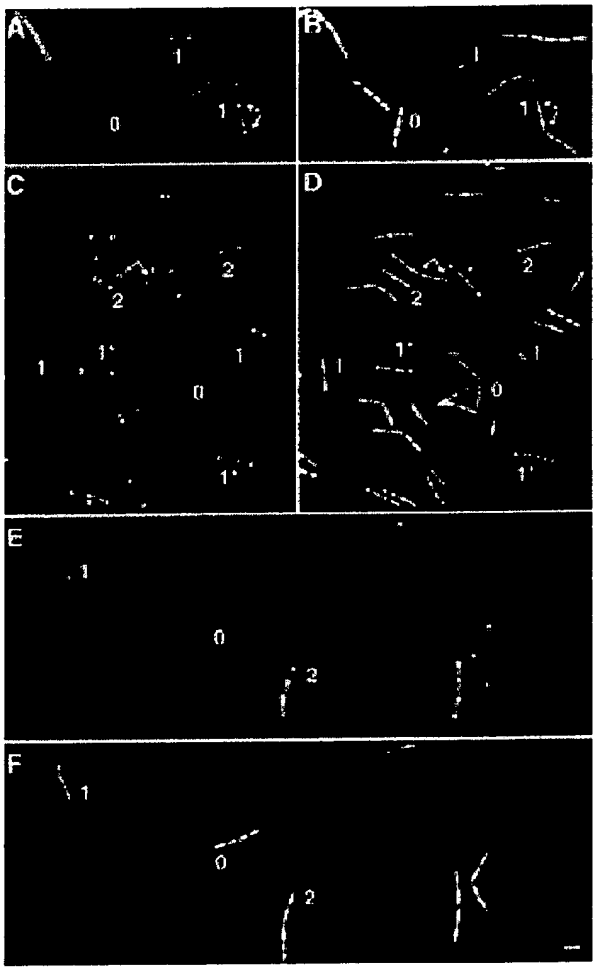

Figure 3. SpoIIE band formation and development. Strains carrying the *spoIIE-gfp* fusion were induced to sporulate, and live DAPI-stained cells were examined by fluorescence microscopy. (*A,B*) Wild-type (1305) cells at t_{70}; (*C,D*) wild-type cells at t_{105}; (*E,F*) *spoIIG spoIIIE* double mutant (strain 1213) at t_{90}. (*A,C,E*) Localization of SpoIIE-GFP; (*B,D,F*) DAPI images showing the nucleoids of cells in the same fields as in *A*, *C*, and *E*, respectively. (*0*) Examples of cells without SpoIIE bands; (*1*) cells with one relatively weak and straight band, corresponding to cells that have not started to engulf; (*1**) cells with one strong and curving fluorescent band, corresponding to cells undergoing or having completed engulfment; (*2*) cells with two SpoIIE bands. Arrows point to the asymmetric septa in cells that have not yet completed transfer of the prespore chromosome. Scale bar, 2.5 μM.

ing asymmetric septation, often only one very weak SpoIIE band could be observed in each sporulating cell. In most of these cells (e.g., arrowed cells in Fig. 3A–D), the band was at the position of a constriction in the DNA, which corresponds to the site of a nascent asymmetric septum. In slightly later samples, cells with two bands could be observed, with one band brighter than the other (Fig. 3C,D). These cells generally showed a completely condensed prespore nucleoid, indicating that they had formed a septum and completed transfer of the prespore chromosome. Later still, cells with a visible prespore-distal band became less prevalent.

To confirm that the observation of single SpoIIE bands in early sporulating cells was not attributable to degradation in cells that initially had two bands, we examined cells of a *spoIIG spoIIIE* double mutant, in which developmental degradation is abolished (Pogliano et al. 1997; see above). As shown in Figure 3, cells with a single band at the site of nascent septation were readily detected in this mutant background. Therefore, we conclude that the polar bands of SpoIIE protein are generally formed sequentially, first appearing at the pole where the prespore septum forms.

Sequestration of SpoIIE phosphatase to the prespore side of the asymmetric septum

To examine the distribution of the SpoIIE phosphatase, we treated sporulating cells of strain 1305 with lysozyme. Treatment with lysozyme would digest away the thin peptidoglycan layer between the prespore and the mother cell membranes (before engulfment), as well as protoplasting the prespore and the mother cell. Therefore, upon protoplasting the distance between the prespore and the mother cell could be increased and it should be possible to distinguish between one-sided and two-sided distributions of the SpoIIE protein, as illustrated schematically in Figure 4A,B. Figure 4C–F shows the distribution of SpoIIE-GFP in protoplasted sporulating cells either just before (C,D) or just after (E,F) σ^F becomes active (t_{85} and t_{100}, respectively). Both samples were thus taken before developmental degradation of SpoIIE begins. The images show clearly that in both samples the SpoIIE-GFP signal was concentrated, often as a spot, in the prespore. The mother cell showed a weak signal throughout the cell. Weak, evenly distributed signals were also detected in mother cells of live (untreated) cultures from different times of sporulation, before and after developmental degradation of SpoIIE could be detected (Fig. 3A,C; data not shown), suggesting that this weak mother cell signal primarily came from cleaved (see above) or untargeted SpoIIE-GFP.

To check that the protoplasting procedure did not cause degradation of SpoIIE-GFP, we treated some sporulating wild-type cells at t_{90} to make protoplasts, then either pelleted and froze the protoplasts immediately, or left them on ice or at room temperature for 30 min before pelleting them. The samples were then analyzed by Western blot using both anti-SpoIIE and anti-GFP antibodies. As shown in Figure 1B, no degradation products could be detected even 30 min after the protoplasts were incubated at room temperature. This suggests that the fusion protein survived the protoplasting procedure and remained stable for a considerable period at room temperature. This excluded the possibility that the weak signal in the mother cell could be attributable to degradation of the fusion protein caused by the protoplasting procedure.

In the mother cell protoplast sometimes a small SpoIIE spot could also be detected at the pole opposite to the prespore (arrows in Fig. 4C), but no concentrated signals were seen on the face of the mother cell near to the

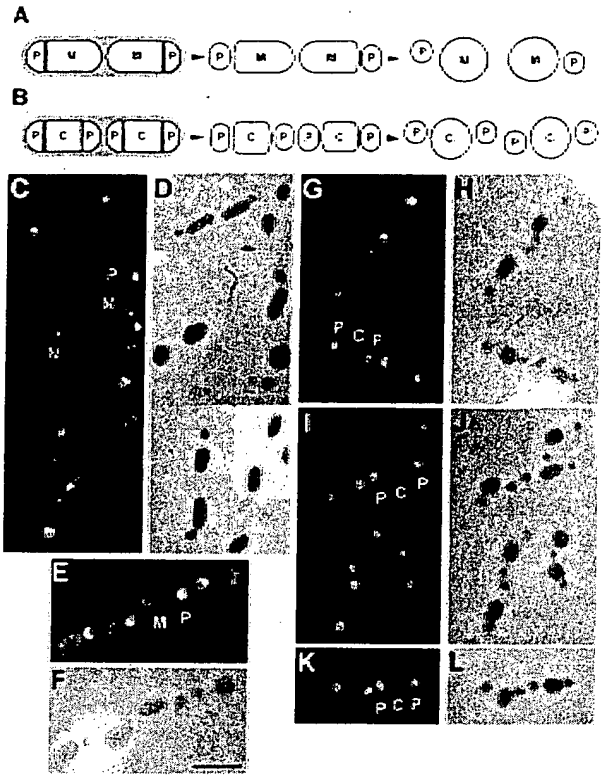

Figure 4. Localization of SpoIIE-GFP in protoplasted cells from sporulating cultures just before and after σ^F becomes active. (*A,B*) Schematic illustration of the consequences of treatment of (*A*) wild-type and (*B*) *spoIIG* mutant cells with lysozyme to make protoplasts. Removal of the cell wall material (shaded) allows the prespore (P), mother cell (M), or central (C) compartments to enlarge and round off and separate, allowing the fate of GFP initially located at the site of the thin division septum to be resolved. The remaining panels show images of typical cells. (*C–F*) Wild type (strain 1305); (*G–J*) *spoIIG spoIIIE* double mutant (strain 1213); (*K,L*) *spoIIG* mutant (strain 1211). (*C,D,G,H*) Cells at an early stage of sporulation (t_{85}), just before activation of σ^F. (*E,F,I–L*) Cells at slightly later stages of sporulation (t_{100}), just after σ^F becomes active. (*C,E,G,I,K*) Fluorescence images showing the distribution of *SpoIIE-GFP*; (*D,F,H,J,L*) phase-contrast images of same fields as *C, E, G, I,* and *K*, respectively. (*N*) Nonseptate cell. Arrows point to some of the SpoIIE spots in the mother cell protoplasts. Scale bar, 2.5 μM.

prespore. Presumably the prespore-distal SpoIIE spots were from the prespore-distal bands. The presence of these spots in some mother cell protoplasts suggested that the prespore-distal SpoIIE band did not always disassemble during protoplasting. However, to examine this further, as well as to exclude the possibility that SpoIIE did exist on the mother cell face but disassembled during protoplasting, we took advantage of a *spoIIG spoIIIE* double mutant. Western blot analysis showed that in both the *spoIIG* and the *spoIIIE* single mutants, developmental degradation of SpoIIE was greatly reduced or delayed (see Fig. 2). Pogliano et al. (1997) also reported that a *spoIIG spoIIIE* double mutant produces elevated levels of SpoIIE and has stable persistent SpoIIE bands at both poles. Therefore, if SpoIIE did exist on the mother cell face of the asymmetric septum and was disassembled upon protoplasting, the central compartment of the double mutant would be expected to show a stronger GFP signal, derived from two bands of SpoIIE rather than one. As shown in Figure 4G–J, this was not the case; the signal in the central compartment was actually much weaker than that observed in the mother cell of the wild-type cells. Furthermore, no SpoIIE spots could be observed in the central compartments. To check that the distribution pattern of the SpoIIE protein observed in the *spoIIG spoIIIE* double mutant was not attributable to some special effect of the *spoIIIE* mutation, we also examined the distribution of SpoIIE-GFP in a *spoIIG* single mutant (strain 1211) and obtained similar distribution patterns as in the double mutant (Fig. 4K,L). These results strongly suggest that there is no SpoIIE protein on the mother cell face of the completed asymmetric septum.

Genetic evidence for sequestration of SpoIIE to the prespore face of the asymmetric septum

Previously we reported that *spoIIIE* null mutants have σ^F activity in the mother cell compartment (Wu and Errington 1994). Studies by Pogliano et al. (1997) showed that the prespore-distal SpoIIE band persists in a *spoIIIE* null mutant and thus that the activation of σ^F in the mother cell of this mutant could be attributable to persistence of the SpoIIE band in the mother cell. If the SpoIIE protein were distributed on both sides of the asymmetric septum, rather than being restricted to the prespore side, one would expect that σ^F would also become active in the central compartment of *spoIIG spoIIIE* double mutants, in which both SpoIIE bands persist. To test this we examined the expression of a σ^F-dependent *gpr–lacZ* fusion in the central compartment during sporulation of the double mutant. *spoIIIE* mutations block prespore chromosome translocation and the *gpr* locus lies in the part of the chromosome that is excluded from the prespore (Wu and Errington 1994). As shown in Figure 5, the reporter gene was expressed in both the *spoIIG* and *spoIIIE* single mutants, but not in the *spoIIG spoIIIE* double mutant. When the reporter gene was moved to the prespore-located *amyE* locus it became highly expressed in the double mutant, suggesting that σ^F is active in the prespores in this mutant. This clearly demonstrates that in the double mutant σ^F activity is restricted to the prespores despite the presence of the *spoIIIE* mutation. Again these results would be consistent with SpoIIE being sequestered to the prespore face of the asymmetric septum.

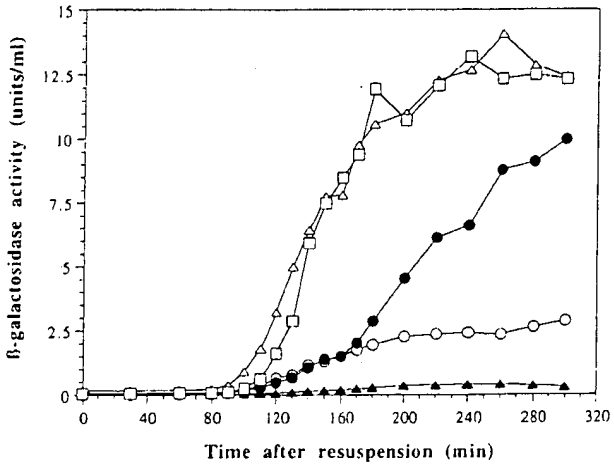

Figure 5. Absence of σ^F activity from the central compartment of a *spoIIG spoIIIE* double mutant. Various strains carrying a σ^F-dependent *gpr–lacZ* fusion located at the *gpr* locus (::pPS1395) or at *amyE* (::pPS1326) were induced to sporulate and β-galactosidase was assayed. (●) Wild-type strain SG38::pPS1395; (▲) *spoIIG spoIIIE* double mutant with the fusion located at the *gpr* locus (919::pPS1395); (△) *spoIIG spoIIIE* double mutant with the fusion located at the *amyE* locus (919::pPS1326); (○) *spoIIG* single mutant 901::pPS1395; (□) *spoIIIE* single mutant 604.6::pSG1395.

Discussion

Previous work showed that the SpoIIE protein localizes in bands at the potential sites of asymmetric septation near each pole early in sporulation (Arigoni et al. 1995). Localization at these sites was likely to play an important role in SpoIIE function because the protein is required for both formation of the asymmetric septum and for activation of σ^F in the polar compartment once formed (Barak and Youngman 1996; Feucht et al. 1996). Now we have used a fully functional *spoIIE-gfp* fusion to examine SpoIIE band formation, development, and degradation in more detail. The results obtained from observations of wild-type and mutant strains are summarized in schematic form in Figure 6A.

Sequential formation of SpoIIE bands

In previous work, mainly on the basis of immunofluorescence microscopy (Arigoni et al. 1995), it was reported that SpoIIE assembles initially in a bipolar pattern. We were surprised to find that when cells containing the SpoIIE-GFP fusion were examined early in sporulation, a monopolar pattern was predominant. Thus, at t_{70} when

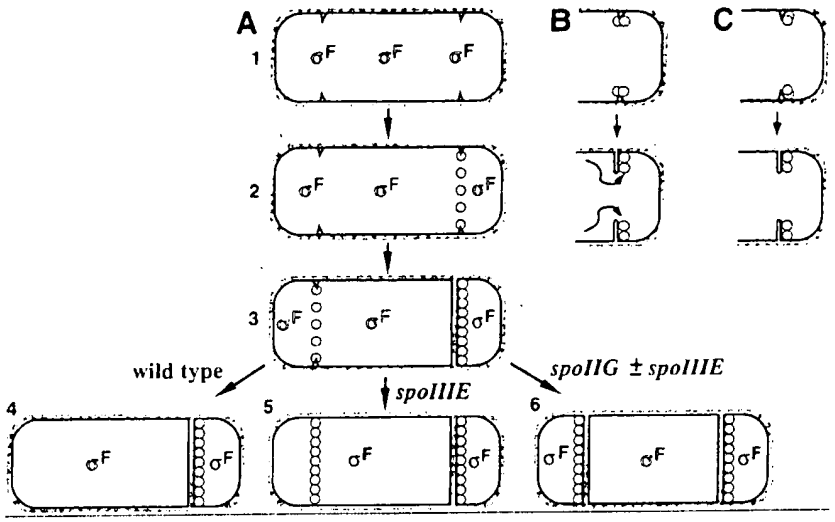

Figure 6. Schematic summary of the localization of SpoIIE protein in wild-type and mutant cells (*A*) and possible models for sequestration of SpoIIE to the prespore compartment (*B,C*). (*A*) *1* represents a preseptational cell soon after the initiation of sporulation; open arrowheads indicate the potential sites for asymmetric septation close to each pole. σ^F is present throughout the cytoplasm but in an inactive state (indicated by outline text). SpoIIE protein (O) then begins to be made (*2*) and is localized initially in a band at the polar septation site where the asymmetric septum will be formed, presumably by association with a component of the division apparatus. When the septum has formed (*3*) the SpoIIE protein is sequestered specifically into the membrane on the prespore side, and a second band of SpoIIE starts to appear at the prespore-distal potential division site. Sequestration of most of the cellular SpoIIE into the small prespore compartment results in activation of σ^F (boldface type). In wild-type cells SpoIIE in the mother cell is then degraded (*4*), probably as a result of activation of σ^E and synthesis of one or more proteases encoded by genes controlled by the new form of RNA polymerase. In *spoIIIE* mutants (*5*), the second SpoIIE ring persists in the mother cell, leading to aberrant activation of σ^F in that compartment. In *spoIIG* single or *spoIIG spoIIIE* double mutant (*6*), the absence of σ^E allows the second polar septum to form. The second SpoIIE ring is thus sequestered into its prespore, leaving the central compartment devoid of SpoIIE, and hence preventing σ^F from being activated in this compartment. (*B*) SpoIIE protein localizes initially to the site of incipient septation. As the septal annulus closes, flux of membrane lipid from the large compartment (where the bulk of new lipid synthesis could conceivably take place) drives the membrane-bound SpoIIE protein into the prespore compartment. (*C*) The SpoIIE band forms just to the polar side of the division site, so that as the septum forms the protein is captured by the prespore.

only the first few cells have formed an asymmetric septum, and long before developmental degradation of SpoIIE could be detected (Fig. 2), most such cells had only one prominent band, at the position of the septum (Fig. 3). The polar constriction in the DNA of these cells shows that they had just formed a septum but had not yet translocated the whole of the prespore chromosome into the small compartment and thus had not yet activated σ^F (Partridge and Errington 1993; Lewis et al. 1994). In later samples, the majority of cells did have two SpoIIE bands, but such cells were generally at a later stage of development, with a completely segregated prespore chromosome (Fig. 3). Eventually, as reported previously (Arigoni et al. 1995), the SpoIIE bands disappeared, first from the prespore-distal pole. Presumably, this reflects the developmental degradation of the protein seen in the Western analysis from about t_{105} (Fig. 2). We conclude, particularly from the analysis of cells in the early samples, that SpoIIE band formation occurs sequentially, rather than in a simultaneous bipolar manner. Because targeting of SpoIIE to these bands requires interaction with one or more components of the division apparatus (Levin et al. 1997), the differential development of the SpoIIE bands probably reflects differential assembly of the division apparatus at the two poles. This would accord well with the previous finding that in disporic mutants, the second asymmetric septum is formed about 15 min later than the first one (Lewis et al. 1994). Taken together, these observations are consistent with the notion that the choice of pole for formation of the prespore septum is attributable to the limited availability of one or more components of the division apparatus (Lewis et al. 1994). Moreover, the finding that in many cells, most of the SpoIIE protein is located at the pole where septation occurs, accords with its proposed role in modification of the form of the sporulation septum (Illing and Errington 1991).

Sequestration of SpoIIE protein to the prespore-face of the asymmetric septum

Both direct microscopic observations and indirect genetic experiments suggested that after formation of the asymmetric septum, the SpoIIE protein in the band marking the site of impending septation is sequestered into the prespore compartment. Microscopic examination of whole living cells did not provide sufficient resolution to be able to distinguish between localization on one or both sides of the septum. However, treatment with lysozyme, leading to formation of protoplasts, resulted in expansion of the space between the septal membranes of the prespore and mother cell, and revealed a strong enrichment of the SpoIIE-GFP in the prespore compartment. In many of the treated cells, especially those in which protoplasting was only partial (e.g., Fig. 4C), the SpoIIE-GFP signal remained highly concentrated, as in the bands of untreated cells, and the concentrated spots were clearly associated with the prespore, rather than with the mother cell. Control experiments showed that the background fluorescence associated

with the mother cell was probably not attributable to degradation of the fusion protein (at least in the early samples). Probably, it represents untargeted protein, as a diffuse background signal was generally visible in the living untreated cells (Fig. 3).

The conclusion that SpoIIE becomes sequestered into the prespore was reinforced by examination of *spoIIG* mutant cells. These mutant studies were useful for two reasons. First, *spoIIG* mutants form a second prespore-like cell at the opposite pole of the cell (see above), therefore, the SpoIIE protein associated with the prespore-distal band should either remain partly associated with the central compartment, or be sequestered into the second prespore leaving only a low background signal in the central compartment. Second, as shown previously by Pogliano et al. (1997), the prespore-distal SpoIIE band persists in *spoIIG* mutants (and both bands in *spoIIG spoIIIE* double mutants), therefore, SpoIIE localization after septation should be more readily evident in these mutants than in the wild type. Microscopic examination of such mutants showed strong signals in the prespore protoplasts but not in the central compartment, strongly supporting our contention that the SpoIIE-GFP from the polar bands is sequestered to the membrane of the prespore compartment after septation (see Fig. 6A).

The disporic phenotype of *spoIIG* mutants also provided an indirect genetic test for sequestration of SpoIIE protein to the prespore side of the septum. If sequestration results in removal of most of the SpoIIE phosphatase activity from the central compartment, σ^F should not become active there. Although the central compartment of these mutants is normally devoid of DNA and thus would not normally contain a σ^F-dependent reporter gene, it was possible to test activity in this compartment by use of a *spoIIIE* mutation, which results in most of the chromosome failing to be segregated into the prespore compartment (Wu and Errington 1994; Wu et al. 1995). As shown in Figure 5, in a *spoIIG spoIIIE* double mutant, strong σ^F activation was detected with a reporter gene segregated into the prespore compartment but not with the same reporter positioned in the central compartment. Although this result strongly supports the sequestration of SpoIIE protein out of the central compartment and into the polar ones, interpretation of the data is made slightly complicated by the 15- or 20-min delay between formation of the first and second polar septa in *spoIIG* mutants (Lewis et al. 1994). The absence of detectable σ^F activity in the large (later central) compartment of the double mutant suggests that σ^F does not become active in the interval before the second septum forms. The notion that aberrant σ^F activation in the large compartment of *spoIIIE* null mutants is delayed would be consistent with the *lacZ* fusion data; for example, the open squares versus open triangles in Figure 5 (also L.J. Wu, P.J. Lewis, and J. Errington, unpubl.). Unfortunately, we do not yet understand the molecular basis for mother cell activation of σ^F in *spoIIIE* null mutants and this aspect of the mutant phenotype may be a misleading, indirect consequence of the unbalanced genetic and physiological state of the cells. Nevetheless, in results to be presented elsewhere, we have found that dephosphorylation of SpoIIAA (attributable to SpoIIE activity) occurs predominantly in the prespore compartment of disporic *spoIIG* mutant cells, even in the absence of the complicating *spoIIIE* mutation (P.J. Lewis and J. Errington, unpubl.). Therefore, we conclude, on the basis of both direct and indirect evidence, that formation of the asymmetric septum results in sequestration of SpoIIE protein onto the prespore face of the asymmetric septum.

How might sequestration of SpoIIE to the prespore face of the septum be achieved? One possibility would be for the SpoIIE protein to be transferred through the septum as it forms (Fig. 6B). As we suggested previously (Feucht et al. 1996), the asymmetric positioning of the septum probably results in a net influx of membrane lipid through the septal annulus as it constricts. Transport of the SpoIIE protein could be driven by this flux. Alternatively, it is possible that the SpoIIE ring is slightly offset from the division apparatus, toward the pole, so that when the septum forms, the topology dictates that SpoIIE becomes trapped in the prespore (Fig. 6C). Our present methods do not provide sufficient resolution to distinguish between the relative positions of SpoIIE and other proteins that contribute to formation of the septum, such as FtsZ, before septation.

Whatever the mechanism of sequestration, our finding that the strongest SpoIIE band tends to lie at the pole where prespore septation takes place, means that most of the cellular SpoIIE is trapped in the small prespore compartment after septation. The resultant high concentration of SpoIIE in the prespore conceivably could provide the trigger for σ^F activation by overwhelming the opposing kinase reaction that maintains the inhibitory state (see introductory section). It could also provide a simple explanation for the dependence of σ^F activation on formation of the septum (Levin and Losick 1994).

Materials and methods

Bacterial strains and plasmids

The bacterial strains and the plasmids used in this study are listed in Table 1. Plasmid pSG1151 (P.J. Lewis, unpubl.) is a derivative of pSG1137 (Lewis and Errington 1996) with an additional mutation (F64L) in the *gfp* gene (Cormack et al. 1996). To make a new *spoIIE-gfp* fusion a 871-bp fragment was amplified by PCR from chromosomal DNA of CW314 (Arigoni et al. 1995), in which the 3′ end of *spoIIE* was joined in-frame to *gfp* through a polylinker sequence. The PCR product was digested with *Hin*dIII and *Msc*I and the resulting 770 bp fragment was subcloned into *Hin*dIII-*Msc*I-digested pSG1151. The oligonucleotides used for the PCR were 5′-CAGCTACAGCATGATGGAGC-3′ and 5′-AGTGACAAGTGTTGGCCATGG-3′. Plasmid pSG1901 was constructed by cloning the 1571-bp *spoIIE* fragment amplified from SG38 chromosomal DNA using PCR and digested with *Bam*HI into pQE-30 (Qiagen), thereby fusing codon 325 of *spoIIE* in-frame with the polyhistidine-encoding sequence of pQE-30. The oligonucleotides used for PCR were 5′-ACGCGGATCCACGAGGAAAGTGCCGAG-3′ and 5′-GCGGATCCCATATATTCCCATCTTCGCCAGAAG-3′, which would create a *Bam*HI site at each end of the PCR product.

Table 1. *Bacterial strains and plasmids*

Strain/plasmid	Relevant genotype[a]	Construction, source, or reference
B. subtilis		
SG38	*trpC2 amyE*	Errington and Mandelstam (1986)
CW314	*spoIIE*::pCW28 *(spoIIE-gfp aph-A3)*	Arigoni et al. (1995)
1305	*trpC2 amyE spoIIE*::pSG1902 *(spoIIE-gfpF64L S65T cat)*	pSG1902 transformed into SG38, with selection for chloramphenicol resistance
604.6	*trpC2 spoIIIE604*	M. Deadman (unpub.)
901	*trpC2* Ω *(spoIIGA::aph-A3)901*	Wu and Errington (1994)
919	*trpC2 spoIIIE604* Ω *(spoIIGA::aph-A3)901*	Wu and Errington (1998)
1210	*trpC2 spoIIIE604 spoIIE*::pSG1902 *(spoIIE-gfpF64L S65T cat)*	pSG1902 transformed into 604.6, with selection for chloramphenicol resistance
1211	*trpC2* Ω *(spoIIGA::aph-A3)901 spoIIE*::pSG1902 *(spoIIE-gfpF64L S65T cat)*	pSG1902 transformed into 901, with selection for chloramphenicol resistance
1213	*trpC2 spoIIIE604* Ω *(spoIIGA::aph-A3)901 spoIIE*::pSG1902 *(spoIIE-gfpF64L S65T cat)*	pSG1902 transformed into 919, with selection for chloramphenicol resistance
E. coli		
DH5α	F⁻*endA1 hsdR17 supE44* λ⁻*thi-1 recA1 gyrA96 relA1 Δ(lacZYA-argF)U169*(ϕ80d*lac*) Δ*(lacZ)M15*	GIBCO BRL
MC1061	F⁻*hsdR mcrB araD139 Δ(araABC-leu)7679 galU galK Δ(lac)X74 rpsL thi*	Meissner et al. (1987)
NM554 (pREP4)	F⁻*hsdR mcrB araD139 Δ(araABC-leu)7679 galU galK Δ(lac)X74 rpsL thi recA13* (pREP4) *lacI*ᵠ	pREP4 (Qiagen) transformed into NM554 of Raleigh et al. (1988)
Plasmids		
pSG1151	*bla cat gfpF64L S65T*	P.J. Lewis (unpub.)
pSG1901	*bla spoIIE* (973-2484)	this paper
pSG1902	*bla cat spoIIE* (1932-2481)-*gfpF64L S65T*	this paper
pPS1395	*gpr-lacZ* in pJF751	P. Setlow (University of Connecticut Health Center, Farmington)
pPS1326	*grp-lacZ* in ptrpBG1	Sun and Setlow (1991)

[a]Numbers in parentheses after *spoIIE* refer to the first and last nucleotides of the insert from the *spoIIE* coding sequence.

Plasmids pSG1901 and pSG1902 were constructed using *Escherichia coli* strains DH5α and MC1061, respectively. Both plasmids were sequenced to ensure that the cloned *spoIIE* fragments did not contain any mutations.

Growth media

Nutrient agar (Oxoid) was used as a solid medium for growing *B. subtilis*. Chloramphenicol (5 μg/ml) or kanamycin sulfate (5 μg/ml) were added as required. Media used for growing *E. coli* were 2× TY (Sambrook et al. 1989) and nutrient agar (Oxoid) supplemented with ampicillin (100 μg/ml) and kanamycin sulfate (25 μg/ml) as necessary.

General methods

B. subtilis cells were made competent for transformation with DNA by the method of Anagnostopoulos and Spizizen (1961), as modified by Jenkinson (1983). *B. subtilis* chromosomal DNA was prepared by a scaled-down method based on the one described by Errington (1984). DNA manipulations and *E. coli* transformations were carried out using standard methods (Sambrook et al. 1989).

Induction of sporulation

B. subtilis cells grown in hydrolyzed casein growth media at 37°C were induced to sporulate by the resuspension method of Sterlini and Mandelstam (1969), as specified by Nicholson and Setlow (1990) and Partridge and Errington (1993). Times (minutes) after resuspension of cells in the starvation medium were denoted t_0, t_{60}, t_{75}, and so forth. β-Galactosidase activity was measured by the method of Errington and Mandelstam (1986). One unit of β-galactosidase catalyzes the production of 1 nmole of 4-methylumbelliferone per minute under the standard reaction conditions.

Measurement of septum formation and sporulation frequency

The frequency of asymmetric septation of strain 1305 and the wild-type strain SG38 were determined at t_{80}, as described by Feucht et al. (1996). The sporulation frequency was determined by counting spores and total cells with a phase contrast microscope at t_{420}.

Antibodies and Western blots

To raise antibodies against SpoIIE the histidine-tagged, carboxy-

terminal fragment of SpoIIE was overexpressed using plasmid pSG1901 in *E. coli* NM554 (pREP4) and the resulting insoluble fusion protein was purified as described in the Qiagen protocol. A rabbit polyclonal antiserum was raised by standard procedures (Harlow and Lane 1988). For the purification of the anti-SpoIIE antibodies the truncated SpoIIE protein was further purified by a Prep Cell (model 491, Bio-Rad) as described by the manufacturer. The antibodies were affinity purified as described by Reznekov et al. (1996) using 4.5 M $MgCl_2$ as eluant. The final purified antiserum was used at a dilution of 1:200 for Western blot analysis (Harlow and Lane 1988). Monoclonal anti-GFP antibody (Clontech) was used at a dilution of 1:1750 for Western blot analysis. The amount of protein samples loaded on SDS-PAGE for Western blot analysis was determined by a Bio-Rad protein assay.

Protoplasting and fluorescence microscopy

Samples of sporulating cultures were centrifuged to harvest the cells (at different times after induction of sporulation) and the cell pellet was resuspended quickly in about half volume of the original sample of 1× SMM [0.5 M sucrose, 20 mM maleic acid; 20 mM $MgCl_2$ (pH 6.5)] containing 4 mg/ml lysozyme, as described by Errington (1990). The mixture was mixed gently for 1 min, then ~1.5 µl was loaded onto a polylysine-treated microscope slide. For live cell examination, a 1.5-µl drop of fresh culture was placed directly onto a polylysine-treated microscope slide. For fixed cells, the conditions described by Harry et al. (1995) were used except that glutaraldehyde was reduced to 0.005%. For either live or fixed cells or protoplasts, DAPI solution (1 µg/ml) was sometimes added directly onto the slides to visualize the nucleoids. Microscopic examination of GFP fluorescence and image grabbing was performed as described previously (Lewis and Errington 1996).

Acknowledgments

We thank Chris D. Webb and Peter Lewis for providing strain CW314 and plasmid pSG1151, respectively. This work was supported by the Biotechnology and Biological Sciences Research Council.

The publication costs of this article were defrayed in part by payment of page charges. This article must therefore be hereby marked "advertisement" in accordance with 18 USC section 1734 solely to indicate this fact.

References

Alper, S., L. Duncan, and R. Losick. 1994. An adenosine nucleotide switch controlling the activity of a cell type-specific transcription factor in B. subtilis. *Cell* **77**: 195-205.

Anagnostopoulos, C. and J. Spizizen. 1961. Requirements for transformation in *Bacillus subtilis*. *J. Bacteriol.* **81**: 741-746.

Arigoni, F., K. Pogliano, C.D. Webb, P. Stragier, and R. Losick. 1995. Localization of protein implicated in establishment of cell type to sites of asymmetric division. *Science* **270**: 637-640.

Arigoni, F., L. Duncan, S. Alper, R. Losick, and P. Stragier. 1996. SpoIIE governs the phosphorylation state of a protein regulating transcription factor σ^F during sporulation in *Bacillus subtilis*. *Proc. Natl. Acad. Sci.* **93**: 3238-3242.

Barak, I. and P. Youngman. 1996. SpoIIE mutants of *Bacillus subtilis* comprise two distinct phenotypic classes consistent with a dual functional role for the SpoIIE protein. *J. Bacteriol.* **178**: 4984-4989.

Barak, I., J. Behari, G. Olmedo, P. Guzman, D.P. Brown, E. Castro, D. Walker, J. Westpheling, and P. Youngman. 1996. Structure and function of the *Bacillus* SpoIIE protein and its localization to sites of sporulation septum assembly. *Mol. Microbiol.* **19**: 1047-1060.

Cormack, B.P., R.H. Valdivia, and S. Falkow. 1996. FACS-optimized mutants of the green fluorescent protein (GFP). *Gene* **173**: 33-38.

Diederich, B., J.F. Wilkinson, T. Magnin, S.M.A. Najafi, J. Errington, and M.D. Yudkin. 1994. Role of interactions between SpoIIAA and SpoIIAB in regulating cell-specific transcription factor σ^F of *Bacillus subtilis*. *Genes & Dev.* **8**: 2653-2663.

Duncan, L. and R. Losick. 1993. SpoIIAB is an anti-σ factor that binds to and inhibits transcription by regulatory protein σ^F from *Bacillus subtilis*. *Proc. Natl. Acad. Sci.* **90**: 2325-2329.

Duncan, L., S. Alper, F. Arigoni, R. Losick, and P. Stragier. 1995. Activation of cell-specific transciption by a serine phosphatase at the site of asymmetric division. *Science* **270**: 641-644.

Errington, J. 1984. Efficient *Bacillus subtilis* cloning system using bacteriophage vector ϕ105J9. *J. Gen. Microbiol.* **130**: 2615-2628.

———. 1990. Gene cloning techniques. In *Molecular biological methods for* Bacillus (ed. C.R. Harwood and S.M. Cutting), pp. 175-220. Wiley, Chichester, UK.

———. 1993. *Bacillus subtilis* sporulation: Regulation of gene expression and control of morphogenesis. *Microbiol. Rev.* **57**: 1-33.

———. 1996. Determination of cell fate in *Bacillus subtilis*. *Trends Genet.* **12**: 31-34.

Errington, J. and J. Mandelstam. 1986. Use of a *lacZ* gene fusion to determine the dependence pattern of sporulation operon *spoIIA* in *spo* mutants of *Bacillus subtilis*. *J. Gen. Microbiol.* **132**: 2967-2976.

Feucht, A., T. Magnin, M.D. Yudkin, and J. Errington. 1996. Bifunctional protein required for asymmetric cell division and cell-specific transcription in *Bacillus subtilis*. *Genes & Dev.* **10**: 794-803.

Glaser, P., M.E. Sharpe, B. Raether, M. Perego, K. Ohlsen, and J. Errington. 1997. Dynamic, mitotic-like behavior of a bacterial protein required for accurate chromosome partitioning. *Genes & Dev.* **11**: 1160-1168.

Guzman, P., J. Westpheling, and P. Youngman. 1988. Characterization of the promoter region of the *Bacillus subtilis spoIIE* operon. *J. Bacteriol.* **170**: 1598-1609.

Harlow, E. and D.P. Lane. 1988. *Antibodies: A laboratory manual*. Cold Spring Harbor Laboratory, Cold Spring Harbor, NY.

Harry, E.J., K. Pogliano, and R. Losick. 1995. Use of immunofluorescence to visualize cell-specific gene expression during sporulation in *Bacillus subtilis*. *J. Bacteriol.* **177**: 3386-3393.

Illing, N. and J. Errington. 1991. Genetic regulation of morphogenesis in *Bacillus subtilis*: Roles of σ^E and σ^F in prespore engulfment. *J. Bacteriol.* **173**: 3159-3169.

Jenkinson, H.F. 1983. Altered arrangement of proteins in the spore coat of a germination mutant of *Bacillus subtilis*. *J. Gen. Microbiol.* **129**: 1945-1958.

Levin, P.A. and R. Losick. 1994. Characterization of a cell division gene from *Bacillus subtilis* that is required for vegetative and sporulation septum formation. *J. Bacteriol.* **176**: 1451-1459.

Levin, P.A., R. Losick, P. Stragier, and F. Arigoni. 1997. Localization of the sporulation protein SpoIIE in *Bacillus subtilis* is dependent upon the cell division protein FtsZ. *Mol. Microbiol.* **25**: 839-846.

Lewis, P.J. and J. Errington. 1996. Use of green fluorescent protein for detection of cell-specific gene expression and subcellular protein localization during sporulation in *Bacillus subtilis*. *Microbiology* **142**: 733–740.

Lewis, P.J., S.R. Partridge, and J. Errington. 1994. σ factors, asymmetry, and the determination of cell fate in *Bacillus subtilis*. *Proc. Natl. Acad. Sci.* **91**: 3849–3853.

Lewis, P.J., T. Magnin, and J. Errington. 1996. Compartmentalized distribution of the proteins controlling the prespore-specific transcription factor σ^F of *Bacillus subtilis*. *Genes Cells* **1**: 881–894.

Magnin, T., M. Lord, J. Errington, and M.D. Yudkin. 1996. Establishing differential gene expression in sporulating *Bacillus subtilis*: Phosphorylation of SpoIIAA (anti-anti-σ^F) alters its conformation and prevents formation of a SpoIIAA/SpoIIAB/ADP complex. *Mol. Microbiol.* **19**: 901–907.

Magnin, T., M. Lord, and M.D. Yudkin. 1997. Contribution of partner switching and SpoIIAA cycling to regulation of σ^F activity in sporulating *Bacillus subtilis*. *J. Bacteriol.* **179**: 3922–3927.

Margolis, P., A. Driks, and R. Losick. 1991. Establishment of cell type by compartmentalized activation of a transcription factor. *Science* **254**: 562–565.

Meissner, P.S., W.P. Sisk, and M.L. Berman. 1987. Bacteriophage λ cloning system for the construction of directional cDNA libraries. *Proc. Natl. Acad. Sci.* **84**: 4171–4175.

Min, K.-T., C.M. Hilditch, B. Diederich, J. Errington, and M.D. Yudkin. 1993. σ^F, the first compartment-specific transcription factor of B. subtilis, is regulated by an anti-σ factor that is also a protein kinase. *Cell* **74**: 735–742.

Najafi, S.M.A., A.C. Willis, and M.D. Yudkin. 1995. Site of phosphorylation of SpoIIAA, the anti-anti-sigma factor for sporulation-specific σ^F of *Bacillus subtilis*. *J. Bacteriol.* **177**: 2912–2913.

Nicholson, W.L. and P. Setlow. 1990. Sporulation, germination and outgrowth. In *Molecular biological methods for Bacillus* (ed. C.R. Harwood and S.M. Cutting), pp. 391–450. Wiley, Chichester, UK.

Partridge, S.R. and J. Errington. 1993. The importance of morphological events and intercellular interactions in the regulation of prespore-specific gene expression during sporulation in *Bacillus subtilis*. *Mol. Microbiol.* **8**: 945–955.

Piggot, P.J. and J.G. Coote. 1976. Genetic aspects of bacterial endospore formation. *Bact. Rev.* **40**: 908–962.

Pogliano, K., A.E. Hofmeister, and R. Losick. 1997. Disappearance of the σ^E transcription factor from the forespore and the SpoIIE phosphatase from the mother cell contributes to establishment of cell-specific gene expression during sporulation in *Bacillus subtilis*. *J. Bacteriol.* **179**: 3331–3341.

Raleigh, E.A., N.E. Murray, H. Revel, R.M. Blumenthal, D. Westaway, A.D. Reith, P.W.J. Rigby, J. Elhai, and D. Hanahan. 1988. McrA and McrB restriction phenotypes of some *E. coli* strains and implications for gene cloning. *Nucleic Acids Res.* **16**: 1563–1575.

Reznekov, O., S. Alper, and R. Losick. 1996. Subcellular localization of proteins governing the proteolytic activation of a developmental transcription factor in *Bacillus subtilis*. *Genes Cells* **1**: 529–542.

Sambrook, J., E.F. Fritsch, and T. Maniatis. 1989. *Molecular cloning: A laboratory manual*. Cold Spring Harbor Laboratory Press, Cold Spring Harbor, NY.

Sterlini, J.M. and J. Mandelstam. 1969. Committment to sporulation in *Bacillus subtilis* and its relationship to the development of actinomycin resistance. *Biochem. J.* **113**: 29–37.

Stragier, P. and R. Losick. 1996. Molecular genetics of sporulation in *Bacillus subtilis*. *Annu. Rev. Genet.* **30**: 297–341.

Sun, D. and P. Setlow. 1991. Cloning, nucleotide sequence, and expression of the *Bacillus subtilis ans* operon, which codes for L-asparaginase and L-aspartase. *J. Bacteriol.* **173**: 3831–3845.

Wu, L.J. and J. Errington. 1994. *Bacillus subtilis* SpoIIIE protein required for DNA segregation during asymmetric cell division. *Science* **264**: 572–575.

———. 1998. Use of asymmetric cell division and *spoIIIE* mutants to probe chromosome orientation and organization in *Bacillus subtilis*. *Mol. Microbiol.* **27**: 777–786.

Wu, L.J., P.J. Lewis, R. Allmansberger, P.M. Hauser, and J. Errington. 1995. A conjugation-like mechanism for prespore chromosome partitioning during sporulation in *Bacillus subtilis*. *Genes & Dev.* **9**: 1316–1326.

Regulation of ZAP-70 Intracellular Localization: Visualization with the Green Fluorescent Protein

By Joanne Sloan-Lancaster,* Weiguo Zhang,* John Presley,‡ Brandi L. Williams,§ Robert T. Abraham,§ Jennifer Lippincott-Schwartz,‡ and Lawrence E. Samelson*

*From *the Section on Lymphocyte Signaling and ‡the Unit of Organelle Biology, Cell Biology and Metabolism Branch, National Institute of Child Health and Human Development, National Institutes of Health, Bethesda, Maryland 20892; and §The Department of Immunology, Mayo Clinic, Rochester, Minnesota 55905*

Summary

To investigate the cellular dynamics of ZAP-70, we have studied the distribution and regulation of its intracellular location using a ZAP-70 green fluorescent protein chimera. Initial experiments in epithelial cells indicated that ZAP-70 is diffusely located throughout the quiescent cell, and accumulates at the plasma membrane upon cellular activation, a phenotype enhanced by the coexpression of Lck and the initiation of ZAP-70 kinase activity. Subsequent studies in T cells confirmed this phenotype. Intriguingly, a large amount of ZAP-70, both chimeric and endogenous, resides in the nucleus of quiescent and activated cells. Nuclear ZAP-70 becomes tyrosine phosphorylated upon stimulation via the T cell receptor, indicating that it may have an important biologic function.

The TCR has a multisubunit structure composed of the polymorphic αβ heterodimer, responsible for antigen recognition, and the invariant CD3 γ, δ, ε, and TCR-ζ subunits, required for receptor surface expression and signal transduction. Engagement of the TCR leads to a rapid rise in intracellular protein tyrosine phosphorylation, followed by a series of other biochemical events, eventually resulting in gene expression and effector function (for reviews see references 1, 2). The earliest biochemical event after TCR occupancy appears to be the activation of the Src family protein tyrosine kinases (PTKs)[1] Lck and/or Fyn. These activated kinases phosphorylate the various immunoreceptor tyrosine-based activation motifs (ITAMs) of the TCR (3, 4), providing binding sites for molecules containing SH2 domains capable of binding phosphotyrosine in the proper context (5). One such molecule is ZAP-70, also a PTK, which binds via its tandem SH2 domains to the two phosphotyrosine residues of individual ITAMs (6, 7). Subsequent phosphorylation of ZAP-70 by Lck and/or Fyn induces its activation (3, 8, 9). Thereafter, a number of other signaling and adaptor molecules are phosphorylated and recruited to the activated TCR and ZAP-70, and may subsequently be activated (10). These include phospholipase Cγ1 (PLCγ1) (11, 12), the proto-oncogenes Vav and Cbl (13, 14), and SLP-76 and pp36 whose functions are still unknown (15). Thus, a multicomponent protein complex is formed at the TCR soon after activation, though the stoichiometry and kinetics of assembly of its components have remained largely unexplored.

A critical role for ZAP-70 in the initiation of T cell signaling has been demonstrated by several lines of evidence. For example, disruption of ZAP-70 recruitment to the activated TCR results in a loss of T cell signaling (16, 17). Moreover, a mutant Jurkat T cell line lacking ZAP-70, P116, shows no functional or biochemical evidence of TCR-mediated activation (B.L. Williams, manuscript in preparation) and patients with ZAP-70 mutations as well as ZAP-70 knockout mice display profound SCID phenotypes (18–21). Despite the information available regarding the function of ZAP-70 in T cells, little is known about its intracellular location or dynamics. Upon cellular activation, ZAP-70 is rapidly tyrosine phosphorylated and it transiently translocates to the TCR. However, subcellular fractionation experiments have indicated that most ZAP-70 remains in the cytosol, and only a fraction of the kinase becomes tyrosine phosphorylated when the cells are activated (W. Zhang, unpublished observations). Though interest has focused on the TCR-associated fraction of ZAP-70, clearly the function of the majority of ZAP-70 molecules has been insufficiently analyzed.

To further explore ZAP-70 intracellular localization and dynamics, we have used the green fluorescent protein (GFP) of the jellyfish *Aequorea victoria*. The fluorescent signal gen-

[1] *Abbreviations used in this paper:* cfb3, cytosolic fragment of erythrocyte band 3; GFP, green fluorescent protein; IF, immunofluorescence; IP, immunoprecipitation; IRP, iron regulatory protein; ITAM, immunoreceptor tyrosine-based activation motif; KD, kinase dead; PTK, protein tyrosine kinase; PV, pervanadate; NLS, nuclear localization signal; ROI, region of interest; RT, room temperature.

erated by GFP is stable, species-independent, and can be monitored noninvasively in living cells (22, 23). GFP-tagged proteins have been used to assess the regulation of gene expression, the dynamics of intracellular organelles, and the subcellular localization and movement of many proteins in intact cells (see review in reference 23). Moreover, refined GFP variants are now available, which are codon-optimized for expression in mammalian cells and have fluorescence intensities up to 35-fold higher than the wild-type GFPs (24).

Here we have used a chimeric protein composed of ZAP-70 fused to the variant GFP, EGFP, as a tool to begin to visually define the kinetics and regulation of ZAP-70 movement. Our results show that, when expressed in epithelial cells, ZAP-70 GFP is found diffusely throughout the quiescent cell. However, upon pharmacological stimulation, redistribution of a pool of ZAP-70 GFP to the plasma membrane occurs. This phenotype is enhanced by coexpression of an active form of Lck (F505 Lck), but can occur in the absence of any TCR chains. Although maximal membrane accumulation requires full phosphorylation and activation of ZAP-70 kinase, significant translocation of a kinase-dead (KD) form of ZAP-70 GFP occurs. Subsequent studies in T lymphocytes also indicate a cellular redistribution of the enzyme upon activation via the TCR. Intriguingly, ZAP-70 GFP is present in the nucleus of both resting and activated cells. This nuclear location was confirmed for the endogenous protein in Jurkat T cells, both by immunofluorescence staining with an anti-ZAP-70 antiserum, and by biochemical purification of the nuclear material. Similarly to cytosolic ZAP-70, the nuclear pool demonstrates an increase in phosphotyrosine content upon cellular stimulation, implying that it acquires kinase activity (8, 9). Our observations provide visual evidence to support many previous biochemical data, as well as revealing some unexpected findings that will provoke further study. The movement of ZAP-70 to the plasma membrane in the absence of a TCR suggests that other peripheral or transmembrane proteins can serve as docking molecules for this kinase. Moreover, the presence of ZAP-70 in the nucleus leads one to reassess its role as merely a plasma membrane PTK, suggesting instead that it may have additional nuclear functions.

Materials and Methods

Cells, Antibodies, and Reagents. Complete D10 (for Cos 7 cells) or R10 (Jurkat and its ZAP-70 negative mutant, P116) medium was used for cell culture (8). The P116/ZAP-70 GFP subclones C8, C11, and H9 were derived from the parent subclone 2G1, whereas F4 was derived from the independent parent subclone 1C2. All stably transfected lines were cultured in R10 complete medium supplemented with 1 mg/ml Geneticin (G418; GIBCO BRL, Gaithersburg, MD) for maintenance of transgene expression.

mAbs used include antiphosphotyrosine, 4G10 (UBI, Lake Placid, NY); anti-TCR α chain, A2B4 (25); the $F(ab')_2$ fragment of OKT3 (anti-CD3 ε; reference 26); and anti-Lck, 3A5 (Santa Cruz Biotechnology, Santa Cruz, CA). Rabbit sera are anti-ZAP-70 (8), anti-GFP (Clontech, Palo Alto, CA), and anti-IRP-1 (27). Rhodamine-coupled goat anti-mouse and goat anti-rabbit IgG (Southern Biotechnology, Birmingham, AL), and Cy™ 3 donkey anti-rabbit IgG (Jackson ImmunoResearch Labs Inc., West Grove, PA) were used. The cytosolic fragment of erythrocyte band 3 (cfb3), a substrate of ZAP-70, has been described elsewhere (28).

Plasmids and Constructs. The generation of pSXSRα-Lck F505 has been described previously (8). An oligonucleotide linker method was used to create the ZAP-70 GFP fusion protein expressed in the Clontech pEGFP-N1 vector (pEGFP/ZAP-70). The oligonucleotide, 5′-CTA GGG CCC CCA GGC AGC ACA CAG AAG GCT GAG GCT GCC TGT GCC TCG-3′, encoding the COOH terminus of ZAP-70, was cloned into the Xba 1/Bam H1 sites of pBluescript KS plasmid. The Apa 1 fragment was subcloned into pSXSRα-ZAP-Myc, and the EcoR1/BamH1 fragment from this was subcloned into the corresponding sites of the pEGFP-N1 expression vector. A KD form of ZAP-70, created by site-directed mutagenesis of the lysine at position 369 to an alanine, replaced ZAP-70 GFP in the pEGFP/ZAP-70 vector.

Transfection. Cos 7 cells were electroporated using 15 μg of each DNA construct at 250 V and 500 μF using a Gene Pulser (Bio Rad Labs., Hercules, CA) and used at 20–26 h after transfection. P116 T cells (2×10^6) were electroporated using 20 μg DNA at 310 V and 500 μF. First stage subclones of P116/ZAP-70 GFP, 2G1, and 1C2, were selected from a bulk population by limiting dilution analysis, and these were further subcloned to produce C8, C11, H9 (from 2G1), and F4 (from 1C2), respectively.

Immunoprecipitation, Immunoblotting, Immune-complex Kinase Assays, Cytosol/Membrane and Nuclear Fraction Purification. Transfected Cos 7 cells were harvested and lysed in Brij 97 lysis buffer (8). The cells were stimulated for 10 min at room temperature (RT) in the presence or absence of pervanadate (PV) before lysis. Jurkat, P116, and ZAP-70 GFP subclones were left untreated or stimulated with $F(ab')_2$ fragments of OKT3 for 2 min at 37°C before lysis. Postnuclear lysates were analyzed by SDS-PAGE or were subjected to immunoprecipitation (IP) using the appropriate Ab adsorbed to protein A–Sepharose. An immune-complex kinase assay was performed using cfb3 as an exogenous substrate (1 μg/IP; reference 8).

For preparation of cytosolic/membrane and nuclear fractions, Jurkat cells (4×10^7) were suspended in homogenization buffer (10 mM Tris, pH 7.6, 0.5 mM $MgCl_2$, 1 mM PMSF, 10 μg/ml Aprotinin, 10 μg/ml Leupeptin, 5 mM EDTA, 1 mM Na_3VO_4), with (see Fig. 9 *a*) or without (see Fig. 9 *b*) 0.1% Tween 20, and incubated on ice for 20 min. Swollen cells were then homogenized by aspirating 50 times using a 25-gauge needle and 1-ml syringe, and the percentage of broken cells was >95%. NaCl (150 mM final) and Hepes (pH 7.5, 50 mM final) were added, and cells were centrifuged at 2,000 rpm for 5 min to pellet the nuclei. Supernatants were considered the cytosolic/membrane fraction. Nuclear pellets were washed three times with homogenization buffer with (Fig. 9 *a*) or without (Fig. 9 *b*) 0.1% Triton X-100, resuspended in the same buffer (400 μl), and sonicated (four times, 30 s each). Samples were boiled for 15 min, centrifuged at 15,000 rpm × 10 min, and supernatants collected as purified nuclear material. A portion of each cellular fraction was used to determine enrichment of nuclear material and percent contamination from cytosol. The remainder of each was immunoprecipitated with anti-ZAP-70 antiserum after adding Brij 97 to 1% final concentration.

A densitometer (Molecular Dynamics, Sunnyvale, CA) and ImageQuant software were used for quantitation analysis of autoradiographs.

Immunofluorescence Staining and Confocal Microscopy. Transfected Cos 7 cells were grown on sterile glass coverslips (10 or 25 mM diameter, No. 1 thickness). ZAP-70 GFP subclones were adhered to coverslips precoated with poly L-lysine (100 μg/ml; Sigma

Chemical Co., St. Louis, MO; see Figs. 5 and 6) for 2 h at 37°C. Cells were stimulated directly on the coverslips (PV × 10 min for Cos 7 or $F(ab')_2$ of OKT3 × 2 min for 2G1), fixed in 2% formaldehyde in PBS for 15 min at RT, and examined directly or permeabilized and stained with the appropriate antibody. Antibody staining was performed with T cells in suspension in all other experiments, and cells were mounted onto coverslips immediately before microscopy analysis. The cells were fixed using 3.7% paraformaldehyde in PBS for 30 min at RT, washed (three times) in PBS containing 10% fetal bovine serum (PBS/FBS), permeabilized using 0.1% Triton X-100 in PBS for 4 min at RT, washed (three times), and incubated for 45 min in PBS/FBS for preblocking. Cells were then incubated with first stage antibody (anti-ZAP-70, anti-GFP, or anti-Lck) in PBS/FCS for 45 min at RT, washed and incubated with second stage antibody (rhodamine-coupled goat anti-mouse or anti-rabbit IgG or (see Fig. 7) Cy™ 3 donkey anti-rabbit IgG) for 45 min, followed by washing with PBS (three times). Cells were resuspended in Fluoromount G added (Southern Biotechnology) and pipetted onto microscope slides with a coverslip mounted on top. Hoechst stain (20 μg/ml) was included during the second antibody incubation (See Fig. 7, *c* and *d*). These cells were viewed using a Zeiss Axioskop microscope equipped with both UV and rhodamine optics and cells photographed directly. All other fixed cells were viewed as 0.5 μM dual color optical sections, or composites of a complete Z section analysis in (see Fig. 2) using a Zeiss lasor scanning microscope 410 confocal microscope having a 100 × Zeiss planapo objective (numerical aperature 1.4) and optics for both fluorescein (GFP) and rhodamine (antibody stains). For experiments using live cells, the coverslips were affixed to a Leiden coverslip dish and mounted on a custom-made 37°C stage of the confocal microscope using the 100× objective. The GFP molecule was excited with the 488 line of a krypton-argon laser and imaged using a 515–540-nm bandpass filter. Images were averaged 16 times to improve image quality. Two images of each cell were taken before addition of stimulant, and subsequent images were taken at 20-s intervals thereafter until 5 min after stimulation, with the same cell slice being viewed in each image.

Quantitation measurements (see Fig. 6, *c* and *d*) were determined using IP Lab Spectrum software. The middle section of a complete Z series (0.5-μM slices) was selected from a field of each subclone to ensure that a slice through the nucleus was being examined. Regions of interest (ROIs) were drawn around the entire cell and around the nucleus, and the sum of pixels in each ROI calculated. The following equation was used to determine the percent of ZAP-70 GFP in the nucleus: (sum of intensities of total pixels in nucleus)/(sum of intensities of total pixels in cell) × 100%. The mean fluorescence intensity for the entire cell is reported to compare the expression level of ZAP-70 GFP between individual cells.

Results

ZAP-70 GFP Chimera Retains the Antigenic and Kinase Properties of Native ZAP-70. The ZAP-70 GFP fusion protein was constructed in a mammalian expression vector fusing the GFP coding sequence to the COOH terminus of ZAP-70 kinase (Fig. 1 *a*). To assess the enzymatic activity of the chimeric protein, Cos 7 cells were transfected with ZAP-70 GFP and Lck F505, left untreated, or stimulated with PV, and an in vitro kinase assay was performed on the anti-ZAP-70 IPs (Fig. 1 *b*, *top*). Enzymatic activity was measured by detection of autophosphorylation and phosphorylation of cfb3, a substrate for ZAP-70. ZAP-70 GFP showed significant kinase activity, which was increased upon cellular stimulation, indicating that the fusion protein retained the enzymatic properties of the native ZAP-70 molecule (8). An anti-ZAP-70 immunoblot of the membrane demonstrated the amounts of protein in the lanes and confirmed that the antigenic properties of ZAP-70 had been retained (Fig. 1 *b*, *bottom*). Anti-GFP antiserum also identified this single species (data not shown), whereas an irrelevant mAb failed to IP the chimeric protein (Fig. 1 *b*).

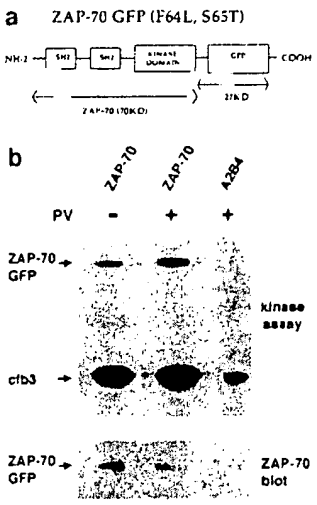

Figure 1. In vitro functional activity and apparent molecular weight of the ZAP-70 GFP fusion protein. (*a*) Schematic of the ZAP-70 GFP fusion protein, showing the position of the GFP (F64L, S65T) molecule at the COOH terminus of ZAP-70, with a predicted molecular weight of ~97 kD. (*b*) Cos 7 cells expressing pEGFP/ZAP-70 and pSXSRαLck F505, were incubated for 10 min with or without PV as indicated. Immunoprecipitation of lysed cells was performed with either anti-ZAP-70 antiserum or A2B4 mAb, and the phosphorlyated proteins from an in vitro kinase assay analyzed (*top*). An anti-ZAP-70 Western blot of the same membrane is shown (*bottom*).

ZAP-70 GFP Is Located throughout Cos 7 Cells, and Migrates to the Plasma Membrane upon Activation. Cos 7 cells were next transfected with ZAP-70 GFP, and the fixed cells were viewed using confocal microscopy. The kinase was located diffusely throughout the cells, which frequently included a heavy concentration in the perinuclear region, as shown in Fig. 2 *a*. Little, if any, plasma membrane–associated ZAP-70 was detected. Unexpectedly, marked nuclear localization was also observed in many cells. Upon cellular stimulation (Fig. 2 *b*, *3 min PV*), ZAP-70 redistributed significantly with cytosolic clearing and simultaneous accumulation at the plasma membrane, indicating that there was a correlation between ZAP-70 activation and its movement to the cell surface.

Since Lck F505 induces ZAP-70 kinase activity (3, 8, 9), we next examined if simply coexpressing the two proteins resulted in more plasma membrane–associated ZAP-70. To compare cellular distribution of the two enzymes, transfected cells were immunostained with an anti-Lck antibody and a rhodamine-coupled secondary mAb. Thus, the green image represents ZAP-70, the red indicates Lck, and the yellow image indicates where the two molecules colocalize. Coexpression of active Lck had a dramatic influence on the distribution of ZAP-70. A significant amount was observed at the plasma membrane in the unstimulated cell, and further rapid membrane accumulation occurred as soon as 1 min after PV stimulation (Fig. 2, *c* and *d*). Lck colocalized at the plasma membrane with ZAP-70 in both instances.

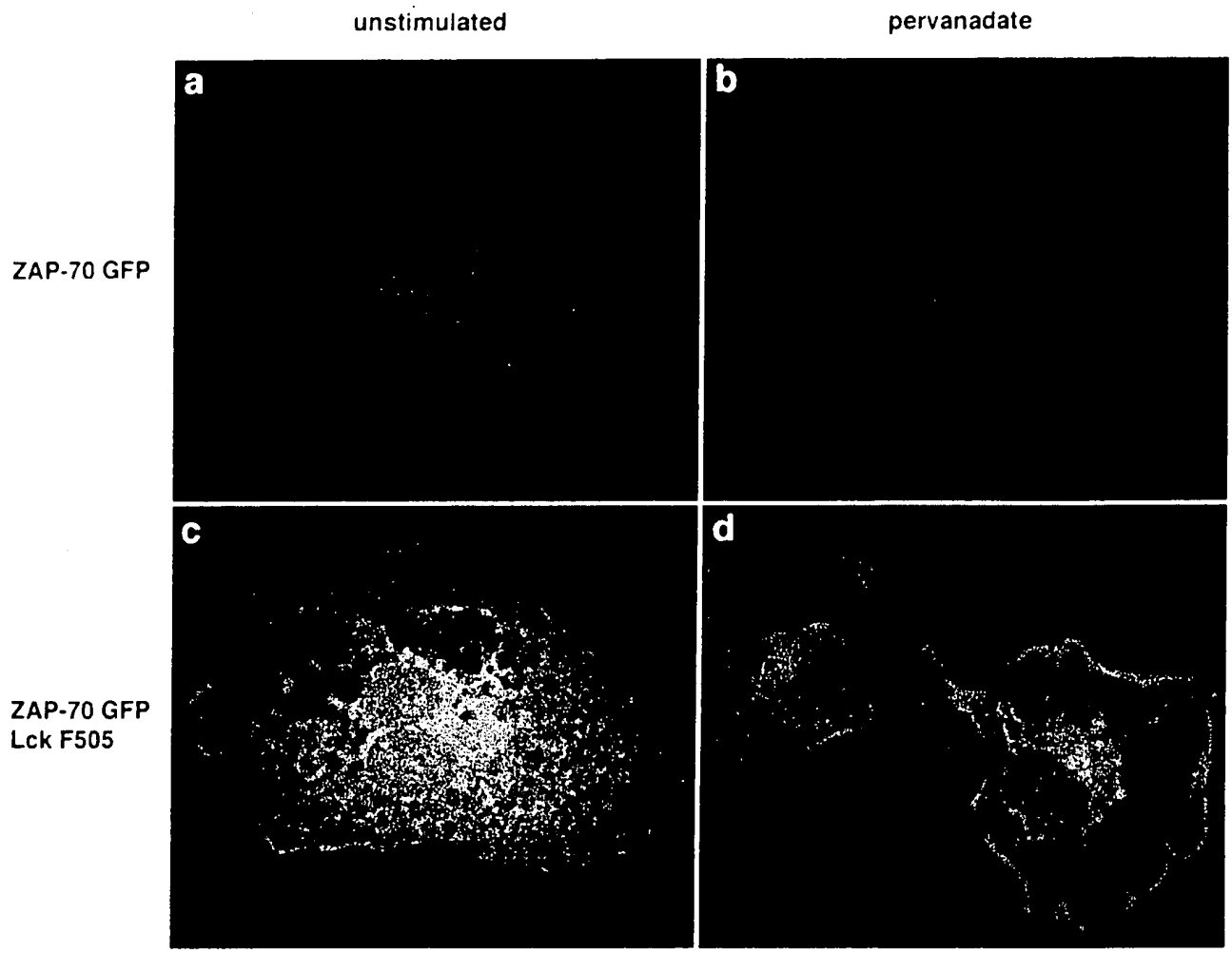

Figure 2. ZAP-70 GFP expression and cellular location in Cos 7 cells. Cos 7 cells expressing pEGFP/ZAP-70 alone (*a* and *b*) or together with pSXS-RαLck F505 (*c* and *d*) were left untreated (*a* and *c*) or stimulated with pervanadate for 1 (*d*) or 3 min (*b*). Coverslips were mounted directly (*a* and *b*) or after first staining with anti-Lck (*c* and *d*). The optical sections of a complete Z series were then projected to produce the composite single (*a* and *b*) or dual (*c* and *d*) color images shown (*green*, ZAP-70 GFP fusion protein; *red*, immunostain of Lck F505). Areas of yellow represent colocalization of ZAP-70 GFP and Lck F505 (*c* and *d*).

Several intriguing observations were made from this initial experiment. ZAP-70 becomes closely associated with the plasma membrane specifically upon activation, apparently independent of the TCR, since Cos 7 cells do not express any TCR components. In addition, the presence of active Lck enhanced the membrane association of ZAP-70 GFP, suggesting that the phosphorylation and subsequent activation of ZAP-70 are prerequisites for its translocation to and association at the membrane. Furthermore, ZAP-70 was detected abundantly in the nucleus, a phenotype that was unaffected by cellular stimulation.

Active Lck Enhances Plasma Membrane Accumulation of ZAP-70. Although it seemed that F505 Lck coexpression enhanced ZAP-70 localization to the plasma membrane, these observations were made using fixed cells, preventing a comparison of the same cell at different stimulation time points. To more accurately study the role of F505 Lck on the quantitation and kinetics of ZAP-70 movement to the cell surface, we monitored individual live cells over time, both before and after stimulation. Transfected cells were treated as described in Materials and Methods, and monitored before and after PV stimulation, for a total of 5 min after stimulation, with images taken at 20-s intervals. Upon subsequent comparison of the images for ZAP-70 distribution, the kinetics of its movement to the plasma membrane in a single cell could be visualized.

A representative cell, expressing ZAP-70 GFP alone, was observed before and after stimulation with PV (Fig. 3, *top*). Consistent with the data acquired using fixed cells, the unstimulated cell displayed a diffuse pattern of ZAP-70 expression, with only a small amount of fluorescence at the plasma membrane (*unstim*). Upon pharmacologic stimulation, little change in ZAP-70 distribution was apparent during the first minute or so after stimulation (*1 min PV*). However, after 2 min, plasma membrane accumulation of ZAP-70 was evident (*2 min PV*, arrow highlights area of accu-

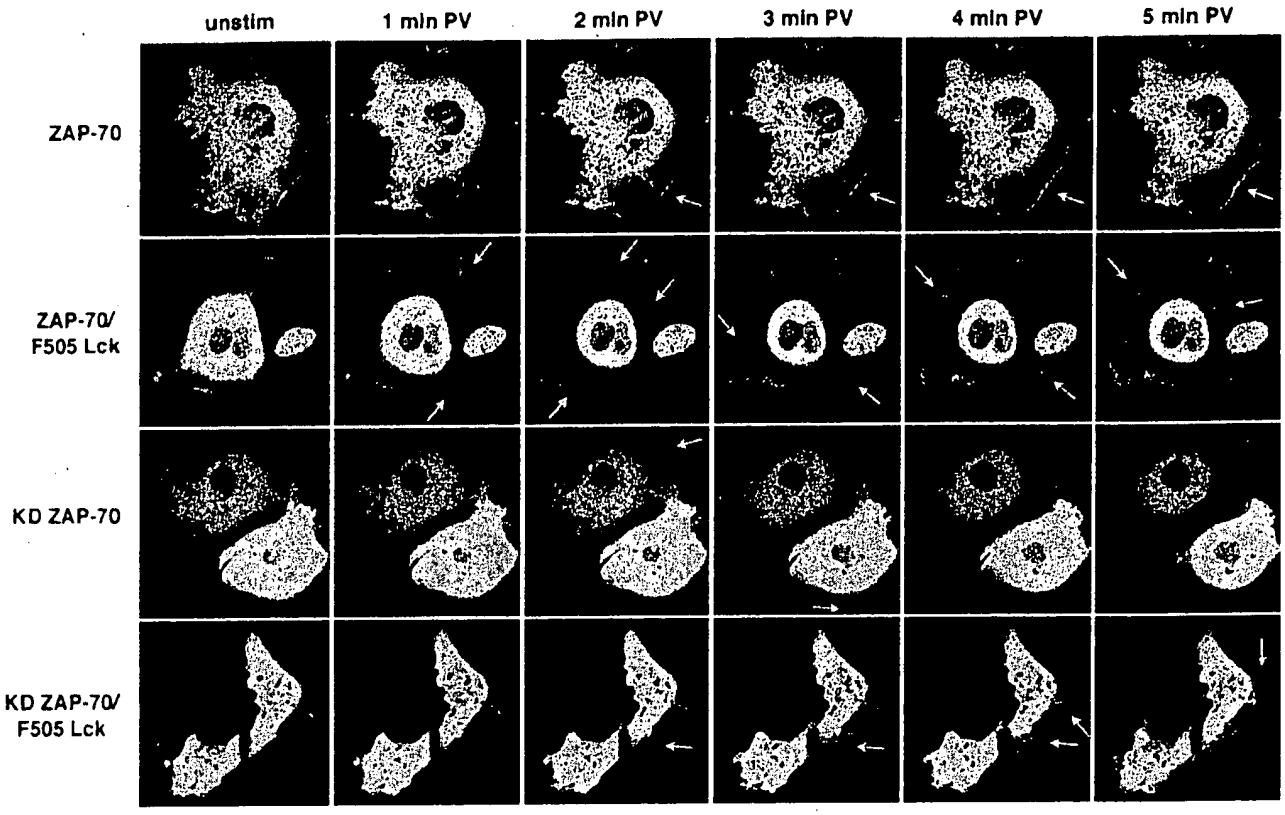

Figure 3. Effects of F505 Lck and cellular stimulation on the kinetics of plasma membrane acquisition of ZAP-70 GFP and KD ZAP-70 GFP. Individual live Cos 7 cells were examined by confocal microscopy and plasma membrane acquisition of ZAP-70 GFP assessed as described in Materials and Methods. A single image of each cell is shown before activation (*unstim*) with subsequent images shown at 1-min intervals after the addition of PV. Arrows highlight specific areas of plasma membrane accumulation of the ZAP-70 GFP fusion proteins.

mulation). This redistribution to the cell surface steadily continued throughout the 5-min stimulation period (*5 min PV*).

A qualitatively different pattern was observed when cells cotransfected with ZAP-70 GFP and F505 Lck were monitored (Fig. 3, *ZAP-70/F505*). Unlike the cells transfected with ZAP-70 GFP alone, those coexpressing F505 Lck consistently showed a high concentration of perinuclear and intranuclear ZAP-70, and minimal diffuse cytosolic location. Moreover, a significant quantity of ZAP-70 was already at the cell surface in the resting cell (*unstim*). Further accumulation to the cell surface began immediately after PV addition (*1 min PV*), was rapidly and steadily enhanced with the entire cell surface outlined by ZAP-70 GFP as early as 3 min before stimulation, and increased until the conclusion of the experiment (*5 min PV*). Thus, active Lck has a dramatic positive influence on the kinetics and quantity of ZAP-70 redistribution to the plasma membrane.

Redistribution of KD ZAP-70 to the Plasma Membrane Is Highly Inefficient in Cos 7 Cells. Phosphorylation of specific tyrosine residues, and the subsequent activation of ZAP-70 kinase, result from interaction with active Lck or stimulation by PV (29). The phosphorylation and/or kinase activation may be responsible for ZAP-70 translocation to the plasma membrane. To determine whether an inactive form of ZAP-70 would demonstrate the same dynamics, a KD form of ZAP-70 (KD ZAP-70) was fused to GFP and the chimera used in live cell experiments as above. When expressed in Cos 7 cells alone, KD ZAP-70 GFP was abundantly expressed in the cytosol, but not at the cell surface (Fig. 3). Furthermore, PV stimulation had no effect on redistributing the protein at the early time points, in contrast to the wild-type chimera (compare *ZAP-70* and *KD ZAP-70, 1 min PV*). At later time points, a small amount of KD ZAP-70 could be seen around the cell surface (*2, 3 min PV*, arrows indicate membrane accumulation), but this was not enhanced as the cells were stimulated further (*4, 5 min PV*). The addition of active Lck increased the redistribution significantly (Fig. 3, *bottom*). As with the wild-type chimera, some KD ZAP-70 was already at the cell surface in the resting cell, although the quantity was much less (*unstim*). Further movement to the membrane occurred after addition of PV, but again the total amount was less and the kinetics slower than with native ZAP-70. Thus, ZAP-70 kinase activity is required for optimal redistribution to the plasma membrane in TCR-negative epithelial cells.

Although the activation data suggest that Lck facilitates ZAP-70 redistribution by phosphorylating and ultimately activating it, a physical interaction between the two proteins is also possible. Membrane association of ZAP-70 could be mediated via this direct interaction since Lck associates

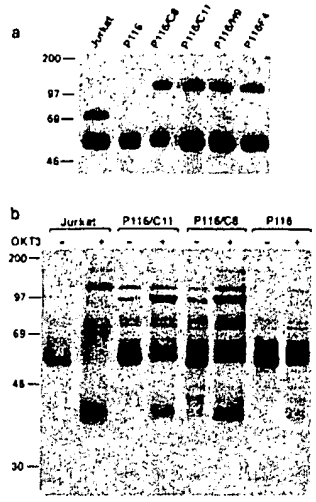

Figure 4. Quantitation and functional reconstitution analyses of ZAP-70 GFP in stably transfected P116 subclones. (*a*) Cell lysates of Jurkat, P116, or P116/ZAP-70 GFP subclones were immunoprecipitated with anti-ZAP-70. Immunoprecipitated proteins were analyzed by SDS-PAGE and Western blot using anti-ZAP-70 (2×10^6 cells/lane). Levels of ZAP-70 GFP expression in each subclone, presented as a percent of endogenous ZAP-70 in Jurkat cells, were as follows: 97% for C8, 143% for C11, 131% for H9, and 94% for F4. (*b*) Cells were lysed directly or first stimulated for 2 min with OKT3 $F(ab')_2$ at 37°C, and antiphosphotyrosine Western blot analysis of whole cellular lysates (2×10^5 cells/lane) performed.

with the plasma membrane via its NH_2-terminal myristylation site. Thus, we used a mutant form of F505 Lck in which the myristylation site had been destroyed (30), and determined its efficiency at facilitating ZAP-70 membrane association. Transition of ZAP-70 to the cell surface was similar regardless of whether Lck could associate with the lipid bilayer, supporting the thesis that Lck kinase activity is responsible for ZAP-70 movement (data not shown).

ZAP-70 GFP Reconstitutes Early Activation Events in P116 Cells Lacking ZAP-70. To study the intracellular location and redistribution of ZAP-70 in T cells, we reconstituted a mutant Jurkat T cell line, P116, which lacks ZAP-70 (Williams, B.L., and R.T. Abraham, manuscript submitted for publication). Individual subclones were selected from stable bulk cultures by limiting dilution analysis and two, 2G1 and 1C2, were used for further study. These lines were further subcloned to derive C8, C11, H9 (from 2G1), and F4 (from 1C2). Anti-ZAP-70 IP and Western blot analysis (Fig. 4 *a*) with subsequent densitometry measurements indicated that the relative expression of ZAP-70 GFP compared to endogenous ZAP-70 in Jurkat cells was 97% for C8, 143% for C11, 131% for H9, and 94% for F4.

Jurkat, P116 cells and the stably reconstituted subclones were left untreated or stimulated through the TCR with OKT3 $F(ab')_2$ for 2 min at 37°C. Ab-mediated TCR cross-linking led to rapid increases in the phosphorylation of several proteins in Jurkat T cells, as expected (Fig. 4 *b*). In contrast, only a slight increase in tyrosine phosphorylated substrates was observed in the stimulated P116 cells, consistent with our previous observations (Zhang, W., B.L. Williams, and R.T. Abraham, unpublished data). The defect in TCR-inducible protein tyrosine phosphorylation in P116 cells was reversed in all subclones, regardless of the level of expression of ZAP-70 GFP (Fig. 4 *b*, and data not shown). Thus, ZAP-70 GFP was able to reconstitute early signaling events, which correlate with the kinetics of ZAP-70 localization to the plasma membrane, in reconstituted P116 cells.

ZAP-70 GFP Redistributes Around the Cell Periphery in T Cells After anti-TCR Stimulation. We next used the subclones to determine the distribution of ZAP-70 in resting and activated cells. 2G1 cells were stained with anti-Lck and a rhodamine-coupled secondary mAb to colocalize the two proteins. As expected, Lck was found exclusively around the plasma membrane and in the cytosol, and provided a clear counterstain surrounding the nucleus (Fig. 5 *a*). In contrast, ZAP-70 GFP, while colocalizing with Lck in the cytosol (*yellow*), was also abundant in the cell nucleus, displaying a typical nucleolar exclusion pattern.

To assess if ZAP-70 redistribution to the plasma membrane could be visualized in T cells, 2G1 cells were adhered to coverslips and then fixed immediately or after stimulation with OKT3 $F(ab')_2$ for 2 min (Fig. 5, *b* and *d*). Cytoplasmic ZAP-70 GFP was observed in the unstimulated cells (*b*). In the population stimulated with anti-TCR antibody, some cells showed a peripheral rim of enhanced GFP (Fig. 5 *c*, *arrows*), and others showed membrane blebs with GFP (*arrowhead*). Whether this protein redistribution is analogous to that seen in the Cos 7 cells is difficult to determine. Regardless, anti-TCR stimulation of T cells induces rapid ZAP-70 redistribution, consistent with its movement to and function at the plasma membrane.

Nuclear ZAP-70 GFP Location Is Independent of Protein Expression Levels. ZAP-70 GFP was clearly identified in the nucleus of the reconstituted subclones (Fig. 5). Although the biochemical analysis showed that these cell lines expressed comparable levels of ZAP-70 to Jurkat, the possibility remained that the nuclear ZAP-70 GFP was an artifact of overexpression in individual cells. To rule this out, we took advantage of the ability to quantitate the GFP fusion protein by pixel intensity computation. Subclones F4 and H9 were selected as representatives expressing comparable and 1.3-fold higher levels of ZAP-70 to endogenous protein by biochemical analysis (see Fig. 4 *a*). A complete Z series of adhered cells was carried out in several random fields, and the middle section from each field was selected for analysis to ensure that the nucleus was represented. Quantitative measurements were taken of individual cells, and the percent of ZAP-70 GFP in the nucleus determined. Data from a representative field of each subclone is presented (Fig. 6).

Interestingly, although the cell lines had been subcloned twice, a range of protein expression levels was observed in each population, highlighting the sensitivity of the assay system at the single cell level (Fig. 6, *a* and *b*). For F4, two cells expressed ZAP-70 GFP at about the lowest level of detection (Fig. 6 *a*, cells *1* and *2*), reflected in the mean pixel intensity for each cell (Fig. 6 *c*). Other cells in the F4 population expressed intermediate protein levels (e.g., cell *4*). ROIs encompassing the entire cell and the nucleus were quantified for total fluorescence intensity, and the percent of ZAP-70 residing in the nucleus was determined using the formula described in Materials and Methods. In most cells, about half of the ZAP-70 detected in the section was in the nucleus. More importantly, there was no correlation between nuclear location and overall protein expression

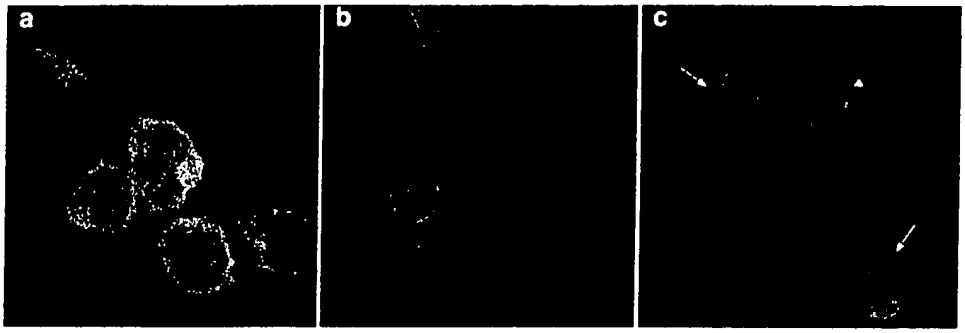

Figure 5. Intracellular location of ZAP-70 GFP in stably transfected P116 T cells, and its movement to the plasma membrane upon cellular activation. (*a*) Nuclear expression of ZAP-70 GFP in P116/2G1 cells is highlighted by the nucleolar exclusion pattern. Endogenous Lck, stained with anti-Lck and a rhodamine-coupled secondary mAb, is entirely extranuclear in all cells, and areas of yellow indicate the cytosolic colocalization of ZAP-70 GFP and Lck. (*b* and *c*) P116/2G1 cells were left untreated (*b*) or stimulated with $F(ab')_2$ of OKT3 for 2 min at 37°C (*c*). Arrows and arrowheads indicate peripheral rims and membrane blebs of ZAP-70 GFP, respectively (*c*).

levels (Fig. 6 *c*). This was further verified when the H9 subclone was similarly assessed, whereas cells expressing much higher total cellular amounts of ZAP-70 GFP showed no significant increase in the amount residing in the nucleus (Fig. 6, *b* and *d*, cells *7*, *8*, and *9*). Thus, nuclear ZAP-70 is not an artifact of overexpression since it exists at physiological protein levels. It should be noted that, although close to 50% of the material was nuclear in the slices quantitated, this may not reflect the percent nuclear ZAP-70 in the entire cell. To determine this value, the sum of values from all slices through an individual cell must be calculated for a population of cells.

Endogenous ZAP-70 Is Detected in the Nucleus of Jurkat Cells by Immunofluorescence. To rule out the possibility that nuclear ZAP-70 GFP was an artifact of the chimera, immunofluorescence (IF) staining was first performed on P116 cells reconstituted with ZAP-70 containing a COOH-terminal Myc epitope tag. As with ZAP-70 GFP, nuclear ZAP-70 was evident in about half of the cells (data not shown). Next, an anti–ZAP-70 antiserum was affinity purified against its immunizing epitope and then used to identify the location of endogenous ZAP-70. Jurkat cells were immunostained in suspension to maintain their three dimensional structure and eliminate the possibility of misinterpreting cellular location due to cell flattening. Immediately after mounting, complete Z series analysis of immunostained cells was performed. An assessment of the immunostaining pattern in all cell slices verified that endogenous ZAP-70 is indeed present in the nucleus. Two slices (0.5-μM–thick) through the middle of a typical field of Jurkat cells, 1 μM apart, are displayed in Fig. 7 (*a* and *b*). The staining pattern clearly indicates that ZAP-70 is not only in the cytosol (note the intense peripheral staining), but also highly abundant in the nucleus, with a typical nucleolar exclusion pattern. The specificity of the staining pattern was verified when ZAP-70–negative P116 cells, treated in a similar manner, failed to show any IF staining (*e*), although cells were present in the field as seen under the reflector light (*f*). In addition, the secondary Ab alone did not significantly stain the Jurkat cells (data not shown). The nuclear location of endogenous ZAP-70 was further confirmed when Jurkat cells were costained with anti–ZAP-70 and a Hoechst DNA stain. Although only the Ab stained the cytosol, both anti–ZAP-70 and Hoechst showed a superimposable staining pattern in the nucleus (*c* and *d*). Thus, endogenous ZAP-70 is present in the nucleus of normal Jurkat T cells.

Efficiency of Ab Staining Is Hindered by the Nuclear Membrane. A recent study reported that ZAP-70 is found ex-

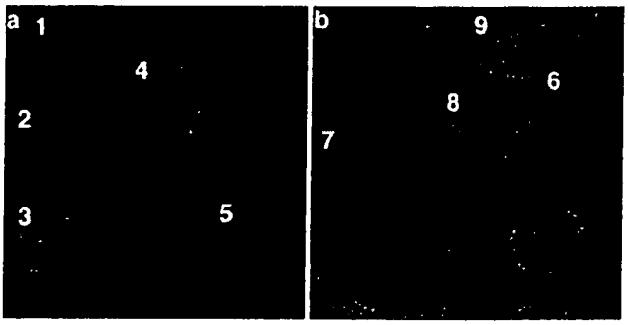

c

P116/F4

Cell #	Mean pixel intensity	% nuclear ZAP-70 GFP
1	54.27	47.3
2	57.32	47.4
3	105.2	45.5
4	119	35.9
5	83.26	49.5

d

P116/H9

Cell #	Mean pixel intensity	% nuclear ZAP-70 GFP
6	58.82	46.7
7	123.55	43
8	159.93	53.8
9	163.01	51

Figure 6. Quantitation of nuclear ZAP-70 GFP, and its relationship to expression levels, in individual cells of stably transfected P116 subclones. The middle section from a complete Z series of 0.5 μM optical sections through a field of F4 (*a*) and H9 (*b*) subclones is shown. Numbered cells correlate with the corresponding quantitation analyses reported in (*c*) for F4 and (*d*) for H9. Mean pixel intensity throughout individual cells is reported as a method to accurately compare GFP expression levels between cells. Percent nuclear ZAP-70 GFP was determined as described in Materials and Methods.

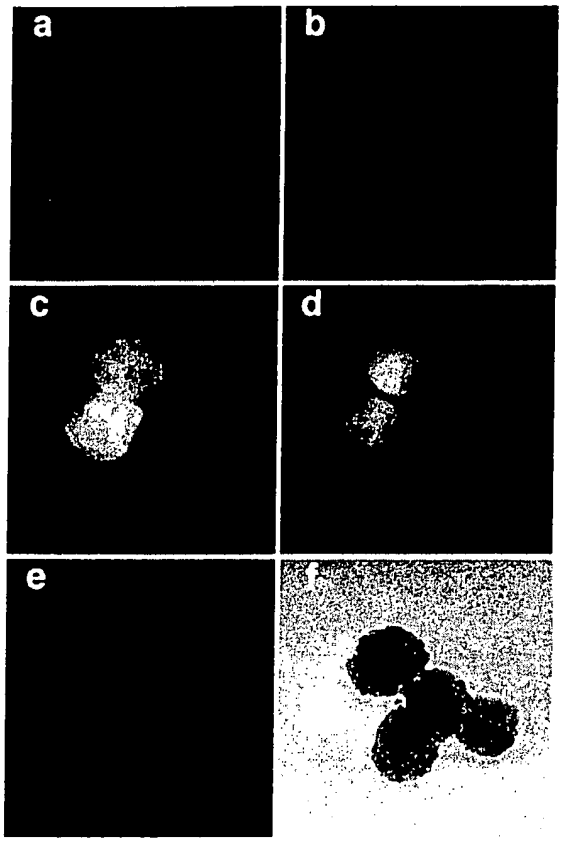

Figure 7. Identification of endogenous ZAP-70 in the nucleus of Jurkat cells by IF staining. Jurkat (*a*, *b*, *c*, and *d*) and P116 (*e* and *f*) cells were stained with affinity-purified anti-ZAP-70 antiserum. 0.5 μM slices through the middle of the cells are displayed (*a*, *b*, *e*, and *f*). Two 0.5 μM slices, 1 μM apart, are shown for anti-ZAP-70-stained Jurkat cells (*a* and *b*), and one for P116 cells (*e*). An image of the same field as in *e*, using the reflector optics, indicates the specificity of the Ab stain (*f*). The nuclear staining of the anti-ZAP-70 is further verified by colocalization of anti-ZAP-70 (*c*) with the Hoechst DNA stain (*d*) in the same cells.

clusively in a cortical region of Jurkat cells, with no evidence of the protein in the nucleus (31). This is inconsistent with the findings presented here. However, a comparison of our results using Ab staining versus GFP to detect ZAP-70 revealed an interesting pattern that may explain this apparent discrepancy. Although the ZAP-70 GFP was present in the nucleus of all T cells examined, Ab staining using either anti-Myc or anti-ZAP-70 consistently detected nuclear ZAP-70 in only about half of the cells, indicating that some nuclear structure was acting as a physical barrier, preventing efficient access of the Abs to the nucleus (data not shown).

To formally test this hypothesis, Cos 7 cells expressing ZAP-70 GFP were immunostained with either anti-GFP or anti-ZAP-70 and a rhodamine-coupled secondary Ab. Individual cells were then viewed, using dual-color optics for fluorescein and rhodamine, to compare the location of ZAP-70 using the two detection methods. A complete Z series analysis was performed, and the center slice of a typical cell is shown for cells immunostained for GFP (Fig. 8, *a–c*) or ZAP-70 (*d–f*). Although GFP indicated a high concentration of the chimera in the nucleus (Fig. 8 *a*), this was completely unrecognized by the anti-GFP (Fig. 8 *b*). In contrast, expression of the protein elsewhere in the cell was detected comparably by either method (*c*, yellow indicates overlay of both signals). Although the anti-ZAP-70 appeared to be somewhat more accessible to the nucleus (*e*), some exclusion was apparent since the GFP signal was much stronger than the Ab signal (compare *d*, *e*, and overlay in *f*). The partial exclusion of anti-ZAP-70 is consistent with the detection of only ~50% of examined T cells displaying nuclear ZAP-70 using this Ab. Our studies demonstrate two strengths of the ZAP-70 GFP chimeric system. Intracellular locations of proteins, which are overlooked by conventional IF techniques, are efficiently detected. Also, accurate quantitative intracellular distribution measurements can be made.

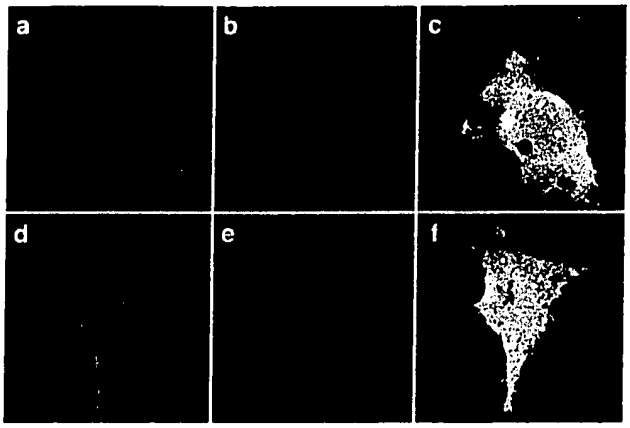

Figure 8. Demonstration of inaccessibility of Abs to nuclei. Cos 7 cells, expressing ZAP-70 GFP, were immunostained with anti-GFP (*a–c*) or anti-ZAP-70 (*d–f*). ZAP-70 GFP (*a* and *d*). Ab signals (*b* and *e*) and the dual-color overlays (*c* and *f*) are shown for a 0.5 μM slice through an individual cell stained with either anti-GFP (*a–c*) or anti-ZAP-70 (*d–f*).

ZAP-70 Can Be Isolated from Jurkat Nuclei and Is Tyrosine Phosphorylated after Anti-TCR Stimulation. To understand the role of nuclear ZAP-70 in T cell signaling, a biochemical cell fractionation procedure was used to yield highly purified cytosol/membrane and nuclear pools from Jurkat cells. ZAP-70 was abundant in both the cytosolic/membrane and nuclear fractions, as indicated by anti-ZAP-70 immunoblotting of whole lysate preparations (Fig. 9 *b*, *top*). About 35% of total cellular ZAP-70 was nuclear, but this value varied between experiments, a reflection of the inefficiency of nuclear material recovery (32). The membrane was then immunoblotted with anti-iron regulatory protein (IRP)-1 as a control for cytosolic contamination in the nuclear fraction (Fig. 9 *b*, *bottom*), since IRP-1 is purely cytosolic (27, 33). Densitometric analysis indicated that the ratio of nuclear/cytosolic ZAP-70 was 0.53, whereas that for IRP-1 was 0.1. Thus, ZAP-70 in the nucleus was enriched 5.3-fold as compared to IRP-1, and as much as 6.2-fold in other experiments; confirming that ZAP-70 truly resides in the cell nucleus. Similar results were found when nuclear material

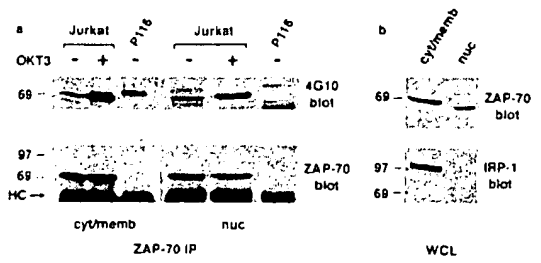

Figure 9. Biochemical isolation of ZAP-70 from nuclei of Jurkat cells, and demonstration of its increased tyrosine phosphorylation after anti-TCR stimulation. (*a*) Cytosol/membrane (1.2×10^7 cells) and nuclear fractions (2.6×10^7 cells) of Jurkat or P116 cells, immunoprecipitated with anti-ZAP-70, were analyzed by antiphosphotyrosine Western blotting (*top*). The stripped membrane was reprobed with anti-ZAP-70 (*bottom*). Specific activity of ZAP-70 after cellular stimulation was 2.4 for cytosolic/membrane ZAP-70 and 1.4 for nuclear ZAP-70. A nonspecific band appears in the 4G10 blot of P116 cells, which migrates more slowly than the phosphorylated ZAP-70. (*b*) Whole lysate samples from the purified material (6×10^5 cells/lane) was immunoblotted with anti-ZAP-70, and then reprobed with anti-IRP-1. Densitometric analysis confirmed that there was a 5.3 fold enrichment of ZAP-70 in the nuclear fraction as compared to IRP-1. This was confirmed in 3 independent experiments, with enrichment of ZAP-70 as compared to IRP-n1 ranging from 5 fold to 6.2 fold.

was isolated from Jurkat cells in the presence (Fig. 9 *a*) or absence (Fig. 9 *b*) of 0.1% mild detergent, and also in transfected Cos 7 cells using a sucrose gradient separation technique (data not shown). Moreover, the enrichment of nuclear material was confirmed by immunoblotting with an Ab against a nuclear pore complex protein (data not shown; reference 34).

To compare the function of cytosolic and nuclear ZAP-70, anti-ZAP-70 IPs of the purified cell fractions were performed from unstimulated or OKT3 $F(ab')_2$ stimulated cells, and the phosphotyrosine content examined. A specific increase in ZAP-70 phosphotyrosine content was observed after anti-TCR stimulation, both in cytosolic and nuclear ZAP-70 (Fig. 9 *a*, *top*). When compared to ZAP-70 protein levels in the IPs (*bottom*), the increase in specific activity was calculated to be 2.4-fold in the cytosolic fraction and 1.4-fold in the nuclear fraction. P116 cells did not contain any ZAP-70, although an unidentified nonspecific species was present in the antiphosphotyrosine, but not anti-ZAP-70, immunoblots which migrated more slowly than the ZAP-70 protein (Fig. 9, *top*). Thus, nuclear ZAP-70 increases its phosphotyrosine content after anti-TCR stimulation, and therefore likely acquires enzymatic activity. Interestingly, the insoluble material remaining after sonication of the nuclear/cytoskeletal pellet, which was separated from the soluble nuclear material and considered to contain cytoskeletal and nuclear matrix-associated proteins, showed little or no evidence of ZAP-70 presence, either by direct immunoblotting or by anti-ZAP-70 IP.

Discussion

Since the identification of ZAP-70 as a T cell-specific protein tyrosine kinase, a number of biochemical studies have focused on its activity, regulation, and molecular interactions (for reviews see references 29, 35). Although such research has been critical, a complementary cell biological study is necessary to fully understand ZAP-70 function. Here, we provide an analysis of ZAP-70 subcellular location and demonstrate its dynamics under different conditions. The visualization of ZAP-70 movement to the plasma membrane supports previous biochemical data. Our work also demonstrates that only a small fraction of total enzyme translocates to the membrane. That this membrane localization can be independent of TCR expression suggests that our knowledge of the sequence of events occurring after T cell stimulation may be incomplete. Moreover, the discovery that there is a large pool of ZAP-70 in the nucleus, which is activated upon cellular stimulation, suggests that the kinase has additional, heretofore unexpected functions.

Compelling evidence exists indicating that a physical interaction between ZAP-70 and TCR chains takes place soon after T cell stimulation. Early studies showed that ZAP-70 coprecipitates with TCR-ζ and the CD3 chains after activation (36, 37). This interaction depends on the highly specific binding of the tandem SH2 domains of ZAP-70 with tyrosine phosphorylated ITAMs of the TCR (6, 7). Our results, revealing plasma membrane translocation of ZAP-70 in the absence of any TCR chains, suggest that there are alternative mechanisms of ZAP-70 localization at the plasma membrane. Cos 7 cells may express a molecule at the surface with cytoplasmic tyrosine residues or ITAMs, available for phosphorylation and SH2 binding. SH2-mediated binding could also be independent of phosphotyrosine as seen in the cases of Src family PTK SH2 domains binding to Raf and other proteins, Abl SH2 binding Bcr and Syk SH2 domains binding Cbl (38-40). However, the enhanced translocation of ZAP-70 to the membrane in response to pervanadate makes this possibility less likely. Thus, the kinase can likely be retained at the membrane by additional, non-SH2 mechanisms.

The tyrosine phosphorylation and subsequent activation of ZAP-70 by Lck are the critical parameters in the facilitation of its membrane localization. The observation that KD ZAP-70 could redistribute to the cell surface less efficiently than the native molecule suggests that ZAP-70 tyrosine phosphorylation or kinase activity is involved in the mechanism of translocation. Perhaps a phosphorylation-dependent conformational change in ZAP-70 occurs leading to its activation and/or redistribution, similar to that reported for other protein kinases (41-43). The activated kinase may then enhance the translocation either by increasing its own phosphotyrosine content by transphosphorylation or that of downstream substrates which may then serve as vehicles for ZAP-70 movement to the cell surface. We have found that only about half of phospho-ZAP-70 is retrieved from the membrane fraction of T cells. The rest is in the cytoplasm, indicating that the enzyme may indeed be activated before its accumulation at the cell surface (Zhang, W., unpublished observations).

The majority of known protein tyrosine kinases are involved in the transduction of extracellular signals, exerting

their effects at or near the plasma membrane. The discovery that several nuclear proteins contain phosphotyrosine raised the possibility that some tyrosine kinases may reside and have additional functions in the nucleus (for review see reference 44). Indeed, several PTKs have a nuclear location, the best characterized of which is c-Abl (44). This PTK is found in both the cytoplasm and in the nucleus of cultured fibroblasts, and has a classical nuclear localization signal (NLS) and a DNA binding domain. Kinase activity and DNA binding of nuclear c-Abl is regulated during the cell cycle (45). The significance of Abl cellular localization is corroborated by the observation that oncogenic forms reside exclusively in the cytoplasm (45). Other nuclear PTKs include two members of the Src family of PTKs, which can be found in the nucleus as well as in the cytosol. The nuclear localization of Fgr appears to be constitutive, whereas that of Src is induced by Ca^{2+} ionophore (44). Two NLS sequences have been identified in the SH2 and tyrosine kinase domains of Fgr, but no analogous sites have yet been discovered in Src. The specific nuclear functions of these two kinases remains unknown (44).

Although unexpected, nuclear ZAP-70 was seen both as a chimeric protein overexpressed in endothelial cells or at physiological levels in T cells, and as the native endogenous protein by immunofluorescence and biochemical analyses. The advantages of using GFP chimeras to study cell localization were highlighted in the comparison of the GFP and immunofluorescence assay results. Ab detection of nuclear ZAP-70 was hindered by the nuclear membrane, leading to inaccurate results regarding the fraction of the molecule in different cellular compartments, both within a single cell and in the population as a whole. In contrast, the ZAP-70 GFP protein, produced within the cell, was detected efficiently in the nucleus of all cells, regardless of their expression levels. Moreover, the ability to quantitate the amount of ZAP-70 GFP in individual cell fractions (46) facilitates the acquisition of accurate data regarding the percent of the protein in different compartments under several stimulation conditions. Preliminary biochemical results suggest that one third of the total cellular ZAP-70 resides within the nucleus of resting T cells (Fig. 6). Finally, the ability to visually study GFP-tagged proteins in living cells allows one to acquire precise and detailed kinetic measurements regarding protein redistribution in response to cellular stimulation, as shown by the results in Fig. 3.

The details of ZAP-70 nuclear localization remain to be defined. Because nuclear pores set a physical barrier to proteins above ~40 kD, transit of ZAP-70 into the nucleus must be an active mechanism involving specific localization signals (47). Although no classical NLSs are obvious in the amino acid sequence, several candidate basic-rich regions can easily be highlighted (37). Moreover, the recent discovery of a novel receptor-mediated nuclear import pathway, using a nonclassical NLS, suggest other mechanisms for nuclear localization (48, 49). Interestingly, the lack of an NH_2-terminal myristylation may facilitate nuclear localization of ZAP-70. Indeed, nuclear forms of Fgr lack the conventional NH_2-terminal myristylation site, and addition of such a motif actually inhibits nuclear entry (45). The function of nuclear ZAP-70 is likewise uncertain. However, the clear demonstration of its increased phosphotyrosine content after anti-TCR stimulation (Fig. 9) strongly suggests that nuclear ZAP-70 is active. Indeed, many nuclear tyrosine phosphorylated proteins were apparent after stimulation (data not shown), suggesting that nuclear PTKs are active in the cells. Further investigation should reveal informative data identifying which of these phosphorylated proteins are substrates of nuclear ZAP-70. Finally, the mechanism of phosphorylation of nuclear ZAP-70 remains to be defined. The protein may be phosphorylated in the cytosol and subsequently shuttle into the nucleus, or alternatively be activated directly in the nuclear compartment. The mechanism of nuclear ZAP-70 phosphorylation and the identity of its nuclear substrates will require further investigation.

The authors wish to thank Dr. Noah Isakov for the generation of KD ZAP-70, and Dr. Stephen Lee for his experimental suggestions.

Dr. Sloan-Lancaster is a fellow of the Damon-Runyon/Walter Winchell Cancer Research Fund. Dr. Zhang is supported by the Leukemia Society of America. Dr. Abraham is supported by a National Institutes of Health grant GM47286.

Address correspondence to Lawrence E. Samelson, NICHD, CBMB, Bldg. 18T, Rm 101, Bethesda, MD 20892. Phone: 301-496-6368; FAX: 301-402-0078; E-mail: samelson@helix.nih.gov

Received for publication 1 April 1997 and in revised form 30 June 1997.

References

1. Samelson, L.E., and R.D. Klausner. 1992. Tyrosine kinases and tyrosine-based activation motifs. *J. Biol. Chem.* 267: 24913–24916.
2. Weiss, A., and D.R. Littman. 1994. Signal transduction by lymphocyte antigen receptors. *Cell.* 76:263–274.
3. Iwashima, M., B.A. Irving, N.S.C. van Oers, A.C. Chan, and A. Weiss. 1994. Sequential interactions of the TCR with two distinct cytoplasmic tyrosine kinases. *Science (Wash. DC).* 263: 1136–1139.
4. van Oers, N.S., N. Killeen, and A. Weiss. 1996. Lck regulates the tyrosine phosphorylation of the T cell receptor subunits and ZAP-70 in murine thymocytes. *J. Exp. Med.* 183:1053–1062.
5. Pawson, T. 1995. Protein modules and signalling networks.

Nature (Lond.). 373:573–580.
6. Isakov, N., R.L. Wange, W.H. Burgess, J.D. Watts, R. Aebersold, and L.E. Samelson. 1995. ZAP-70 binding specificity to T cell receptor tyrosine-based activation motifs: the tandem SH2 domains of ZAP-70 bind distinct tyrosine-based activation motifs with varying affinity. *J. Exp. Med.* 181:375–380.
7. Bu, J.-Y., A.S. Shaw, and A.C. Chan. 1995. Analysis of the interaction of ZAP-70 and syk protein-tyrosine kinases with the T-cell antigen receptor by plasmon resonance. *Proc. Natl. Acad. Sci. USA*. 92:5106–5110.
8. Wange, R.L., R. Guitian, N. Isakov, J.D. Watts, R. Aebersold, and L.E. Samelson. 1995. Activating and inhibitory mutations in adjacent tyrosines in the kinase domain of ZAP-70. *J. Biol. Chem.* 270:18730–18733.
9. Kong, G., M. Dalton, J.B. Wardenburg, D. Straus, T. Kurosaki, and A.C. Chan. 1996. Distinct tyrosine phosphorylation sites within ZAP-70 mediate activation and negative regulation of antigen receptor function. *Mol. Cell. Biol.* 16:5026–5035.
10. Peri, K.G., and A. Veillette. 1994. Tyrosine protein kinases in T lymphocytes. *Chem. Immunol.* 59:19–39.
11. Park, D.J., H.W. Rho, and S.G. Rhee. 1991. CD3 stimulation causes phosphorylation of phospholipase C-γ1 on serine and tyrosine residues in a human T cell line. *Proc. Natl. Acad. Sci. USA*. 88:5453–5456.
12. Weiss, A., G. Koretzky, R.C. Schatzman, and T. Kadlecek. 1991. Functional activation of the T-cell antigen receptor induces tyrosine phosphorylation of phospholipase C-γ1. *Proc. Natl. Acad. Sci. USA*. 88:5484–5488.
13. Bustelo, X.R., J.A. Ledbetter, and M. Barbacid. 1992. Product of vav proto-oncogene defines a new class of tyrosine protein kinase substrates. *Nature (Lond.)*. 356:68–71.
14. Donovan, J.A., R.L. Wange, W.Y. Langdon, and L.E. Samelson. 1994. The protein product of the c-cbl protooncogene is the 120-kDa tyrosine-phosphorylated protein in Jurkat cells activated via the T cell antigen receptor. *J. Biol. Chem.* 269:22921–22924.
15. Jackman, J.K., D.G. Motto, Q. Sun, M. Tanemoto, C.W. Turck, G.A. Peltz, G.A. Koretsky, and P.R. Findell. 1995. Molecular cloning of SLP-76, a 76-kDa tyrosine phosphoprotein associated with Grb-2 in T cells. *J. Biol. Chem.* 270: 7029–7032.
16. Wange, R.L., N. Isakov, T. Burke, Jr., A. Otaka, P.P. Roller, J.D. Watts, R. Aebersold, and L.E. Samelson. 1995. $F_2(Pmp)_2$-TAMζ$_3$, a novel competitive inhibitor of the binding of ZAP-70 to the T cell antigen receptor, blocks early T cell signaling. *J. Biol. Chem.* 270:944–948.
17. Qian, D., M.N. Mollenauer, and A. Weiss. 1996. Dominant-negative ζ associated protein 70 inhibits T cell antigen receptor signaling. *J. Exp. Med.* 183:611–620.
18. Chan, A.C., T.A. Kadlecek, M.E. Elder, A.H. Filipovich, W.-L. Kuo, M. Iwashima, T.G. Parslow, and A. Weiss. 1994. ZAP-70 deficiency in an autosomal recessive form of severe combined immunodeficiency. *Science (Wash. DC)*. 264:1599–1601.
19. Arpaia, E., M. Shahar, H. Dadi, A. Cohen, and C.M. Roifman. 1994. Defective T cell receptor signaling and $CD8^+$ thymocyte selection in humans lacking ZAP-70 kinase. *Cell*. 76:947–958.
20. Elder, M.E., D. Lin, J. Clever, A.C. Chan, T.J. Hope, A. Weiss, and T.G. Parslow. 1994. Human severe combined immunodeficiency due to a defect in ZAP-70, a T cell tyrosine kinase. *Science (Wash. DC)*. 264:1596–1599.
21. Negishi, I., N. Motoyama, K.-I. Nakayama, K. Nakayama, S. Senju, S. Hatakeyama, Q. Zheng, A.C. Chan, and D.Y. Loh. 1995. Essential role for ZAP-70 in both positive and negative selection of thymocytes. *Nature (Lond.)*. 376:435–438.
22. Cubitt, A.B., R. Heim, S.R. Adams, A.E. Boyd, L.A. Gross, and R.Y. Tsein. 1995. Understanding, improving and using green fluorescent proteins. *Trends Biochem. Sci.* 20:448–455.
23. Gerdes, H.H., and C. Kaether. 1996. Green fluorescent protein: applications in cell biology. *FEBS Lett.* 389:44–47.
24. Heim, R., A.B. Cubitt, and R.Y. Tsein. 1995. Improved green fluorescence. *Nature (Lond.)*. 373:663–664.
25. Samelson, L.E., R.N. Germain, and R.H. Schwartz. 1983. Monoclonal antibodies against the antigen receptor on a cloned T-cell hybrid. *Proc. Natl. Acad. Sci. USA*. 80:6972–6976.
26. Kung, P., G. Goldstein, E.L. Reinherz, and S.F. Schlossman. 1979. Monoclonal antibodies defining distinctive human T cell surface antigens. *Science (Wash. DC)*. 206:347–349.
27. Kim, H.Y., T. LaVaute, R.D. Klausner, and T.A. Rouault. 1996. Identification of a conserved and functional iron-responsive element in the 5′-untranslated region of mammalian mitochondrial aconitase. *J. Biol. Chem.* 271:24226–24230.
28. Wang, C.C., J.A. Badylak, S.E. Lux, R. Moriyama, J.E. Dixon, and P.S. Low. 1992. Expression, purification, and characterization of the functional dimeric cytoplasmic domain of human erythrocyte band 3 in *Escherichia coli*. *Protein Sci.* 9:1206–1214.
29. Wange, R.L. and L.E. Samelson. 1996. Complex complexes: signaling at the TCR. *Immunity*. 5:197–205.
30. Abraham, N., and A. Veillette. 1990. Activation of $p56^{lck}$ through mutation of a regulatory carboxy-terminal tyrosine residue requires intact sites of autophosphorylation and myristylation. *Mol. Cell. Biol.* 10:5197–5206.
31. Huby, R.D.J., M. Iwashima, A. Weiss, and S.C. Ley. 1997. ZAP-70 protein tyrosine kinase is constitutively targeted to the T cell cortex independently of its SH2 domains. *J. Cell Biol.* 137:1639–1649.
32. Nagasawa, M., I. Melamed, A. Kupfer, E.W. Gelfand, and J.J. Lucas. 1997. Rapid nuclear translocation and increased activity of cyclin-dependent kinase 6 after T cell activation. *J. Immunol.* 158:5146–5154.
33. Klausner, R.D., T.A. Rouault, and J.B. Harford. 1997. Regulating the fate of mRNA: the control of cellular iron metabolism. *Cell*. 72:19–28.
34. Davis, L.I., and G. Blobel. 1986. Identification and characterization of a nuclear pore complex protein. *Cell*. 45:699–709.
35. Weiss, A. 1995. Zapping tandem SH2 domains. *Nature (Lond.)*. 377:17–18.
36. Chan, A.C., M. Iwashima, C.W. Turck, and A. Weiss. 1992. ZAP-70: a 70 kd protein-tyrosine kinase that associates with the TCR zeta chain. *Cell*. 71:649–662.
37. Wange, R.L., S.N. Malek, S. Desiderio, and L.E. Samelson. 1993. Tandem SH2 domains of ZAP-70 bind to T cell antigen receptor ζ and CD3ε from activated jurkat T cells. *J. Biol. Chem.* 268:19797–19801.
38. Muller, A.J., A.-M. Pendergast, M.H. Havlik, L. Puil, T. Pawson, and O.N. Witte. 1992. A limited set of SH2 domains binds BCR through a high-affinity phosphotyrosine-independent interaction. *Mol. Cell. Biol.* 12:5087–5093.
39. Cleghon, V., and D.K. Morrison. 1994. Raf-1 interacts with Fyn and Src in a non-phosphotyrosine-dependent manner. *J. Biol. Chem.* 269:17749–17755.
40. Ota, Y., L.O. Beitz, A.M. Scharenberg, J.A. Donovan, J.-P.

Kinet, and L.E. Samelson. 1996. Characterization of Cbl tyrosine phosphorylation and a Cbl-Syk complex in RBL-2H3 cells. *J. Exp. Med.* 184:1713–1723.
41. Newton, A.C. 1995. Protein kinase C: structure, function, and regulation. *J. Biol. Chem.* 270:28495–28498.
42. Xu, W., S.C. Harrison, and M.J. Eck. 1997. Three-dimensional structure of the tyrosine kinase c-Src. *Nature (Lond.).* 385:595–602.
43. Sicheri, F., I. Moarefi, and J. Kuriyan. 1997. Crystal structure of the Src family tyrosine kinase Hck. *Nature (Lond.).* 385: 602–609.
44. Wang, J.Y.J. 1994. Nuclear protein tyrosine kinases. *TIBS (Trends Biochem. Sci.).* 19:373–376.
45. Wang, J.Y.J. 1993. Abl tyrosine kinase in signal transduction and cell-cycle regulation. *Curr. Opin. Genet. Dev.* 3:35–43.
46. Presley, J.F., N.B. Cole, T.A. Schroer, K. Hirschberg, K.J.M. Zaal, and J. Lippincott-Schwartz. 1997. ER to Golgi transport visualized in living cells. *Nature (Lond.).* 389:81–85.
47. Davis, L.I. 1995. The nuclear pore complex. *Annu. Rev. Biochem.* 64:865–896.
48. Siomi, H., and G. Dreyfuss. 1995. A nuclear localization domain in the hnRNP A1 protein. *J. Cell Biol.* 129:551–559.
49. Pollard, V.W., W.M. Michael, S. Nakielny, M.C. Siomi, F. Wang, and G. Dreyfuss. 1996. A novel receptor-mediated nuclear protein import pathway. *Cell.* 86:985–994.

Nieren- und Hochdruckkrankheiten, Jahrgang 27, Nr. 3/1998, S. 123–131

Molekulare Mechanismen der Entzündung

Signaltransduktion von Interleukin-6-Typ-Zytokinen über den Jak/STAT-Weg

P.C. Heinrich[1], I. Behrmann[1], L. Graeve[1], J. Grötzinger[1], S. Haan[1], F. Horn[1], U. Horsten[1], I. Kerr[2], P. May[1], G. Müller-Newen[1], L. Terstegen[1] und S. Thiel[1]

[1] *Institut für Biochemie, Rheinisch-Westfälische Technische Hochschule, Aachen,*
[2] *Imperial Cancer Research Fund, London, England*

Schlüsselwörter
Inflammatorische Zytokine – Interleukin-6 – Janus-Kinasen – STAT-Faktoren – Signaltransduktion – Endozytose.

Key words
Inflammatory cytokines – Interleukin-6 – Janus kinases – STAT factors – signal transduction – endocytosis.

Abkürzungen
CNTF: ciliary neurotrophic factor, CT: Kardiotrophin-1, G-CSF: granulocyte colony stimulating factor, GFP: green fluorescent protein, IL = Interleukin, JAB: Jak-binding protein, LIF: leukemia inhibitory factor, OSM: Onkostatin-M, SOCS: supressor of cytokine signaling, SSI: STAT-induced STAT inhibitor, TGF: transforming growth factor.

Molekulare Mechanismen der Entzündung: Signaltransduktion von Interleukin-6-Typ-Zytokinen über den Jak/STAT-Weg

Wir haben gefunden, daß IL-6 und die IL-6-Typ-Zytokine IL-11, Onkostatin-M, leukemia inhibitory factor, ciliary neurotrophic factor und Kardiotrophin-1 über den Jak/STAT-Weg signalisieren. IL-6 wird zunächst mit niedriger Affinität an seinen spezifischen Rezeptor (gp80) gebunden, der IL-6/gp80-Komplex interagiert in der Folge mit 2 Molekülen des Signaltransduktors gp130. Die Dimerisierung von gp130 im hochaffinen Komplex aus IL-6, gp80 und gp130 führt zu einer Aktivierung von Tyrosinkinasen der Jak-Familie. Hierbei spielt Jak1 eine sehr wichtige Rolle für die Phosphorylierung von gp130 und die Aktivierung der Transkriptionsfaktoren STAT1 und STAT3. Von den 6 Tyrosinresten in der zytoplasmatischen Domäne von gp130 sind die 4 distalen Tyrosinreste fähig, STAT3 zu aktivieren, während STAT1 nur von den letzten 2 Tyrosinresten aktiviert werden kann. STAT5 läßt sich nicht über gp130 tyrosinphosphorylieren. Die aktivierten STAT-Faktoren homo- oder heterodimerisieren und translozieren in den Zellkern, wo sie an Enhancer-Elemente von IL-6-Zielgenen binden. Die IL-6-induzierte STAT-Faktor-Translokation konnte in transfizierten COS- und HeLa-Zellen mit Hilfe eines STAT3-GFP(green fluorescence protein)-Fusionsproteins nachgewiesen werden. Mit Hilfe spezifischer Aktivierung von STAT1, -3 und -5 und des Einsatzes von CAT-Reportergen-Assays in Hepatoma(HepG2)-Zellen ließ sich eindeutig zeigen, daß IL-6-Zielgene wie γ-Fibrinogen, Haptoglobin, Hämopexin und C-reaktives Protein hauptsächlich durch STAT3 induzierbar sind. Bei der Diskussion der möglichen IL-6-Signalabschaltmechanismen werden Ergebnisse zur Endozytose von IL-6/IL-6-Rezeptorkomplexen vorgestellt. Es wird mit Hilfe heterochimärer Rezeptoren gezeigt, daß Internalisierung und Signaltransduktion zwei voneinander unabhängige Prozesse sind.

Molecular mechanisms of inflammation: interleukin-6-type cytokine signaling through the Jak/STAT pathway

We have found that IL-6 and the IL-6-type cytokines (IL-11, oncostatin-M, LIF, CNTF, CT-1) signal through the Jak/STAT pathway. IL-6 first binds to its specific receptor (gp80), the IL-6/gp80 complex subsequently interacts with 2 molecules of the signal transducer gp130 resulting in a high affinity complex. Ternary complex formation of IL-6, gp80, and gp130 results in the activation of the Jak family tyrosine kinases Jak1, Jak2, and Tyk2. Using mutant fibrosarcoma cells lacking the different Jak kinases, Jak1 was found to play a major role in the tyrosine phosphorylation of gp130 and activation of the transcription factors STAT1 and STAT3. Out of the 6 tyrosine residues present in the cytoplasmic region of gp130 we have found that the 4 distal tyrosine residues are able to activate STAT3, the last 2 tyrosine residues lead to STAT1 activation, whereas STAT5 could not be activated via gp130. After tyrosine phosphorylation the STAT factors homo- or hetero-dimerize and translocate to the nucleus where they bind to response elements of IL-6 target genes. The IL-6-induced STAT translocation could be shown in COS- and HeLa cells with a STAT3-GFP fusion protein. By specific activation of STAT1, 3, and 5 together with the use of CAT reporter gene assays in hepatoma (HepG2) cells we could show that IL-6 target genes (γ-fibrinogen, haptoglobin, hemopexin, CRP) are mainly induced by STAT3. In previous studies we have shown that IL-6 is internalized and its receptor is down-regulated. A di-leucine motif in the cytoplasmic tail of gp130 was found to be responsible for the endocytosis of IL-6/gp80 complexes. Using a heterochimeric receptor system we now show that internalization and signal transduction are 2 independent processes.

Die ursprünglich definierten 5 Kardinalsymptome der Entzündung Calor, Rubor, Tumor, Dolor und Functio laesa sind heute zwar noch akzeptiert, aber durch eine enorme Zahl an zellbiologischen, biochemischen und molekularbiologischen Befunden auf eine außerordentlich komplexe molekulare Ebene verschoben worden.

Aus der Vielzahl der am Entzündungsgeschehen beteiligten Moleküle soll im vorliegenden Beitrag die Gruppe der sogenannten Zytokine – dies sind hormonähnliche Polypeptide – ausgewählt und deren Signaltransduktion diskutiert werden.

Zytokine

Zytokine sind ein wichtiger Bestandteil des Kommunikationssystems vielzelliger Organismen. Als interzelluläre Mediatoren regulieren sie in nano- bis picomolaren Konzentrationen Wachstum, Differenzierung und spezifische Effektorfunktionen von Zellen. Zytokine werden im Unterschied zu Hormonen nicht als präformierte Moleküle in Drüsen gespeichert, sondern von einer Vielzahl verschiedener Zellen meist nach Stimulation rasch synthetisiert und sezerniert. Sie wirken auf zahlreiche verschiedene Zielzellen (Pleiotropie) und beeinflussen die Wirkung anderer Zytokine in additiver, synergistischer oder antagonistischer Weise. Neben ihrer pleiotropen Wirkung ist die Wirkung der Zytokine in hohem Maße redundant, d.h. viele biologische Antworten können durch unterschiedliche Zytokine hervorgerufen werden.

Ihre Wirkungen, die auto-, para- oder auch endokrin sein können, entfalten Zytokine über spezifische Rezeptoren auf der Oberfläche ihrer Zielzellen (Übersicht [13]).

Zytokine spielen für die Immunantwort und während entzündlicher Prozesse eine sehr wichtige Rolle.

Entzündliche Prozesse

Entzündliche Prozesse treten u.a. nach Infektionen (Sepsis), bei Gelenkerkrankungen (rheumatoide Arthritis, Osteoarthritis), neurologischen Erkrankungen (multiple Sklerose, Morbus Alzheimer), entzündlichen Nierenerkrankungen (Glomerulonephritis), endokrinologischen Autoimmunerkrankungen (Thyreoiditis, Diabetes Typ I und entzündlichen Gefäßerkrankungen (Atherosklerose) auf.

Inflammatorische Zytokine

Die inflammatorischen Zytokine lassen sich in 3 Gruppen unterteilen:

- frühe oder proinflammatorische Zytokine: Interleukin-1, Tumornekrosefaktor α, Interferon γ, Interleukin-8,
- Interleukin-6-Familie: Interleukin-6, Interleukin-11, leukemia inhibitory factor, Onkostatin M, ciliary neurotrophic factor, Kardiotrophin-1,
- antiinflammatorische Zytokine: Interleukin-4, Interleukin-10, Interleukin-13, transforming growth factor β.

Die Mitglieder der IL-6-Familie können sowohl pro- als auch antiinflammatorische Wirkungen entfalten.

Im folgenden soll auf diese Zytokin-Familie und insbesondere auf das hier bestuntersuchte Zytokin IL-6 näher eingegangen werden, wobei besonderes Gewicht auf der Signaltransduktion liegen soll.

Interleukin-6-Typ-Zytokine

Die Interleukin-6-Typ-Zytokine gehören zu den sogenannten long chain 4-α-helical bundle Zytokinen. Hierzu zählen neben IL-6, IL-11, LIF, OSM, CNTF und CT-1 auch Erythropoietin, Granulozytenkolonie-stimulierender Faktor, Interleukin-12, Wachstumshormon, Prolaktin, Interleukin-10, Interferon α/β und Leptin. Obwohl diese Zytokine sich in ihrer Aminosäuresequenz stark unterscheiden, weisen sie eine vergleichbare Tertiärstruktur auf. Diese ist am Beispiel von Interleukin-6 (Abb. 1) gezeigt. Die IL-6-Typ-Zytokine zeichnen sich dadurch aus, daß ihre Plasmamembranrezeptoren eine gemeinsame signaltransduzierende Untereinheit (gp130) besitzen (Abb. 2).

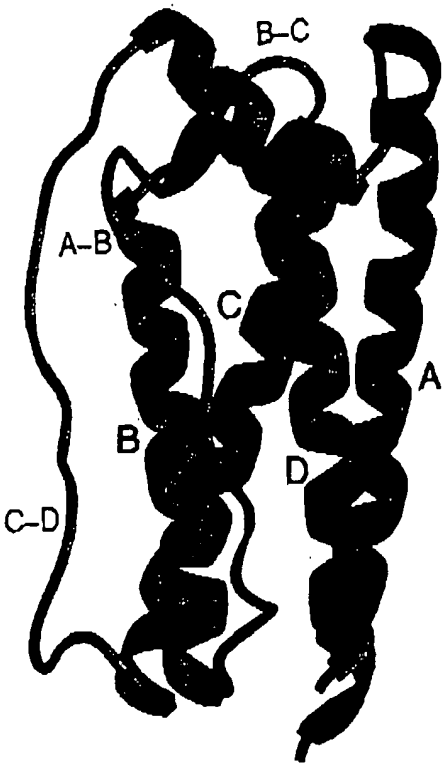

Abb. 1. Strukturmodell von Interleukin-6 [6].

nom- und Melanomzellen zu hemmen [1]. Wir haben 1987 Interleukin-6 als Hepatozyten-stimulierenden Faktor identifiziert [2]. Das Zytokin wirkt auf Hepatozyten der Leber und induziert die Synthese von Akutphase-Proteinen wie C-reaktives Protein, Fibrinogen, Haptoglobin, Hämopexin, α_1-Antichymotrypsin und α_1-saurem Glykoprotein [9]. Die Akutphase-Proteine spielen eine wichtige Rolle als Inhibitoren proteolytischer Prozesse, wie der Blutgerinnung und der Fibrinolyse, sowie als Transportproteine im Blut. Die Regulation ihrer Synthese, wie auch das Abschalten der Reaktion nach Beseitigung der Störungsursache, erfolgen auf transkriptioneller Ebene. Eine Störung in diesem sensiblen Regulationsmechanismus kann zu überschießenden Reaktionen und damit zu chronischen Entzündungszuständen führen [9].

Wie Interleukin-6, zeigen auch die verwandten IL-6-Typ-Zytokine eine pleiotrope Wirkung.

Interleukin-6

Interleukin-6 spielt bei der Hämatopoese, bei der Differenzierung von Nervenzellen, T-Zellen sowie B-Zellen, die zu Plasmazellen differenzieren, eine wichtige Rolle. IL-6 ist ein Wachstumsfaktor für Keratinozyten, Plasmazytom- und Mesangialzellen. Andererseits vermag IL-6 das Wachstum von Brustkarzi-

Interleukin-6-Signaltransduktion

Unserer Arbeitsgruppe ist es 1994 gelungen, den Signaltransduktionsweg von IL-6 über seinen Oberflächenrezeptor bis hin zur Genregulation der Zielgene im Zellkern in seinen wesentlichen Schritten aufzuklären [11] (Abb. 3).

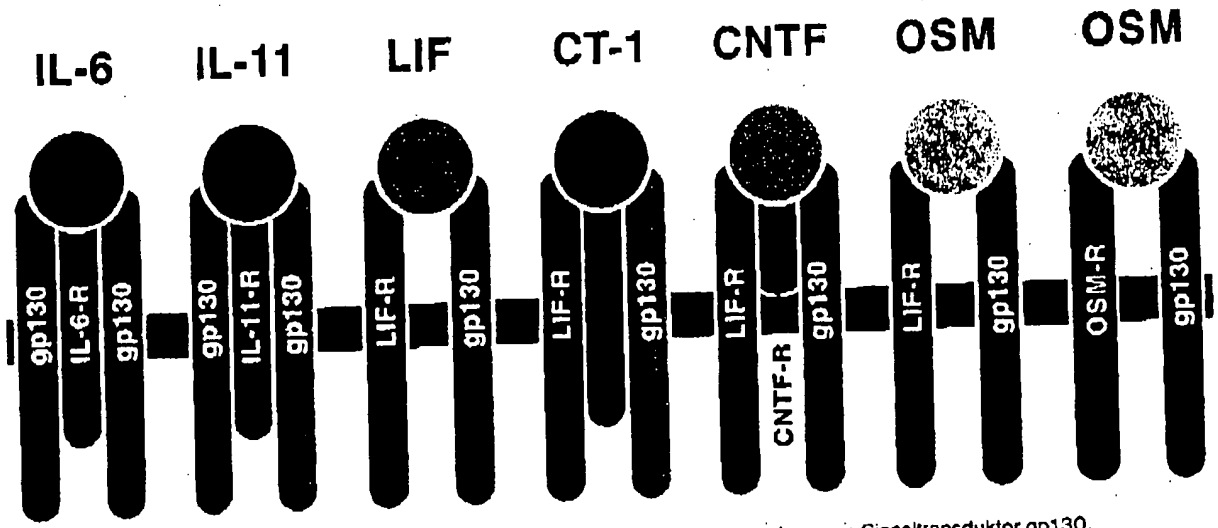

Abb. 2. IL-6-Typ-Zytokinrezeptoren benutzen den gemeinsamen Signaltransduktor gp130.

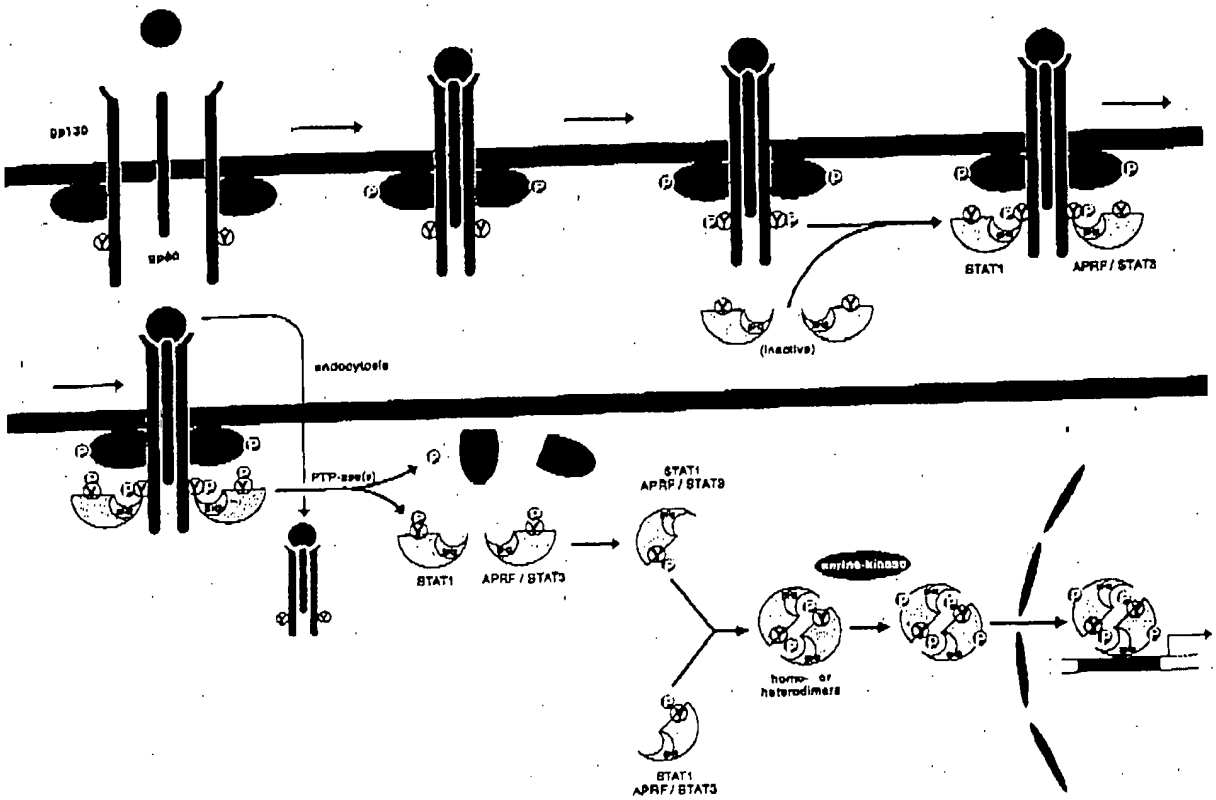

Abb. 3. Schematische Darstellung der IL-6-Signaltransduktion.

IL-6 bindet zunächst mit niedriger Affinität an seinen spezifischen Rezeptor gp80. Der IL-6/gp80-Komplex – der selbst kein Signal auslösen kann – interagiert in der Folge mit 2 Rezeptoruntereinheiten, die als Signaltransduktor-Moleküle (gp130) bezeichnet werden. Im Verband von gp80 und den dimerisierten gp130-Molekülen wird IL-6 mit hoher Affinität (50 pM) gebunden. Die IL-6-Rezeptorstöchiometrie wird zur Zeit kontrovers diskutiert. Während Grötzinger und Mitarbeiter [6] einen Rezeptorkomplex aus einem IL-6, einem gp80 und zwei gp130 diskutieren, zeigen Untersuchungen anderer Gruppen, daß der IL-6-Rezeptorkomplex als Hexamer, bestehend aus zwei IL-6-, zwei gp80- und zwei gp130-Molekülen vorliegt [14, 17]. Die gp130-Dimerisierung setzt eine Phosphorylierungskaskade in Gang, deren erster Schritt die gegenseitige Phosphorylierung von Tyrosinkinasen der Jak-Familie ist. Die Janus-Kinasen Jak1, Jak2 und Tyk2, die konstitutiv and den membranproximalen Bereich der zytoplasmatischen Domäne von gp130 binden, werden Tyrosin-phosphoryliert und damit enzymatisch aktiv. In der Folge werden verschiedene Tyrosinreste im zytoplasmatischen Teil von gp130 phosphoryliert. Die Phosphotyrosine fungieren als Andockstellen für Transkriptionsfaktoren der STAT(signal transducer and activator of transcription)-Familie. Die STAT-Faktoren STAT1 und STAT3, die an ihren C-terminalen Enden eine Tyrosinphosphorylierungsstelle und eine Src-Homologiedomäne (SH2-Domäne) besitzen, binden über ihre SH2-Domänen an Phosphotyrosin-Reste im zytoplasmatischen Teil von gp130. Die Jak-Kinasen können nun auch die STAT-Faktoren an C-terminalen Tyrosin-Resten phosphorylieren. Während die Tyrosin-phosphorylierten STAT-Faktoren den Rezeptorkomplex verlassen, wird letzterer durch Endozytose in die Zelle aufgenommen. Die aktivierten STAT-Faktoren homo- und/oder heterodimerisieren über Phosphotyrosin-SH2-Interaktionen. Es schließt sich eine Serin-Phosphorylierung von STAT1 bzw. STAT3 im Zytoplasma an. Die hierfür verantwortliche, durch H7 hemmbare Serinkinase konnte bisher noch nicht identifiziert werden. Nach Translokation der

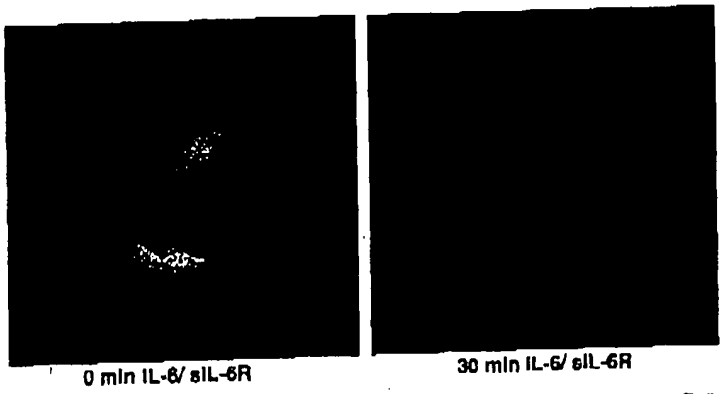

Abb. 4. Translokation von STAT3-GFP in den Zellkern nach Stimulation mit IL-6 und seinem löslichen Rezeptor.

dimeren STAT-Faktoren in den Zellkern binden diese an Enhancer-Elemente von IL-6-Zielgenen und regulieren deren Transkription. Die Translokation der STAT-Faktoren konnte nach Transfektion von STAT1/3-GFP(green fluorescence protein)-Fusionsproteinen in COS- und in HeLa-Zellen, die mit IL-6 und seinem löslichen Rezeptor stimuliert wurden, nachgewiesen werden. Die Fluoreszenz, die in unstimulierten Zellen zunächst über die gesamte Zelle verteilt ist, ließ sich schon 30 Minuten nach Stimulation mit IL-6 im Zellkern beobachten (Abb. 4).

Der Einsatz von humanen Fibrosarkom-Zellinien, die bezüglich der Jak-Kinasen Jak1, Jak2 oder Tyk2 defizient sind, erlaubte die Beantwortung der Frage, welche der 3 Jak-Kinasen die zentrale Rolle in der IL-6-Signaltransduktion spielt. Es wurde nach Stimulation der verschiedenen Jak-defizienten Fibrosarkomzellen mit IL-6 und seinem löslichen Rezeptor eindeutig nachgewiesen, daß nur die Jak1-defizienten Zellen eine nahezu vollständig eingeschränkte Tyrosinphosphorylierung von gp130, keine Tyrosinphosphorylierung von STAT1 und eine stark verminderte Tyrosinphosphorylierung von STAT3 aufwiesen [7]. Diese Versuche unterstreichen die zentrale Rolle von Jak1 im Interleukin-6-Signalweg.

Welche Tyrosinreste aktivieren welche STAT-Faktoren?

Da der zytoplasmatische Teil des Signaltransduktors gp130 sechs Tyrosinreste enthält, haben wir mit Hilfe chimärer Rezeptoren versucht, die Frage zu beantworten: Welche Tyrosine aktivieren welche STAT-Faktoren? Dazu wurden die in Abbildung 5 dargestellten Rezeptor-Chimären benutzt (Extrazellulär-Domäne des Erythropoietin-Rezeptors, Transmembran-Domäne von gp130 sowie 60 Aminosäuren der sogenannten Box1- und Box2-Region von gp130, an die die verschiedenen gp130-Tyrosinpeptide fusioniert wurden). Nach Ko-Expression dieser Chimären mit STAT1 oder STAT3 in COS-Zellen ließ sich zeigen, daß die distalen Tyrosine 915, 905, 814 und 767 imstande sind, STAT3 zu aktivieren und daß STAT1 nur von den Tyro-

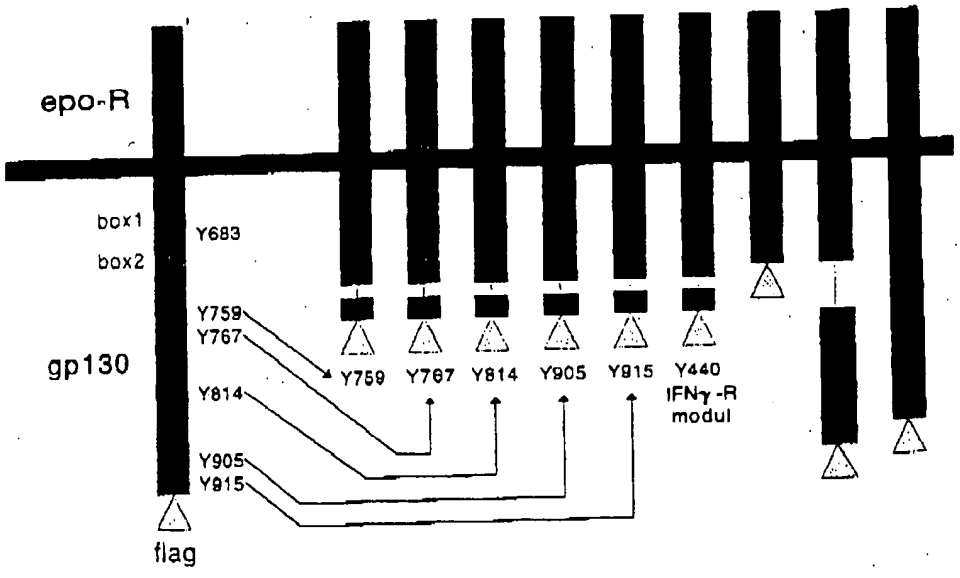

Abb. 5. Erythropoietin-gp130-Rezeptor-Chimäre.

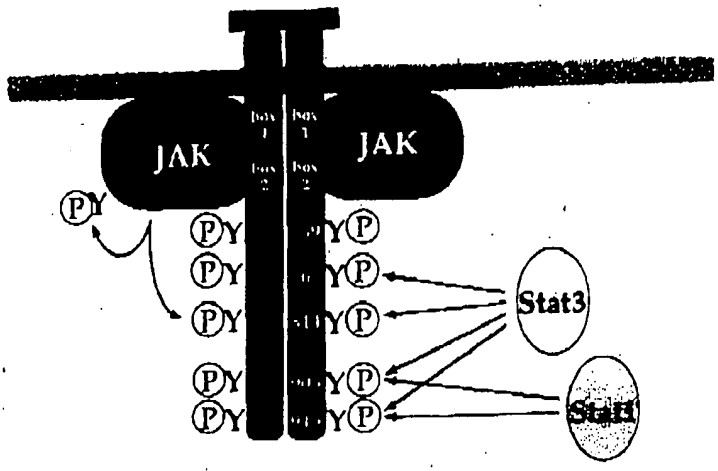

Abb. 6. STAT1- und STAT3-Aktivierung durch Phosphotyrosin-Module im zytoplasmatischen Teil von gp130.

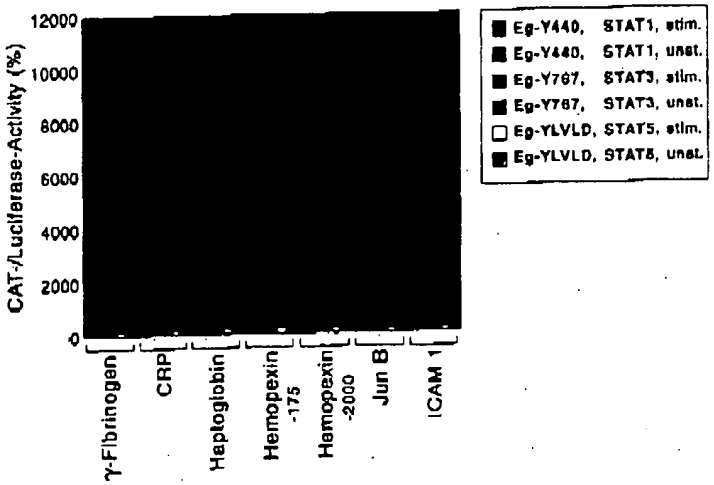

Abb. 7. STAT3 spielt bei der Regulation von Akutphase-Protein- und Immediate-early-Gen-Promotoren gegenüber STAT1 und STAT5 eine herausragende Rolle.

sinmodulen 915 und 905 aktiviert werden kann [5].

Abbildung 6 zeigt schematisch unsere Befunde. Auch im Kontext des gesamten zytoplasmatischen Teils von gp130, in dem sämtliche Tyrosinreste durch Phenylalanin ausgetauscht und nachfolgend die einzelnen Tyrosine zurück"mutiert" wurden, ergab sich das gleiche Bild der Aktivierbarkeit der STAT-Faktoren 1 und 3 (Schaper, Eck, Schmitz, unveröffentlichte Ergebnisse).

Spezifität der STAT-Faktoren 1, 3 und 5 bei der Regulation von Akutphase- und Immediate-early-Genpromotoren

Der Jak/STAT-Signaltransduktionsweg wird von einer Vielzahl von Zytokinen und Wachstumsfaktoren genutzt, die so verschiedene Effekte wie die Synthese von Akutphase-Proteinen, die Sekretion von Milchproteinen und die Zellteilung oder Differenzierung vermitteln. Es stellte sich daher die Frage, wie hierbei mit nur 4 Jak-Kinasen und 7 STAT-Faktoren für jedes Zytokin die Spezifität seiner Antwort erreicht wird. Dabei spielt sicherlich eine Rolle, daß jedes Zytokin nur einen oder auch mehrere bestimmte STAT-Faktoren aktiviert. Damit diese gezielte Aktivierung von STAT-Faktoren auch tatsächlich zur Spezifität der Antwort führt, muß angenommen werden, daß die verschiedenen STATs selektiv bestimmte Gene regulieren. Wir haben daher die Promotoren verschiedener Gene, die durch IL-6 und damit also potentiell durch STAT1, -3 oder -5 reguliert werden, auf ihre Induzierbarkeit durch die drei genannten STAT-Faktoren untersucht.

Ebenfalls mit Hilfe von chimären Erythropoetin/gp130-Rezeptoren, die spezifisch STAT1, STAT3 oder STAT5 nach Stimulation mit Erythropoetin zu aktivieren vermögen, konnte in mit STAT3 und verschiedenen Akutphase - Protein -Promotor -Reportergen-Konstrukten transfizierten Hepatoma(HepG2)-Zellen eindeutig gezeigt werden, daß STAT3 eine Hauptrolle in der Aktivierung der Transkription der Akutphase-Gene γ-Fibrinogen, CRP, Haptoglobin und Hämopexin sowie der Immediate-erly-Gene JunB und ICAM1 spielt (May, Dissertation, Aachen 1997) (Abb. 7).

Wie wird das IL-6-Signal abgeschaltet?

Ein wichtiges Problem der Zytokin-Signaltransduktion ist die Frage nach dem Abschaltmechanismus. Hierzu werden verschiedene Möglichkeiten diskutiert:

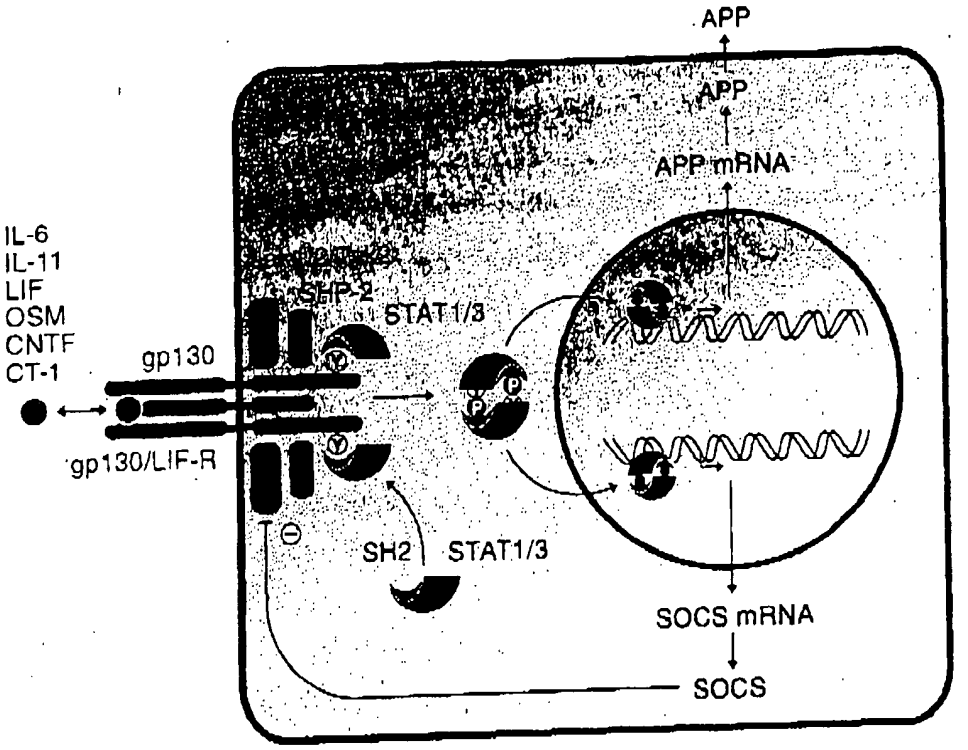

Abb. 8. Schematische Darstellung der IL-6-Typ-Zytokin-Signaltransduktion und deren Feed-back-Regulation durch Jak-Kinase-Inhibitoren der SOCS-Familie.

- eine Tyrosin-Phosphatase im Zellkern dephosphoryliert die aktivierten STAT-Faktoren [8],
- die STAT-Faktoren werden durch nukleäre Proteasomen degradiert [10],
- Phosphotyrosin-Phosphatase(n) dephosphorylieren Rezeptor-assoziierte Proteine wie Jak-Kinasen und STAT-Faktoren,
- intrazelluläre Jak/STAT-Inhibitoren werden synthetisiert [4, 12, 15],
- die Zytokinrezeptoren werden via Endozytose internalisiert [3, 16].

Während eine STAT1-Degradation durch nukleäre Proteasomen nachgewiesen wurde [10], konnte für STAT3 dieser Weg der Inaktivierung nach Verwendung des Proteasomen-Inhibitors Laktazystin nicht beobachtet werden (Küster und Heinrich, unveröffentlicht). Neueste Befunde verschiedener Arbeitsgruppen [4, 12, 15] zeigen, daß es nach IL-6-Einwirkung zur Induktion und Synthese von Jak-Kinase-Inhibitoren kommt (Abb. 8).

Endozytose von IL-6, gp80 und gp130

Die Untersuchungen in unserer Arbeitsgruppe haben ergeben, daß es zwischen 30 und 60 Minuten nach Bindung von IL-6 an seine Rezeptor-Untereinheiten gp80 und gp130 zu einer Internalisierung des gesamten Rezeptorkomplexes kommt. Verantwortlich für die Endozytose ist ein Di-Leuzin-Motiv (STQPLL) in der zytoplasmatischen Region von gp130. Dieses Motiv bewirkt auch schon eine Liganden-unabhängige Internalisierung von gp130 [3]. Der Austausch der Leuzinreste durch Alanin führt zum Verlust der Internalisierungsfähigkeit von gp130 [3].

Mit Hilfe heterochimärer Rezeptoren, die als Extrazellulär-Domänen die α- bzw. β-Rezeptor-Untereinheiten des IL-5-Rezeptors tragen, war es uns möglich nachzuweisen, daß Internalisierung und STAT-Aktivierung zwei voneinander unabhängige Prozesse sind [16]. Nach Co-Transfektion von COS-Zellen mit IL-5-Rezeptor-α bzw. -β/gp130-Heterochimären werden die Internalisierung von radioaktiv markiertem IL-5 und eine STAT1-Akti-

Tab. 1. JAK/STAT-Aktivierung durch Zytokine.

	Zytokine	JAK-Kinasen				STAT-Faktoren						
		JAK1	JAK2	JAK3	TYK2	STAT1	STAT2	STAT3	STAT4	STAT5A	STAT5B	STAT6
Zytokin-R-Superfamilie (= hämatopoietische Superfamilie)	GH	×	×			×		×		×	×	
	PRL		×			×		×		×	×	
	Epo		×							×	×	
	Tpo		×		×			×		×	×	
	G-CSF	×	×		×	×		×				
	IL-12		×					×	×			
γ_c chain user	IL-2	×		×		×		×		×	×	
	IL-4	×		×								×
	IL-7	×		×						×	×	
	IL-9	×		×		×						
	IL-13	×		×								×
	IL-15	×	×	×				×				
β_c chain user	IL-3		×							×	×	
	IL-5		×			×		×		×	×	
	GM-CSF		×							×	×	
gp 130 users	IL-6	×	×		×	×		×		×	×	
	IL-11	×	×		×	×		×				
	LIF	×	×		×	×		×		×	×	
	OSM	×	×		×	×		×			×	
	CNTF	×	×		×	×		×				
	CT	×	×		×			×				
IFN-R-Superfamilie	IFNα/β	×			×	×	×	×				
	IFNγ	×	×			×		×		×	×	
	IL-10		×			×		×				
Protein-Tyrosinkinase-R-Superfamilie	EGF	×				×		×				
	PDGF					×		×				
	M-CSF					×				×	×	

vierung nach Stimulation mit IL-5 beobachtet. Die Deletion der zytoplasmatischen Domäne von gp130 resultiert in einem Verlust der Internalisierungsfähigkeit und der STAT1-Aktivierung. Wird im heterochimären Rezeptor im zytoplasmatischen Teil von gp130 das Di-Leuzin-Motiv durch Ala-Ala ausgetauscht, geht die Fähigkeit zur Internalisierung verloren, während die STAT-Aktivierung erhalten bleibt. Nach Deletion des Membran-proximalen Teils von gp130, der für die Bindung der Jak-Kinasen verantwortlich ist, wird eine nahezu unveränderte Internalisierung beobachtet, die STAT1-Aktivierung bleibt aber aus. Diese Befunde zeigen eindeutig, daß Internalisierung und Signaltransduktion zwei unabhängig voneinander ablaufende Prozesse sind [16].

Aus Tabelle 1 soll klar werden, daß eine große Zahl von Zytokinen und Wachstumsfaktoren, die in entzündlichen Prozessen eine wichtige Rolle spielen, über den Jak-/STAT-Weg signalisieren. Nicht aufgeführt sind Zytokine/Hormone, die über G-Protein gekoppelte Rezeptoren ebenfalls STAT-Faktoren zu aktivieren vermögen.

Danksagung

The authors like to thank Silvia Cottin and Ria Lindt for secretarial assistance. The experiments described in this article have been supported by grants from the Deutsche Forschungsgemeinschaft (Bonn), by the Interdisciplinary Center for Clinical Research in Biomaterials and Tissue-Material-Interaction in Implants (BIOMAT), and the Fonds der Chemischen Industrie (Frankfurt a.M.).

Literatur

[1] *Akira S., T. Taga, T. Kishimoto:* Interleukin-6 in biology and medicine. Adv. Immunol. *54*, 1-78 (1993).

[2] *Andus T., T. Geiger, T. Hirano, H. Northoff, U. Ganter, J. Bauer, T. Kishimoto, P.C. Heinrich:* Recombinant human B cell stimulatory factor 2 (BSF-2/IFN-β2) regulates β-fibrinogen and albumin mRNA levels in FAO-9 cells. FEBS Lett. *221*, 18-22 (1987).

[3] *Dittrich E., C.R. Haft, L. Muys, P.C. Heinrich, L. Graeve:* A di-leucine motif and an upstream serine in the interleukin-6 signal transducer gp130 mediate ligand-induced endocytosis and down-regulation of the IL-6 receptor. J. Biol. Chem. *271*, 5487-5494 (1996).

[4] *Endo T.A., M. Masuhara, M. Yokouchi, R. Suzuki, H. Sakamoto, K. Mitsui, A. Matsumoto, S. Tanimura, M. Ohtsubo, H. Misawa, T. Miyazaki, N. Leonor, T. Taniguchi, T. Fujita, Y. Kanakura, S. Komiya, A. Yoshimura:* A new protein containing an SH2 domain that inhibits JAK kinases. Nature *387*, 921-924 (1997).

[5] *Gerhartz C., B. Heesel, J. Sasse, U. Hemman, C. Landgraf, J. Schneider-Mergener, F. Horn, P.C. Heinrich, L. Graeve:* Differential activation of acute phase response factor/STAT3 and STAT1 via the cytoplasmatic domain of the interleukin-6 signal transducer gp130. J. Biol. Chem. *271*, 12991-12998 (1996).

[6] *Grötzinger J., G. Kurapkat, A. Wollmer, M. Kalai, S. Rose-John:* The family of the IL-6-type cytokines: Specificity and promiscuity of the receptor complexes. Proteins *27*, 96-109 (1997).

[7] *Guschin D., N. Rogers, J. Briscoe, B. Witthuhn, D. Watling, F. Horn, S. Pellegrini, K. Yasukawa, P.C. Heinrich, G.R. Stark, J.N. Ihle, I.M. Kerr:* A major role for the protein tyrosine kinase Jak1 in the Jak/STAT signal transduction pathway in response to interleukin-6. EMBO J. *14*, 1421-1429 (1995).

[8] *Haspel R.L., M. Salditt-Georgieff, J.E. Darnell, Jr.:* The rapid inactivation of nuclear tyrosine phosphorylated Stat1 depends upon a protein tyrosine phosphatase. EMBO J. *15*, 6262-6268 (1996).

[9] *Heinrich P.C., J.V. Castell, T. Andus:* Interleukin-6 and the acute phase response. Biochem. J. *265*, 621-636 (1990).

[10] *Kim T.K., T. Maniatis:* Regulation of interferon-gamma-activated STAT1 by the ubiquitin-proteasome pathway. Science *273*, 1717-1719 (1996).

[11] *Lütticken C., U.M. Wegenka, J. Yuan, J. Buschmann, C. Schindler, A. Ziemiecki, A.G. Harpur, A.F. Wilks, K. Yasukawa, T. Taga, T. Kishimoto, G. Barbieri, S. Pellegrini, M. Sendtner, P.C. Heinrich, F. Horn:* Association of transcription factor APRF and protein kinase JAK1 with the interleukin-6 signal transducer gp130. Science *263*, 89-92 (1994).

[12] *Naka T., M. Narazaki, M. Hirata, T. Matsumoto, S. Minamoto, A. Aono, N. Nishimoto, T. Kajita, T. Taga, K. Yoshizaki, S. Akira, T. Kishimoto:* Structure and function of a new STAT-induced STAT inhibitor. Nature *387*, 924-929 (1997).

[13] *Nicola N.A.:* Guidebook to cytokines and their receptors. Oxford University Press, Oxford 1994.

[14] *Paonessa G., R. Graziani, R. De Serio, R. Savino, L. Ciapponi, A. Lahm, A.L. Salvati, C. Toniatti, G. Ciliberto:* Two distinct and independent sites on IL-6 trigger gp130 dimer formation and signaling. EMBO J. *14*, 1942-1951 (1995).

[15] *Starr R., T.A. Willson, E.M. Viney, L.J.L. Murray, J.R. Rayner, B.J. Jenkins, T.J. Gonda, W.S. Alexander, D. Metcalf, N.A. Nicola, D.J. Hilton:* A family of cytokine-inducible inhibitors of signaling. Nature *387*, 917-921 (1997).

[16] *Thiel S., I. Behrmann, E. Dittrich, L. Muys, J. Tavernier, J. Wijdenes, P.C. Heinrich, L. Graeve:* Internalization of the IL-6 signal transducer gp130 does not require activation of the Jak/STAT pathway. Biochem. J. *330*, 47-54 (1998).

[17] *Ward L.D., G.J. Howlett, G. Discolo, K. Yasukawa, A. Hammacher, R.L. Moritz, R.J. Simpson:* High affinity interleukin-6 receptor is a hexameric complex consisting of two molecules each of interleukin-6, interleukin-6 receptor, and gp130. J. Biol. Chem. *269*, 23286-23289 (1994).

Prof. Dr. rer. nat. P.C. Heinrich
Institut für Biochemie
Rheinisch-Westfälische Technische Hochschule
Pauwelsstraße 30
D-52057 Aachen

Secretory-granule dynamics visualized *in vivo* with a phogrin–green fluorescent protein chimaera

Aristea E. POULI*, Evaggelia EMMANOUILIDOU*, Chao ZHAO*, Christina WASMEIER†, John C. HUTTON†, and Guy A. RUTTER*[1]

*Department of Biochemistry, School of Medical Sciences, University Walk, University of Bristol, Bristol BS8 1TD, U.K., and †Barbara Davis Center for Childhood Diabetes, University of Colorado Health Services Center, Box B140, 4200 East, 9th Avenue, Denver, CO 80262, U.S.A.

To image the behaviour in real time of single secretory granules in neuroendocrine cells we have expressed cDNA encoding a fusion construct between the dense-core secretory-granule-membrane glycoprotein, phogrin (phosphatase on the granule of insulinoma cells), and enhanced green fluorescent protein (EGFP). Expressed in INS-1 β-cells and pheochromocytoma PC12 cells, the chimaera was localized efficiently (up to 95%) to dense-core secretory granules (diameter 200–1000 nm), identified by co-immunolocalization with anti-(pro-)insulin antibodies in INS-1 cells and dopamine β-hydroxylase in PC12 cells. Using laser-scanning confocal microscopy and digital image analysis, we have used this chimaera to monitor the effects of secretagogues on the dynamics of secretory granules in single living cells. In unstimulated INS-1 β-cells, granule movement was confined to oscillatory movement (dithering) with period of oscillation 5–10 s and mean displacement < 1 μm. Both elevated glucose concentrations (30 mM), and depolarization of the plasma membrane with K^+, provoked large (5–10 μm) saltatory excursions of granules across the cell, which were never observed in cells maintained at low glucose concentration. By contrast, long excursions of granules occurred in PC12 cells without stimulation, and occurred predominantly from the cell body towards the cell periphery and neurite extensions. Purinergic-receptor activation with ATP provoked granule movement towards the membrane of PC12 cells, resulting in the transfer of fluorescence to the plasma membrane consistent with fusion of the granule and diffusion of the chimaera in the plasma membrane. These results illustrate the potential use of phogrin–EGFP chimeras in the study of secretory-granule dynamics, the regulation of granule–cytoskeletal interactions and the trafficking of a granule-specific transmembrane protein during the cycle of exocytosis and endocytosis.

INTRODUCTION

Glucose activates exocytosis of insulin from islet β-cells through an increase in intracellular free $[Ca^{2+}]$, prompting the fusion of granules located close to or docked at the plasma membrane [1]. Glucose may also promote the recruitment to the plasma membrane of granules located deeper within the β-cell interior [2,3]. Similarly, in adrenal chromaffin cells, neurotransmitter-induced $[Ca^{2+}]$ increases provoke the release of stored catecholamines [4]. Whether granules remote from the plasma membrane are recruited in this cell type is unclear.

Investigation of granule dynamics in living cells represents a considerable technical challenge. Techniques used in the past include cinematography and video-imaging of the movement of dense bodies (assumed to be secretory granules) in flattened cells, using a phase-contrast light microscope [2,3,5]. Recent studies [6–8] have employed granule-membrane cargo proteins, fused to green fluorescent protein (GFP) [9], to measure vesicle dynamics and exocytosis. However, these studies are hampered by the fact that only a proportion (40% [8] to 70% [6]) of the expressed fluorescent reporters are targeted correctly to mature secretory granules. Instead, there is significant retention of the proteins in the endoplasmic reticulum and trans-Golgi network [8] and direction of the proteins to other vesicles, possibly of the non-regulated secretory pathway [6]. This problem is also compounded by the uncertain stability and fluorescence properties of GFP in the low-pH environment of the granule lumen. Although the exocytotic event can be imaged by this approach, it is not possible to monitor the fate of the granule membrane, or membrane proteins, after fusion with the plasma membrane.

To monitor granule movement and exocytosis in single living cells we have constructed a recombinant cDNA encoding a chimaera between the granule-specific transmembrane glycoprotein phogrin (phosphatase on the granule of insulinoma cells) and an enhanced form of green fluorescent protein (EGFP) [9]. Phogrin was originally identified using antibodies to highly enriched insulinoma dense-core granule membranes to probe a rat insulinoma cDNA-expression library [10]. Phogrin (1004 amino acids) is a type I transmembrane glycoprotein of mature M_r 60000–64000, consisting of an N-terminal intralumenal domain, a transmembrane domain and a C-terminal cytosolic protein tyrosine phosphatase domain. When expressed in anterior pituitary AtT-20 cells in native form (J. C. Hutton, unpublished work), or as a fusion with aequorin in insulin-secreting INS-1 cells [11], phogrin is sorted efficiently to dense-core secretory granules, which constitute the major intracellular pool of the protein. Fusion of EGFP at the C-terminus of phogrin therefore is predicted to place EGFP exclusively on the outer surface of the granule, exposed to the cytosolic environment.

Using the phogrin–EGFP chimaera, we have examined the behaviour of dense-core secretory granules in two neuroendocrine cell types; islet INS-1 β-cells are a highly differentiated [12] and glucose-sensitive insulinoma cell line that provides a model of islet β-cells [13,14]. Pheochromocytoma cells are derived from

Abbreviations used: phogrin; phosphatase on the granule of insulinoma cells; GFP, green fluorescent protein; EGFP, enhanced green fluorescent protein; D-βH, dopamine β-hydroxylase.

[1] To whom correspondence should be addressed (e-mail g.a.rutter@bris.ac.uk).

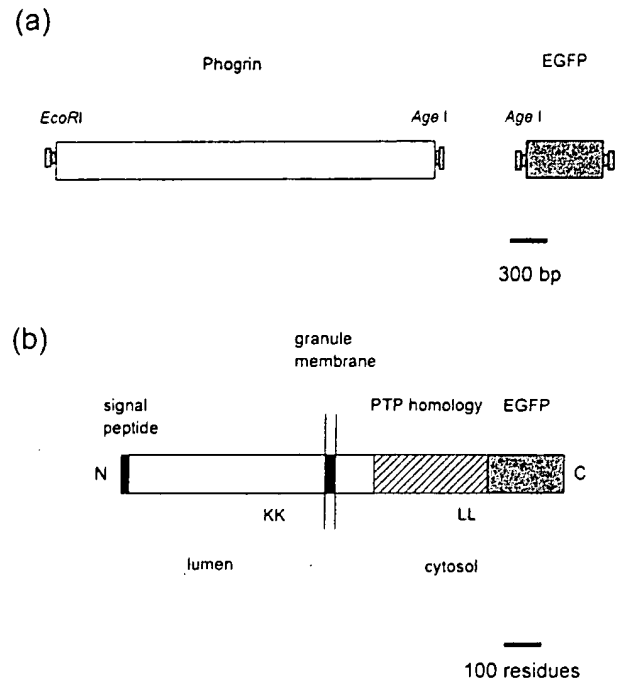

Figure 1 Construction and expression of phogrin–EGFP

(a) Strategy for phogrin–EGFP construction. cDNA encoding full-length phogrin, minus TAG stop codon (1003 amino acids), was generated by PCR amplification (see Methods section) with flanking *Eco*R1 and *Age*1 restriction sites. Ligation with *Age*1-digested plasmid pEGFP-N1 produced cDNA encoding the in-frame phogrin–EGFP chimaera. (b) Predicted type I membrane topology of the expressed chimaera, with EGFP lying on the cytosolic surface of the granule. The protein tyrosine phosphatase (PTP) domain, likely di-lysine (KK) cleavage site and di-leucine (LL) localization domain are shown.

an adrenal chromaffin cell tumour [15], secrete catecholamines, and are a widely used model of sympathetic neurones. We demonstrate that the phogrin–EGFP chimaera is targeted efficiently to dense-core secretory granules in each of these cell types. This allows the monitoring of granule movement before exocytosis, and the fate of this granule membrane protein after vesicle fusion.

Time-lapse movies accompany this paper, and are presented on the World Wide Web at the URLs given in the Figure legends.

MATERIALS AND METHODS

Materials

Tissue-culture reagents were obtained from Gibco-BRL Ltd. Guinea-pig anti porcine (pro-)insulin antiserum was obtained from Dako Ltd., Bucks, U.K, and rabbit anti-dopamine β-hydroxylase (D-βH) antibodies from Biogenesis (Poole, Dorset, U.K.). Other reagents were from Boehringer Mannheim (Mannheim, Germany) or Sigma (Poole, Dorset, U.K.).

Methods

Plasmid construction

cDNA encoding the entire coding region of phogrin was amplified by PCR using ExpandTaq® (Boehringer Mannheim) with forward primer 5′-T.TTT.GAA.TTC.GAC.GAG.ATG.GGG.-CTA.CCG.CTC.CG-3′, including an *Eco*R1 restriction site (underlined), and a Kozak sequence, and reverse primer 5′-TTT.TAC.CGG.TCC.CTG.GGG.AAG.GGC.CTT.CAG-3′ (with *Age*1 site underlined). The 3.01 kb PCR product was digested and subcloned into plasmid pN1-EGFP (Clontech) encoding EGFP ($S^{65}T$, $F^{64}L$, and codon-usage mutations) under cytomegalovirus immediate-early gene promoter control.

Cell culture and microinjection

INS-1 [12,14] and PC12 [11] cells were cultured as described previously, on poly-L-lysine (Sigma) or collagen (murine type IV; Becton-Dickinson Labware, MA, U.S.A.)-coated coverslips, respectively. cDNA was introduced by microinjection at 0.35 mg·ml^{-1} in 2 mM Tris/HCl/0.2 mM EDTA (pH 8.0) as described [16]. Following microinjection, cells were incubated for 16–24 h in an atmosphere of 5% CO_2.

Immunocytochemistry

Cells were fixed and permeabilized 24 h after microinjection with 4% (v/v) paraformaldehyde/0.2% Triton X-100. Intrinsic EGFP fluorescence was maintained under these conditions. Primary polyclonal antibodies to (pro-)insulin (1:100 dilution) and to D-βH (1:100 dilution) were revealed with tetramethylrhodamine-conjugated secondary antibodies, in 0.1% (v/v) BSA. Cells were washed with PBS between incubations and mounted on coverslips with Mowiol before analysis. Confocal images were captured using a laser-scanning confocal microscope (Leica TCS 4D/DM IRBE; 63×/1.32 NA PL-Apo oil-immersion lens) equipped with a krypton/argon laser (488 and 568 nm excitation lines), and analysed off-line using Adobe Photoshop 3.0®.

In vivo confocal imaging

Prior to imaging, cells were incubated for 30 min in Krebs-Ringer medium comprising 125 mM NaCl, 3.5 mM KCl, 1.5 mM $CaCl_2$, 0.5 mM $MgSO_4$, 0.5 mM KH_2PO_4, 2.5 mM $NaHCO_3$, 3 mM glucose, and 10 mM HepesNa$^+$ (pH 7.4), equilibrated with a 95:5 O_2:CO_2 mixture. Cells were then transferred to the thermostat-controlled (37 °C) stage of a Leica TCS 4D/DM IRBE inverted-optics confocal microscope, fitted with a 40×/1.0 NA PL Fluotar oil-immersion objective, and controlled by TCS-NT4 software (Leica). Cells were maintained in Krebs-Ringer medium (0.5 ml), which was replaced with the same medium but containing additions (pre-warmed to 37 °C) when required (exchange time < 15 s). Two scans were performed for each image; this allowed capture of images of sufficient quality for image analysis every 5 s, and ensured minimum bleaching of EGFP fluorescence. Laser power did not exceed 50% and typical pinhole sizes and photomultiplier gains were 0.4 μm and 500–580/1000, respectively.

Image analysis

Images were exported as TIFF files and processed using Adobe Photoshop 3.0®. After conversion of files to GIF format (PaintShop Pro), time-lapse image sequences were prepared using a GIF construction set (Shareware, URL http://www.mindshop.com). Scale bars were calculated using the Leica software; in a typical experiment (40× objective magnification, 4× zoom) the 512×512-pixel image corresponded to a 60×60 μm box (i.e. 0.117 μm pixel width).

Granule movement was analysed using NIH Image (freeware from ftp://zippy.nimh.nih.gov/pub/image/) and GIF construction sets. The velocity of individual granules was calculated from the movement between successive images.

Insulin radio-immunoassay

INS-1 cells were cultured, for 48 h in 96-well microtitre plates, before the assay of insulin release in Krebs-Ringer medium (for details see above) [13] by competitive radio-immunoassay (Linco Res. Inc., MO, U.S.A.).

Statistical analysis

Data are given as the mean ± S.E.M. for the number of observations shown. Statistical significance was calculated with paired Student's *t*-tests, assuming equal variances.

RESULTS

Imaging granule movement in INS-1 β-cells with expressed phogrin–EGFP

The structure of the chimaeric phogrin–EGFP cDNA construct, and the domain structure and predicted topology of the expressed recombinant protein, are shown in Figure 1.

Using immuno-electron microscopy and an incorporated epitope tag, we have demonstrated previously that a chimaera similar to phogrin–EGFP, phogrin aequorin [11], is targeted efficiently at (pro-)insulin-containing granules in INS-1 cells. In the present study, we used confocal microscopy to determine the subcellular distribution of the intrinsic fluorescence of the phogrin–EGFP chimaera, compared with that of immunostained insulin. This approach was complicated by the fact that permeabilization adequate to allow labelling of secretory granules with anti-insulin antibodies caused a loss of EGFP-derived fluorescence. Thus, strong EGFP-derived fluorescence was usually observed in cells that were not labelled with anti-insulin antibodies. Nevertheless, under optimal permeabilization conditions, expressed phogrin–EGFP was localized in INS-1 cells to > 95% of insulin-containing vesicles (Figures 2a–c). However, approx. 60% co-localization to (pro-)insulin-containing structures (Figures 2d–f) was observed more usually, as a result of the above limitation. In cells where close co-localization between the chimaera and insulin was revealed, we could not detect phogrin–EGFP-positive, insulin-negative, nor phogrin–EGFP-negative, insulin-positive structures (data taken from > 50 individual INS-1 cells from 4 separate cultures). However, there were significant differences in the ratio of phogrin : insulin-derived

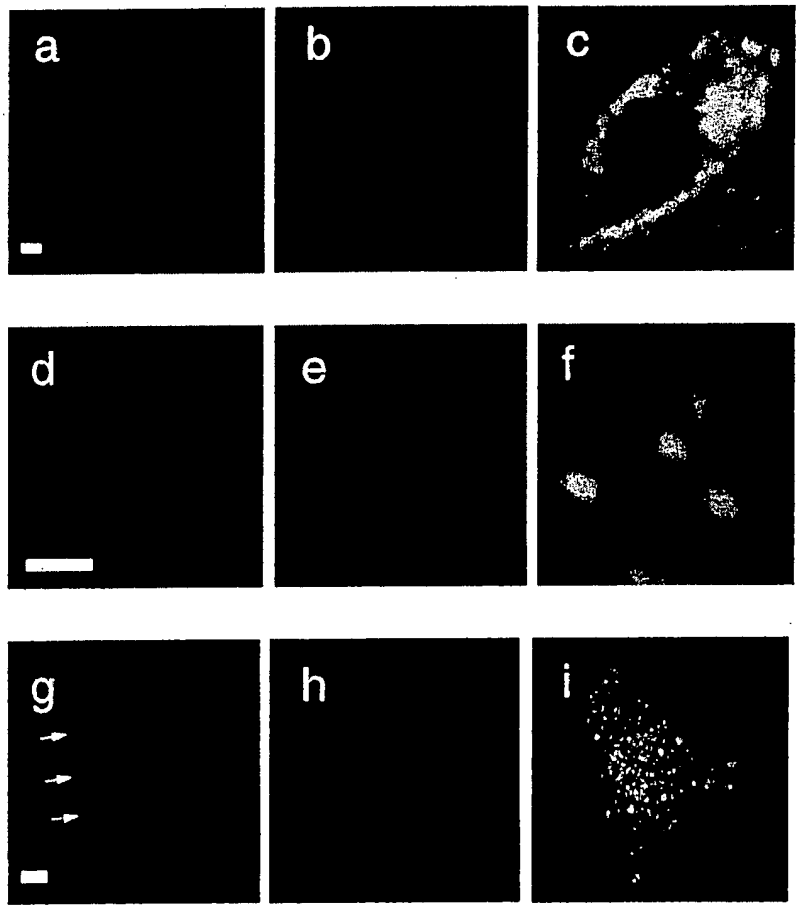

Figure 2 Localization of phogrin–EGFP to dense-core secretory vesicles in INS-1 and PC12 cells

(**a–c**) Co-localization with (pro-)insulin in INS-1 β-cells. Cells expressing phogrin–EGFP were fixed and probed with polyclonal anti-(pro-)insulin antiserum, followed by tetramethyl-rhodamine (TRITC)-conjugated rabbit anti-guinea-pig IgG as secondary antibody. (**a**) Intrinsic EGFP fluorescence (488 nm excitation); (**b**) TRITC-fluorescence (568 nm excitation); (**c**) overlay of (**a**) and (**b**). (**d**, **e**) As (**a–c**) but with a different individual cell, examined at higher magnification (scale bar = 1 μm). (**f**) Overlay of (**d**) and (**e**). (**g–i**) Co-localization of phogrin–EGFP with D-βH in fixed PC12 cells probed with polyclonal rabbit anti-D-βH primary antibody, and TRITC-conjugated anti-rabbit IgG as secondary antibody. Note the close colocalization observed in the arrowed granules. Scale bars = 2 μm.

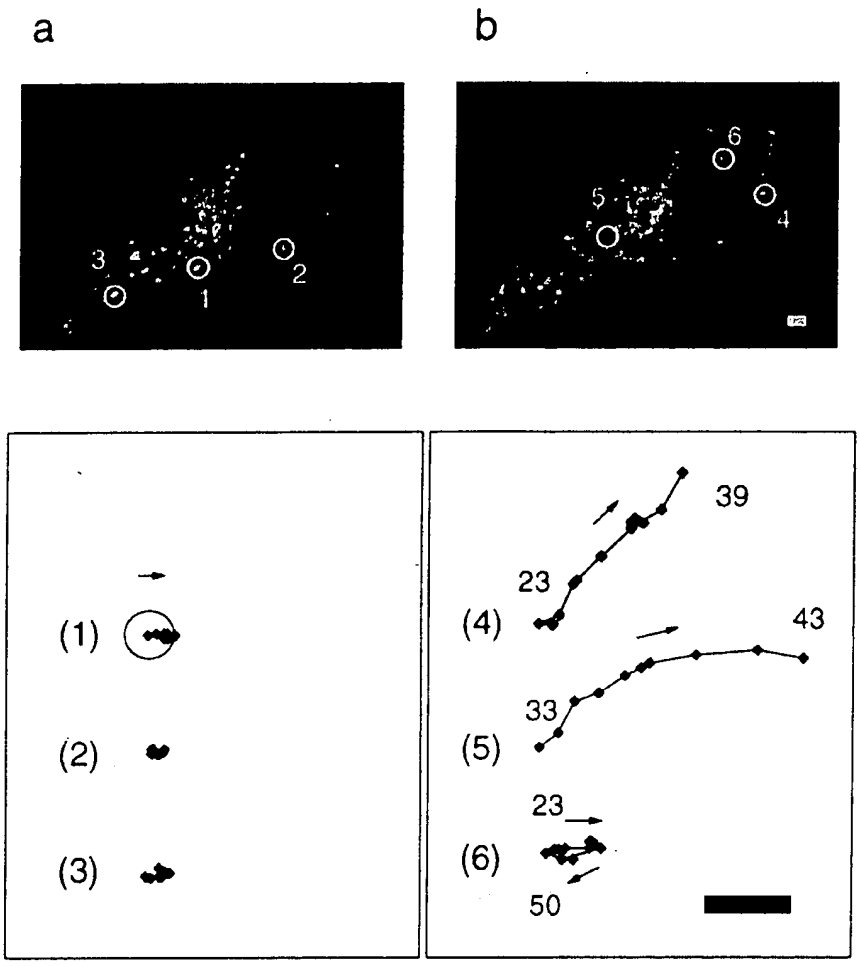

Figure 3 Effect of glucose on dense-core secretory-vesicle dynamics in living INS-1 cells

Fluorescence was monitored in a single INS-1 cell expressing phogrin–EGFP, by scanning confocal microscopy. Images were the mean of two scans obtained within a 5 s interval, as described in the Methods section. (**a**) One image of 15 obtained in the presence of 3 mM glucose; (**b**) Image 16 of 35 obtained after addition of 30 mM glucose. Images were corrected off-line for progressive fluorescence loss by photobleaching (approx. 20% during the course of the experiment). These images are presented as time-lapse movies that can be accessed through the World Wide Web by connecting to URL: http://www.BiochemJ.org/bj/333/bj3330193add.htm. The presence of glucose at 30 mM is indicated in the time-lapse movie. The movement of the individual granules shown (lower panels) was plotted from the obtained confocal images using NIH Image. The initial position of the centre of each granule (approx. size indicated by the circle) was that in image 1 (left panel, 3 mM glucose). In the right panel (30 mM glucose), numbers indicate the frame number in which the granule occupied the position shown. Scale bars = 2 μm.

fluorescence between individual granules (Figure 2, a versus b). The dimensions of the doubly labelled structures (200–500 nm) corresponded closely with those of dense-core secretory vesicles [17].

The majority of granules that could be observed in the focal plane (approx. 500 nm deep) of an individual living INS-1 cell displayed linear, back-and-forth movements, with a period (5–7 s) close to that of the rate of data acquisition (Figure 3). The amplitude of these movements was within 2–3 times the diameter of the granule. Analysis of the movement of granules in a further single cell is presented in Table 1. Maintained in low glucose concentration (3 mM), no granule was observed to move more than 1 μm (approx. 5 granule diameters) from its point of origin during a typical 2.5 min observation (data taken from 18 individual cells from separate cultures). Elevation of the glucose concentration to 30 mM, sufficient to provoke a 2.2-fold increase in insulin release from cell populations (Table 1), increased markedly the movement of the granules (Figure 3; Table 1). Under these conditions, it was possible to detect the movement of individual granules over much longer distances (up to 5 μm). For example, elevation of glucose concentration provoked the excursion of two granules in the cell shown in Figure 3(b) (granules #4 and #5). In this experiment, granules can also be seen to be moving in and out of the focal plane (i.e. along the z axis) after the addition of 30 mM glucose. In seven out of eight separately cultured cells examined in the presence of 30 mM glucose, the movement of two or more granules in this manner was detectable in a 2.5 min data-acquisition period.

This effect of glucose was also mimicked by cell depolarization provoked with 70 mM KCl. Measured in cell populations, stimulation with high K^+ concentration (56 mM), led to a 2.7-fold stimulation of insulin release (Table 1). In Figure 4, a single INS-1 cell was maintained initially in the presence of 3 mM glucose before the addition of 70 mM K^+ (indicated in the time-lapse movie). The granule in the centre of the cell (over the nuclear region, granule #5) remains fixed during three acquisition

Table 1 Effect of glucose and KCl on granule movement and insulin secretion in INS-1 cells

Granule movement was determined for a single INS-1 cell. Individual granules were identified and the maximum distance moved (in granule diameters) by each granule from its starting position was calculated during 15 data acquisitions (75 s). The number of individual granules examined is given in parentheses. High [KCl] = 70 mM (granule movement) or 56 mM (insulin release). Insulin release (ng of insulin · 100000 cells^{-1} · 30 min^{-1}) was measured in four separate cultures. $^{*}p < 0.05$, $^{***}p < 0.001$ for the effect of 30 mM glucose.

Concentration (glucose or K^+)	Granule movement (diameters)	Insulin secretion
3 mM glucose	0.7 ± 0.17 (26)	9.1 ± 2.1
30 mM glucose	3.2 ± 0.58*** (20)	17.1 ± 2.3*
3 mM glucose	1.08 ± 0.26 (15)	9.1 ± 2.1
3 mM glucose + high KCl	4.42 ± 2.03* (13)	24.5 ± 2.4*

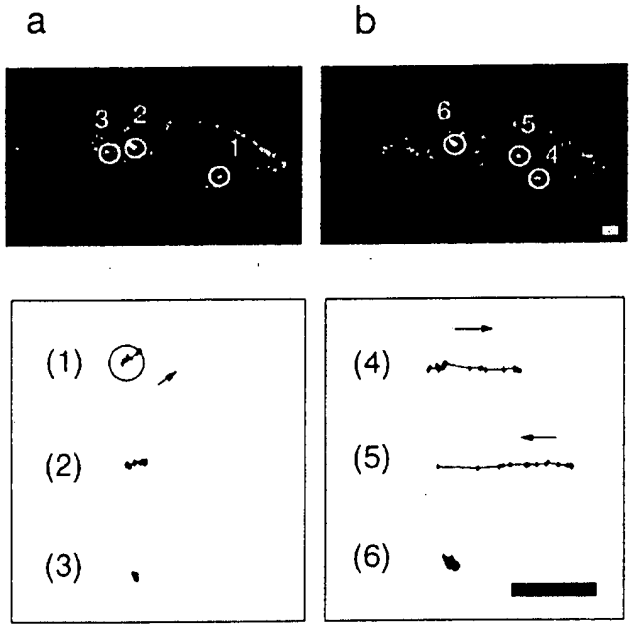

Figure 4 Effect of K^+ on secretory-vesicle dynamics in living INS-1 cells

Fluorescence was monitored as described in the Figure 3 legend. (**a**) Image 1 of 15 acquired in the presence of 3 mM glucose alone. (**b**) Image 1 of 24, obtained in the presence of 70 mM KCl. Note the movement of the indicated granules (see the Results section for further details). Bleaching of fluorescence was minimal in this experiment, and the images are shown as raw data. These images are presented as time-lapse movies that can be accessed through the World Wide Web by connecting to URL: http://www.BiochemJ.org/bj/333/bj3330193add.htm. Movement of the indicated granules is shown in the corresponding panels. Scale bars = 2 μm.

periods after K^+ addition, before moving approx. 2 μm in the next three frames, pausing and then moving approx. 4 μm in the next three frames. This represents a maximum velocity of approx. 0.2 $\mu m \cdot s^{-1}$. Similar behaviour was noted in a further granule (#4), whereas a third (#6) barely moved from its point of origin.

No clear evidence of fusion of phogrin–EGFP-containing granules with the plasma membrane was apparent in INS-1 cells. This may reflect either (i) the relatively low exocytotic activity of this cell type, or (ii) a transient interaction between phogrin–EGFP and the plasma membrane, which does not lead to net accumulation of fluorescence. We therefore sought evidence for membrane fusion in an alternative neuroendocrine cell type, PC12 cells, which exhibit a substantially higher secretion rate in terms of percentage loss of cellular hormone content over time.

Granule movement and exocytosis in PC12 cells

We have reported previously [11] that PC12 cells respond dramatically to stimulation with the purinergic receptor agonist, providing robust exocytosis, monitored by the recruitment to the plasma membrane of the lipophilic dye, FM1-43 [18]. Phogrin–EGFP was targeted efficiently to dense-core granules in PC12 cells, again co-localizing closely with the dense-core granule marker, D-βH (Figures 2d–f). In these cells, which had evident neurite extensions, movement of vesicles from the centre of the cells and into the neurites was clearly apparent, even in this absence of a stimulus (Figure 5a). The maximum velocity achieved in these long excursions was similar to that of INS-1 granules, i.e. approx. 0.2–0.5 $\mu m \cdot s^{-1}$. Stimulation of PC12 cells with ATP activates P_{2U} purinergic receptors and produces sustained increases in intracellular [Ca^{2+}] [11]. ATP challenge caused apparently directed movement of granules towards the plasma membrane (Figure 5b). This led to a clear increase in plasma-membrane luminescence (Figure 5, c versus b), presumably the result of the arrival and diffusion of the labelled phogrin during exocytosis, followed by diffusion into the plasma membrane.

DISCUSSION

We have compared the dynamics of vesicle movements in INS-1 β-cells and PC12 neurones, using a phogrin–EGFP chimaera. This chimaera was targeted to secretory vesicles in both cell types, causing the intense fluorescence of individual granules. This allows granule movement to be monitored readily by laser-scanning confocal microscopy. As such, the technique offers a number of advantages over those used previously to monitor granule movement and exocytosis in living β-cells. The complete co-localization of the chimaera with insulin or D-βH eliminates concerns about the identity of the observed granule, a problem which hampers the use of cargo proteins to target GFP to granules [6–8]. Compared with phase-contrast video-microscopy, the use of phogrin–EGFP only detects the movement of granules, with other dense-core bodies (lysosomes, for example) being unlabelled. Furthermore, the use of digital confocal imaging allows analysis of cells with unflattened morphology, which is difficult or impossible with phase-contrast microscopy [2]. Finally, this technique allows conventional confocal microscopy to be employed to monitor the recruitment of a vesicle-membrane protein to the plasma membrane during exocytosis. This eliminates the need for specialized evanescence-wave approaches [6].

In the two cell types examined, the behaviour of secretory granules was quite distinct, both in unstimulated cells and after stimulation with [Ca^{2+}]-raising secretagogues. In unstimulated INS-1 β-cells, granule movement was confined to small oscillatory movements, typically of less than 2–3 granule diameters from the starting location during a 2.5 min observation period. High glucose or K^+ concentrations increased the likelihood of these movements (Table 1), and also provoked longer, saltatory excursions of the granules (Figures 3 and 4). These appeared linear, undirected, and occurred with equal probability towards or away from the plasma membrane. Since these movements can only be detected if they occur in the focal plane, our observation of up to three granules making this movement per cell is a

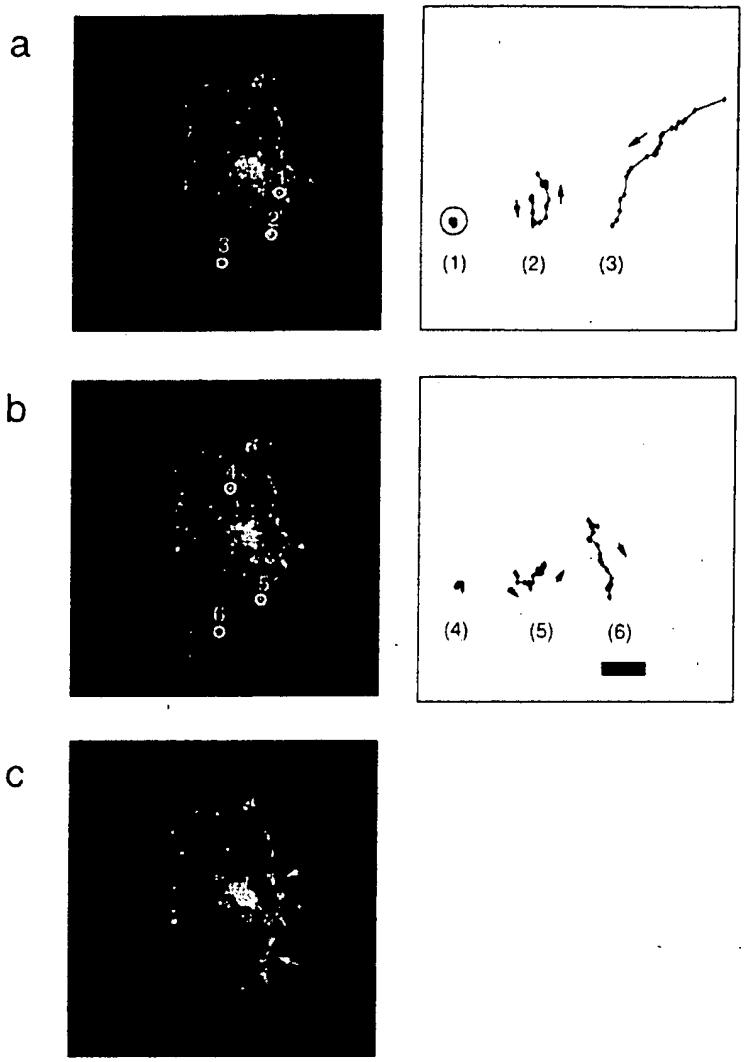

Figure 5 Effect of ATP on secretory-granule dynamics in living PC12 cells

Vesicle dynamics were measured by image acquisition at 5 s intervals in a cell incubated (**a**) in unmodified Krebs-bicarbonate medium containing 3 mM glucose (image 1 of 30; note the movement of vesicles towards neurite extensions; granule #3); (**b**) after the addition of 50 μM ATP (image 1 of 30); or (**c**) 175 s after the addition of ATP (image 30 of 30). Note the accumulation of membrane fluorescence after stimulation with ATP (29 and 62.5% increases in a 30 × 50-pixel box corresponding to the regions marked by the upper and lower arrows, respectively). A smaller (19%) increase in fluorescence was also apparent in the perinuclear region, whereas a decrease (21%) was observed in a region of the cell distant from the nucleus (in the bottom left of the image). Scale bar = 2 μm. These images are presented as time-lapse movies that can be accessed through the World Wide Web by connecting to URL: http://www.BiochemJ.org/bj/333/bj3330193add.htm.

considerable underestimate of the total number occurring throughout the whole cell. These movements are likely to represent the previously described motion of secretory vesicles in islet β-cells [2,3], most probably along microtubular tracks [19]. An intriguing possibility is that the pauses during movements might correspond to the transfer of a granule between successive microtubular tracks.

The rate of movement of the granules measured in these studies with phogrin–EGFP were comparable with those measured by video microscopy in long-term cultures of islet β-cells [2,3] and in the HIT-T15 β-cell line [5]. Although it is impossible to be certain that the measurements made in the earlier studies described only the movement of secretory granules (and not other dense bodies such as lysosomes), the fact that similar behaviour could be detected in granules bearing phogrin–EGFP suggests that the expressed chimaera did not interfere with the machinery responsible for granule movement. Furthermore, in the current studies with INS-1 β-cells, the effect of increasing glucose from 3 to 30 mM (Figure 3; Table 1) was more dramatic than observed in earlier work [2,3] and exceeded the stimulation of exocytosis measured in cell populations. In particular, we failed to observe any long saltatory granule movements in unstimulated INS-1 cells. This suggests that these may play an important role in the activation of exocytosis by nutrient secretagogues, including glucose. Consistent with an important role for glucose-induced increases in intracellular [Ca^{2+}], the effects of glucose could be mimicked by the activation of Ca^{2+} influx by cell depolarization with KCl.

By contrast, long saltatory granule movements were apparent in PC12 cells even in the absence of intracellular [Ca^{2+}]-raising

agents (Figure 5). These appeared to be directed from the cell interior outwards, i.e. towards the plasma membrane and into neurite extensions. This apparent, predominantly anterograde, movement is therefore compatible with previous observations in which the movement of acidic granules was monitored by enhanced video microscopy after loading AtT-20 cells with acridine orange [20]. This technique, which involved fixation *post-facto* and immunocytochemistry to reveal adrenocorticotrophin-containing granules, indicated that the majority of these secretory granules moved in the anterograde direction. In further agreement with the results of Kreis et al. [20], we also observed that phogrin–EGFP-labelled vesicles undergoing long saltatory jumps did not usually change direction (Figures 5a and 5b, granules #3 and #6). Such behaviour is suggestive of movement along linear microtubules, driven by anterograde motors. Nevertheless, shorter excursions were associated with reversal of direction (Figures 5a and 5b, granules #2 and #5), indicating that 'hopping' between microtubules could occur under these circumstances.

In our studies, increases in intracellular [Ca^{2+}] provoked with ATP apparently increased the number of directed movements of vesicles in PC12 cells. This resulted in clear increases in fluorescence associated with the plasma membrane (Figures 5b and 5c). Thus, secretion in PC12 cells appeared to be associated with the recruitment of the secretory-vesicle granule protein phogrin into the membrane. In this respect, the behaviour of phogrin–EGFP may be similar to that of the granule membrane protein D-βH, examined in intact chromaffin cells [21].

In summary, we describe a new method of selectively monitoring dense-core secretory-granule movement in single living neuroendocrine cells. This involves the use of a granule-membrane-located EGFP fusion protein, and laser-scanning confocal microscopy. This approach reveals important differences in the behaviour of secretory granules in islet INS-1 β-cells and in a model of sympathetic neurones, the PC12 cell. These differences may be related to the regulation of secretion from these cell types by distinct secretagogues *in vivo*, i.e. responsiveness of β-cells to nutrient secretagogues plus modulatory neurotransmitters [22], and of chromaffin cells to neurotransmitters alone. The molecular basis of these differences remains unknown, and will require analysis of the motor and other proteins involved in the transport of secretory granules in these cell types [19].

Received 13 March 1998/14 April 1998; accepted 24 April 1998

We thank the Wellcome Trust, the Medical Research Council (U.K.), the Royal Society, the British Diabetic Association, the Juvenile Diabetes Foundation and the Christine Wheeler Bequest for financial support. We also thank the Medical Research Council for providing an Infrastructure Award to establish the Bristol School of Medical Sciences Cell Imaging Facility, and Dr M. Jepson, A. Leard and E. Basham for technical assistance. A. E. P. is a Bristol University Research Scholar.

REFERENCES

1 Ashcroft, F. M. and Kakei, M. (1989) J. Physiol. (London) **416**, 349–367
2 Lacy, P. E., Finke, E. H. and Codilla, R. C. (1975) Lab. Invest. **33**, 570–576
3 Somers, G., Blondel, B., Orci, L. and Malaisse, W. J. (1979) Endocrinology **104**, 255–264
4 Augustine, G. J. and Neher, E (1992) J. Physiol. (London) **450**, 247–271
5 Hisatomi, M., Hidaka, H. and Niki, I. (1996) Endocrinology **137**, 4644–4649
6 Lang, T., Wacker, I., Steyer, J., Kaether, C., Wunderlich, I., Soldati, T., Gerdes, H. H. and Almers, W. (1997) Neuron **18**, 857–863
7 Wacker, I., Kaether, C., Kromer, A., Migala, A., Almers, W. and Gerdes, H. H. (1997) J. Cell Sci. **110**, 1453–1463
8 Pouli, A. E., Kennedy, H. J., Schofield, J. G. and Rutter, G. A. (1998) Biochem. J. **331**, 669–675
9 Heim, R., Cubitt, A. B. and Tsien, R. Y. (1995) Nature (London) **373**, 663–664
10 Wasmeier, C. and Hutton, J. C. (1996) J. Biol. Chem. **271**, 18161–18170
11 Pouli, A. E., Karagenc, N., Arden, S., Bright, N., Schofield, G. S., Hutton, J. C. and Rutter, G. A. (1998) Biochem. J. **330**, 1399–1404
12 Asfari, M., Janjic, D., Meda, P., Li, G., Halban, P. A. and Wollheim, C. B. (1992) Endocrinology **130**, 167–178
13 Sekine, N., Cirulli, V., Regazzi, R., Brown, L. J., Gine, E., Tamarit-Rodriguez, J., Girotti, M., Marie, S., MacDonald, M. J., Wollheim, C. B. and Rutter, G. A. (1994) J. Biol. Chem. **269**, 4895–4902
14 Rutter, G. A., Theler, J.-M., Murta, M., Wollheim, C. B., Pozzan, T. and Rizzuto, R. (1993) J. Biol. Chem. **268**, 22385–22390
15 Greene, L. A. and Tischler, A. S. (1976) Proc. Natl. Acad. Sci. U.S.A. **73**, 2424–2428
16 Rutter, G. A., Burnett, P., Rizzuto, R., Brini, M., Murgia, M., Pozzan, T., Tavare, J. M. and Denton, R. M. (1996) Proc. Natl. Acad. Sci. U.S.A. **93**, 5489–5494
17 Bonner-Weir, S. (1988) Diabetes **37**, 616–621
18 Smith, C. B. and Betz, W. J. (1996) Nature (London) **380**, 531–534
19 Hirokawa, N. (1998) Science **279**, 519–526
20 Kreis, T. E., Matteoni, R., Hollinshead, M. and Tooze, J. (1989) Eur. J. Cell Biol. **49**, 128–139
21 Hurtley, S. M. (1993) J. Cell Sci. **106**, 649–655
22 Rorsman, P. (1997) Diabetologia **40**, 487–495

[CANCER RESEARCH 58, 4752–4757, October 15, 1998]

Transforming Growth Factor β Signaling through Smad1 in Human Breast Cancer Cells[1]

Xiaojie Liu, Jianho Yue, Randall S. Frey, Qichao Zhu, and Kathleen M. Mulder[2]

Department of Pharmacology, Pennsylvania State University College of Medicine, Hershey, Pennsylvania 17033

ABSTRACT

Previous results have suggested that Smad1 transduces signals in response to bone morphogenetic proteins (BMPs), but not in response to transforming growth factor β (TGF-β). Here we investigated the ability of TGF-β to regulate Smad1 phosphorylation, hetero-oligomerization with Smad4, translocation to the nucleus, and transcriptional activation of 3TP-luciferase reporter activity in TGF-β- and BMP-responsive Hs578T human breast cancer cells. We demonstrate that Smad1 was rapidly phosphorylated *in vivo* in response to both TGF-β_3 and BMP2 as determined using an antibody against the epitope-tagged Smad1 being expressed. In addition, both TGF-β_3 and BMP2 increased Smad1-Smad4 hetero-oligomerization in Hs578T cells. Visualization of Smad1 nuclear translocation with the aid of green fluorescent protein (GFP) in live cells demonstrated nuclear accumulation of GFP-Smad1 fluorescence in response to either TGF-β or BMP2 stimulation. After ligand stimulation, approximately 60–70% of transfected cells displayed prominent nuclear fluorescence. Expression of Smad1 in Hs578T cells increased the activity of the TGF-β-responsive reporter 3TP-Lux. Moreover, TGF-β treatment further potentiated the effect of Smad1 on 3TP-luciferase activity. Collectively, our results demonstrate that TGF-β as well as BMP can signal through Smad1.

INTRODUCTION

TGF-β[3] is a multifunctional factor that regulates a number of cellular responses including cell growth, differentiation, extracellular matrix production, and apoptosis, depending on the cell type (1–3). This polypeptide signals through two types of transmembrane serine/threonine kinase receptors, RI and RII. The ligand binds to RII, which appears to recruit and result in RI phosphorylation (4–8). Activation of these receptors mediates the cellular effects of TGF-β. Thus far, events downstream of TGF-β receptor activation are poorly understood, although several distinct types of signaling components have been described as participants in the TGF-β signaling cascade in untransformed epithelial cells. These include protein kinase C, phospholipase C, protein phosphatase 1, Ras, mitogen-activated protein kinases, stress-activated protein kinases, and the Smads (Sma and Mad homologues; Refs. 1 and 9–19).

Among those components mentioned above, Smads were recently identified as important signaling components for several members of the TGF-β superfamily (15–19). Smads contain highly conserved regions at the amino- and carboxyl-terminal domains, which are connected by a proline-rich linker region. A pathway-restricted phenomenon has been reported for Smad1, Smad2, Smad3, and Smad5 (16–17). For example, it has been suggested that Smad1 and Smad5 are relatively specific for BMP signaling, whereas Smad2 and Smad3 mediate TGF-β and activin signaling. The current working model for Smad regulation consists of sequential activation events that occur after receptor activation. These include phosphorylation of pathway-restricted Smads (*i.e.*, Smad1, Smad2, and Smad3), heteromeric complex formation of these Smads with Smad4 (the common partner Smad), translocation to the nucleus, and activation of gene transcription (20–25). This model is currently being tested by a number of laboratories in the TGF-β field.

The involvement of Smad1 in BMP signaling has been clearly demonstrated (26–29). In contrast, studies in TGF-β-resistant cell lines, which have been transfected with TGF-β receptors, suggest that Smad1 is not a signaling intermediate for TGF-β. It is possible that overexpression of TGF-β receptors in these cells may not be sufficient to transduce TGF-β signals. Several investigators have previously reported that TGF-β induced endogenous Smad1 phosphorylation *in vivo* (30, 31). However, the anti-Smad1 antibodies used in these studies recognized other Smad family members. Thus far, studies have not directly examined the effects of TGF-β on each of the Smad1 activation events in epithelial cells that are naturally sensitive to TGF-β.

In this study, we examined whether TGF-β could regulate each of the activation steps for Smad1. For these studies, we used a model system that displays natural sensitivity to both TGF-β and BMPs. Our results demonstrate that TGF-β and BMP are equally effective in inducing Smad1 phosphorylation, heteromeric complex formation with Smad4, and nuclear translocation. Furthermore, expression of Smad1 increases the activity of the TGF-β-responsive reporter 3TP-Lux in these cells. TGF-β treatment potentiates the effects of Smad1 on 3TP-luciferase activity. Together, this report provides strong evidence that Smad1 can be activated by TGF-β in a manner similar to that of BMPs.

MATERIALS AND METHODS

Materials. Rabbit anti-HA, anti-Flag, and anti-His polyclonal antibodies were obtained from Santa Cruz Biotechnology, Inc. (Santa Cruz, CA). The anti-Flag M2 monoclonal antibody was obtained from Eastman Kodak Co. (Rochester, NY). The 6XHis monoclonal antibody and pEGFP-C1 protein fusion vector were purchased from Clontech Laboratories, Inc. (Palo Alto, CA). The pcDNA3.1 expression vector was obtained from Invitrogen Corp. (Carlsbad, CA). [^{3}H]Thymidine and [^{32}P]orthophosphate were purchased from DuPont New England Nuclear (Boston, MA).

Construction of Smad1 Expression Vectors. RSmad1 was cloned by screening a cDNA library derived from an untransformed rat IEC line, IEC 4-1 (1, 34). Mammalian expression vectors (pCGN and pcDNA3.1) containing the entire coding region of RSmad1 were constructed. These constructs included either HA or 6XHis epitopes at the amino terminus of RSmad1 and were used in *in vivo* phosphorylation and in the Smad1-Smad4 heteromeric complex formation assays. To construct the GFP-RSmad1 plasmid, a 1.57-kb cDNA fragment of RSmad1 was blunted at both ends and inserted into the multiple cloning site (*Xmal*) of the pEGFP-C1 protein fusion vector (Clontech Laboratories, Inc.). The correct orientation and reading frame of the recombinant plasmids were verified by DNA sequencing. The pRK5-Smad4 Flag plasmid (21) and the p3TP-Lux reporter construct (35) were generous gifts from Dr. R. Derynck (University of California at San Francisco, San Francisco, CA) and Dr. J. Massague (Memorial Sloan-Kettering Cancer Center, New York, NY), respectively.

Received 5/8/98; accepted 8/17/98.

The costs of publication of this article were defrayed in part by the payment of page charges. This article must therefore be hereby marked *advertisement* in accordance with 18 U.S.C. Section 1734 solely to indicate this fact.

[1] Supported by NIH Grants CA51425, CA54816, and CA68444 (to K. M. M.). K. M. M. is a recipient of NIH Research Career Development Award K04 CA59552.

[2] To whom requests for reprints should be addressed, at Department of Pharmacology (H078), Pennsylvania State University College of Medicine, 500 University Drive, Hershey, PA 17033. Phone: (717) 531-6789; Fax: (717) 531-5013; E-mail: kmm15@psu.edu.

[3] The abbreviations used are: TGF-β, transforming growth factor β; BMP, bone morphogenetic protein; RSmad1, rat Smad1; IEC, intestinal epithelial cell; PAI-1, plasminogen activator inhibitor 1; BCC, breast cancer cell; GFP, green fluorescent protein.

Cell Culture. Hs578T MCF-7 human BCCs were obtained from the American Type Culture Collection and maintained as described previously (12, 13).

Thymidine Incorporation. Hs578T cells were plated at cell densities of 6.66×10^4 cells/cm^2 in 12-well plates. Twelve h later, the medium was changed to serum-free conditions for 13 h. TGF-β_3 (10 ng/ml) or BMPs (50 ng/ml) were added to the appropriate wells, followed by incubation for an additional 24 h. The above concentrations for TGF-β_3 and BMPs were chosen to give optimal responses according to previous publications (12, 20, 26). Incorporation of [^{3}H]thymidine into DNA was determined as described previously (12, 13).

***In Vivo* Phosphorylation of Smad1 in Hs578T Cells.** Hs578T cells were transfected with 10 μg of HA-tagged RSmad1 by calcium phosphate coprecipitation for 21 h in a 3% CO_2 atmosphere at 35°C (36). Cells were then labeled with [^{32}P]orthophosphate (1 mCi/ml) for 3 h at 37°C in phosphate-free, serum-free DMEM, followed by treatment with TGF-β_3 or BMP2 for the indicated times. Samples were normalized for radioactivity as determined by trichloroacetic acid precipitation. Samples were then immunoprecipitated with an anti-HA antibody (Santa Cruz Biotechnology, Inc.) for 1 h at 4°C. Immunocomplexes collected on protein A-Sepharose beads were resolved by 12% SDS-PAGE. Gels were stained with Coomassie Blue, dried, and exposed to X-ray film at −70°C.

Smad1-Smad4 Heteromeric Complex Formation. Hs578T or MCF-7 cells were plated as described above in 100-mm tissue culture dishes (12–13). Twenty-four h later, cells were cotransfected with 10 μg of Flag-tagged Smad4 and His-tagged RSmad1 by the calcium phosphate method. Forty-eight h later, the medium was changed to serum-free conditions for 30 min. Transfected cells were treated with TGF-β_3 or BMP2 for 1 h and lysed in lysis buffer [10 mM Tris (pH 7.8), 150 mM NaCl, 0.5% NP40, 1 mM phenylmethylsulfonyl fluoride, 5 mM benzamidine, 10 μg/ml aprotinin, 10 μg/ml leupeptin, and 1% Triton X-100]. Cell lysates were immunoprecipitated with either 6XHis monoclonal antibody (Clontech Laboratories, Inc.) or anti-Flag M2 monoclonal antibody (Eastman Kodak Co.). Immunoprecipitates were separated by 12% SDS-PAGE and transferred to Immobilon-P membranes (Millipore). Tagged proteins were detected by Western blotting using rabbit polyclonal anti-Flag or anti-His antibodies (Santa Cruz Biotechnology, Inc.). Smad1-Smad4 heteromeric complex formation was quantified by densitometry and corrected for the expression levels of Smad4.

Visualization of GFP-Smad1 Cytoplasmic to Nuclear Translocation in Hs578T Cells *in Vivo*. Hs578T cells were plated in 60-mm tissue culture dishes and transiently transfected with 4 μg of GFP or GFP-RSmad1 plasmid DNA by the calcium phosphate method. Cells were treated as described for the Smad1-Smad4 heteromeric complex formation assay. Fluorescent cells were visualized using an inverted Nikon Diaphot Epi-fluorescence microscope. The total number of fluorescent cells and the number of cells with nuclear fluorescence were recorded. GFP-Smad1 nuclear accumulation was detected at 1 h after treatment with ligands, and images were captured by a Nikon high-resolution color digital camera at ×400 magnification.

3TP-Lux Reporter Assays. Hs578T cells were cotransfected with 0.25 μg of 3TP-Lux, 0.125 μg of renilla-luciferase control reporter (pRL-SV40; Promega), and 2.5 μg of either RSmad1 or human Smad1 by the calcium phosphate coprecipitation method as described above. Twenty-four h later, the medium was changed to serum-free conditions for 13 h. The cells were then treated with TGF-β_3 or TGF-β_1 at a concentration of 10 ng/ml for an additional 24 h. 3TP-luciferase activities were corrected using renilla luciferase activities.

RESULTS

Inhibition of DNA Synthesis by TGF-β and BMPs in Hs578T Human BCCs. Previous reports (20, 26–29) of Smad1 activation events used cell lines that either did not naturally respond to TGF-β (R-1B/L-17 or COS cells) or were not epithelial cells (MC3T3 osteoblast cells). To investigate the role of Smad1 in TGF-β signaling, we used cell lines that were natively sensitive to both TGF-β and BMPs. We previously reported that the growth of Hs578T cells was potently inhibited by TGF-β_1, TGF-β_2, and TGF-β_3 (12, 13). As shown in Fig. 1, TGF-β_3 inhibited DNA synthesis by 80% in Hs578T cells, whereas BMP2 or BMP4 decreased DNA synthesis by 70 or 60%, respectively. These data demonstrate that Hs578T cells are sensitive to both TGF-β and BMPs without the need to transfect cells with exogenous TGF-β or BMP receptors.

TGF-β-induced Phosphorylation of Smad1 in Hs578T Human BCCs. Previous studies of endogenous Smad1 phosphorylation in TGF-β-sensitive cell lines (A549, NmuMg, and L6) used antibodies that recognized other Smad family members (30, 31). Other studies examining exogenous Smad1 phosphorylation were performed in epithelial cells that were not naturally sensitive to TGF-β (26, 27, 29). Therefore, it was of interest to determine whether TGF-β could phosphorylate Smad1 in epithelial cells that were naturally sensitive to TGF-β. To investigate this, we constructed a mammalian expression vector that contained the entire coding region of RSmad1 with an HA epitope at the amino terminus. Fig. 2 displays the results of *in vivo* phosphorylation of transiently transfected RSmad1 in Hs578T cells. In the absence of ligands, Smad1 was weakly phosphorylated. However, the phosphorylation of Smad1 was strongly induced by TGF-β_3 within 15–30 min. Likewise, BMP2 treatment resulted in a rapid increase in Smad1 phosphorylation by 15 min that then declined toward baseline levels by 30 min. Quantitation of Smad1 phosphorylation by densitometry is plotted in Fig. 2*B*. The extent of induced Smad1 phosphorylation by BMP2 is similar to that reported previously (26, 29). Moreover, in TGF-β-sensitive untransformed IEC 4-1 cells, we observed a rapid (>5-fold) increase in the phosphorylation of endogenous Smad1 by TGF-β_1 when a Smad1-specific polyclonal antisera (26) was used (33–34). Thus, TGF-β can stimulate the phosphorylation of both exogenous and endogenous Smad1 in TGF-β-responsive epithelial cells.

TGF-β-induced Smad1-Smad4 Heteromeric Complex Formation in Hs578T Human BCCs. Previous studies have indicated that BMP2 and BMP4, but not TGF-β, stimulated Smad1-Smad4 heteromeric complex formation in COS and R1B/L-17 cells (20, 26, 27, 29). Because we observed a TGF-β-mediated phosphorylation of Smad1 in Hs578T cells, it was of interest to examine the effects of TGF-β on Smad1-Smad4 hetero-oligomerization in these human BCCs. In these experiments, Hs578T cells were cotransfected with Flag-tagged Smad4 and His-tagged Smad1, followed by treatment with TGF-β_3 or BMP2 for 1 h. Anti-His immunoprecipitates were separated by 12% SDS-PAGE, and tagged proteins were detected by blotting with rabbit polyclonal anti-Flag antibodies. As shown in Fig. 3*A*, in the absence of ligands (*Lane 2*), low basal levels of Smad1-Smad4 heteromeric complexes were observed. TGF-β_3 (*Lane 3*) and BMP2 (*Lane 4*)

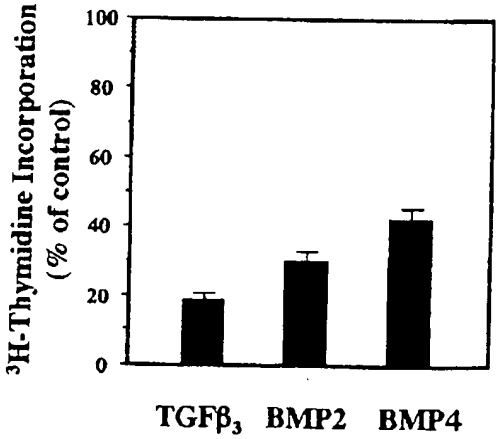

Fig. 1. TGF-β_3 and BMPs inhibit DNA synthesis in Hs578T human BCCs. Hs578T cells were plated and incubated in serum-free medium before treatment with TGF-β_3 (10 ng/ml) or BMPs (50 ng/ml) for 24 h as described in "Materials and Methods." Incorporation of [^{3}H]thymidine into DNA was plotted as a percentage of the levels in untreated cells. *Error bars*, mean ± SE (n = 3).

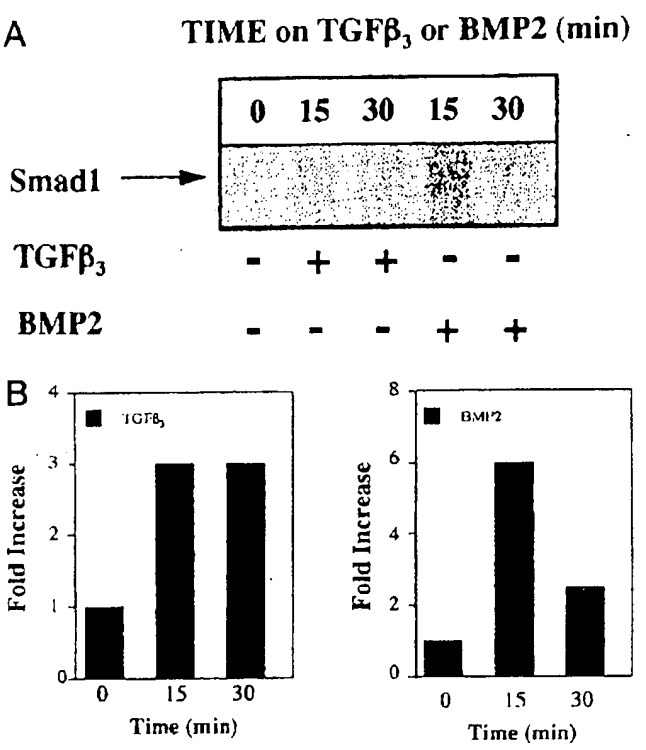

Fig. 2. TGF-β_3 and BMP2 induce Smad1 phosphorylation in Hs578T human BCCs. *A*, proliferating cultures of Hs578T cells were transiently transfected with 10 μg of HA-tagged Smad1. Cells were labeled with [^{32}P]orthophosphate (1 mCi/ml) for 3 h, followed by treatment with TGF-β_3 (10 ng/ml) or BMP2 (50 ng/ml) for the indicated times. Samples were normalized for radioactivity as determined by trichloroacetic acid precipitation. Labeled proteins were immunoprecipitated with anti-HA antibody and analyzed by SDS-PAGE and autoradiography. *B*, quantitation of Smad1 phosphorylation in Hs578T cells. The Smad1 phosphorylation bands were quantitated by densitometry. Results are representative of two independent experiments.

treatment increased Smad1-Smad4 heteromeric complex formation by 3- or 2.7-fold, respectively, after correction for differences in Smad4 expression. The results of three independent experiments performed in Hs578T cells were also summarized in Fig. 3*A*. Similar data were also obtained in the MCF-7 human BCCs (Fig. 3*B*), for which TGF-β_3 and BMP2 increased Smad1-Smad4 interaction by 3- or 4-fold, respectively. These results demonstrate that TGF-β can promote Smad1-Smad4 interactions as effectively as BMP2.

Nuclear Translocation of Smad1 in Hs578T Cells after Stimulation with TGF-β and BMP2. To extend the above findings, it was of interest to determine whether TGF-β could also stimulate Smad1 nuclear translocation. To investigate Smad1 nuclear translocation in live Hs578T human BCCs, we prepared the GFP-RSmad1 constructs by inserting GFP at the amino terminus of RSmad1. Hs578T cells were transiently transfected with GFP or GFP-RSmad1 and treated with TGF-β or BMP2 for 1 h. As depicted in Fig. 4*A*, the majority of the cells transfected with GFP alone (*a*) or GFP-Smad1 (*b*) displayed a diffuse fluorescent signal throughout the cells. In contrast, cells treated with either BMP2 (*c*) or TGF-β_3 (*d*) demonstrated strong nuclear fluorescence and a relatively weak fluorescent signal in the cytoplasm. Approximately 60–70% of the fluorescent cells transfected with GFP-Smad1 displayed prominent nuclear translocation on ligand addition (Fig. 4*B*). In the absence of ligand stimulation, only 20% of cells displayed prominent nuclear fluorescence. The percentage of transfected cells that displayed prominent nuclear Smad1 was similar to that in other reports for which immunocytochemistry was used (37). Furthermore, we have obtained similar results after the transfection of human Smad1 in Hs578T cells. These results demonstrate that TGF-β can stimulate Smad1 cytoplasmic to nuclear translocation as efficiently as BMP2 in Hs578T cells.

Induction of 3TP-Lux Reporter Activity by Smad1 and TGF-β in Hs578T Human BCCs. Because we have demonstrated that TGF-β triggered Smad1 activation events (*i.e.*, phosphorylation, hetero-oligomerization with Smad4, and nuclear translocation) in Hs578T cells, we next explored whether Smad1 expression could induce transcriptional responses in these cells. In these studies, Hs578T cells were transiently transfected with the TGF-β-responsive luciferase reporter 3TP-Lux. The 3TP-Lux construct contains three repeats of the TPA-responsive element fused to a portion of the PAI-1 promoter (35). This reporter construct has been used previously to evaluate TGF-β and activin responsiveness in transient transfection assays (23, 33, 36–40). As shown in Fig. 5*A*, TGF-β_3 alone induced 3TP-luciferase activity by 5-fold, whereas expression of RSmad1 in the absence of ligand induced 3TP-luciferase activity by 6-fold. However, the combination of Smad1 and TGF-β_3 resulted in a further increase in 3TP-luciferase activity in Hs578T cells (values obtained from four independent experiments ranged from 17–27-fold). In contrast, BMP2 at a dosage of 50 ng/ml failed to increase 3TP-luciferase

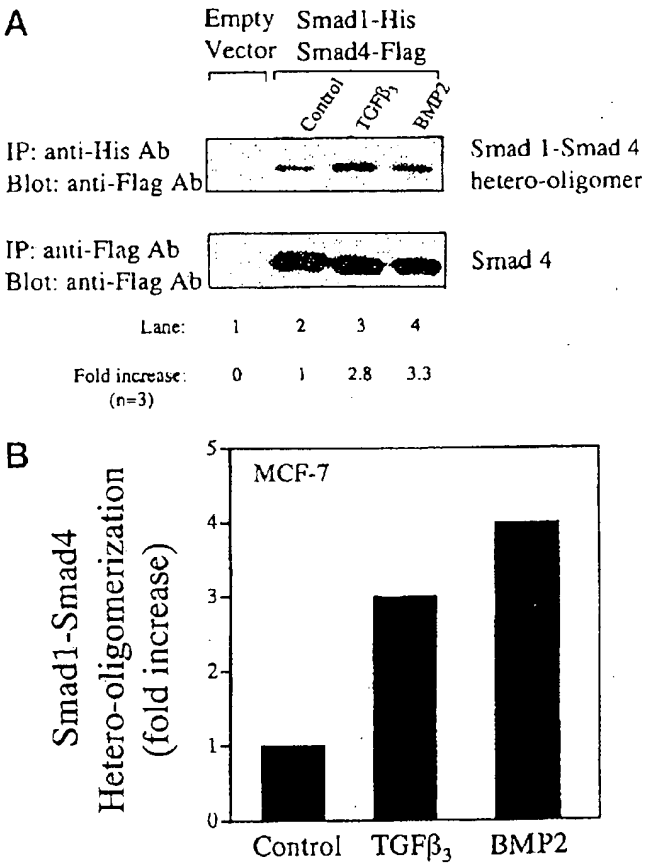

Fig. 3. TGF-β_3 and BMP2 promote Smad1-Smad4 heteromeric complex formation in Hs578T human BCCs. *A*, immunoprecipitation/blot analysis of Smad1-Smad4 interactions in Hs578T cells. Hs578T cells were transiently cotransfected with Flag-tagged Smad4, His-tagged Smad1 (*Lanes 2–4*), or empty vectors (*Lane 1*). Cells were incubated in serum-free medium before treatment with TGF-β_3 (*Lane 3*) or BMP2 (*Lane 4*) for 1 h. Cell lysates were analyzed by immunoprecipitation and subsequent immunoblot analysis to detect either Smad1-Smad4 interactions (*top*) or Smad4 expression levels among samples (*bottom*). Western blot analysis of the same lysates also demonstrated relatively equal expression of Smad1 among samples (data not shown). Results are representative of three separate experiments. Fold increase values represent three independent experiments, as indicated ($n = 3$). *B*, quantification of Smad1-Smad4 heteromeric complex formation in MCF-7 cells. Immunoprecipitation/blot analysis of Smad1-Smad4 interactions was performed in MCF-7 cells. Bands were scanned by densitometry and corrected for the expression levels of Smad4. The plot is representative of two separate experiments.

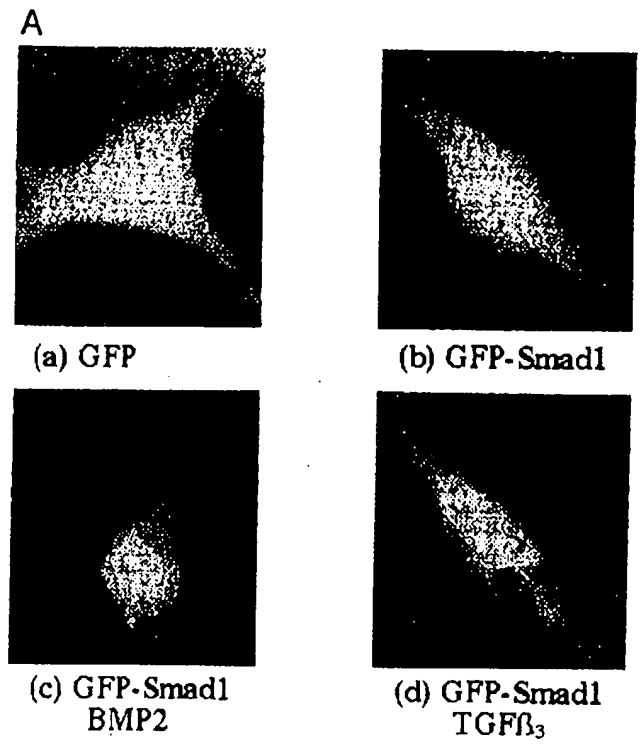

Fig. 4. Both TGF-β and BMP2 stimulate GFP-Smad1 cytoplasmic to nuclear translocation in Hs578T human BCCs *in vivo*. Hs578T BCCs were transiently transfected with 2–4 μg of GFP or GFP-Smad1 plasmid DNA. Forty-eight h later, the medium was changed to serum-free conditions for 30 min, and TGF-β_1 or (10 ng/ml) TGF-β_1 or BMP2 (50 ng/ml) was added for 1 h. *A*, photomicrographs of individual fluorescent cells transfected with GFP alone (*a*) or GFP-Smad1 (*b–d*). Cells were treated with BMP2 (*c*) or TGF-β, (*d*) for 1 h. GFP-Smad1 cytoplasmic to nuclear translocation was visualized at 1 h after treatment with ligands, and images were captured by a Nikon high-resolution color digital camera (×400). *B*, quantitation of GFP-Smad1 nuclear fluorescence in transfected Hs578T cells. Hs578T cells were transfected and treated as described above. The total number of fluorescent cells and the number of cells with nuclear translocation were recorded after treatment with either TGF-β or BMP2 for 1 h. Results were expressed as a percentage of the total number of transfected cells with prominent nuclear fluorescence by counting 200–250 transfected cells for each sample. The plot is representative of three similar experiments. *Error bars*, mean ± SE (n = 3).

activity (data not shown). This lack of effect was also observed by other investigators, presumably due to the fact that BMP does not regulate PAI-1 gene expression (43).

For the majority of experiments, we have transfected RSmad1 into human BCCs. To rule out the possibility that RSmad1 may act differently than human Smad1 in BCCs, we decided to examine whether human Smad1 could regulate the 3TP-Lux reporter in a manner similar to that of RSmad1. As shown in Fig. 5*B*, expression of human Smad1 also stimulated this TGF-β-responsive reporter. Like RSmad1, TGF-β potentiated the effect of Smad1 on 3TP-Lux activity. Thus, our results demonstrate that RSmad1 and human Smad1 affect nuclear translocation and 3TP-Lux transcription similarly.

DISCUSSION

Previous work has demonstrated that Smad1 is activated in a pathway-restricted fashion by TGF-β superfamily members (26–29). Specifically, Smad1 was shown to be a signaling component for BMP, but not for TGF-β. In this study, we demonstrate that TGF-β can trigger Smad1 activation events (phosphorylation, heteromeric complex formation with Smad4, nuclear translocation, and transcriptional activation of the 3TP-Lux reporter) in the absence of serum or other growth/differentiation factors. We also provide evidence that these events occur in TGF-β-sensitive Hs578T BCCs without overexpression of exogenous TGF-β receptors. In addition, we have observed

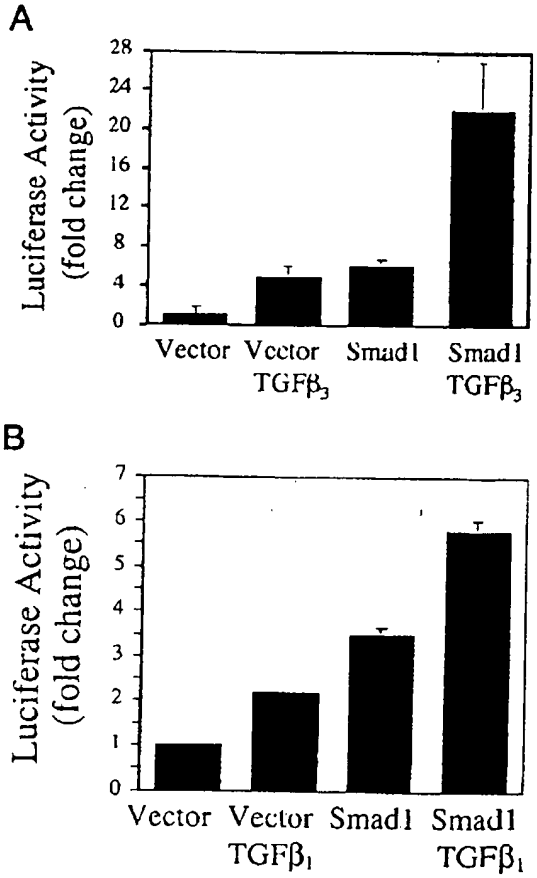

Fig. 5. TGF-β and Smad1 stimulate TGF-β-mediated transcriptional activation of 3TP-Lux reporter activity in Hs578T human BCCs. *A*, Hs578T BCCs were cotransfected with 0.25 μg of 3TP-Lux, 0.125 μg of renilla luciferase control reporter, and 2.5 μg of either RSmad1 or empty vector pCGN. Twenty-four h later, the medium was changed to serum-free conditions for 13 h. The cells were then treated with TGF-β_3 (10 ng/ml) for an additional 24 h. The 3TP-luciferase activities were corrected for transfection efficiencies using renilla luciferase activities. The plot is representative of four independent experiments performed in triplicate. *Error bars*, mean + SE (n = 4). *B*, Hs578T cells were transfected with 3TP-Lux, renilla luciferase control reporter, and human Smad1 or empty vector pcDNA 3.1. Cells were changed to serum-free conditions for 13 h and treated with TGF-β_1 (10 ng/ml) for 24 h. The plot is representative of two independent experiments performed in triplicate. *Error bars*, mean ± SE.

these effects in other epithelial cells (*i.e.*, MCF-7 BCCs and untransformed IEC 4-1 cells) (33, 34) that are natively sensitive to TGF-β. Therefore, our data support the hypothesis that Smad1 is a signaling intermediate for both TGF-β and BMP.

We also report that expression of Smad1 stimulates 3TP-Lux reporter activity, a finding that has not been reported previously. These results are in contrast to those of Chen *et al.* (44), who described an inhibition of 3TP-Lux activity by expression of Smad1 in Mv1Lu cells. The different results obtained in these two cell lines may be due to differences in the relative amounts of DNA transfected or to differences in the expression levels of endogenous Smads (*i.e.*, Smad4). The latter point was also suggested by Zhang *et al.* (21, 45), who previously reported that Smad1, alone or in combination with TGF-β, failed to increase PAI-1 reporter activity in the TGF-β-resistant human colon carcinoma cell line SW480.7; cotransfection of Smad4 was required to increase PAI-1 reporter activity. Therefore, in cell types either deficient in Smad4 or expressing this Smad at lower levels, Smad1 alone may be insufficient to activate 3TP-luciferase activity.

As mentioned above, published data suggest that TGF-β does not activate Smad1 (26–29). More recent reports have indicated that the L45 loop of the RI receptor kinase domain and the L3 loop of Smad1 mediate and specify interaction between Smad1 and BMP receptors (29, 43). Furthermore, these reports suggest that the different structural motif in the L3 loop of Smad1 may not be optimal for the interaction between Smad1 and TGF-β receptors. A number of possibilities may explain the ability of TGF-β to activate Smad1 in some cell types but not in others. These possibilities include: (*a*) specific cell types may express unique yet unidentified TGF-β RI receptors, which can directly interact with and phosphorylate Smad1; (*b*) under certain circumstances or in specific cell types, TGF-β may be capable of signaling through receptors that also transmit signals for other TGF-β superfamily members. There is a precedent for this type of promiscuous utilization of receptors among TGF-β superfamily members, as illustrated by the ability of BMP to signal though activin receptors (16, 46, 47); and (*c*) TGF-β RII receptors may actually play a more direct role in TGF-β signaling than originally thought; these receptors may influence TGF-β activation of Smad1. Each of these possibilities may also explain the cell-type specificity frequently encountered with respect to the intracellular components that mediate specific TGF-β responses.

It is also possible that the inability of TGF-β to stimulate Smad1 activation events may have derived from the lack of intact endogenous TGF-β signaling components in the cell lines used for the previous studies. These studies were performed only in COS or R1B/L-17 cells transfected with exogenous TGF-β or BMP receptors. Furthermore, an inability of the transfected receptors to interact naturally with downstream signaling components may also play a role. The differences that we have observed may also relate to the possibility that inhibitory Smads are expressed in some cell types; these may have counteracted the effect of TGF-β on Smad1 activation (48–53). Along these lines, TGF-β has been shown to regulate expression of the inhibitory Smads (Smad6 and Smad7) in Mv1Lu cells (51, 53).

In summary, we demonstrate that TGF-β is at least as effective as BMP in stimulating Smad1 activation in some cell types. Our studies also indicate that utilization of Smad1 by TGF-β may be cell-type specific, or that Smad1 activation by TGF-β may require intact endogenous receptors and signaling components. Thus, the concept of a pathway-restricted pattern for Smad signaling may be overgeneralized under certain circumstances.

ACKNOWLEDGMENTS

We gratefully acknowledge Dr. R. Derynck (University of California at San Francisco, San Francisco, CA) for the pRK5-Smad4 Flag plasmid and Dr. J. Massague (Memorial Sloan-Kettering Cancer Center, New York, NY) for the human Smad1 and p3TP-Lux reporter constructs. We also thank Dr. M. Morin (Pfizer Pharmaceuticals, Groton, CT) and Dr. V. Rosen (Genetics Institute, Cambridge, MA) for generously supplying the TGF-β_3 and BMPs, respectively.

REFERENCES

1. Hartsough, M. T., and Mulder, K. M. Transforming growth factor-β signaling in epithelial cells. Pharmacol. Ther., *75:* 21–41, 1997.
2. Wrana, J. L. TGF-β receptors and signalling mechanisms. Miner. Electrolyte Metab., *24:* 120–130, 1998.
3. Roberts, A. B. Molecular and cell biology of TGF-β. Miner. Electrolyte Metab., *24:* 111–119, 1998.
4. Wrana, J. L., Attisano, L., Wieser, R., Ventura, F., and Massague, J. Mechanism of activation of TGF-β receptor. Nature (Lond.), *370:* 341–347, 1994.
5. Chen, R-H., and Derynck, R. Homomeric interactions between type II transforming growth factor-β receptors. J. Biol. Chem., *269:* 22868–22874, 1994.
6. Lu, K. X., and Lodish, H. F. Signalling by chimeric erythropoietin-TGF-β receptors: homodimerization of the cytoplasmic domain of type I TGF-β receptor and heterodimerization with type II receptor are both required for intracellular signal transduction. EMBO J., *15:* 4485–4496, 1996.
7. Feng, X-H., and Derynck, R. Ligand-independent activation of transforming growth factor (TGF) β signaling pathways by heteromeric cytoplasmic domains of TGF-β receptors. J. Biol. Chem., *271:* 13123–13129, 1996.
8. Wieser, R., Wrana, J. L., and Massague, J. GS domain mutations that constitutively activate TβR-I, the downstream signaling component in the TGF-β receptor complex. EMBO J., *14:* 2199–2208, 1995.
9. Hartsough, M. T., and Mulder, K. M. Transforming growth factor β activation of $p44^{mapk}$ in proliferating cultures of epithelial cells. J. Biol. Chem., *270:* 7117–7124, 1995.
10. Hartsough, M. T., Frey, R. S., Zipfel, P. A., Buard, A., Cook, S. J., McCormick, F., and Mulder, K. M. Altered transforming growth factor β signaling in epithelial cells when Ras activation is blocked. J. Biol. Chem., *271:* 22368–22375, 1996.
11. Mulder, K. M., and Morris, S. L. Activation of $p21^{ras}$ by transforming growth factor β in epithelial cells. J. Biol. Chem., *267:* 5029–5031, 1992.
12. Frey, R. S., and Mulder, K. M. Involvement of extracellular signal-regulated and stress-activated protein kinase/Jun N-terminal kinase activation by transforming growth factor β in the negative growth control of breast cancer cells. Cancer Res., *57:* 628–633, 1997.
13. Frey, R. S., and Mulder, K. M. TGFβ regulation of mitogen activated protein kinases in human breast cancer cells. Cancer Lett., *117:* 41–50, 1997.
14. Yue, J., Buard, A., and Mulder, K. M. Blockade of TGFβ$_3$ up-regulation of $p27^{Kip1}$ and $p21^{Cip1}$ by expression of RasN17 in epithelial cells. Oncogene, *17:* 47–56, 1998.
15. Wrana, J., and Pawson, T. Mad about Smads. Nature (Lond.), *388:* 28–29, 1997.
16. Heldin, C-H., Miyazono, K., and ten Dijke, P. TGF-β signalling from cell membrane to nucleus through SMAD proteins. Nature (Lond.), *390:* 465–471, 1997.
17. Kretzschmar, M., and Massague, J. SMADs: mediators and regulators of TGF-β signaling. Curr. Opin. Genet. Dev., *8:* 103–111, 1998.
18. Zhang, Y., and Derynck, R. Intracellular signalling: the Mad way to do it. Curr. Biol., *6:* 1226–1229, 1996.
19. Nakao, A., Imamura, T., Souchelnytskyi, S., Kawabata, M., Ishisaki, A., Oeda, E., Tamaki, K., Hanai, J-I., Heldin, C-H., Miyazono, K., and ten Dijke, P. TGF-β receptor-mediated signalling through Smad2, Smad3 and Smad4. EMBO J., *16:* 5353–5362, 1997.
20. Lagna, G., Hata, A., Hemmati-Brivanlou, A., and Massague, J. Partnership between DPC4 and SMAD proteins in TGF-β signalling pathways. Nature (Lond.), *383:* 832–836, 1996.
21. Zhang, Y., Musci, T., and Derynck, R. The tumor suppressor Smad4/DPC 4 as a central mediator of Smad function. Curr. Biol., *7:* 270–276, 1996.
22. Eppert, K., Scherer, S. W., Ozcelik, H., Prioni, R., Hoodless, P., Kim, H., Tsui, L. C., Bapat, B., Gallinger, S., Andrulis, I. L., Thomsen, G. H., Wrana, J. L., and Attisano, L. MadR2 maps to 18q21 and encodes a TGF β-regulated Mad-related protein that is functionally mutated in colorectal carcinoma. Cell, *86:* 543–552, 1996.
23. Yingling, J. M., Datto, M. B., Wong, C., Frederick, J. P., Liberati, N. T., and Wang, X-F. Tumor suppressor Smad4 is a transforming growth factor β-inducible DNA binding protein. Mol. Cell. Biol., *17:* 7019–7028, 1997.
24. Wu, R-Y., Zhang, Y., Feng, X-H., and Derynck, R. Heteromeric and homomeric interactions correlate with signaling activity and functional cooperativity of Smad3 and Smad4/DPC4. Mol. Cell. Biol., *17:* 2521–2528, 1997.
25. Padgett, R. W., Cho, S-H., and Evangelista, C. Smads are the central component in transforming growth factor-β signaling. Pharmacol. Ther., *78:* 47–52, 1998.
26. Kretzschmar, M., Liu, F., Hata, A., Doody, J., and Massague, J. The TGF-β family mediator Smad1 is phosphorylated directly and activated functionally by the BMP receptor kinase. Genes Dev., *11:* 984–995, 1997.
27. Kretzschmar, M., Hata, A., Doody, J., and Massague, J. Opposing BMP and EGF signalling pathways converge on the TGF-β family mediator Smad1. Nature (Lond.), *389:* 618–622, 1997.

28. Hoodless, P. A., Huerry, T., Abdollah, S., Stapleton, M., O'Connor, M. B., Attisano, L., and Wrana, J. L. MADR1, a MAD-related protein that functions in BMP2 signaling pathways. Cell, *85:* 489–500, 1996.
29. Lo, R. S., Chen, Y-G., Shi, Y., Pavletich, N. P., and Massague, J. The L3 loop: a structural motif determining specific interactions between SMAD proteins and TGF-β receptors. EMBO J., *17:* 996–1005, 1998.
30. Lechleider, R. J., de Caestecker, M. P., Dehejia, A., Polymeropoulos, M. H., and Roberts, A. B. Serine phosphorylation, chromosomal location, and transforming growth factor-β signal transduction by human bsp-1. J. Biol. Chem., *271:* 17617–17620, 1996.
31. Yingling, J. M., Das, P., Savage, C., Zhang, M., Padgett, R. W., and Wang, X-F. Mammalian dwarfins are phosphorylated in response to transforming growth factor β and are implicated in control of cell growth. Proc. Natl. Acad. Sci. USA, *93:* 8940–8944, 1996.
32. Mulder, K. M., Segarini, P. R., Morris, S. L., Ziman, J. M., and Choi, H. G. Role of receptor complexes in resistance or sensitivity to growth inhibition by TGFβ in intestinal epithelial cell clones. J. Cell. Physiol., *154:* 162–174, 1993.
33. Yue, J., Hansough, M. T., Frey, R. S., Frielle, T., and Mulder, K. M. Cloning and expression of rat Smad1: role in TGFβ signaling and modulation by Ras and MEK. J. Cell Physiol., in press, 1998.
34. Yue, J., Frey R. S., and Mulder, K. M. Cross-talk between Smad1 and Ras/MEK signaling pathways for TGFβ. Oncogene, in press, 1998.
35. Wrana, J. L., Attisano, L., Carcamo, J., Zentella, A., Doody, J., Laiho, M., Wang, X-F., and Massague, J. TGF-β signals through a heteromeric protein kinase receptor complex. Cell, *71:* 1003–1014, 1992.
36. Chen, C., and Okayama, H. High efficiency transformation of mammalian cells by plasmid DNA. Mol. Cell. Biol., *7:* 2745–2752, 1987.
37. Liu, F., Pouponnot, C., and Massague, J. Dual role of the Smad4/DPC4 tumor suppressor in TGFβ-inducible transcriptional complexes. Genes Dev., *11:* 3157–3167, 1997.
38. Wieser, R., Attisano, L., Wrana, J. L., and Massague, J. Signaling activity of transforming growth factor β type II receptors lacking specific domains in the cytoplasm region. Mol. Cell. Biol., *13:* 19637–19640, 1993.
39. Carcamo, J., Weis, F. M., Ventura, F., Wieser, R., Wrana, J. L., Attisano, L., and Massague, J. Type I receptors specify growth-inhibitory and transcriptional responses to transforming growth factor β and activin. Mol. Cell. Biol., *14:* 3810–3821, 1994.
40. Bassing, C. H., Yingling, J. M., Howe, D. J., Wang, T., He, W. W., Gustafson, M. L., Shah, P., Donahoe, P. K., and Wang, X F. A transforming growth factor β type I receptor that signals to activate gene expression. Science (Washington DC), *263:* 87–89, 1994.
41. Attisano, L., Carcamo, J., Ventura, F., Weis, F. M., Massague, J., and Wrana, J. L. Identification of human activin and TGFβ type I receptors that form heteromeric kinase complexes with type II receptors. Cell, *75:* 671–680, 1993.
42. Attisano, L., Wrana, J. L., Montalvo, E., and Massague, J. Activation of signalling by the activin receptor complex. Mol. Cell. Biol., *16:* 1066–1073, 1996.
43. Chen, Y-G., Hata, A., Lo, R. S., Wotton, D., Shi, Y., Pavletich, N., and Massague, J. Determinants of specificity in TGF-β signal transduction. Genes Dev., *12:* 2144–2152, 1998.
44. Chen, Y., Lebrun J-L., and Vale, W. Regulation of transforming growth factor-β and activin-induced transcription by mammalian Mad proteins. Proc. Natl. Acad. Sci. USA, *93:* 12992–12997, 1996.
45. Zhang, Y., Feng, X-H., Wu, R-Y., and Derynck, R. Receptor-associated Mad homologues synergize as effector of TGFβ response. Nature (Lond.), *383:* 168–172, 1996.
46. Persson, U., Souchelnytskyi, S., Franzen, P., Miyazono, K., ten Dijke, P., and Heldin, C-H. Transforming growth factor (TGF-β)-specific signaling by chimeric TGF-β type II receptor with intracellular domain of activin type IIB receptor. J. Biol. Chem., *272:* 21187–21194, 1997.
47. Yamashita, H., ten Dijke, P., Huylebroeck, D., Sampath, T. K., Andries, M., Smith, J. C., Heldin, C-H., and Miyazono, K. Osteogenic protein-1 binds to activin type II receptors and induces certain activin-like effects. J. Cell Biol., *130:* 217–226, 1995.
48. Whitman, M. Feedback from inhibitory SMADs. Nature (Lond.), *389:* 245–247, 1997.
49. Imamura, T., Takase, M., Nishihara, A., Oeda, E., Hanai, J., Kawabata, M., and Miyazono, K. Smad6 inhibits signalling by the TGF-β superfamily. Nature (Lond.), *389:* 622–626, 1997.
50. Hata, A., Lagna, G., Massague, J., and Hemmati-Brivanlou, A. Smad6 inhibits BMP/Smad1 signaling by specifically competing with the Smad4 tumor suppressor. Genes Dev., *12:* 186–197, 1998.
51. Nakao, A., Afrakhte, M., Moren, A., Nakayama, T., Christian, J. L., Heuchel, S. I., Kawabata, M., Heldin, N-E., Heldin, C-H., and ten Dijke, P. Identification of Smad7, a TGF-β-inducible antagonist of TGF β signalling. Nature (Lond.), *389:* 631–635, 1997.
52. Hayashi, H., Abdollah, S., Qiu, Y., Cai, J., Xu, Y-Y., Grinnell, B. W., Richardson, M. A., Topper, J. N., Grimbrone, M. A., Jr., Wrana, J. L., and Falb, D. The MAD related protein Smad7 associates with TGF-β receptor and functions as an antagonist of TGF-β signaling. Cell, *89:* 1165–1173, 1997.
53. Takase, M., Imamura, T., Sampath, T. K., Takeda, K., Ichijo, H., Miyazono, K., and Kawabata, M. Induction of Smad6 mRNA by bone morphogenetic proteins. Biochem. Biophys. Res. Commun., *244:* 26–29, 1998.

ZAP-70 Association with T Cell Receptor ζ (TCRζ): Fluorescence Imaging of Dynamic Changes upon Cellular Stimulation

Joanne Sloan-Lancaster,* John Presley,‡ Jan Ellenberg,‡ Tetsuo Yamazaki,* Jennifer Lippincott-Schwartz,‡ and Lawrence E. Samelson*

*The Section on Lymphocyte Signaling, ‡The Unit of Organelle Biology, Cell Biology and Metabolism Branch, National Institute of Child Health and Human Development, National Institutes of Health, Bethesda, Maryland 20892

Abstract. The nonreceptor protein tyrosine kinase ZAP-70 is a critical enzyme required for successful T lymphocyte activation. After antigenic stimulation, ZAP-70 rapidly associates with T cell receptor (TCR) subunits. The kinetics of its translocation to the cell surface, the properties of its specific interaction with the TCRζ chain expressed as a chimeric protein (TTζ and Tζζ), and its mobility in different intracellular compartments were studied in individual live HeLa cells, using ZAP-70 and Tζζ fused to green fluorescent protein (ZAP-70 GFP and Tζζ–GFP, respectively). Time-lapse imaging using confocal microscopy indicated that the activation-induced redistribution of ZAP-70 to the plasma membrane, after a delayed onset, is of long duration. The presence of the TCRζ chain is critical for the redistribution, which is enhanced when an active form of the protein tyrosine kinase Lck is coexpressed. Binding specificity to TTζ was indicated using mutant ZAP-70 GFPs and a truncated ζ chimera. Photobleaching techniques revealed that ZAP-70 GFP has decreased mobility at the plasma membrane, in contrast to its rapid mobility in the cytosol and nucleus. Tζζ–GFP is relatively immobile, while peripherally located ZAP-70 in stimulated cells is less mobile than cytosolic ZAP-70 in unstimulated cells, a phenotype confirmed by determining the respective diffusion constants. Examination of the specific molecular association of signaling proteins using these approaches has provided new insights into the TCRζ–ZAP-70 interaction and will be a powerful tool for continuing studies of lymphocyte activation.

Key words: ZAP-70 • TCRζ • protein tyrosine kinase • intracellular signaling • GFP

ENGAGEMENT of the T cell receptor (TCR)[1] by antigenic ligand, in the form of a short linear peptide bound in the cleft of a major histocompatibility complex (MHC) class I or II molecule, is the critical binding event leading to T cell activation (Babbitt et al., 1985; Townsend et al., 1986; Bentley and Mariuzza, 1996; Garcia et al., 1996). The TCR is comprised of multiple integral membrane proteins (Jorgensen et al., 1992; Weiss, 1993; Weissman, 1994) and serves to initiate intracellular signaling, leading to new gene expression, protein synthesis, induction of multiple effector functions, and clonal expansion (Samelson and Klausner, 1992; Weiss and Littman, 1994). The αβ heterodimer binds to the antigen-MHC ligand, and the CD3 γ, δ, ε, and TCRζ chains translate this event into biochemical signals within the cell (Cantrell, 1996; Garcia et al., 1996; Wange and Samelson, 1996; Qian and Weiss, 1997). Since none of these molecules contains any intrinsic enzymatic activity, they recruit and bind signaling proteins via their conserved immunoreceptor tyrosine-based activation motifs (ITAMs), which are present as a single copy in each of the CD3 chains and in triplicate in TCRζ (Reth, 1989; Weiss and Littman, 1994; Wange and Samelson, 1996). The CD3 and TCRζ chains are phosphorylated on the tyrosines within their ITAMs within seconds of TCR engagement by the Src kinases Lck and Fyn (Iwashima et al., 1994; van Oers et al., 1996; Sloan-Lancaster and Samelson, 1998). The phospho-ITAMs are then able to bind SH2 domain–containing proteins, allow-

J. Sloan-Lancaster's current address is Division of Research Technologies and Proteins, Eli Lilly and Company, Lilly Corporate Center, Indianapolis, IN 46285.

Address all correspondence to Lawrence E. Samelson, NICHD, CBMB, Bldg. 18T, Rm 101, Bethesda, MD 20892. Tel.: (301) 496-6368. Fax: (301) 402-0078. E-mail: samelson@helix.nih.gov

1. *Abbreviations used in this paper*: FLIP, fluorescence loss in photobleaching; FRAP, fluorescence recovery after photobleaching; GFP, green fluorescent protein; ITAM, immunoreceptor tyrosine-based activation motif; MHC, major histocompatibility complex; PV, pervanadate; ROI, region of interest; TCR, T cell antigen receptor; TTζ, Tac Tac zeta; Tζζ, Tac zeta zeta.

ing a multiprotein complex to form under the membrane, which includes enzymes and adaptors responsible for triggering the various intracellular signaling pathways for successful T cell activation (Weiss and Littman, 1994; Wange and Samelson, 1996).

ZAP-70, a nonreceptor protein tyrosine kinase expressed exclusively in T cells, thymocytes, and natural killer cells, is a critical enzyme in early T cell signaling (Chan et al., 1992; Wange et al., 1992; Arpaia et al., 1994; Chan et al., 1994; Elder et al., 1994; Negishi et al., 1995). After binding via its tandem SH2 domains to the two phosphotyrosines of an individual ITAM during TCR engagement (Wange et al., 1993), ZAP-70 is phosphorylated by Lck and/or Fyn and is thus activated (Iwashima et al., 1994; Wange et al., 1995*a*; Kong et al., 1996). Subsequently, these kinases phosphorylate other specific substrates, resulting in the activation of the various intracellular signaling pathways required for T cell function. Although the absolute requirement of functional ZAP-70 for T cell activation has been clearly demonstrated both biochemically and genetically (Wange et al., 1995*b*; Qian et al., 1996; Williams et al., 1998), few studies have examined its intracellular localization and how this is affected by cellular stimulation. The primary structure predicts that ZAP-70 is a cytosolic protein (Chan et al., 1992), and biochemical data have shown that it rapidly translocates to the TCR upon activation (Wange et al., 1992; Chan et al., 1991). We have recently developed a cellular approach to examine the location and movement of ZAP-70 in single cells over real time, using a chimera of ZAP-70 fused to the green fluorescent protein (GFP) and time-lapse imaging confocal microscopy (Sloan-Lancaster et al., 1997). Our initial study revealed that ZAP-70 GFP was present not only throughout the cytosol but also in the nucleus, in both transiently transfected COS 7 cells and ZAP-70–deficient T cells stably reconstituted with the chimera. In COS 7 cells, ZAP-70 GFP rapidly moved from the cytosol to the cell surface in response to pharmacological stimulation. This was surprising since COS 7 cells do not express any TCR chains or other molecules known to contain ITAMs. We reasoned that another membrane-associated protein, which becomes tyrosine phosphorylated upon cellular stimulation, was able to bind ZAP-70 in order for this translocation and apparent binding to occur (Sloan-Lancaster et al., 1997).

Since the current model of T cell activation dictates that ZAP-70 is bound and concentrated at the region of activated TCR via a specific interaction with the phosphorylated ITAMs of TCR subunits, we wanted to refine our experimental system to study this association. This would enable us not only to assess the real time binding kinetics, but also to demonstrate the fine specificity of the molecular interaction in individual living cells. In addition, we wanted to measure the mobility of ZAP-70 in the different intracellular compartments to understand the mechanisms of retention at the plasma membrane. Here we report the stimulation-dependent translocation of ZAP-70 to the cell surface in HeLa cells is dependent on expression of a chimeric TCRζ chain. We describe the kinetics of this interaction and show that ZAP-70 translocation is enhanced by coexpressing active Lck. Moreover, we provide evidence that relocated ZAP-70 is specifically bound to the chimeric ζ chain, with properties that correspond precisely with the data generated biochemically (Wange et al., 1993; Koyasu et al., 1994). Using photobleaching techniques, we have revealed the highly mobile and freely diffusible nature of cytosolic and nuclear ZAP-70 and its conversion to a more static state accompanying its translocation to the cell periphery. Cell surface–located ZAP-70 is more diffusible than TCRζ, a transmembrane protein, a phenotype confirmed by calculating the diffusion constants for the individual proteins, which indicated that peripheral ZAP-70 diffuses 20-fold faster than TCRζ. Such observations suggest that the interaction between ZAP-70 and TCRζ upon cellular stimulation is dynamic.

Materials and Methods

Cells, Antibodies, and Reagents

HeLa cells were grown in complete D10 medium (DME containing 10% FBS, 2 mM glutamine, and 50 μg/ml gentamicin). All stably transfected lines were cultured in complete D10 medium supplemented with 1 mg/ml geneticin (G418; GIBCO BRL, Gaithersburg, MD) for maintenance of transgene expression. H/TTζ, H/Tζζ, and H/Tζζ truncated (H/Tζζ trunc) cells stably expressed the appropriate fusion protein as determined by frequent FACS® and immunoprecipitation analyses.

mAbs used include anti–IL-2 receptor α chain, 33B3.1 (Immunotech, Inc., Westbrook, ME), for FACS® analysis; rabbit anti–ZAP-70 antiserum (Wange et al., 1995*a*); mouse anti–human α-tubulin (Sigma Chemical Co., St. Louis, MO); rhodamine-coupled goat anti–mouse IgG; and fluorescein-coupled goat anti–rat IgG (KPL, Inc., Gaithersburg, MD).

Plasmids, Constructs, and Transfection

The generation of pSXSRα-Lck F505, pEGFP/ZAP-70, and pEGFP/kin.neg. (with deleted kinase domain) ZAP-70 have been described previously (Wange et al., 1995*a*; Sloan-Lancaster et al., 1997). pEGFP/double SH2 was made by ligating the NheI/XmnI fragment from pEGFP/ZAP-70, containing both SH2 domains and both interdomains, to the NheI/SmaI-digested pEGFP-N1 vector. For construction of pEGFP/ZAP-70 kin.dom. (expressing the kinase domain alone), the NheI/XmnI fragment was removed from pEGFP/ZAP-70, and the vector was religated using the oligos 5′ CTA GCA CCG GTG GAT CCT CTA GAA TGA AGC 3′ and 5′ GCT TCA TTC TAG AGG ATC CAC CGG TG 3′. For pEGFP/SH2(C) + kin.dom., the NheI/KpnI fragment of pEGFP/ZAP-70 was removed, and the vector religated using the oligos 5′ CTA GCG ATA TCA TGC CAG ACC CCG CGG CGC ACC TGC CCT GGT AC 3′ and 5′ CAG GGC AGG TGC GCC GCG GGG TCT GGC ATG ATA TCG 3′. pEGFP/SH2(N) + kin.dom. was made in two steps. First, an intermediate vector, ZAP 1 + 2, encoding the kinase domain alone with an inserted KpnI site, was derived by annealing the NheI/XmnI-digested pEGFP/ZAP-70 to the oligos 5′ CTA GCG ATA TCT GCA GGG TAC CTC GAG AAG C 3′ and 5′ GCT TCT CGA GGT ACC CTG CAG ATA TCG 3′. The NheI/KpnI fragment of pEGFP/ZAP-70, encoding the NH_2-terminal SH2 and interdomain 1, was then ligated to the NheI/KpnI-cut ZAP 1 + 2. pEGFP/Tζζ was constructed as follows: the EcoRI/BamHI fragment from pXSSRα/Tζζ (Letourneur and Klausner, 1991) was ligated to EcoRI/BamHI-digested pEGFP-N1 vector to create the intermediate plasmid pEGFP/Tζζ/BamHI. A PCR fragment from the BamHI site of Tζζ was created with an introduced COOH-terminal AgeI site, using the oligos 5′ GCA GGG ATC CAG AGA TGG GAG GC 3′ and 5′ GAC GAC CGG TGA GCG AGG GGC CAG GGT CTG 3′. Then BamHI/AgeI-digested PCR product and BamHI/AgeI-digested pEGFP/Tζζ/BamH1 vector were ligated together to produce the final construct, pEGFP/Tζζ. The construction of the TTζ, Tζζ, and Tζζ trunc chimeras have been described elsewhere (Letourneur and Klausner, 1991). All three contain the extracellular domain of the human IL-2 receptor α chain and the intracellular domain of TCRζ. TTζ includes the transmembrane region of the IL-2 receptor α chain, while Tζζ contains the transmembrane region of TCRζ. Tζζ trunc is a shortened form of the latter chimera, terminated after TCRζ amino acid residue 65, and thus lacks all three ITAMs (Letourneur and Klausner, 1991). HeLa cells, or their stably transfected counterparts, were electroporated using 15 μg of each DNA construct at

250 V and 500 μF using a Gene Pulser (Bio-Rad Labs., Hercules, CA) and used 20–24 h after transfection.

Immunofluorescence Staining

HeLa cells were grown overnight on sterile glass coverslips (10-mm diameter, No. 1 thickness). Cells, untreated or pretreated with nocodazole (33 μM, 30 min incubation at 4°C, followed by 30 min at 37°C), were then fixed in 3.7% paraformaldehyde in PBS for 30 min at room temperature, washed (three times) in PBS containing 10% fetal bovine serum (PBS/FBS), permeabilized using 0.1% Triton X-100 in PBS for 4 min at room temperature, washed (three times), and incubated for 45 min in PBS/FBS for preblocking. Cells were then incubated with a mouse anti-human tubulin Ab in PBS/FBS for 45 min at room temperature, washed, and incubated with rhodamine-coupled goat anti-mouse IgG for 45 min, followed by washing with PBS (three times). The coverslips were then mounted onto glass slides using Fluoromount G (Southern Biotechnology Associates, Inc., Birmingham, AL) and viewed using the 568-nm laser line of a confocal laser scanning microscope (model LSM 410; Carl Zeiss, Inc., Thornwood, NY) with a 100× planapochromat oil immersion objective (NA 1.4) and optics for rhodamine.

Fluorescence Microscopy, Time-Lapse Imaging, and Image Processing

Transfected cells were grown overnight in coverglass chambers (LabTek, Naperville, IL) in complete D10 medium. For time-lapse imaging experiments, the slides were mounted on a custom-made platform (of a confocal laser scanning microscope; Yona Microscope and Instrument Co., Rockville, MD) equipped with a triple line Kr/Ar laser, a 100× 1.4 NA Planapochromat oil immersion objective, a 25× 0.8 NA Neofluar immersion corrected objective, and a temperature-controlled stage. Time-lapse sequences were recorded with macros programmed with the Zeiss LSM software package that allow autofocusing on the coverslip surface in reflection mode before taking confocal fluorescence images. The media was replaced by PBS supplemented with magnesium and calcium salts before the start of imaging. In Fig. 4 *d*, cells were treated with nocodazole as above before beginning the time-lapse imaging. Two images of each cell were taken before addition of the pervanadate (PV) stimulant directly to the chambered coverglass, and subsequent images were taken at 30-s intervals thereafter until 15 min after stimulation, as previously described (Sloan-Lancaster et al., 1997).

Photobleaching Experiments

Fluorescence loss in photobleaching (FLIP) experiments were performed at room temperature on a custom-made stage of a confocal microscope (model LSM 410; Carl Zeiss, Inc.) using the 63× objective and the 488-nm line of a 400-mW Kr/Ar laser, which delivered 0.9 mW power (Cole et al., 1996). In brief, HeLa cells expressing ZAP-70 GFP alone, ZAP-70 GFP together with Lck F505, or Tζζ GFP were left untreated or stimulated with PV for 12 min before beginning the FLIP experiment, as indicated in figure legends. A small rectangular region defined by the boxed area was repeatedly illuminated with the laser at 100% power, 100% transmission. Between each intense illumination, the entire field of view was imaged at low-power laser light (20% power, 1% transmission) to assess the extent of loss of fluorescence outside the box as a consequence of photobleaching within the box. The time lapse between images was ~25 s. The possibility that regions on the edge of the illuminated box are progressively bleached by light leakage during FLIP was ruled out by repeating FLIP identically on fixed cells, which showed bleaching only in the area exposed to illumination. Furthermore, there was no significant photobleaching while imaging the recovering cell since control cells in the field did not lose any significant fluorescence intensity during the time followed.

Fluorescence recovery after photobleaching (FRAP; Edidin, 1994) was performed at room temperature on a confocal microscope (model LSM 410; Carl Zeiss, Inc.) essentially as described (Ellenberg et al., 1997). For the qualitative *D* measurements shown in Fig. 7, cells were stimulated for 12 min before commencement of photobleaching. The width of the rectangular regions of interest used were 2 μm (Tζζ GFP, some ZAP-70 GFP) or 4 μm (ZAP-70 GFP). Fluorescence within the strip was measured at low laser power (20% power, 1% transmission) before the bleach (prebleach intensity) and then photobleached with full laser power (100% power, 100% transmission) for 0.218 s (Tζζ GFP) or 0.436 s (ZAP-70 GFP) (which effectively reduced the fluorescence to background levels in fixed material). Recovery was followed after 2 s with low laser power at 2-s intervals for 200 s (Tζζ GFP) or 1-s intervals for 50 s (ZAP-70 GFP) and then at 10-s intervals until the recovered fluorescence intensity within the strip had reached a plateau. Zero of time *t*, taken as the midpoint of the bleach, was 2.399 s for Tζζ GFP and 2.513 s for ZAP-70 GFP. Numerical simulations were used to determine *D* using the prebleach intensity of entire cells (to assess the effects of geometry and nonuniform fluorescence density) and compared with experimentally derived *D* values, as described (Ellenberg et al., 1997; Sciaky et al., 1997).

Results

Redistribution of ZAP-70 to the Plasma Membrane in HeLa Cells Requires Both Cellular Activation and Coexpression of a TCR Chain

In a previous report, we made use of a ZAP-70 GFP chimera to study the intracellular location of this protein tyrosine kinase, and how it changed in response to cellular stimulation, using time-lapse imaging (Sloan-Lancaster et al., 1997). This approach revealed the very rapid redistribution of cytosolic ZAP-70 to the cell surface, with significant membrane accumulation detected as early as 1 min after stimulation. The phenotype was enhanced when an active form of Lck was coexpressed, which itself induced some ZAP-70 translocation. These results were somewhat surprising since the COS 7 cells, in which the chimeric ZAP-70 GFP was expressed, do not contain any TCR chains. We were therefore curious to determine whether the introduction of a TCR chain in this experimental system had any observable effect on the redistribution of ZAP-70.

To compare results in the presence or absence of a TCR chain, we made use of the HeLa cell line, which lacks any TCR chains, and its transfected derivative, H/TTζ, which stably expresses a chimeric form of TCRζ comprised of the extracellular and transmembrane portions of the human IL-2 receptor α chain, Tac, fused to the entire intracellular region of TCRζ (Letourneur and Klausner, 1991). The fusion protein is successfully expressed on the cell surface as an integral membrane protein independent of any other TCR component and provides an experimental system in which the contribution of the tandem ITAMs of TCRζ can be examined apart from the CD3 molecules (Letourneur and Klausner, 1991). In non-T cells, cross-linking TTζ at the cell surface does not induce cellular activation. Thus, to stimulate the cells, we used the pharmacological agent pervanadate (PV). PV inhibits intracellular phosphatases, thereby creating a steady state in which tyrosine residues are phosphorylated normally but not dephosphorylated and which is used as a surrogate for antigen or anti-TCR cross-linking (O'Shea et al., 1992; Secrist et al., 1993). Both HeLa and H/TTζ cells were transfected with ZAP-70 GFP, and time-lapse imaging was used to monitor the movement of the chimeric fluorescent molecule in response to pharmacological stimulation. Two images were taken before PV addition, with subsequent images taken at 30-s intervals thereafter.

Little if any ZAP-70 redistributed to the plasma membrane in HeLa cells with PV stimulation (Fig. 1, *top row*), while significant membrane accumulation was evident as early as 2 min after stimulation in COS 7 cells (Sloan-Lancaster et al., 1997). The lack of a similar phenotype in

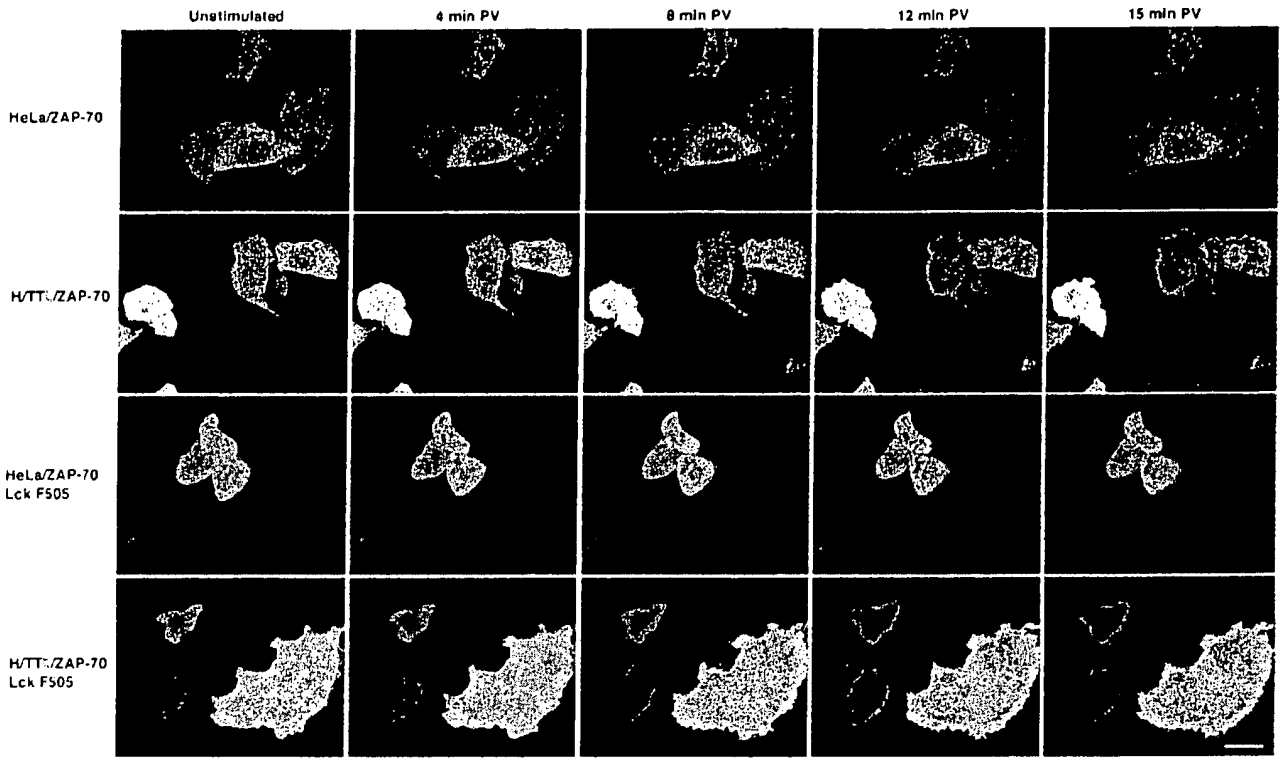

Figure 1. Activation-induced movement of ZAP-70 to the cell surface in TCRζ-expressing HeLa cells and its enhancement by Lck F505. Individual live HeLa or H/TTζ cells were monitored by time-lapse imaging confocal microscopy. Lck F505 was cotransfected with ZAP-70 GFP in the bottom two rows. Two images were taken before PV addition, with subsequent images collected every 30 s thereafter. One prestimulation image is shown for each experimental group, followed by those at 4, 8, 12, and 15 min after stimulation. Bar: (Rows *1*, *3*, and *4*) 21 μm; (row *2*) 27 μm.

HeLa cells suggests that no phosphotyrosine- or ITAM-containing proteins capable of binding ZAP-70 are expressed in these cells. Thus, in the absence of a TCR chain, pharmacological stimulation had little effect on ZAP-70 redistribution in HeLa cells. However, when H/TTζ cells were stimulated with PV, ZAP-70 dramatically redistributed to the cell surface in all cells examined (Fig. 1, *second row*). Unlike its rapid accumulation to the plasma membrane in COS 7, there was a significant delay in H/TTζ, with little detectable redistribution until 8–10 min after stimulation. At this time, movement to the plasma membrane, accompanied by cytosolic clearing, continued steadily around each cell until ~15 min after stimulation, when ZAP-70 was uniformly distributed over the inner surface. Results from a semiquantitative analysis of individual cells confirmed this phenotype, in which mean fluorescence intensity in a region of interest (ROI) over the center of each cell (cytosol and plasma membrane) was compared with an ROI at the edge (plasma membrane). These data indicated that there was, on average, a 1.1-fold increase in the surface to cytosolic fluorescence ratio 4 min after stimulation, which increased to 1.5-fold by 8 min and to 3.1-fold by 15 min after PV addition. The uniform distribution around the cell surface was consistent with ZAP-70 binding specifically to the chimeric TTζ molecule, which is localized throughout the plasma membrane under these conditions (data not shown).

Lck F505 Enhances ZAP-70 GFP Movement to the Cell Surface

The current model of physiological early T cell signaling suggests that ZAP-70 binds to the ITAMs of TCRζ only after they have been phosphorylated by Lck and/or Fyn (Iwashima et al., 1994; Wange and Samelson, 1996; Qian and Weiss, 1997). Our earlier studies in COS 7 suggested that expression of active Lck followed by PV stimulation enhances the redistribution of ZAP-70 to the cell surface over that induced by PV alone (Sloan-Lancaster et al., 1997). Thus, we performed time-lapse imaging in cells coexpressing the constitutively active Lck F505 to determine if this kinase influenced the recruitment of ZAP-70 and its binding to TCRζ. In HeLa cells, the coexpression of Lck F505 had no apparent effect on the location of ZAP-70 before or after PV stimulation, since ZAP-70 was not detected at the plasma membrane at any time point (Fig. 1, *third row*). This further confirmed the lack of other ZAP-70–binding proteins in HeLa cells, and thus the specificity of the interaction with the ITAMs in H/TTζ. With the expression of the chimeric TCRζ chain, Lck F505 enhanced the redistribution of ZAP-70 to the cell surface, and presumably its binding to TTζ (Fig. 1, *bottom row*). The time-lapse imaging results suggested that Lck F505 kinetically enhanced the accumulation of ZAP-70 at the cell surface. ZAP-70 accumulation was detected at the plasma mem-

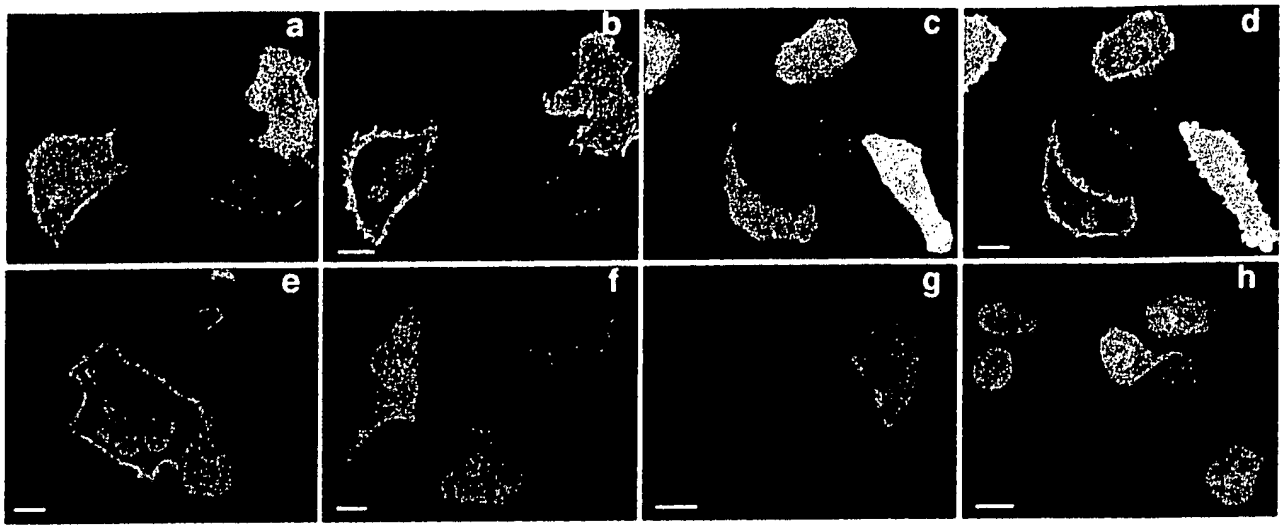

Figure 2. Analysis of the redistribution of ZAP-70 GFP mutants. H/TTζ cells expressing Lck F505 were cotransfected with the following ZAP-70 GFP constructs: wild-type (*a* and *b*), kinase-dead (*c* and *d*), tandem SH2 domains (*e*), kinase domain alone (*f*), SH2(N) + kinase (*g*), or SH2(C) + kinase (*h*). Protein movement in response to PV stimulation was followed by time-lapse imaging. Images are shown for unstimulated conditions (*a* and *c*) and 15 min after stimulation (*b* and *d–h*). Bars, 14 μm.

brane as early as 4–5 min after stimulation, reaching a plateau by 8 min (Fig. 1, *bottom row*). This was determined in several cells by comparing fluorescence intensities within ROIs over the center of the cell (cytoplasm and plasma membrane) and at the edge (plasma membrane only) with time. These data showed an increase in fluorescence intensity at the plasma membrane at a much earlier time after stimulation in cells coexpressing Lck F505. However, there was no apparent quantitative enhancement by Lck F505, since surface fluorescence increased threefold compared with cytosolic levels whether or not Lck F505 was coexpressed.

The Specificity of ZAP-70–TTζ Interaction

The above experiments indicated that, in the HeLa system, the specific molecular interaction of ZAP-70 and TTζ in response to cellular stimulation could be monitored at the single cell level. We next used this assay system to assess the basis of this interaction. To do so, we constructed various chimeras consisting of mutant ZAP-70 with GFP and used them to determine the contribution of individual protein domains in the translocation and binding of the kinase to TTζ (Fig. 2). Lck F505–expressing H/TTζ cells were cotransfected with the indicated ZAP-70 GFP mutant, and cells were monitored before and after addition of PV. Accumulation of ZAP-70 at the cell surface was monitored in response to PV stimulation in cells expressing wild-type ZAP-70 (Fig. 2 *a*, unstimulated, and *b*, 15 min PV). A similar pattern of redistribution was observed using a kinase-dead form of ZAP-70 (Fig. 2 *c*, unstimulated, and *d*, 15 min PV, and data not shown), and an analysis of multiple cells in several experiments indicated that the kinetics and amount of wild-type and kinase-dead ZAP-70 translocated to the cell surface did not differ significantly (data not shown). These data confirm that the kinase activity of ZAP-70 is not necessary for its binding to TCRζ (Wange et al., 1993; Hatada et al., 1995).

We next assessed the roles of the individual protein domains of ZAP-70 in its binding to TCRζ. While a mutant ZAP-70 GFP, containing the tandem SH2 domains without the kinase domain, redistributed to the cell surface with kinetics indistinguishable from those of the entire molecule (Fig. 2 *e*, 15 min PV, and data not shown), neither SH2 domain expressed alone with the kinase domain moved to the plasma membrane (Fig. 2 *g*, NH_2-terminal SH2, and *h*, COOH-terminal SH2, 15 min PV). Moreover, the kinase domain by itself could not bind to TTζ (Fig. 2 *f*, 15 min PV). These data agree with biochemical evidence showing that the tandem SH2 domains of ZAP-70, but not the kinase domain, are absolutely required for a stable interaction with any individual phosphorylated ITAM (Wange et al., 1993; Iwashima et al., 1994; Koyasu et al., 1994).

A similar in vivo analysis of the molecular properties of ζ required to bind to ZAP-70 was also undertaken. For this, two additional HeLa cell lines, which stably express distinct forms of the ζ chimera, were used. The first expresses Tζζ, which differs from TTζ in that its transmembrane domain is derived from TCRζ instead of from Tac. This ensures that Tζζ is expressed as a disulfide-linked homodimer on the cell surface. The second expresses a shorter form of Tζζ, called Tζζ trunc, terminated after ζ amino acid 65 and resulting in a homodimer with no ITAMs (Letourneur and Klausner, 1991). A schematic of the structures of these ζ chimeras is shown in Fig. 3 *A*. We tested the ability of these ζ chimeras to acquire phosphotyrosine, since only phospho-ITAMs can bind ZAP-70 biochemically (Bu et al., 1995; Isakov et al., 1995). The ζ chimeras were examined for phosphotyrosine content before

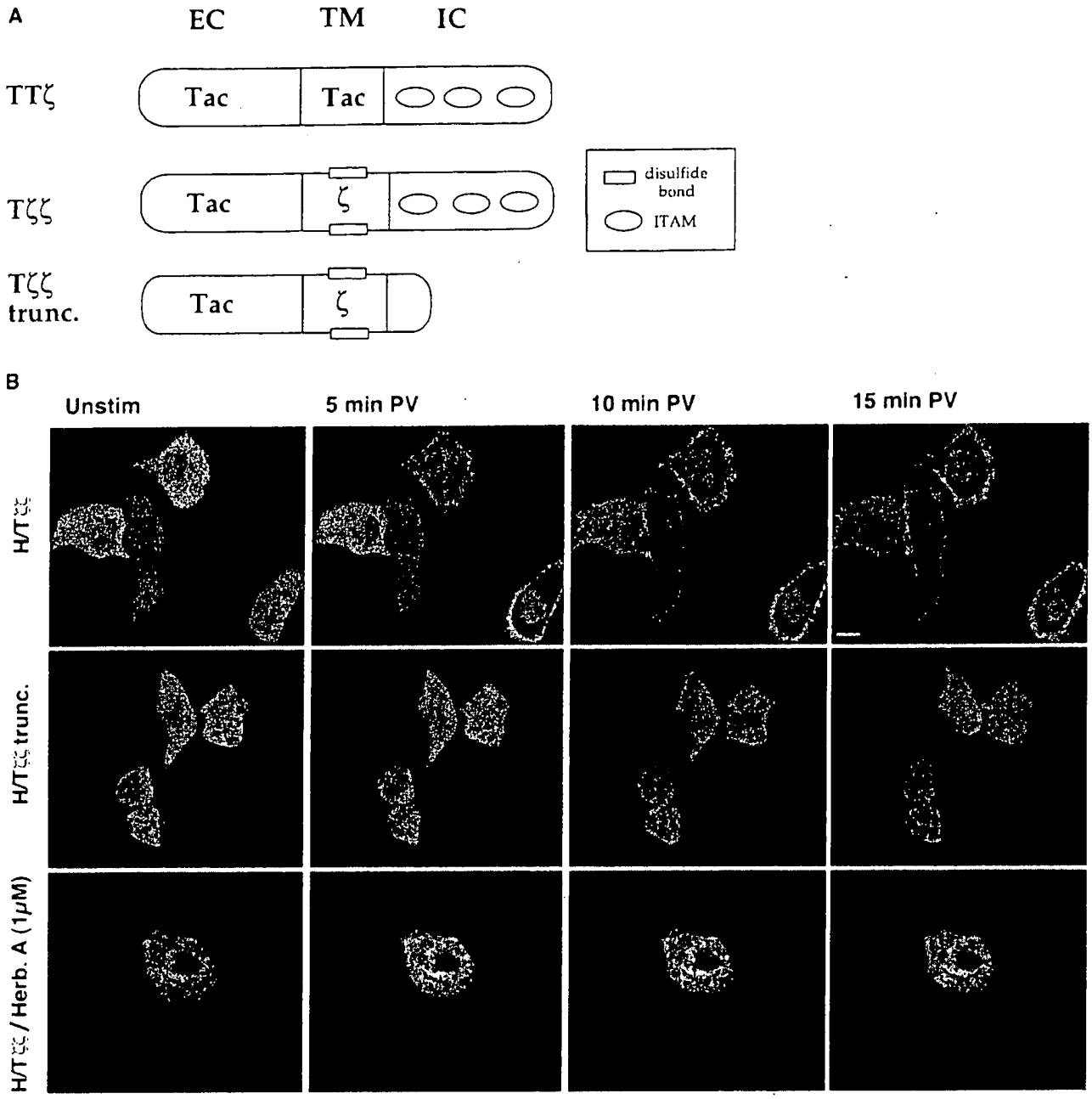

Figure 3. Requirements of TCRζ for ZAP-70 redistribution. (*A*) Schematic of the molecular domains of the various chimeric ζ molecules used. (*B*) H/Tζζ (*top* and *bottom rows*) or H/Tζζ trunc (*middle row*) cells, expressing Lck F505 and ZAP-70 GFP, were monitored by time-lapse imaging. Images were taken at 30-s intervals, and those at 5-min increments are shown. Bar, 13.3 μm.

or after PV stimulation of the respective cell lines. As expected, only H/TTζ and H/Tζζ, but not HeLa or H/Tζζ trunc, displayed a phosphoprotein at the apparent molecular weight for chimeric ζ, verifying the activation-dependent requirement of phosphorylation of chimeric ζ and the lack of intramolecular phosphate-binding sites in Tζζ trunc (data not shown). We also determined that the tyrosine kinase inhibitor, herbimycin A (1 μM), inhibited stimulation-dependent cellular phosphorylation (data not shown).

H/Tζζ (Fig. 3 *B*, *top* and *bottom rows*) and H/Tζζ trunc (*middle row*) cells, expressing ZAP-70 GFP and Lck F505 and including herbimycin A (1 μM, *bottom row*), were PV stimulated and monitored using digital imaging confocal microscopy. As expected, cells expressing full-length Tζζ were successful in recruiting ZAP-70 to the plasma membrane with kinetics similar to those defined earlier (Fig. 1). In contrast, H/Tζζ trunc cells showed no evidence of ZAP-70 redistribution to the cell surface even after 15 min PV stimulation (*middle row*), similarly to HeLa cells without a

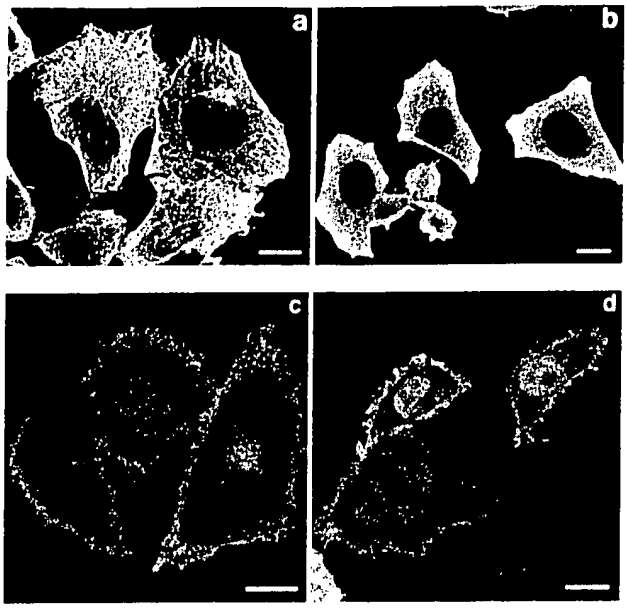

Figure 4. Testing microtubule involvement in ZAP-70's redistribution. H/TTζ cells, cotransfected with Lck F505 and ZAP-70 GFP, were left untreated (*a* and *c*) or pretreated with nocodazole (33 μM; *b* and *d*). In *a* and *b*, cells were fixed and immunostained with antitubulin mAb, followed by a rhodamine-coupled anti-mouse secondary mAb. In *c* and *d*, cells were stimulated with PV and monitored by time-lapse imaging. Time points 15 min after stimulation are shown. Bars, 15 μm.

TCR chain (Fig. 1, *first* and *third rows*). While herbimycin A pretreatment prevented ZAP-70 redistribution to the plasma membrane, there was some redistribution of the chimera under these conditions (Fig. 3, *bottom row*). This drug is likely causing several effects in the cells, many of which may be tyrosine kinase dependent. However, the lack of redistribution of ZAP-70 to the plasma membrane in the presence of herbimycin A is consistent with its inhibition of ITAM phosphorylation. Thus, the cytosolic tail of TCR containing ITAMs and tyrosine phosphorylation after activation were critical for movement of ZAP-70 to the membrane. TTζ and Tζζ appeared to perform equivalently for ZAP-70 recruitment, suggesting that TCRζ dimerization has no effect on the binding efficiency for ZAP-70 in this system (data not shown).

Intact Microtubules or Actin Cytoskeleton Are Not Required for ZAP-70 Translocation to the Cell Surface

Biochemical studies on ZAP-70 have not addressed how this kinase accumulates at the plasma membrane upon cellular stimulation. In fact, the model suggesting that it moves from the cytosol to the cell surface has only been an assumption. Our results confirm that translocation indeed occurs. To explore the mechanism of this translocation, we tested whether microtubules or the actin cytoskeleton were required. H/TTζ cells were treated with nocodazole, which leads to disassembly of the intracellular microtubule lattice. Antitubulin antibody staining of cells showed complete disassembly of the microtubule array in cells treated with nocodazole (33 mM, Fig. 4 *b*), but not in untreated cells (Fig. 4 *a*). Time-lapse imaging of ZAP-70 GFP– and Lck F505–transfected H/TTζ cells indicated that ZAP-70 translocated to the plasma membrane in response to cellular stimulation in both nocodazole-treated and untreated cells with similar kinetics (Fig. 4 *d*, nocodazole-treated, and *c*, untreated, both 15 min PV, and data not shown). Other cells from the population, treated identically, were stained with antitubulin mAb to confirm that nocodazole had disrupted the microtubule lattice. Moreover, treatment of cells with up to 100 μM nocodazole still did not impair ZAP-70 translocation to the cell surface. In addition, the breakdown of actin filaments by cytochalasin B had no effect on ZAP-70 redistribution (data not shown). These data indicate that the microtubule array and the actin cytoskeleton are not required for the intracellular translocation of ZAP-70.

Redistribution of ZAP-70 from the Cytosol to the Cell Surface Correlates with Its Conversion to a Less Mobile State

The ability to photobleach GFP chimeras makes them attractive tools for studying molecular dynamics in real time proteins (Cole et al., 1996). Using photobleaching techniques, we initially took a qualitative approach to determine whether there were any gross changes in ZAP-70 diffusibility after its redistribution within the cell. For this, we repetitively photobleached a small area within the cell and looked for fluorescence loss in the entire cellular compartment due to diffusional exchange of unbleached with bleached molecules (Cole et al., 1996; Ellenberg et al., 1997). The length of time required for fluorescence loss under these conditions depends on the diffusional mobility of the fluorescent protein and the extent of continuity of the cellular compartments. This approach, termed FLIP, was used to compare the dynamics of cytosolic and nuclear ZAP-70 in resting H/TTζ cells expressing ZAP-70 GFP (Fig. 5 *A*). Both pools of ZAP-70 were extremely mobile, with a rapid loss of fluorescence in cells repetitively bleached in the cytosol and in the nucleus. Fluorescence was significantly depleted after only two bleaches (<60 s), and a complete loss was apparent after five bleaches (Fig. 5 *A*, *bottom right cell*). In cells in which the bleached region encompassed only the cytosol, nuclear ZAP-70 GFP remained detectable for a longer time period (Fig. 5 *A*, *top right cell*). These data indicate that cytosolic and nuclear ZAP-70 are both highly mobile and that they are not freely interchangeable with each other. Also, the coexpression of Lck F505 had no effect on the mobility of ZAP-70 during the time frame of the experiment (Fig. 5, compare *B* to *A*).

The time-lapse imaging studies showed that ZAP-70 redistributed from the cytosol to a more peripheral location in TTζ-expressing cells in response to stimulation (Fig. 1). This phenotype was biochemically consistent with a specific molecular interaction between ZAP-70 and the ζ chimera (Figs. 2 and 3). We wanted to determine if this shift of ZAP-70 to the periphery correlated with a change in its diffusional properties. H/TTζ cells expressing ZAP-70 GFP and Lck F505 were stimulated with PV for 12 min before the commencement of FLIP to induce maximal ZAP-70 redistribution to the cell surface. After repetitive pho-

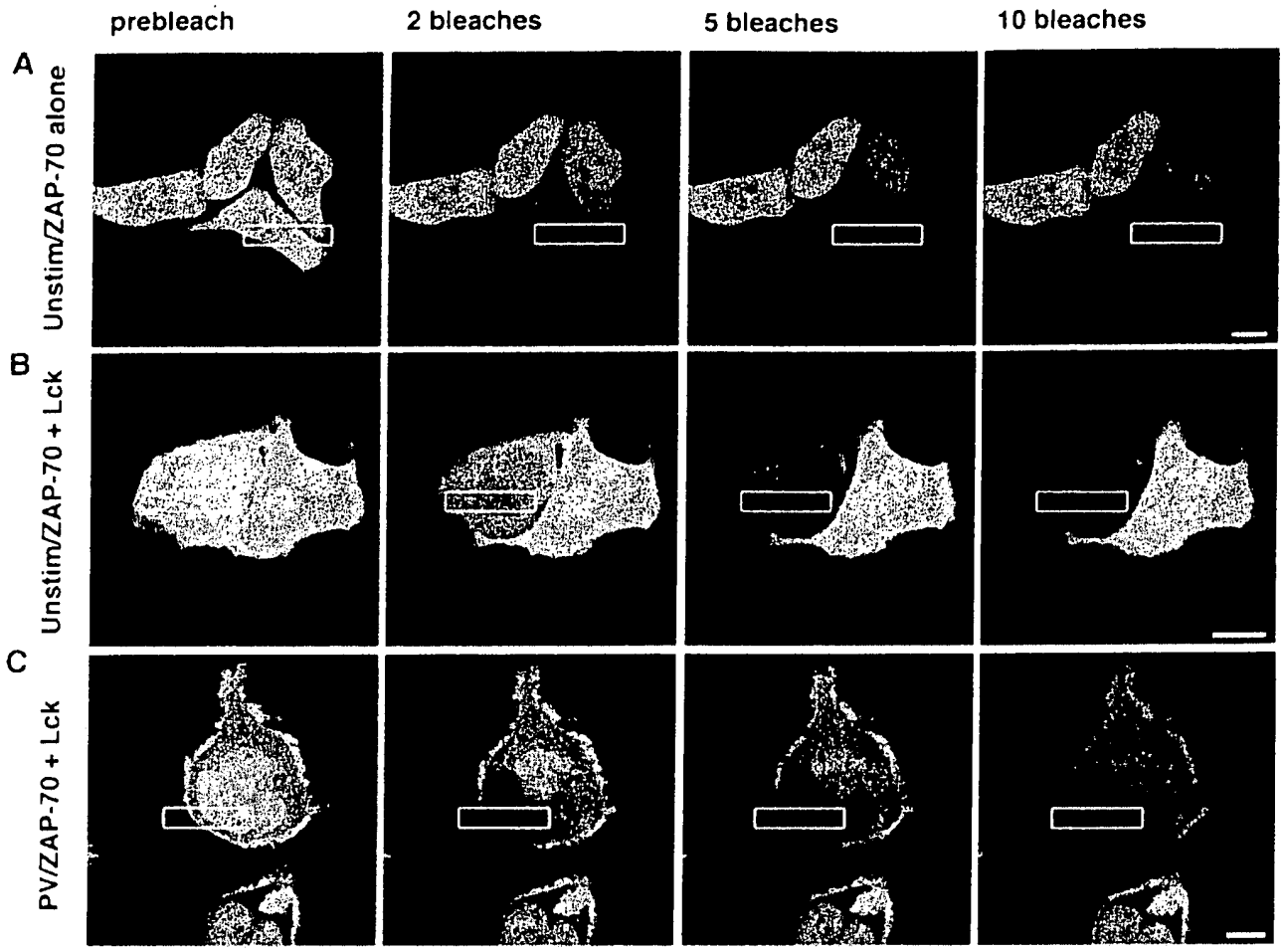

Figure 5. ZAP-70 becomes less mobile when it moves to the cell surface. H/TTζ cells expressing ZAP-70 GFP alone (*A*) or together with Lck F505 (*B* and *C*) were left unstimulated (*A* and *B*) or were stimulated with PV for 12 min before commencement of FLIP (*C*). FLIP was then carried out as described in Materials and Methods, with the boxed rectangle indicating the area being repetitively bleached. Images collected before bleaching and after 2, 5, and 10 bleaches are shown. Bars, 15 μm.

tobleaching of a region of the cell, it was obvious that the diffusional mobility of ZAP-70 had been altered (Fig. 5 *C*). Specifically, surface-localized ZAP-70 was less mobile and no longer able to exchange with the intracytoplasmic pool. A strong fluorescent signal was still apparent at the end of the bleaching sequence (~300 s). There are two possible explanations for this. Either all of the cytosolic ZAP-70 redistributes to the cell periphery, or some remains in the cytosol but converts to a less mobile phenotype, perhaps because of an activation-induced interaction with cytoskeletal proteins. The first hypothesis is the more likely since the conversion to the less mobile state only occurs after stimulation of TTζ-expressing cells, which is consistent with a molecular interaction between these two molecules (data not shown). Regardless, activation-dependent redistribution of ZAP-70 to the cell surface is accompanied by a decrease in its mobility.

Membrane-associated ZAP-70 Is More Mobile than TCRζ

Biochemical studies have indicated that cell surface–located ZAP-70 is physically bound to TCRζ, via the tandem SH2 domains of ZAP-70 and the phospho-ITAMs of TCRζ (Figs. 2 and 3) (Isakov et al., 1995; Bu et al., 1995). One prediction from these data would be that peripherally located ZAP-70 would acquire the same diffusion mobility as TCRζ. We therefore compared the diffusion mobility of the translocated ZAP-70 to that of the ζ chimera, Tζζ. A Tζζ–GFP fusion protein was constructed and expressed in HeLa cells and was expressed exclusively on the cell membrane, as expected for an integral membrane protein (Fig. 6 *C*). H/TTζ cells expressing ZAP-70 GFP alone or together with Lck F505 and HeLa cells expressing Tζζ–GFP were then stimulated with PV for 12 min, and FLIP was performed to compare the mobilities of the two proteins at the cell surface (Fig. 6). As before, peripheral ZAP-70 was relatively stable, showing a similar phenotype whether Lck F505 was coexpressed or not. However, when repetitive photobleaching inside the rectangular box was continued, complete loss of ZAP-70 GFP fluorescence outside the box occurred between 750 and 870 s (Fig. 6, *A* and *B*). In contrast, fluorescence of Tζζ–GFP remained prominently visible on the cell membrane after repetitive photobleaching for 30 min (Fig. 6 *C*, and data not shown). The mobility of Tζζ–GFP was not affected by PV stimulation since it

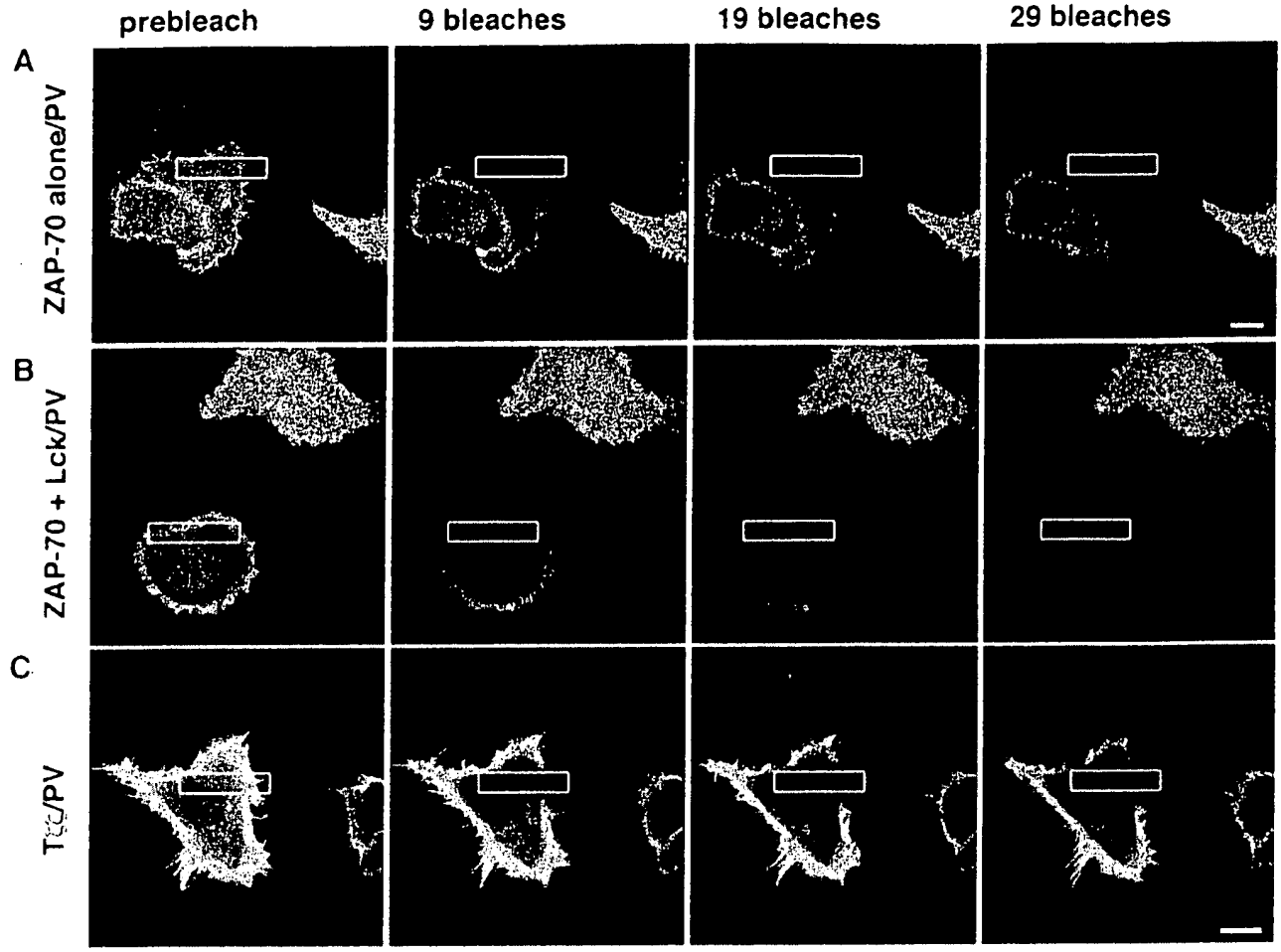

Figure 6. Membrane-associated ZAP-70 is more mobile than TCRζ. H/TTζ cells expressing ZAP-70 GFP alone (*A*) or together with Lck F505 (*B*), or HeLa cells expressing Tζζ–GFP (*C*), were stimulated for 12 min before commencement of FLIP. The area repetitively photobleached is indicated by the rectangle. Images collected before bleaching and after 9, 19, and 29 photobleaches are shown. Bars, 12 μm.

photobleached at a comparable rate in untreated cells. Furthermore, when a TTζ–GFP chimera was used, a similar phenotype was noted, indicating that ζ dimerization has no effect on its mobility in the plasma membrane (data not shown). Thus, it was apparent that the peripherally located ZAP-70 was more mobile than the integral membrane ζ chimera.

FLIP is limited to determining qualitative assessments since the rate at which a cell loses its fluorescence signal is a function of both the diffusion out of the surrounding areas to the bleach zone as well as the size of the bleach zone relative to the entire cell. To better understand the nature of the interaction between ZAP-70 and TCRζ, we wanted to be able to make quantitative measurements of protein diffusion. For this, we used the FRAP technique, in which fluorescence recovery into a bleached region of the cell after a single photobleach is monitored until recovery is complete (Edidin, 1994; Ellenberg et al., 1997; Lippincott-Schwartz, 1998). Experimental data are then plotted versus time and are fit to an empirical formula (Fig. 7 *c*) to determine the diffusion coefficient, *D*, for the protein. A representative plot of fluorescence recovery versus time is shown for both Tζζ–GFP and membrane-associated ZAP-70 GFP (Fig. 7 *a*). These data indicate that Tζζ moves slowly within the membrane, since a plateau of fluorescence recovery is not approached until >440 s for Tζζ compared with about 120 s for ZAP-70. Moreover, the *D* value derived for Tζζ indicated that it diffused slowly in the membrane and was similar to those derived for other plasma membrane proteins (Fig. 7 *b*; 0.011 ± 0.001 $\mu m^2/s$) (Pal et al., 1991). However, the *D* value derived for peripherally located ZAP-70 was >20-fold higher (Fig. 7 *b*; 0.234 ± 0.036 $\mu m^2/s$). These data thus provide strong evidence against the possibility that ZAP-70 irreversibly binds to TCR subunits at the plasma membrane and instead suggest that it interacts dynamically with TCRζ, continually exchanging on and off the plasma membrane. The extremely rapid motion of cytosolic ZAP-70 made it difficult to determine an accurate *D* value with our experimental setup, but it is greater than 1 $\mu m^2/s$.

A

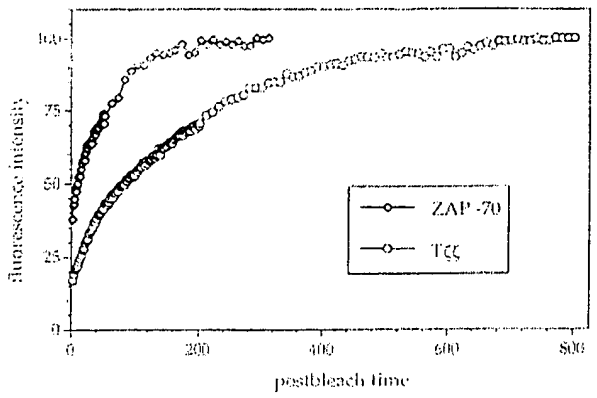

B

$D\,T\zeta\zeta = 0.011 \pm 0.001\ \mu m^2/sec$

$D\,ZAP\text{-}70 = 0.234 \pm 0.036\ \mu m^2/sec$

C Equation for determination of diffusion constants:

$$I_{(t)} = I_{(final)}\,(1 - (W^2\,(W^2 + 4\pi Dt)^{-1})1/2)$$

Figure 7. Quantitative FRAP experiments to determine diffusion constants for ZAP-70 GFP and Tζζ–GFP. (*A*) Fluorescence intensities in recovery after photobleaching, normalized to maximal levels (100%) for both ZAP-70 GFP and Tζζ–GFP, are plotted versus time. Data points were taken at 2-s intervals for 200 s (Tζζ–GFP) or at 1-s intervals for 50 s (ZAP-70 GFP) and then at 10-s intervals until they had reached a steady plateau. (*B*) Diffusion constants ± SD, expressed as a mean from five (Tζζ–GFP) or six (ZAP-70 GFP) independent experiments, are given. Simulated values were 0.016 and 0.09 $\mu m^2/s$ for Tζζ–GFP and ZAP-70 GFP, respectively. (*C*) Equation used to derive diffusion constants assuming one-dimensional recovery.

The equation used for FRAP *D* value measurements assumes one-dimensional recovery since the membranes are bleached all across their length and entire depth. To assess the effect of geometry, the calculated *D* values were checked against a numerical simulation that used the prebleach intensity of the entire cell as input to simulate diffusion recovery into the bleached strip (Ellenberg et al., 1997; Sciaky et al., 1997). For Tζζ GFP, the experimental *D* value correlated well with that derived from the simulated calculation, which was 0.016 $\mu m^2/s$ (compared with 0.011 $\mu m^2/s$). In contrast, the *D* value derived experimentally for ZAP-70 GFP (0.234 $\mu m^2/s$) was much faster than its simulated counterpart (0.090 $\mu m^2/s$). Moreover, the fits generated by the simulation for ZAP-70 GFP were poor and variable. These observations, together with the fact that ζ-associated ZAP-70 moves 20-fold faster than TCRζ, supports the hypothesis that the movement of ZAP-70 at the plasma membrane is more complex than simple diffusion and likely involves other dynamic parameters, such as exchange of ZAP-70 with the cytosolic pool.

Discussion

We have used GFP technology to study the movement, kinetics, and associations of key proteins used in signal transduction pathways coupled to the T cell antigen receptor. Biochemical data have suggested that ZAP-70 undergoes rapid intracellular translocation (Chan et al., 1991; Wange et al., 1992). Thus, we were curious to study its intracellular distribution and visualize its changes in response to cellular stimulation in live cells. Our earlier report provided preliminary data defining where ZAP-70 resides in resting cells and how it translocates to the cell surface upon cellular stimulation (Sloan-Lancaster et al., 1997). However, the specific nature of the translocation, and the subsequent binding to TCR subunits at the plasma membrane, could not be investigated. Here we analyze ZAP-70–TCRζ interaction in real time and the intramolecular properties required for this association. The kinetics of ZAP-70 translocation to the plasma membrane and its diffusional mobility in the different intracellular locations were measured.

The activation-induced movement of ZAP-70 to the cell surface in HeLa cells expressing TTζ, but not in HeLa, was a strong indication that we were monitoring the specific molecular interaction of two proteins over real time. This redistribution was much more dramatic than that in COS 7 cells, with an impressive clearing from the cytosol accompanying a uniform redistribution to the plasma membrane. Biochemically, the interaction of ZAP-70 and the ITAMs has been shown to require the tandem SH2 domains of ZAP-70 and a doubly phosphorylated ITAM (Wange et al., 1993; Iwashima et al., 1994; Koyasu et al., 1994). The crystal structure of the SH2 domains of ZAP-70 bound to a phospho-ITAM verified the molecular properties of this association (Hatada et al., 1995). Based on these data, we designed mutants of ZAP-70 and truncated Tζζ constructs to study the interaction of the two molecules in living cells. Our results validate the imaging approach taken, since they correlated exactly with the biochemical analyses. Moreover, they have allowed us to monitor for the first time the dynamics of these two proteins together in living cells. The tandem SH2 domains of ZAP-70 and an ITAM with phosphorylated tyrosines are clearly critical for any association to occur since there was no detectable redistribution at any time point for more than an hour after stimulation unless both of these criteria were met (Figs. 2 and 3 and data not shown).

How does ZAP-70 translocate to and remain at the plasma membrane? Because it is a cytosolic protein without any identified retention signal, it is likely freely diffusible within the cell, a phenotype supported by our FLIP data (Fig. 5). As the kinase moves randomly throughout the cytoplasm, it will be in a state in which some molecules are in close proximity to the cell surface at any time, and should therefore bind any available unoccupied phospho-ITAMs. After TCR engagement, when the CD3 and TCRζ ITAMs quickly become phosphorylated, the likelihood that ZAP-70 will bind to them and be retained at the

membrane increases tremendously. This should result in an accumulation of ZAP-70 at the cell surface and a reciprocal decrease in its cytosolic concentration, as seen in our time-lapse imaging studies (Fig. 1). Thus, the phosphorylation of the TCR ITAMs seems to be the only triggering event for ZAP-70 redistribution. Our data using mutant ZAP-70 GFPs indicate that the domains required for its redistribution and membrane retention parallel those required to bind TTζ (Fig. 2). Moreover, the enhancement of ZAP-70 redistribution accompanied by coexpression of Lck F505 indicates that simply increasing the level of ITAM phosphorylation results in more ZAP-70 at the plasma membrane (Fig. 1). Finally, neither the organized microtubular network nor the actin microfilaments are required for successful movement of ZAP-70 to the cell surface (Fig. 4).

The data reported by Huby et al. (1998) indicated that nocodazole treatment of T cells can prevent ZAP-70 activation, independently of the location of ZAP-70 at the cell surface. Moreover, in that study ZAP-70 appeared to be in a membrane proximal region in resting T cells, before cellular activation. The differences between this study and our data might reflect the presence of additional proteins in T cells that engage ZAP-70 and affect its dynamics and activation. Our studies in HeLa cells represent an early effort in studying these molecules in real time. The dynamic properties of ZAP-70 must now be analyzed with these methods in T cells.

The kinetics by which ZAP-70 relocated to the HeLa cell surface were much slower than would be predicted from the biochemical analyses in T cells, which indicate that ZAP-70 binds TCRζ within seconds of TCR cross-linking (Chan et al., 1991; Wange et al., 1992). Surprisingly, there was a significant delay between cellular activation and any detectable, redistributed ZAP-70 (Fig. 1). Perhaps the rate-limiting step is the tyrosine phosphorylation of proteins within the cells due to time required for PV, when delivered in the media, to be incorporated into the cells. Moreover, the live cell experiments were conducted at room temperature, and we anticipate that increasing the temperature to 37°C would also result in a faster translocation initiation time. Of course, the system employed here using HeLa cells and recombinant proteins is a simplification of the complexity of early T cell signaling events, in which multiple protein–protein interactions participate to initiate signal transduction. In the T cell environment, such interactions might affect the mobility of both ZAP-70 and TCRζ. However, in the HeLa system, once ZAP-70 began to translocate to the cell surface it quickly reached a steady state, without evidence of any reaccumulation in the cytosol even as long as several hours after PV addition (data not shown). Whether it moves back after the pharmacological or physiological stimulus ceases or is degraded at the plasma membrane is not known.

The data derived using the photobleaching techniques allowed us not only to qualitatively compare the movement of different pools of ZAP-70 with itself and with chimeric ζ, but also to calculate diffusion constants for these molecules. While a role for nuclear ZAP-70 has still not been defined, it clearly is not rapidly interchangeable with the cytosolic pool (Fig. 5 *A*). Both nuclear and cytosolic ZAP-70 are extremely mobile, so we could not determine a lower limit for their diffusion constants. This suggests that the protein is not associated with any anchoring molecules in these compartments. However, membrane-associated ZAP-70 in stimulated cells has dramatically different characteristics in that it is much less mobile. Clearly, membrane-associated ZAP-70 moves slowly relative to the cytosolic pool of unstimulated cells and is likely part of a large multiprotein lattice under the cell surface, containing many of the downstream molecules involved in intracellular signaling.

The peripherally located ZAP-70 had a faster diffusion rate than the chimeric ζ molecule. This was confirmed when the diffusion constants were determined, indicating that ZAP-70 moved ~20-fold faster than ζ (Fig. 7). This indicated that the binding between ζ and ZAP-70 is more complex than an irreversible and stationary interaction. The simulation data also confirmed that the movement of ZAP-70 at or near the membrane is not explained by a single diffusion constant. Instead, it seems that the SH2–phosphotyrosine interaction is dynamic, with specific on- and off-rates. Indeed, this dynamic relationship could explain how an immune response is regulated at the cellular level. Once initiated, T cell activation must eventually be turned off as antigen is cleared from the system. ITAM phosphorylation is a key initiating event of intracellular T cell activation, but dephosphorylation of these domains is critical for the disassembly of the activating lattice under the membrane. In fact, a proposed role of ZAP-70 is that it protects the phosphates of the TCR ITAMs by binding via its SH2 domains, thus maintaining the receptor in an "on" state (Iwashima et al., 1994). Only if ZAP-70 has a dynamic relationship with TCRζ will the phospho-ITAMs be exposed to phosphatases, which will then have an opportunity to dephosphorylate the tyrosine residues. As a result, the now dephosphorylated ITAMs will no longer be suitable targets for ZAP-70, which may eventually recycle to the cytosol or be degraded over time. As fewer active ZAP-70 molecules remain at the cell surface, all subsequent signaling events in the cell will also sequentially be turned off, until the cell returns to its quiescent state.

The ability to study intracellular signal transduction in real time now provides one with the tools to begin to answer many unaddressed questions. With the availability of several GFP variants that excite and emit at different wavelengths (Heim et al., 1994; Heim and Tsien, 1996; Ormo et al., 1996), the movements of several proteins have been successfully monitored simultaneously by time-lapse imaging (Rizzuto et al., 1995; Ellenberg et al., 1998). Moreover, the relationship of protein location and second messenger stimulation has also been studied (Miyawaki et al., 1997; Oancea et al., 1998; Stauffer et al., 1998). Fluorescence resonance energy transfer to assess protein–protein interactions will provide detailed information regarding how intracellular networks are established and maintained (Miyawaki et al., 1997; Romoser et al., 1997; Tsien and Miyawaki, 1998). As these techniques are refined and applied, more studies on how intracellular complexes form in many signaling systems should be performed.

J. Sloan-Lancaster is a fellow of the Damon Runyon-Walter Winchell Cancer Research Fund. T. Yamazaki is a fellow of the Japan Society for the Promotion of Science.

Received for publication 16 July 1998 and in revised form 11 September 1998.

References

Arpaia, E., M. Shahar, H. Dadi, A. Cohen, and C.M. Roifman. 1994. Defective T cell receptor signaling and $CD8^+$ thymocyte selection in humans lacking ZAP-70 kinase. *Cell.* 76:947–958.

Babbitt, B.P., P.M. Allen, G. Matsueda, E. Haber, and E.R. Unanue. 1985. Binding of immunogenic peptides to Ia histocompatibility molecules. *Nature.* 317:359–361.

Bentley, G.A., and R.A. Mariuzza. 1996. The structure of the T cell antigen receptor. *Annu. Rev. Immunol.* 14:563–590.

Bu, J.-Y., A.S. Shaw, and A C. Chan. 1995. Analysis of the interaction of ZAP-70 and syk protein-tyrosine kinases with the T-cell antigen receptor by plasmon resonance. *Proc. Natl. Acad. Sci. USA.* 92:5106–5110.

Cantrell, D. 1996. T cell antigen receptor signal transduction pathways. *Annu. Rev. Immunol.* 14:259–274.

Chan, A.C., B. Irving, J.D. Fraser, and A. Weiss. 1991. TCRζ chain associates with a tyrosine kinase and upon TCR stimulation associates with ZAP-70, a 70K M_r tyrosine phosphoprotein. *Proc. Natl. Acad. Sci. USA.* 88:9166–9170.

Chan, A.C., M. Iwashima, C.W. Turck, and A. Weiss. 1992. ZAP-70: a 70 kd protein-tyrosine kinase that associates with the TCRζ chain. *Cell.* 71:649–662.

Chan, A.C., T.A. Kadlecek, M.E. Elder, A.H. Filipovich, W.-L. Kuo, M. Iwashima, T.G. Parslow, and A. Weiss. 1994. ZAP-70 deficiency in an autosomal recessive form of severe combined immunodeficiency. *Science.* 264:1599–1601.

Cole, N.B., C.L. Smith, N. Sciaky, M. Terasaki, M. Edidin, and J. Lippincott-Schwartz. 1996. Diffusional mobility of Golgi proteins in membranes of living cells. *Science.* 273:797–801.

Edidin, M. 1994. Fluorescence photobleaching and recovery, FPR, in the analysis of membrane structure and dynamics. *In* Mobility and Proximity in Biological Membranes. S. Damjanocich, M. Edidin, and J. Szollosi, editors. CRC Press, Inc., Boca Raton, FL. 109–135.

Elder, M.E., D. Lin, J. Clever, A.C. Chan, T.J. Hope, A. Weiss, and T.G. Parslow. 1994. Human severe combined immunodeficiency due to a defect in ZAP-70, a T cell tyrosine kinase. *Science.* 264:1596–1599.

Ellenberg, J., E.D. Siggia, J.E. Moreira, C.L. Smith, J.F. Presley, H.J. Worman, and J. Lippincott-Schwartz. 1997. Nuclear membrane dynamics and reassembly in living cells: targeting of an inner nuclear membrane protein in interphase and mitosis. *J. Cell Biol.* 138:1193–1206.

Ellenberg, J., J. Lippincott-Schwartz, and J.F. Presley. 1998. Two color green fluorescent protein time-lapse imaging. *Biotechniques.* In press.

Garcia, K.C., M. Degano, R.L. Stanfield, A. Brunmark, M.R. Jackson, P.A. Peterson, L. Teyton, and I.A. Wilson. 1996. An αβ T cell receptor structure at 2.5 Å and its orientation in the TCR-MHC complex. *Science.* 274:209–219.

Hatada, M.H., X. Lu, E.R. Laird, J. Green, J.P. Morgenstern, M. Lou, C.S. Marr, T.B. Phillips, M.K. Ram, K. Theriault, M.J. Zoller, and J.L. Karas. 1995. Molecular basis for interaction of the protein tyrosine kinase ZAP-70 with the T-cell receptor. *Nature.* 377:32–38.

Heim, R., and R.Y. Tsien. 1996. Engineering green fluorescent protein for improved brightness, longer wavelengths and fluorescence resonance energy transfer. *Curr. Biol.* 6:178–182.

Heim, R., D.C. Prasher, and R.Y. Tsein. 1994. Wavelength mutations and posttranslational autoxidation of green fluorescent protein. *Proc. Natl. Acad. Sci. USA.* 91:12501–12504.

Huby, R.D., A. Weiss, and S.C. Ley. 1998. Nocodazole inhibits signal transduction by the T cell antigen receptor. *J Biol. Chem.* 273:12024–12031.

Isakov, N., R.L. Wange, W.H. Burgess, J.D. Watts, R. Aebersold, and L.E. Samelson. 1995. ZAP-70 binding specificity to T cell receptor tyrosine-based activation motifs: the tandem SH2 domains of ZAP-70 bind distinct tyrosine-based activation motifs with varying affinity. *J. Exp. Med.* 181:375–380.

Iwashima, M., B.A. Irving, N.S.C. van Oers, A.C. Chan, and A. Weiss. 1994. Sequential interactions of the TCR with two distinct cytoplasmic tyrosine kinases. *Science.* 263:1136–1139.

Jorgensen, J.L., P.A. Reay, E.W. Ehrich, and M.M. Davis. 1992. Molecular components of T-cell recognition. *Annu. Rev. Immunol.* 10:835–873.

Kong, G., M. Dalton, J.B. Wardenburg, D. Straus, T. Kurosaki, and A.C. Chan. 1996. Distinct tyrosine phosphorylation sites within ZAP-70 mediate activation and negative regulation of antigen receptor function. *Mol. Cell. Biol.* 16: 5026–5035.

Koyasu, S., A.G.D. Tse, P. Moingeon, R.E. Hussey, A. Mildonian, J. Hannisian, L.K. Clayton, and E.L. Reinherz. 1994. Delineation of a T-cell activation motif required for binding of protein tyrosine kinases containing tandem SH_2 domains. *Proc. Natl. Acad. Sci. USA.* 91:6693–6697.

Letourneur, F., and R.D. Klausner. 1991. T-cell and basophil activation through the cytoplasmic tail of T-cell-receptor zeta family proteins. *Proc. Natl. Acad. Sci. USA.* 88:8905–8909.

Lippincott-Schwartz, J., J. Presley, K. Zaal, K. Hirschberg, C. Miller, and J. Ellenberg. 1998. Monitoring the dynamics and mobility of membrane proteins tagged with green fluorescent protein. *In* GFP Biofluorescence: Imaging Gene Expression and Protein Dynamics in Living Cells. K. Sullivan and S. Kay, editors. Academic Press, New York. In press.

Miyawaki, A., J. Llopis, R. Heim, J.M. McCaffrey, J.A. Adams, M. Ikura, and R.Y. Tsien. 1997. Fluorescent indicators for Ca^{2+} based on green fluorescent proteins and calmodulin. *Nature.* 388:882–887.

Negishi, I., N. Motoyama, K.-i. Nakayama, K. Nakayama, S. Senju, S. Hatakeyama, Q. Zheng, A.C. Chan, and D.Y. Loh. 1995. Essential role for ZAP-70 in both positive and negative selection of thymocytes. *Nature.* 376: 435–438.

O'Shea, J.J., D.W. McVicar, T.L. Bailey, C. Burns, and M.J. Smyth. 1992. Activation of human peripheral blood T lymphocytes by pharmacological induction of protein-tyrosine phosphorylation. *Proc. Natl. Acad. Sci. USA.* 89: 10306–10310.

Oancea, E., M.N. Teruel, A.F.G. Quest, and T. Meyer. 1998. Green fluorescent protein (GFP)-tagged cysteine-rich domains from protein kinase C as fluorescent indicators for diacylglycerol signaling in living cells. *J. Cell Biol.* 140: 485–498.

Ormo, M., A.B. Cubitt, K. Kallio, L.A. Gross, R.Y. Tsien, and S.J. Remington. 1996. Crystal structure of the *Aequorea victoria* green fluorescent protein. *Science.* 273:1392–1395.

Pal, R., B.C. Nair, G.M. Hoke, M.G. Sarngadharan, and M. Edidin. 1991. Lateral diffusion of CD4 on the surface of a human neoplastic T-cell line probed with a fluorescent derivative of the envelope glycoprotein (gp120) of human immunodeficiency virus type 1 (HIV-1). *J. Cell Physiol.* 147:326–332.

Qian, D., and A. Weiss. 1997. T cell antigen receptor signal transduction. *Curr. Opin. Cell Biol.* 9:205–212.

Qian, D., M.N. Mollenauer, and A. Weiss. 1996. Dominant-negative ζ associated protein 70 inhibits T cell antigen receptor signaling. *J. Exp. Med.* 183:611–620.

Reth, M. 1989. Antigen receptor tail clue. *Nature.* 338:383–384.

Rizzuto, R., M. Brini, P. Pizzo, M. Murgia, and T. Pozzan. 1995. Chimeric green fluorescent protein as a tool for visualizing subcellular organelles in living cells. *Curr. Biol.* 5:635–642.

Romoser, V.A., P.M. Hinkle, and A. Persechini. 1997. Detection in living cells of Ca^{2+}-dependent changes in the fluorescence emission of an indicator composed of two green fluorescent protein variants linked by a calmodulin-binding sequence. *J. Biol. Chem.* 272:13270–13274.

Samelson, L.E., and R.D. Klausner. 1992. Tyrosine kinases and tyrosine-based activation motifs. *J. Biol. Chem.* 267:24913–24916.

Sciaky, N., J. Presley, C. Smith, K.J. Zaal, N. Cole, J.E. Moreira, M. Terasaki, E. Siggia, and J. Lippincott-Schwartz. 1997. Golgi tubule traffic and the effects if brefeldin A visualized in living cells. *J. Cell Biol.* 139:1137–1155.

Secrist, J.P., L.A. Burns, L. Karnitz, G.A. Koretzky, and R.T. Abraham. 1993. Stimulatory effects of the protein tyrosine phosphatase inhibitor, pervanadate, on T-cell activation events. *J. Biol. Chem.* 268:5886–5893.

Sloan-Lancaster, J., and L.E. Samelson. 1998. Proximal events in T cell activation. *In* Signal Transduction and Cell Cycle Inhibitors. J.S. Gutkind, editor. Humana Press, Totowa, NJ. In press.

Sloan-Lancaster, J., W. Zhang, J. Presley, B.L. Williams, R.T. Abraham, J. Lippincott-Schwartz, and L.E. Samelson. 1997. Regulation of ZAP-70 intracellular localization: visualization with the green fluorescent protein. *J. Exp. Med.* 186:1713–1724.

Stauffer, T.P., S. Ahn, and T. Meyer. 1998. Receptor-induced transient reduction in plasma membrane $PtdIns(4,5)P_2$ concentration monitored in living cells. *Curr. Biol.* 8:343–346.

Townsend, A.R.M., J. Rothbard, F.M. Gotch, G. Bahadur, D. Wraith, and A.J. McMichael. 1986. The epitopes of influenza nucleoprotein recognized by cytotoxic T clymphocytes can be defined with short synthetic peptides. *Cell.* 44: 959–968.

Tsien, R.Y., and A. Miyawaki. 1998. Seeing the machinery of live cells. *Science.* 280:1954–1955.

van Oers, N.S., N. Killeen, and A. Weiss. 1996. Lck regulates the tyrosine phosphorylation of the T cell receptor subunits and ZAP-70 in murine thymocytes. *J. Exp. Med.* 183:1053–1062.

Wange, R.L., and L.E. Samelson. 1996. Complex complexes: signaling at the TCR. *Immunity.* 5:197–205.

Wange, R.L., A.-N. Kong, and L.E. Samelson. 1992. A tyrosine-phosphorylated 70-KDa protein binds a photoaffinity analogue of ATP and associates with both the ζ chain and CD3 components of the activated T cell antigen receptor. *J. Biol. Chem.* 267:11685–11688.

Wange, R.L., S.N. Malek, S. Desiderio, and L.E. Samelson. 1993. Tandem SH_2 domains of ZAP-70 bind to T cell antigen receptor ζ and CD3ε from activated jurkat T cells. *J. Biol. Chem.* 268:19797–19801.

Wange, R.L., R. Guitian, N. Isakov, J.D. Watts, R. Aebersold, and L.E. Samelson. 1995*a*. Activating and inhibitory mutations in adjacent tyrosines in the kinase domain of ZAP-70. *J. Biol. Chem.* 270:18730–18733.

Wange, R.L., N. Isakov, T. Burke, Jr., A. Otaka, P.P. Roller, J.D. Watts, R. Aebersold, and L.E. Samelson. 1995*b*. $F_2(Pmp)_2$-$TAM\zeta_3$, a novel competitive inhibitor of the binding of ZAP-70 to the T cell antigen receptor, blocks early T cell signaling. *J. Biol. Chem.* 270:944–948.

Weiss, A. 1993. T cell antigen receptor signal transduction: a tale of tails and cytoplasmic protein-tyrosine kinases. *Cell.* 73:209–212.

Weiss, A., and D.R. Littman. 1994. Signal transduction by lymphocyte antigen receptors. *Cell.* 76:263–274.

Weissman, A.M. 1994. The T-cell antigen receptor: a multisubunit signaling complex. *Chem. Immunol.* 59:1–18.

Williams, B.L., K.L. Schreiber, W. Zhang, R.L. Wange, L.E. Samelson, P.J. Leibson, and R.T. Abraham. 1998. Genetic evidence for differential coupling of Syk family kinases to the T-cell receptor: reconstitution studies in a ZAP-70-deficient jurkat T-cell line. *Mol. Cell. Biol.* 18:1388–1399.

Direct Visualization of the Translocation of the γ-Subspecies of Protein Kinase C in Living Cells Using Fusion Proteins with Green Fluorescent Protein

Norio Sakai,* Keiko Sasaki,* Natsu Ikegaki,* Yasuhito Shirai,* Yoshitaka Ono,‡ and Naoaki Saito*

*Laboratory of Molecular Pharmacology, Biosignal Research Center, ‡Department of Biology, Faculty of Science, Kobe University, Kobe 657, Japan

Abstract. We expressed the γ-subspecies of protein kinase C (γ-PKC) fused with green fluorescent protein (GFP) in various cell lines and observed the movement of this fusion protein in living cells under a confocal laser scanning fluorescent microscope. γ-PKC–GFP fusion protein had enzymological properties very similar to that of native γ-PKC. The fluorescence of γ-PKC–GFP was observed throughout the cytoplasm in transiently transfected COS-7 cells. Stimulation by an active phorbol ester (12-*O*-tetradecanoylphorbol 13-acetate [TPA]) but not by an inactive phorbol ester (4α-phorbol 12, 13-didecanoate) induced a significant translocation of γ-PKC–GFP from cytoplasm to the plasma membrane. A23187, a Ca^{2+} ionophore, induced a more rapid translocation of γ-PKC–GFP than TPA. The A23187-induced translocation was abolished by elimination of extracellular and intracellular Ca^{2+}. TPA-induced translocation of γ-PKC–GFP was unidirected, while Ca^{2+} ionophore–induced translocation was reversible; that is, γ-PKC–GFP translocated to the membrane returned to the cytosol and finally accumulated as patchy dots on the plasma membrane. To investigate the significance of C1 and C2 domains of γ-PKC in translocation, we expressed mutant γ-PKC–GFP fusion protein in which the two cysteine rich regions in the C1 region were disrupted (designated as BS 238) or the C2 region was deleted (BS 239). BS 238 mutant was translocated by Ca^{2+} ionophore but not by TPA. In contrast, BS 239 mutant was translocated by TPA but not by Ca^{2+} ionophore. To examine the translocation of γ-PKC–GFP under physiological conditions, we expressed it in NG-108 cells, *N*-methyl-D-aspartate (NMDA) receptor–transfected COS-7 cells, or CHO cells expressing metabotropic glutamate receptor 1 (CHO/mGluR1 cells). In NG-108 cells, K^+ depolarization induced rapid translocation of γ-PKC–GFP. In NMDA receptor–transfected COS-7 cells, application of NMDA plus glycine also translocated γ-PKC–GFP. Furthermore, rapid translocation and sequential retranslocation of γ-PKC–GFP were observed in CHO/mGluR1 cells on stimulation with the receptor. Neither cytochalasin D nor colchicine affected the translocation of γ-PKC–GFP, indicating that translocation of γ-PKC was independent of actin and microtubule. γ-PKC–GFP fusion protein is a useful tool for investigating the molecular mechanism of γ-PKC translocation and the role of γ-PKC in the central nervous system.

Protein kinase C (PKC),[1] a family of phospholipid-dependent serine/threonine kinases and of which there are at least 12 subspecies, plays an important role in various cellular signal transductions (Nishizuka, 1984, 1988, 1992). Regardless of ubiquitous expression of PKCs in various tissues, the central nervous system abundantly contains several unique PKCs. In particular, the γ-subspecies of PKC (γ-PKC) is present only in the central nervous system and is thought to be involved in many neuronal functions including the formation of neural plasticity and memory (Nishizuka, 1986; Abeliovich et al., 1993*a*,*b*; Tanaka and Nishizuka, 1994).

PKC isozymes are divided into three subfamilies based on differences in the regulatory domain: conventional PKC (cPKC), novel PKC (nPKC), and atypical PKC (aPKC). Conventional PKCs have two common regions in the regulatory domain, C1 and C2. The C1 region has two cysteine-rich loops (zinc finger–like motifs) that interact with

Address all correspondence to Naoaki Saito, Laboratory of Molecular Pharmacology, Biosignal Research Center, Kobe University, 1-1 Rokkodai-cho, Nada-ku, Kobe 657, Japan. Tel.: 81-78-803-1251. Fax: 81-78-803-0993. E-mail: naosaito@inherit.biosig.kobe-u.ac.jp

1. *Abbreviations used in this paper*: 4α-PDD, 4α-phorbol 12, 13-didecanoate; DG, diacylglycerol; DO, diolein; GFP, green fluorescent protein; NMDA, *N*-methyl-D-aspartate; MCPG, α-methyl-4-carboxyphenyl-glycine; mGluR1, metabotropic glutamate receptor 1; PKC, protein kinase C; PS, phosphatidylserine; TPA, 12-*O*-tetradecanoylphorbol 13-acetate; *trans*-ACPD, (1S, 3R)-1-aminocyclopentane-1,3-dicarboxylic acid.

diacylglycerol (DG) or phorbol esters (Nishizuka, 1988; Ono et al., 1989). The C2 region mediates calcium binding (Ono et al., 1989) and is only present in cPKCs (Ono et al., 1988*b*), although a region related to C2 region was recently reported in nPKC, a calcium-independent PKC (Parker and Dekker, 1997). Full activation of cPKCs, including γ-PKC, requires DG and calcium. The C1 region is also present in nPKC, and one of the cysteine-rich loops is found in aPKCs.

Conventional PKCs and nPKCs, whose regulatory domains contain C1, are known to be translocated from the cytosol to particulate fraction when activated by DG or phorbol esters (Kraft et al., 1982). Therefore, the translocation of PKCs is a good marker of whether these enzymes are activated. Although this phenomenon is well known, the mechanism and physiological significance of PKC translocation have not yet been clarified. By conventional enzymological or immunohistochemical methods, it is impossible to observe the translocation of PKC in real time, in the same cells, and in living states, except in the investigation using fluorescent probes that directly bind PKC (Chen and Poenie, 1993). In addition, these fluorescent compounds are suggested to inhibit the activity of PKC itself at high concentration.

To resolve these problems and to directly observe the translocation of γ-PKC in living cells, we produced a fusion protein of γ-PKC and green fluorescent protein (GFP). The GFP, isolated from jellyfish *Aequorea victoria*, has fluorescence without additional substrates and cofactors (Cubitt et al., 1995). Recent studies have revealed that GFP is a good candidate as a molecular reporter protein to monitor the alternation of protein localization, gene expression, and protein trafficking in living cells (Cubitt et al., 1995). In this study, we visualized and analyzed the translocation of γ-PKC–GFP fusion protein with confocal laser scanning fluorescence microscopy, using various stimulations, such as phorbol esters, Ca^{2+} ionophore, K^+ depolarization, and receptor-mediated stimulus.

Materials and Methods

Materials

A23187 was purchased from Calbiochem (La Jolla, CA). *N*-methyl-D-aspartate (NMDA), 12-*O*-tetradecanoylphorbol 13-acetate (TPA), and 4α-phorbol 12, 13-didecanoate (4α-PDD) were purchased from Sigma Chemical Co. (St. Louis, MO). (1S, 3R)-1-aminocyclopentane-1,3-dicarboxylic acid (*trans*-ACPD), 2-amino-8-phosphonopentanoic acid (AP-5), and (RS)-α-methyl-4-carboxyphenyl-glycine ([RS]-MCPG) were from Tocris (Bristol, UK). Nicardipine and thapsigargin were from Wako Pure Chemical Ltd. (Osaka, Japan). ω-Conotoxin GVIA was from Peninsula Laboratories Inc. (Belmont, CA). Cytochalasin D and colchicine were from nacalai tesque (Kyoto, Japan). All other chemicals were of analytical grade.

Cell Culture

COS-7 and NIH3T3 cells were purchased from Riken cell bank (Tsukuba, Japan). Mouse neuroblastoma × glioma hybrid cells (NG 108-15 cells) were obtained from Dr. T. Amano (The Mitsubishi-Kasei Institute of Life Science, Tokyo, Japan). The CHO cells, stably expressing metabotropic glutamate receptor 1 (CHO/mGluR1 cells) (Tanabe et al., 1992) were a gift from Dr. Nakanishi (Department of Biological Science, Kyoto University Faculty of Medicine, Kyoto, Japan). COS-7 cells were cultured in DME containing 25 mM glucose, which was buffered with 44 mM $NaHCO_3$ and supplemented with 10% FBS, in a humidified atmosphere containing 5% CO_2 at 37°C. NG 108-15 cells were cultured in the same conditions as for COS-7 cells. NIH3T3 cells were cultured in DME supplemented with 10% calf serum instead of FBS. CHO/mGluR1 cells were cultured as described (Tanabe et al., 1992). All media were supplemented with penicillin (100 U/ml) and streptomycin (100 μg/ml), and the FBS used was not heat-inactivated.

Construct of Plasmids Encoding γ-PKC–GFP Fusion Protein

A plasmid containing GFP cDNA (pGFP 10.1) was donated by Dr. D.C. Prasher (Columbia University, New York) (Prasher et al., 1992). A cDNA fragment encoding GFP with a HindIII site in the 5′-terminal and an EcoRI site in the 3′-terminal end was obtained by PCR using pGFP 10.1 as a template. The sense and antisense primers used were 5′-TTAAGCTTATGGTGAGCAAGGGCCAGGAG-3′ and 5′-CCGAATTCTTACTTGTACAGCTCGTCCAT-3′, respectively. A rat γ-PKC cDNA was obtained from its cDNA clone of λCKRγ1 (Ono et al., 1988*a*). After digestion with EcoRI, an insert fragment encoding rat γ-PKC was subcloned into an expression plasmid for mammalian cells, pTB 701 (Ono et al., 1988*a*) (designated as BS 55) (Fig. 1). A cDNA fragment of γ-PKC with an EcoRI site in the 5′ terminus and a HindIII site in 3′ terminus was also produced by PCR using BS 55 as a template. The sense and antisense primers used were 5′-TTGAATTCATGGCGGGTCTGGGTCCTGG-3′ and 5′-TTAAGCTTATGGCGGGTCTGGGTCCTGG-3′, respectively. PCR products for both GFP and γ-PKC were together subcloned into the EcoRI site in pTB701 (BS 186) (Fig. 1).

We next produced a construct encoding mutant γ-PKC–GFP, whose zinc finger–like motif in the C1 region was mutated. We used pTB966, a plasmid containing a cDNA for mutated C1 region, as a template for PCR (Ono et al., 1989). The protein derived from pTB966 was reported to have no binding activity for TPA (Ono et al., 1989). We also produced a mutant γ-PKC–GFP construct whose C2 region was deleted. For this, pTB971 was used as a template for PCR (Ono et al., 1989). The protein derived from pTB971 no longer had binding activity for Ca^{2+} (Ono et al., 1989). PCR was performed to obtain a cDNA fragment containing C1 and C2 regions with a sense primer (5′-TTGAATTCATGGCGGGTCTGGGTCCTGG-3′) and an antisense primer (5′-TTGGATCCTCTGCGCTCTGCCAG-3′) using pTB966 or pTB971 as templates. These PCR products were digested with EcoRI and BamHI and then subcloned into BS 186, whose EcoRI/ BamHI fragment in γ-PKC was removed. These constructs were designated as BS 238 (C1 mutant) and BS 239 (C2 deletion), respectively. All PCR products were verified by sequencing. The structures of three γ-PKC–GFP proteins (BS 186, BS 238, and BS 239) are summarized in Fig. 1.

Expression of γ-PKC–GFP Protein in Cultured Cells

Transient transfection into COS-7 cells was performed by electroporation. Plasmids (~32 μg) encoding each type of γ-PKC–GFP or γ-PKC were transfected into 6×10^6 cells using a Gene Pulser (960 μF, 220 V; Bio-Rad Labs, Hercules, CA). Transfections into NG-108, NIH3T3, and CHO/mGluR1 cells were carried out by lipofection using Tfx-™-50 (Promega Corp., Madison, WI) according to the manufacturer's standard protocol. After the transfection, cells were cultured at 30°C to obtain the optimal fluorescence of GFP. The fluorescence of γ-PKC–GFP was detected 2 or 3 d after the transfection. Experiments were performed 3–5 d after the transfection.

Coexpression of NMDA Receptor and γ-PKC–GFP in COS-7 Cells

Mouse cDNAs encoding NMDARζ1 and NMDARε1 subunits, kindly donated by Dr. Mishina (Department of Pharmacology, Tokyo University, Faculty of Medicine, Tokyo, Japan) (Ikeda et al., 1992; Meguro et al., 1992; Yamazaki et al., 1992), were subcloned into an expression plasmid, pTB 701. The same amount of γ-PKC–GFP, NMDARζ1, and NMDARε1 plasmids (total 32 μg) was transfected into COS-7 cells by electroporation as described above. To prevent NMDA receptor–mediated cell death, transfected cells were cultured in the presence of 100 μM AP-5, an antagonist of NMDA receptor, until the experiment was performed.

Immunoblotting, Kinase Assay, and Immunoprecipitation of γ-PKC–GFP and γ-PKC

γ-PKC-GFP (BS 186) or γ-PKC (BS 55) cDNAs were transiently trans-

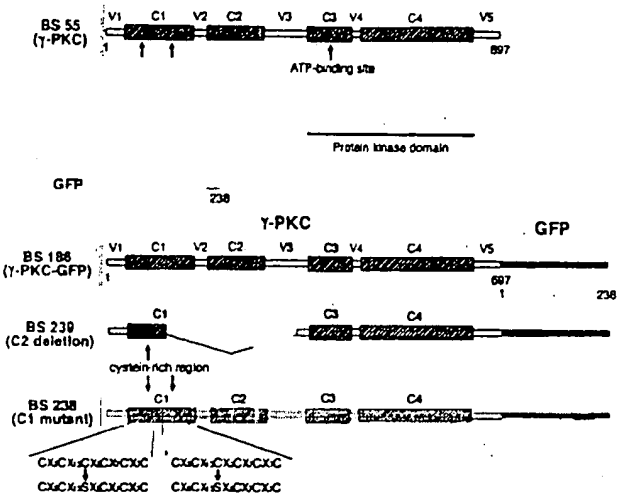

Figure 1. Constructs of γ-PKC–GFP fusion protein and its mutants. BS 186 was a γ-PKC–GFP fusion protein in which γ-PKC (BS 55) and GFP were bound at the COOH terminus of γ-PKC. In the C1 region of γ-PKC, there are two cysteine-rich sequences that interact with DG or phorbol esters, such as TPA. To produce BS 238 (C1 mutant), one cysteine residue in each of the two cysteine-rich regions was substituted with serine by site-directed mutagenesis. The C1 region of BS 238 no longer displayed activity for binding phorbol esters (Ono et al., 1989). The C2 region of γ-PKC, the Ca^{2+} binding domain, was deleted for the production of BS 239 (C2 deletion) as described in the text.

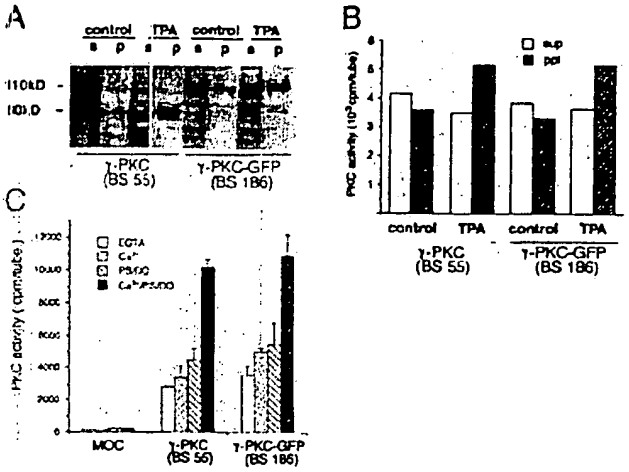

Figure 2. Enzymological property of γ-PKC and γ-PKC–GFP transiently expressed in COS-7 cells. (*A*) Immunoblotting analysis by anti–γ-PKC antibody revealed that expressed γ-PKC (BS 55) and γ-PKC–GFP (BS 186) were proteins with molecular sizes of 80 and 110 kD, respectively. Treatment with 5 μM TPA for 90 min increased the amount of both γ-PKC and γ-PKC–GFP associated with the particulate fraction. *p*, pellet (particulate fraction); *s*, supernatant (cytosol fraction). (*B*) Kinase activity of expressed γ-PKC and γ-PKC–GFP in cytosol and particulate fractions. Kinase activities of both γ-PKC and γ-PKC–GFP were translocated from the cytosol to particulate fraction after treatment with 5 μM TPA for 90 min. *ppt*, pellet (particulate fraction) *sup*, supernatant (cytosol fraction). (*C*) Enzymological property of γ-PKC and γ-PKC–GFP immunoprecipitated by anti–γ-PKC antibody. Kinase activities of expressed γ-PKC and γ-PKC–GFP, which were immunoprecipitated by anti–γ-PKC antibody, were measured in the presence or absence of activators of γ-PKC. The kinase activity of γ-PKC–GFP maximized in the presence of PS, DO, and Ca^{2+}, as did that of γ-PKC. The enzymological properties of γ-PKC and γ-PKC–GFP were very similar.

fected into 6×10^6 COS-7 cells by electroporation. The same number of transfected cells were divided into two culture dishes 8 cm in diameter and cultured at 30°C for 3 d. After treatment with 5 μM TPA for 90 min at room temperature, cells were harvested with PBS(−) and centrifuged. The cell pellet/dish was resuspended in 200 μl homogenate buffer (250 mM sucrose, 10 mM EGTA, 2 mM EDTA, 50 mM Tris/HCl, 200 μg/ml leupeptin, 1 mM PMSF, pH 7.4). After the sonication (UD-210 TOMY SEIKO Co. Ltd., Tokyo, Japan; output 3, duty 50%, 10 times, at 4°C), samples were centrifuged at 19,000 *g* for 30 min at 4°C, and supernatant was collected as the cytosol fraction. The pellet was resuspended with 200 μl of homogenate buffer containing 0.5% Triton-X and used as particulate fraction after the sonication as described above.

For immunoblotting, the samples of each fraction were subjected to 10% SDS-PAGE in the same volume, and the separated proteins were electorophoretically transferred onto polyvinylidine difluoride (PVDF) filters (Millipore Corp., Bedford, MA). Nonspecific binding sites on the PVDF filters were blocked by incubation with 5% gelatine for 18 h. The PVDF filters were then incubated with anti-PKC-γ monoclonal antibody (diluted 1:2,000) (Hashimoto et al., 1988) or anti-GFP polyclonal antibody (diluted 1: 2,000) (CLONTECH Laboratories, Inc., Palo Alto, CA) for 30 min at 25°C. After washing with 0.01 M PBS containing 0.03% Triton X-100, the filters were incubated with goat anti–mouse IgG (for γ-PKC antibody) or anti–rabbit IgG (for GFP antibody) for 15 min and then incubated for 15 min with rabbit peroxidase antiperoxidase complex. After three rinses, the immunoreactive bands were visualized with a chemiluminescence detection kit (ECL; Amersham, Buckinghamshire, UK).

Kinase assays of γ-PKC, γ-PKC–GFP, and its mutants expressed in COS-7 cells were performed as described previously (Kikkawa et al., 1983). The kinase activity in 10 μl of each fraction was assayed by measuring the incorporation of ^{32}Pi into calf thymus H1 histone from [γ-^{32}P]ATP in the presence of 8 μg/ml phosphatidylserine (PS), 0.8 μg/ml diolein (DO), and 0.5 mM Ca^{2+}. Basal activity was measured in the presence of 0.5 mM EGTA instead of PS, DO, and Ca^{2+}.

For immunoprecipitation of γ-PKC–GFP and γ-PKC, transfected cells in a dish 8 cm in diameter were harvested with 1 ml of homogenate buffer containing 1% Triton X-100 and were homogenized by pipetting. After a centrifuge at 19,000 *g* for 5 min at 4°C, the supernatant was rotated with anti–γ-PKC monoclonal antibody for 30 min at 4°C, then with protein A–Sepharose for an additional 30 min. Samples were centrifuged at 2,000 *g* for 5 min at 4°C, and pellets were washed three times with PBS(−). Finally, 10 μl of suspended pellet with 50 μl PBS(−) was used for kinase assay as described above.

Observation of γ-PKC–GFP Translocation

γ-PKC–GFP–transfected cells were spread onto the glass bottom culture dishes (MatTek Corp., Ashland, MA) and cultured for at least 16 h before the observation. For COS-7 cells and CHO/mGluR1 cells, the culture medium was replaced with normal Hepes buffer composed of: 135 mM NaCl, 5.4 mM KCl, 1 mM $MgCl_2$, 1.8 mM $CaCl_2$, 5 mM Hepes, 10 mM glucose, pH 7.3. When necessary, $CaCl_2$ or $MgCl_2$ were eliminated. In the case of NG-108 cells, the buffer used was composed of: 165 mM NaCl, 5 mM KCl, 1 mM $MgCl_2$, 1 mM $CaCl_2$, 5 mM Hepes, 10 mM glucose, pH 7.4.

The fluorescence of γ-PKC–GFP was monitored with a confocal laser scanning fluorescent microscope (model LSM 410 invert; Carl Zeiss, Jena, Germany) at 488-nm argon excitation using a 515-nm-long pass barrier filter. Translocation of γ-PKC–GFP was triggered by a direct application of various stimulants at high concentration into the Hepes buffer to obtain the appropriate final concentration. To observe NMDA-induced translocation, NMDA was applied into the dish in the presence of 10 μM glycine and absence of $MgCl_2$. To induce K^+ depolarization in NG-108 cells, the buffer was exchanged to a high K^+-containing buffer composed of: 52 mM NaCl, 100 mM KCl, 1 mM $MgCl_2$, 10 mM $CaCl_2$, 5 mM Hepes, 10 mM glucose, pH 7.4. All experiments were performed at room temperature.

Immunostaining of γ-PKC–GFP–transfected Cells by Anti–γ-PKC Antibody

The γ-PKC–GFP–transfected COS-7 cells, cultured in glass bottom dishes, were stimulated by TPA or A23187 and it was confirmed that fluores-

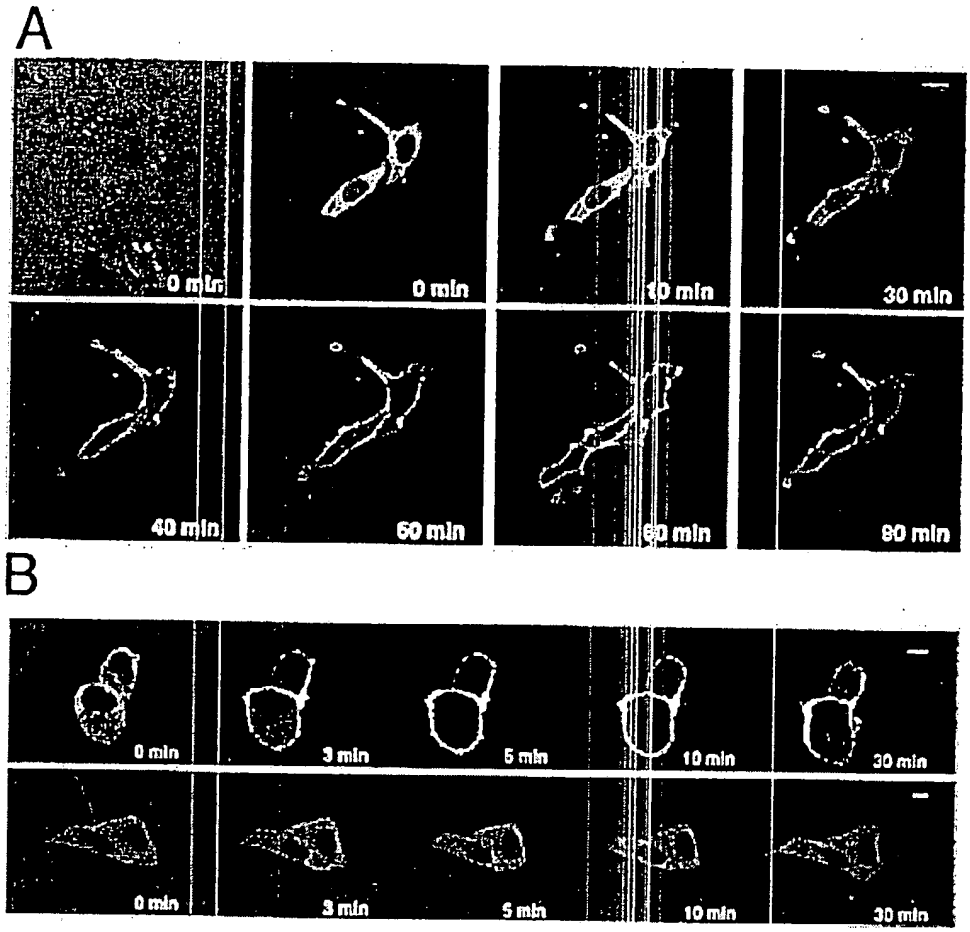

Figure 3. Phorbol ester–induced translocation of γ-PKC–GFP in COS-7 cells. (*A*) Change in the fluorescence of γ-PKC–GFP expressed in COS-7 cells by 5 μM TPA at room temperature. γ-PKC–GFP fusion protein was observed throughout the cytoplasm in transfected COS-7 cells. Activation of PKC by 5 μM TPA induced the obvious translocation of γ-PKC–GFP fluorescence from cytosol to membrane. Translocation was almost completed within 60 min after the treatment with TPA. The same view was taken before the stimulation under Nomarski interference microscope and shown at the upper left corner. (*B*) Change in the fluorescence of γ-PKC–GFP expressed in COS-7 cells by 200 nM TPA and 500 nM 4α-PDD at 37°C. Lower concentration of TPA (200 nM) induced the translocation of γ-PKC–GFP from cytosol to membrane when examined at 37°C (*upper trace*). The translocation occurred more rapidly, and the complete translocation was observed at 10 min after the treatment with TPA. In contrast, 4α-PDD, an inactive phorbol ester, at 500 nM failed to induce the translocation of γ-PKC–GFP even at 37°C. Bars, 10 μm.

cence was completely translocated. Then cells were fixed with 4% paraformaldehyde and 0.2% picric acid in 0.1 M phosphate buffer, pH 7.4, for 30 min. After two washes with 0.1 M PBS, pH 7.4, cells were treated with PBS containing 0.3% Triton X-100 and 5% normal goat serum for 10 min. Cells were sequentially incubated with anti–PKC-γ monoclonal antibody (Hashimoto et al., 1988) (diluted 1:1,000) for 40 min in PBS with 0.03% Triton X-100 (PBS-T) and 5% normal goat serum and then with Cy5-labeled goat anti–mouse IgG for 30 min at room temperature. The fluorescence of γ-PKC–like immunoreactivity was observed with a confocal laser scanning fluorescent microscope at 633-nm argon excitation and a 665-nm red glass filter.

Results

Characteristics of γ-PKC–GFP Fusion Protein

To examine whether γ-PKC–GFP had the characteristics of a phospholipid-dependent/calcium-activated protein kinase (PKC), we carried out immunoblotting and kinase assay of γ-PKC–GFP and γ-PKC expressed in COS-7 cells. As shown in Fig. 2 *A*, γ-PKC and γ-PKC–GFP were recognized as specific bands with the reasonable molecular masses of 80 and 110 kD, respectively. γ-PKC–GFP was also detected as a single 110-kD band by anti-GFP polyclonal antibody (data not shown). The amount of membrane-associated γ-PKC–GFP was increased after the treatment with TPA as seen in the case of γ-PKC (Fig. 2 *A*). The degradative products of γ-PKC–GFP and γ-PKC could not be detected by the antibodies against γ-PKC and GFP. Furthermore, kinase activities of γ-PKC–GFP and of γ-PKC were translocated from cytosol to membrane fractions (Fig. 2 *B*). The kinase assays revealed that both immunoprecipitated γ-PKC and γ-PKC–GFP were dependent on PS/DO and Ca^{2+} (Fig. 2 *C*). These results suggested that γ-PKC–GFP had similar enzymological properties to the native γ-PKC.

Translocation of γ-PKC–GFP Induced by TPA and A23187

Intense fluorescence of γ-PKC–GFP was observed in the perikarya of the transfected COS-7 cells, and faint fluorescence was seen in the nuclei (Fig. 3, *A* and *B*). The activation of γ-PKC–GFP by 5 μM TPA induced the obvious translocation of the fluorescence from the cytoplasm to the membrane. Translocation began at 10 min and was com-

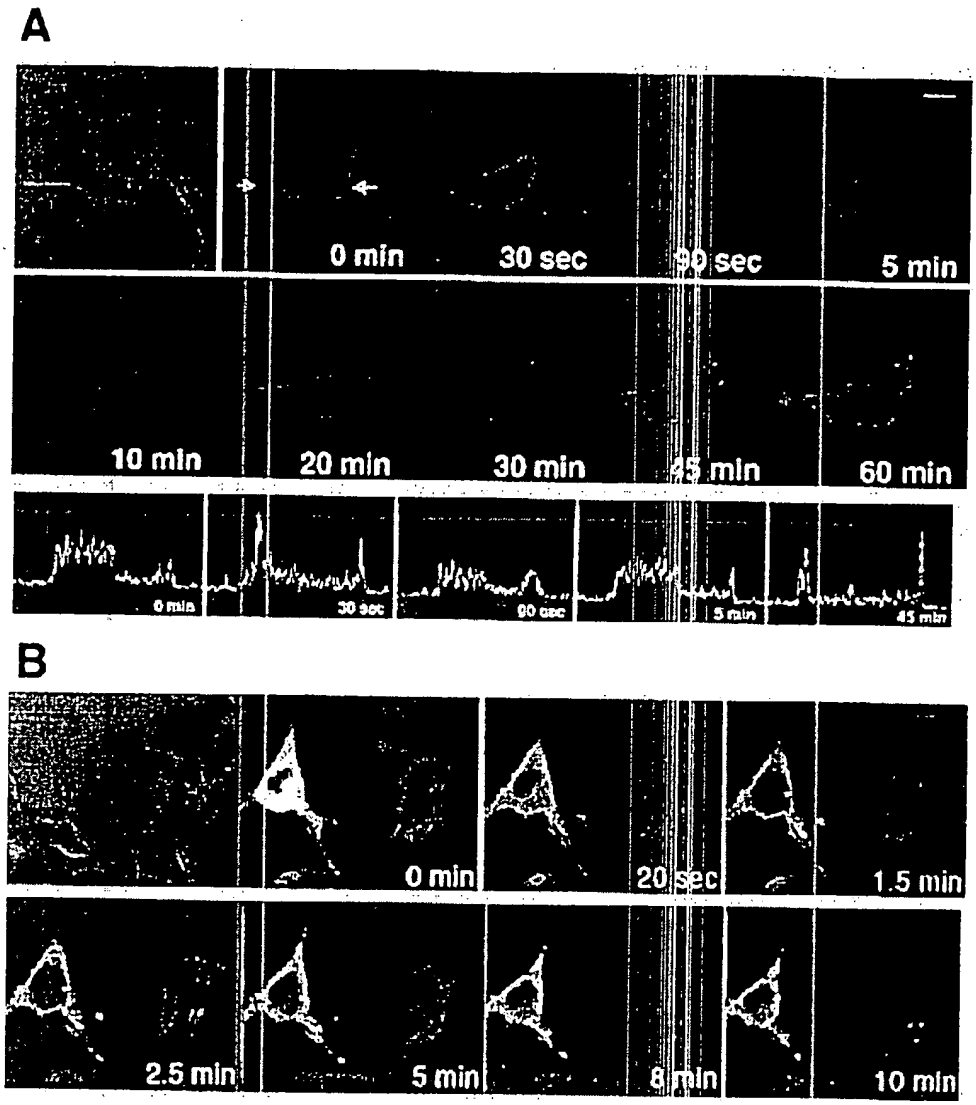

Figure 4. Ca^{2+} ionophore-induced translocation of γ-PKC–GFP in COS-7 cells. (*A*) Change in the fluorescence of γ-PKC–GFP expressed in COS-7 cells by 80 μM A23187, Ca^{2+} ionophore. A23187 also translocated the fluorescence of γ-PKC–GFP from cytosol to membrane; however, the time course of the translocation was significantly different from the TPA-induced one. Ca^{2+} ionophore–induced translocation was rapid and reversible (*upper and middle traces*). In the lower trace, profiles of the GFP intensity on the same line across the cell were shown. (The measured line is between the arrows in the upper left picture.) The translocation was expressed as the increase in the fluorescence at the fringe of the cell at 30 s and 45 min. Comparing the profile of the GFP intensity, very similar profiles were obtained at 0 and 5 min, and the fading of the fluorescence is negligible. (*B*) The γ-PKC–GFP translocation by A23187 was not always reversible. The left cell reveals unidirected translocation, while the right cell shows the reversible translocation, as seen in *A*. Unidirected translocation was more common than reversible translocation. γ-PKC–GFP eventually accumulated as patchy dots on the plasma membrane and in neighboring cytoplasm. Bars, 10 μm.

pleted by 60 min after the treatment with TPA (Fig. 3 *A*). The fluorescence remained on the plasma membrane for at least 90 min after TPA treatment and did not return to the cytoplasm in the cells tested. The γ-PKC–GFP in the nuclei did not appear to be translocated. The TPA-induced translocation of γ-PKC–GFP occurred more rapidly when the experiments were performed at 37°C (Fig. 3 *B*, *upper trace*). The translocation completed 10 min after the treatment with lower concentration of TPA (200 nM). In contrast, an inactive phorbol ester, 4α-PDD, at 500 nM failed to induce the translocation within 30 min (Fig. 3 *B*, *lower trace*).

At 80 μM, A23187, the Ca^{2+} ionophore, also produced γ-PKC–GFP translocation, the time course of which was significantly different from the TPA-induced translocation. The Ca^{2+} ionophore–induced translocation was rapid and reversible (Fig. 4 *A*). The fluorescence of γ-PKC–GFP translocated transiently at only 30 s after the stimulation. The first phase of the translocation was quickly reversed. The γ-PKC–GFP was retranslocated to cytoplasm at 90 s after the stimulation. The second and third phase of the translocation was observed 20 and 45 min after the stimulation, and finally γ-PKC–GFP was accumulated as patchy dots at the plasma membrane 60 min after A23187 treatment (Fig. 4 *A*, *upper and middle traces*). In the lower trace of Fig. 4 *A*, the profiles of the GFP intensity on the same line across the cell at various time points were shown. The translocation of γ-PKC–GFP to the membrane was detected as the increase in the intensity at the fringe of the cell at 30 s and 45 min. Very similar profiles of the GFP intensity were obtained at 0 and 5 min, and the fading of the fluorescence is negligible between the two different time points.

The γ-PKC–GFP translocation by A23187 was not al-

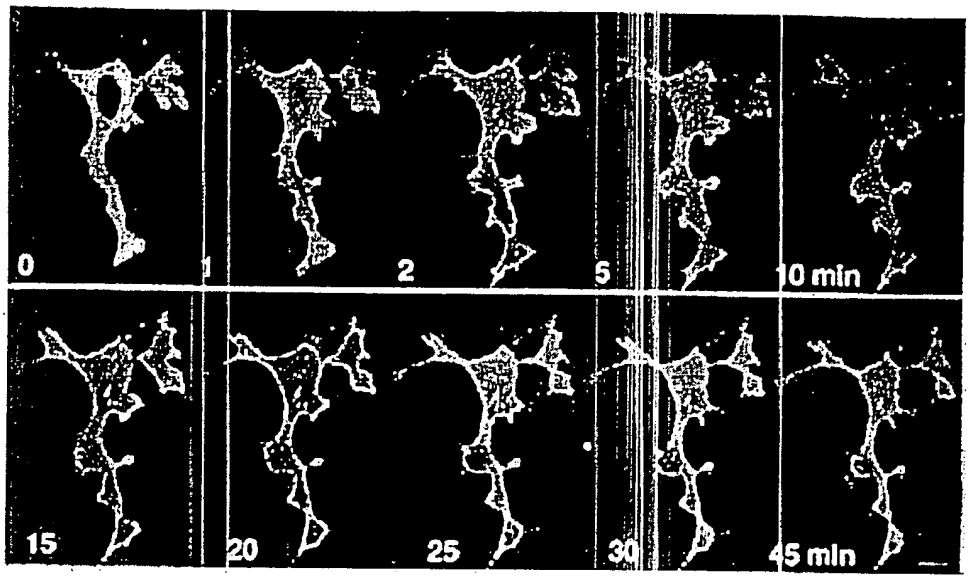

Figure 5. Thapsigargin-induced translocation of γ-PKC–GFP. 5 μM thapsigargin, an inhibitor of the endoplasmic reticulum Ca^{2+}-ATPase, also induced rapid translocation of γ-PKC–GFP. Fluorescence of γ-PKC–GFP accumulated as patchy dots as in A23187-induced translocation. Bar, 10 μm.

ways reversible (Fig. 4 *B*, *left cells*). The unidirected translocation (Fig. 4 *B*, *left cells*) was more common than the reversible translocation (Fig. 4 *B*, *right cells*). However, γ-PKC–GFP was always accumulated on plasma membrane as patchy dots (Fig. 4 *B*). A23187 at lower concentration (10 μM) also showed similar effects (data not shown).

Effects of Thapsigargin on Translocation of γ-PKC–GFP

To examine the influence of Ca^{2+} released from the intracellular Ca^{2+} store on γ-PKC–GFP translocation, we studied the effects of thapsigargin, which inhibits endoplasmic reticulum Ca^{2+}-ATPase and increases the concentration of cytosolic Ca^{2+}, on translocation of γ-PKC–GFP. Application of 5 μM thapsigargin induced a rapid translocation of fluorescence, which began within 1 min after the stimulation (Fig. 5). Finally, fluorescence was accumulated as patchy dots on the plasma membrane as seen in A23187-induced translocation. Accumulation of γ-PKC–GFP also occurred in the perikaryon.

Effects of Ca^{2+} Chelators on γ-PKC–GFP Translocation

To elucidate whether Ca^{2+} ionophore–induced transloca

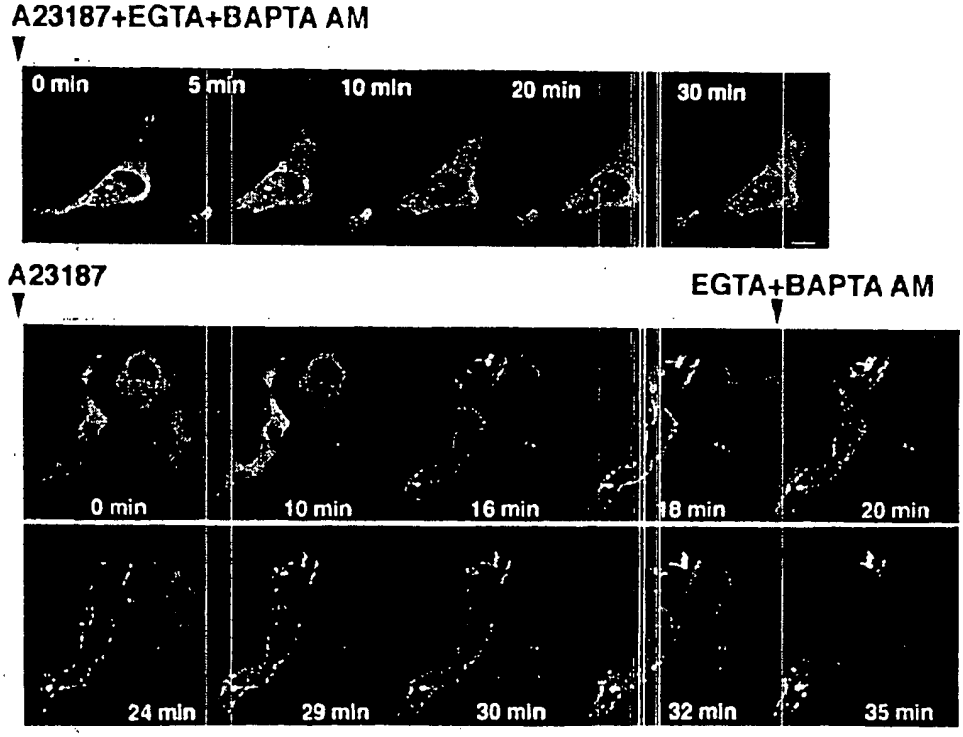

Figure 6. Effects of Ca^{2+} chelators on A23187-induced translocation of γ-PKC–GFP. Pretreatment with 2.5 mM EGTA and 15 μM BAPTA-AM completely blocked A23187 (50 μM)–induced γ-PKC–GFP translocation (*upper trace*). Treatment with 2.5 mM EGTA and 15 μM BAPTA-AM retranslocated γ-PKC–GFP from membrane to cytosol, even after A23187-induced translocation had occurred (*lower trace*). Bars, 10 μm.

tion depends on the increase in the intracellular Ca^{2+} concentration ($[Ca^{2+}]_i$), we examined the effects of Ca^{2+} chelators on A23187-induced translocation. Ca^{2+} ionophore–induced translocation was completely blocked by the pretreatment with Ca^{2+} chelators, 2.5 mM EGTA, and 15 μM BAPTA-AM (Fig. 6, *upper trace*). In addition, A23187-induced translocation was reversed by the treatment with Ca^{2+} chelators after the stimulation of A23187. The fluorescence of γ-PKC–GFP partially returned to the cytoplasm (Fig. 6, *lower trace*). TPA-induced translocation was not inhibited by either pre- or post-treatment with Ca^{2+} chelators (data not shown).

Immunostaining of Translocated γ-PKC–GFP

PKCs are known to be digested between the regulatory and catalytic domains by protease such as calpain (Kishimoto et al., 1983), suggesting that the fluorescence of translocated γ-PKC–GFP did not exactly reveal the localization of γ-PKC. Therefore, we immunostained the transfected cells using a monoclonal anti–γ-PKC antibody that recognizes the regulatory domain of γ-PKC after the translocation was completed. As shown in Fig. 7, γ-PKC-like Cy5 fluorescence was colocalized with the GFP fluorescence even after the TPA- or A23187-induced translocation was completed. These results suggested that fluorescence of GFP showed the localization of γ-PKC itself.

Translocation of Mutant γ-PKC–GFP Fusion Protein

To examine the significance of the C1 and C2 region of γ-PKC in the γ-PKC–GFP translocation, we constructed mutant γ-PKC–GFP, BS 238 (C1 mutant), and BS 239 (C2 deletion), as described above (Fig. 1). BS 238 is a mutant of the C1 region that binds TPA; it therefore was not expected to be activated by TPA. Indeed, TPA did not induce the translocation of BS 238 (C1 mutant), while A23187 did (Fig. 8 *A*). The Ca^{2+} ionophore–induced translocation of BS 238 was insufficient compared with that of wild-type γ-PKC–GFP (BS 186) (Fig. 8 *A* and 4 *A*). BS 239 (C2 deletion) is a deletion mutant of the C2 region that binds calcium ion. In contrast to BS 238, BS 239 was translocated by TPA but not by A23187 (Fig. 8 *B*).

We also examined the kinase character of BS 238 and BS 239. The kinase activity of BS 238 was dependent on Ca^{2+} (157.8 ± 9.1% of the control; control kinase activity was measured in the presence of EGTA), but was not activated by TPA (94.5 ± 5.6% of the control). In contrast, the kinase activity of BS 239 was not activated by neither Ca^{2+} (100.4 ± 5.6% of the control) nor TPA (81.2 ± 7.2% of the control). The kinase activity of BS239, however, was reduced to 27.2% ± 0.4% of the control by the treatment with 1 μM staurosporine, while the activity of BS238 was slightly inhibited by staurosporine (70.9 ± 14.5% of the control).

K^+ Depolarization Induced Translocation of γ-PKC–GFP in Transfected NG 108-15 Cells

The translocation of γ-PKC–GFP protein was further examined under physiological conditions. To investigate whether depolarization and subsequent activation of the voltage-gated Ca^{2+} channel induce γ-PKC translocation, we expressed γ-PKC–GFP fusion protein in NG 108-15 cells,

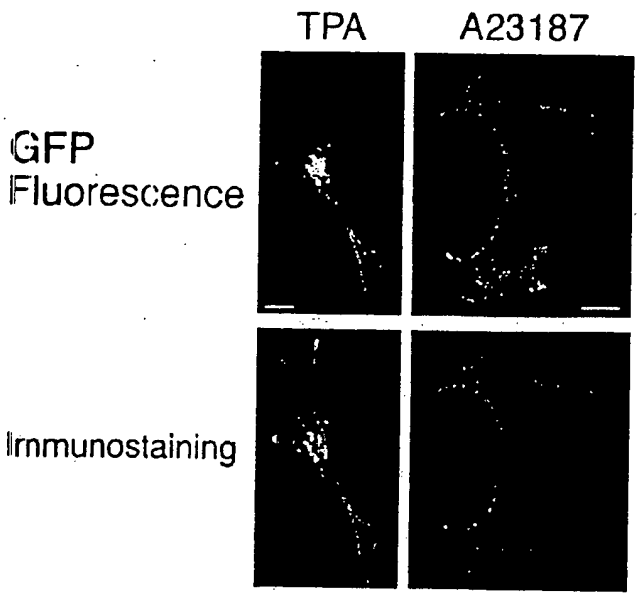

Figure 7. Comparison of the fluorescence of γ-PKC–GFP with the γ-PKC–like immunoreactivity. Immunostaining of γ-PKC–GFP–transfected COS-7 cells by anti–γ-PKC antibody showed that GFP fluorescence and γ-PKC–like immunoreactivity had very similar localizations, even after the TPA- or A23187-induced translocation was completed. Bar, 10 μm.

which have voltage-gated Ca^{2+} channels (Atlas and Adler, 1981). After the extracellular K^+ was elevated from 5 to 100 mM, the fluorescence of γ-PKC–GFP was rapidly translocated from cytosol to membrane (Fig. 9). After the translocation was completed, patchy dotlike fluorescence accumulated in membrane and cytosol as seen in A23187- or thapsigargin-induced translocation (Fig. 9). Reversible translocation, as seen in Fig. 3 *B*, also occurred in the other cells tested (data not shown). K^+ depolarization–induced translocation was abolished by 10 μM nicardipine or 10 μM ω-conotoxin GVIA, blockers of L- and N-type Ca^{2+} channels, respectively, but not by 2 μM tetrodotoxin, a Na^+ channel blocker (data not shown). These findings suggested that translocation was triggered by Ca^{2+} influx through a certain type of voltage-gated Ca^{2+} channel expressed in NG 108-15 cells.

NMDA Receptor–mediated Translocation of γ-PKC–GFP

The translocation of γ-PKC–GFP by receptor-mediated stimulation was further examined. In COS-7 cells coexpressing NMDA receptor channels (ζ1 and ε1 subunits), the treatment with 1 mM NMDA plus 10 μM glycine induced faint but significant translocation of γ-PKC–GFP (Fig. 10). Simultaneous application of 500 μM AP-5, an antagonist of NMDA receptor, blocked NMDA-induced translocation (Fig. 10).

mGluR1–mediated Translocation of γ-PKC–GFP

We transfected γ-PKC–GFP into the CHO cells stably expressing mGluR1 to investigate G-protein–coupled receptor-mediated translocation of γ-PKC. Activation of mGluR1 receptor by 1 mM *trans*-ACPD, an agonist of mGluR1, in-

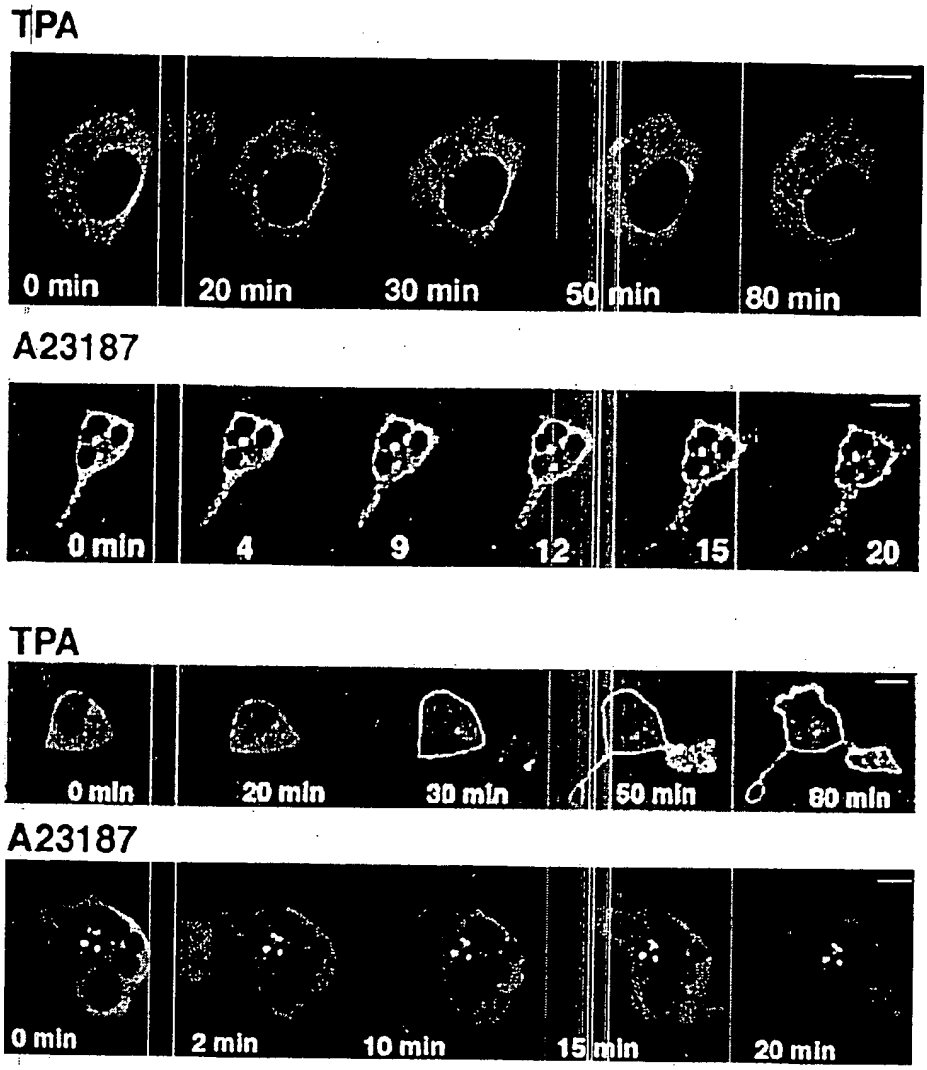

Figure 8. Translocation of mutant γ-PKC–GFPs (BS 238 and BS 239) expressed in COS-7 cells. (*A*) Translocation of BS 238 (C1 mutant γ-PKC–GFP). TPA at 5 μM did not induce the translocation of BS 238, while A23187 at 50 μM did. A23187-induced translocation of BS 238 was insufficient compared with that of BS 186 (control γ-PKC–GFP). (*B*) Translocation of BS 239 (C2 deletion γ-PKC–GFP). In contrast to BS 238, BS 239 was translocated by 5 μM TPA but not by 50 μM A23187. Bars, 10 μm.

duced a rapid translocation of γ-PKC–GFP with re-translocation to the cytoplasm within 20 min (Fig. 11). Simultaneous application of 2.5 mM RS-MCPG, an antagonist of mGluR1, completely blocked mGluR1-mediated translocation of γ-PKC–GFP (Fig. 11).

Effects of Cytochalasin D and Colchicine on γ-PKC–GFP Translocation

To investigate the involvement of filamentous actin in γ-PKC translocation, we studied the effects of cytochalasin D, an inhibitor of actin polymerization, on the translocation of γ-PKC–GFP. Pretreatment with 10 μM cytochalasin D for 25–40 min altered the shapes of cells; however, it did not inhibit the translocation of γ-PKC–GFP induced by either TPA or A23187 (Fig. 12 *A*). We also examined the effects of colchicine, an inhibitor of microtubule polymerization, to investigate the relationship between γ-PKC translocation and microtubules. Colchicine, like cytochalasin D, did not affect the TPA- or A23187-induced translocation of γ-PKC–GFP (Fig. 12 *B*). To assess whether the pretreatment with cytochalasin D or colchicine described above actually acted on cytoskeleton, we stained filamentous actin with rhodamine-phalloidin or microtubules with anti–α-tubulin antibody. Both 10 μM cytochalasin and 100 μM colchicine disrupted actin fibers and microtubules, respectively (data not shown).

Discussion

We first examined the enzymological property of γ-PKC–GFP protein by measuring kinase activity with or without activators of PKC. As shown in Fig. 2 *C*, γ-PKC–GFP protein expressed in COS-7 cells had similar enzymological character to the native γ-PKC. In addition, immunoblotting analysis revealed that γ-PKC–GFP of reasonable molecular size, but not the degradation product of γ-PKC–GFP, was present as a donor of GFP fluorescence, even after the translocation from cytosol to membrane by the stimulation with TPA (Fig. 2 *A*). Kinase activity of γ-PKC–GFP was also translocated from cytosol to membrane (Fig. 2 *B*). These results suggest that γ-PKC–GFP protein did not lose its enzymological character as a γ-PKC, even though a

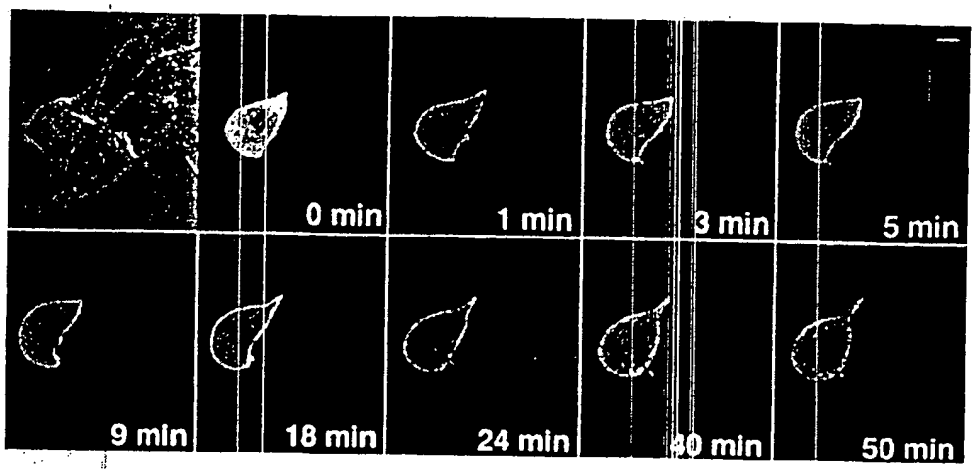

Figure 9. K^+ depolarization–induced translocation of γ-PKC–GFP expressed in NG 108-15 cells. Replacing the external solution with a high K^+–containing one rapidly induced translocation of γ-PKC–GFP. The fluorescence of γ-PKC–GFP accumulated as patchy dots on the plasma membrane and in neighboring cytoplasm, as in Ca^{2+} ionophore–induced translocation. Bar, 10 μm.

GFP, a protein with 238 amino acids, was added to the COOH terminus of γ-PKC. When the GFP was added to the NH_2 terminus of γ-PKC (GFP–γ-PKC), the distribution of GFP–γ-PKC within a cell was similar to the present observation of γ-PKC–GFP (data not shown). The NH_2-terminal methionine of cPKC, however, is known to be posttranslationally cleaved and replaced with an acetyl group (Tsutakawa et al., 1995). Therefore, it is suggested that the fusion protein γ-PKC–GFP, rather than GFP-γ-PKC, is better to monitor the exact localization of γ-PKC itself.

PKCs are reported to be proteolysed by protease such as calpain, a Ca^{2+}-dependent neutral protease (Kishimoto et al., 1983). If γ-PKC–GFP was proteolysed during its translocation, GFP fluorescence did not reveal the exact localization of γ-PKC. Therefore, we also carried out the immunostaining of γ-PKC–GFP with the antibody that recognizes the regulatory domain of γ-PKC when the translocation was completed. As shown in Fig. 7, the immunoreactivity of γ-PKC–GFP coincided with the fluorescence of GFP. Furthermore, the fact that the line intensity profiles across the cell were similar before and after a transient translocation to the membrane (Fig. 4 *A*) suggests that the fluorescence of γ-PKC–GFP exactly revealed the localization of γ-PKC–GFP itself, and the time-dependent movement of GFP fluorescence showed the translocation events of γ-PKC in real time.

Immunohistochemical and enzymological analyses revealed that TPA-induced translocation was completed within 5 min (Kraft et al., 1982), although γ-PKC–GFP was translocated more slowly and a high dose of TPA was nec-

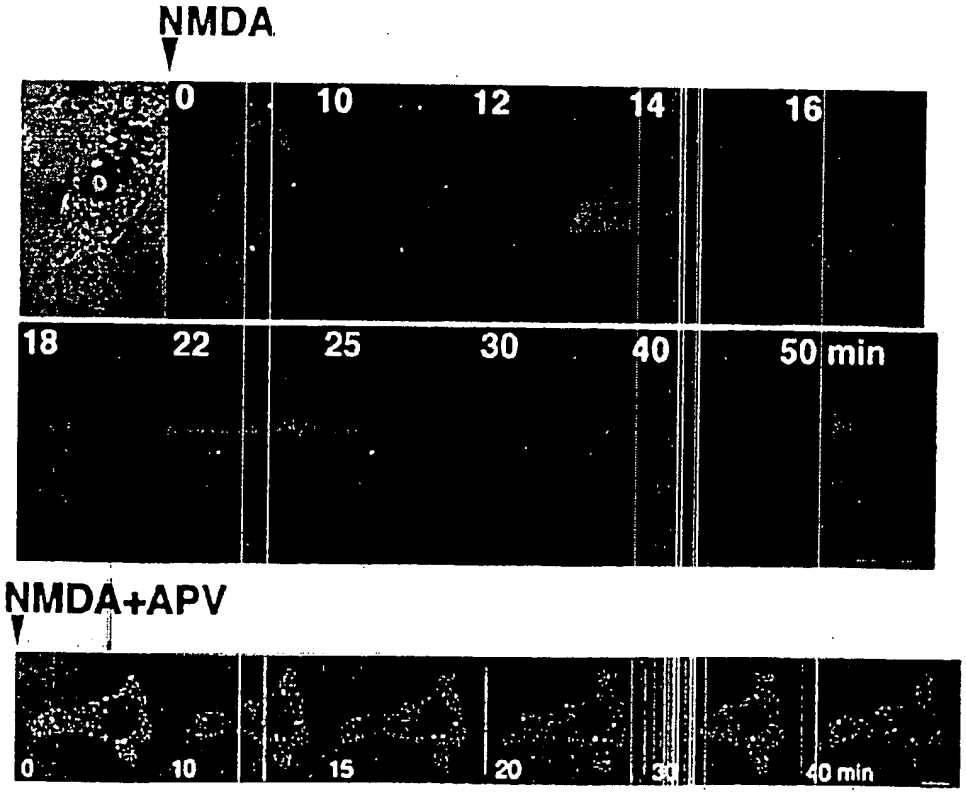

Figure 10. NMDA-induced translocation of γ-PKC–GFP in COS-7 cells coexpressing NMDA receptors. NMDARζ1 and NMDARε1 subunits were cotransfected with γ-PKC–GFP into COS-7 cells by electroporation. NMDA at 1 mM was applied to cells in the absence of Mg^{2+} and presence of 10 μM glycine. NMDA induced faint but significant translocation of γ-PKC–GFP. Simultaneous application of 100 μM AP-5 with 1 mM NMDA blocked NMDA-induced γ-PKC–GFP translocation. Bars, 10 μm.

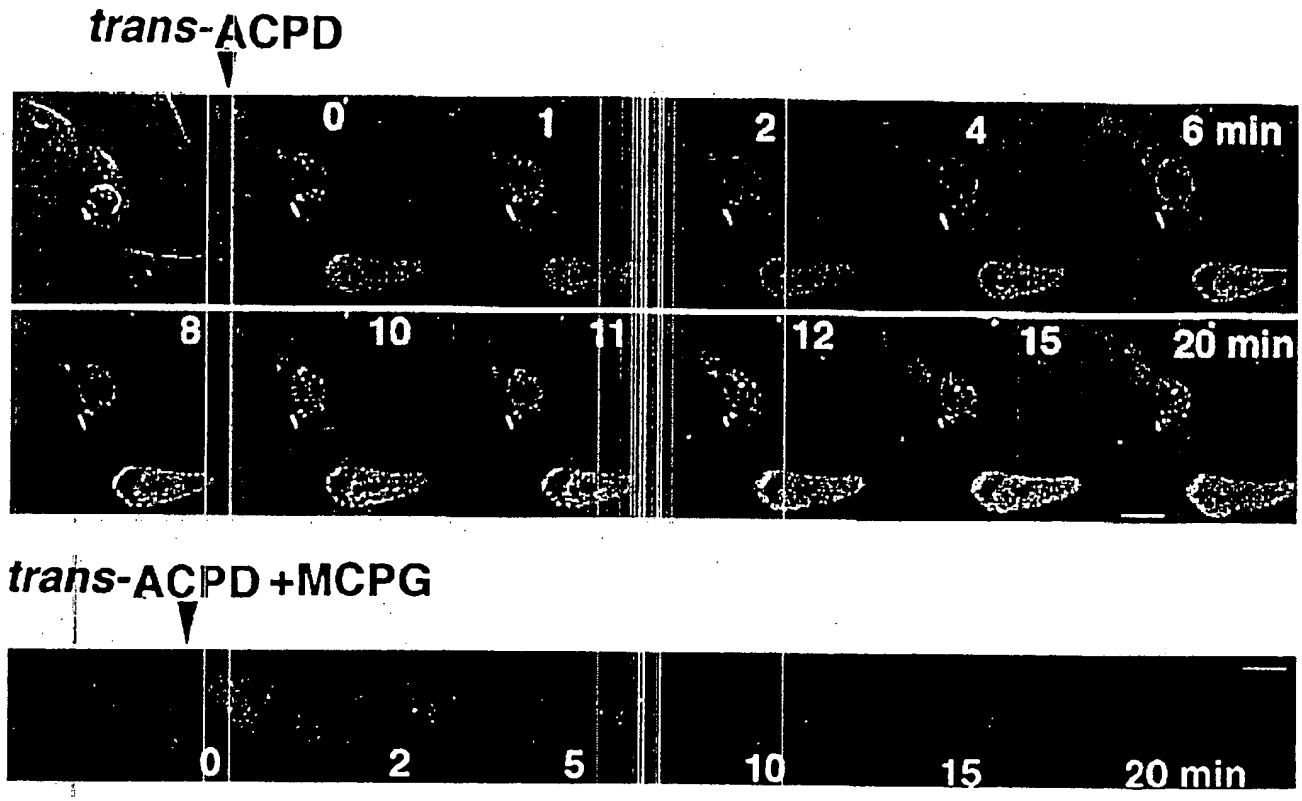

Figure 11. mGluR1-mediated translocation of γ-PKC–GFP. γ-PKC–GFP was transfected into CHO cells stably expressing mGluR1 by lipofection as described in the text. (*Upper trace*) Application of 1 mM *trans*-ACPD rapidly induced the translocation of γ-PKC–GFP from cytosol to membrane. The fluorescence was retranslocated from membrane to cytosol within 20 min. (*Lower trace*) Simultaneous application of 500 μM MCPG with 1 mM *trans*-ACPD completely blocked mGluR1-mediated translocation of γ-PKC–GFP. Bar, 10 μm.

essary for the translocation at room temperature. The discrepancy was due to the temperature since 200 nM TPA was enough to translocate γ-PKC–GFP to the membrane, and the translocation was completed within 10 min when the experiment was performed at 37°C (Fig. 3 *B*).

In contrast with TPA-induced translocation, Ca^{2+} ionophore-induced translocation was rapid and reversible. Even the TPA-induced translocation of γ-PKC–GFP at 37°C was still slower than that induced by Ca^{2+} ionophore. Ca^{2+} chelators blocked the translocation induced by Ca^{2+} ionophore, suggesting that Ca^{2+}-induced translocation depended on the intracellular Ca^{2+} concentration ($[Ca^{2+}]_i$). In this regard, the wavelike translocation by A23187 may reflect the alternation of $[Ca^{2+}]_i$. To prove this, we observed the A23187-induced change in $[Ca^{2+}]_i$ by loading cells with calcium green-1-AM, a fluorescent Ca^{2+} indicator, using a confocal laser fluorescent microscope. A transient elevation of fluorescence was observed; however, no wavelike phenomenon of the $[Ca^{2+}]_i$ could be detected (data not shown). In addition, A23187 commonly induced the unidirected translocation of γ-PKC–GFP, and the typical reversible translocation as shown in Fig. 3 was infrequent. The reason why Ca^{2+} ionophore induced the wavelike translocation of γ-PKC–GFP is unclear at present; however, possible explanations can be proposed. First, a wavelike alternation of $[Ca^{2+}]_i$ is induced by A23187 under certain conditions only, and the experiments using calcium green-1-AM were not performed under such conditions or the calcium green-1-AM was not a suitable drug with which to fine-tune change in $[Ca^{2+}]_i$ becuase of its effect as a Ca^{2+} chelator. Alternatively, when the A23187-induced elevation of $[Ca^{2+}]_i$ was insufficient, the γ-PKC–GFP translocation was incomplete and transient, but subsequent production of phospholipids by various Ca^{2+}-activated phospholipases induced a second or third translocation of γ-PKC–GFP. The results of the kinase assay of γ-PKC–GFP that both phospholipids and Ca^{2+} were needed for the full activation of γ-PKC–GFP support this idea. Thapsigargin also induced rapid translocation of γ-PKC–GFP, indicating that Ca^{2+} influx from intracellular Ca^{2+} stores could translocate γ-PKC–GFP.

When translocation was completed, the localization of γ-PKC in TPA-induced translocation was different from in the Ca^{2+}-induced one. Fluorescence of γ-PKC–GFP was accumulated in plasma membrane in TPA-induced translocation, whereas it was accumulated in plasma membrane and submembrane cytoplasm as patchy dots in Ca^{2+}-induced translocation. These findings suggest that TPA-induced and Ca^{2+}-induced translocation are mediated by different pathways and that the final localization of γ-PKC is distinct after each stimulation.

The treatment with TPA caused subtype-specific subcellular distribution in cardiac myocytes (Disatnik et al., 1994). γ-PKC was also reported to be translocated to Golgi organelle by TPA in NIH3T3 cells stably overexpressing γ-PKC (Goodnight et al., 1995). In contrast, γ-PKC–GFP was

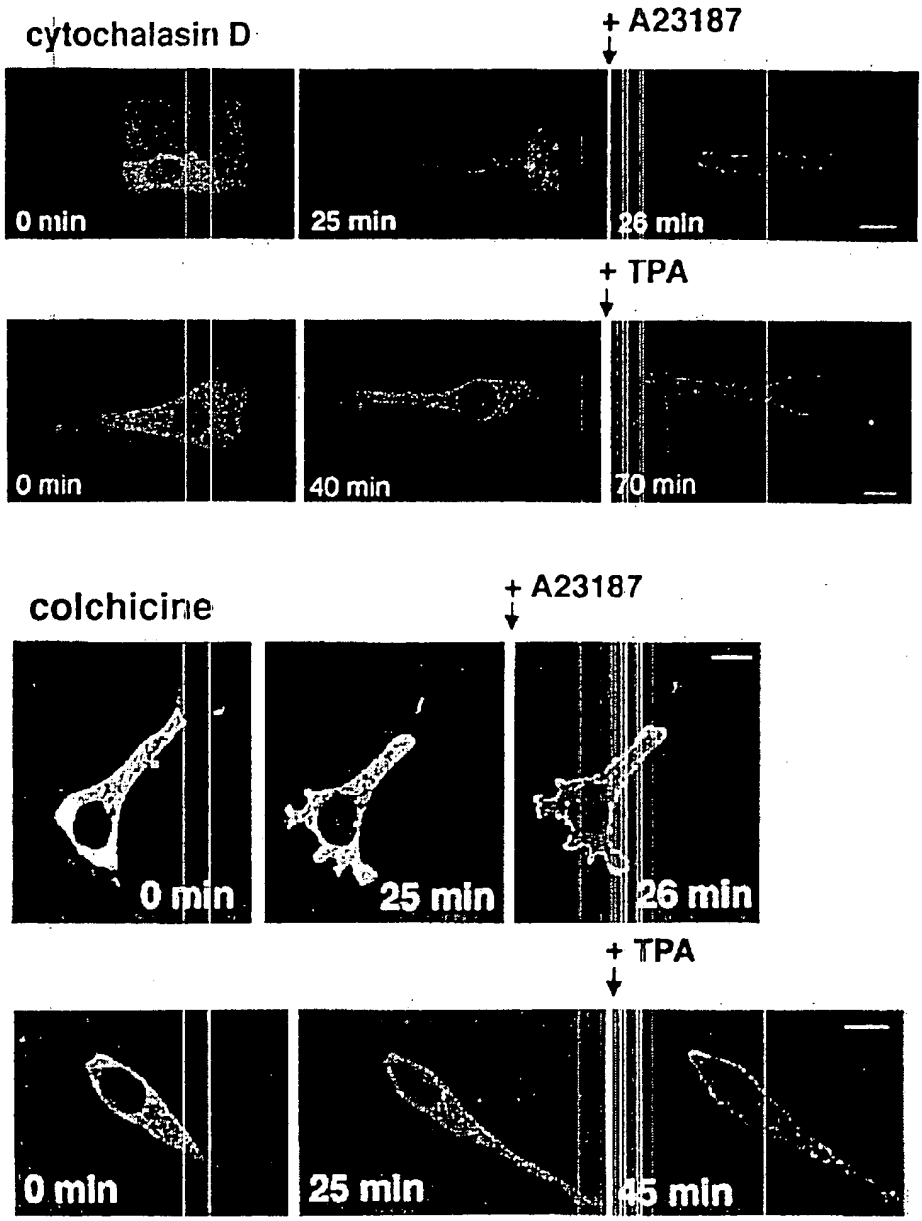

Figure 12. Involvement of γ-PKC–GFP translocation in cytoskeleton. (*A*) Effects of 10 μM cytochalasin D on γ-PKC–GFP translocation. Treatment with 10 μM γ-PKC–GFP affected neither TPA- nor A23187-induced translocation of γ-PKC–GFP. (*B*) Effects of 100 μM colchicine on γ-PKC–GFP translocation. Treatment with 100 μM colchicine did not affect TPA- or A23187-induced translocation. In these experiments, γ-PKC–GFP was transfected into NIH3T3 cells by lipofection as described in the text. The concentrations of TPA and A23187 applied were 1 and 50 μM, respectively. Bars, 10 μm.

mainly translocated from cytosol to membrane by TPA in our study. As far as we could determine in various cells (COS-7, CHO, NG-108, etc.), γ-PKC was not translocated to the Golgi complex. Transiently expressed γ-PKC may have different properties of translocation from native or stably expressed γ-PKC. Otherwise, an addition of GFP may alter the translocation nature of γ-PKC.

In our present study, γ-PKC–GFP was translocated by various physiological stimuli. The findings showed that γ-PKC is activated and translocated in living cells. In addition, receptor mediated-translocation of γ-PKC–GFP were rapid and reversible. In particular, mGluR1-mediated translocation was transient, indicating that γ-PKC translocation induced by receptor-mediated breakdown of phosphatidylinositol was not sustained in living cells. As mGluR1-mediated elevation of Ca^{2+} was found to be transient by measuring fluorescence of intracellular-loaded Ca^{2+} green-1-AM (data not shown), mGluR1-mediated translocation of γ-PKC–GFP may depend on intracellular Ca^{2+}.

To elucidate whether the translocation of γ-PKC is associated with the activation mechanism, we examined the translocation of mutant γ-PKC–GFPs. TPA induced translocation of BS 239 (C2 mutant) but not BS 238 (C1 mutant). In contrast, Ca^{2+} ionophore translocated BS 238 but not BS 239. The kinase activity of BS 238 was dependent on Ca^{2+}, in parallel with the results of BS 238 translocation, while the kinase activity of BS 239 depended on neither Ca^{2+} nor TPA but was blocked by the staurosporine, a potent kinase inhibitor, suggesting that BS 239 may become a constitutively active form by a mutation. TPA-induced translocation of γ-PKC may not be coupled with its kinase

activity, as the staurosporine did not block TPA-induced translocation (data not shown). As shown in Fig. 8 *A*, Ca^{2+} ionophore–induced translocation of BS 238 (C1 mutant) was insufficient in all cells tested. Based on the results of the kinase assay (Fig. 2 *C*), Ca^{2+} alone appears not to induce the complete translocation of γ-PKC. As Ca^{2+} has been reported to activate the production of phospholipids, including DG, both calcium and phospholipids were needed to induce complete translocation of γ-PKC.

Although PKC translocation is a well-known phenomenon, the molecular mechanism and significance of PKC translocation have not yet been clarified. Phorbol esters translocated some subtypes of PKCs from cytosol to particulate fractions including cytoskeleton (Zalewski et al., 1988; Jaken et al., 1989; Papadopoulos and Hall, 1989; Kiley and Jaken, 1990; Mochly-Rosen et al., 1990). In βII-PKC, which was reported to be translocated to actin fiber (Goodnight et al., 1995), it was proposed that receptors for activated C-kinase (RACK), present in the detergent-insoluble fraction and bound activated βII-PKC, play a role in the mechanism of PKC translocation (Mochly-Rosen et al., 1991; Ron and Mochly-Rosen, 1995). To elucidate whether cytoskeleton proteins such as actin or microtubule are involved in PKC translocation, the effects of cytochalasin D, an inhibitor of actin polymerization, and colchicine, an inhibitor of microtubule polymerization, on the translocation of γ-PKC–GFP were examined. As shown in Fig. 12, pretreatment with neither cytochalasin D nor colchicine affected γ-PKC–GFP translocation. Furthermore, γ-PKC–GFP translocation occurred even when the glucose in the external solution was eliminated (data not shown). These results indicated that PKC translocation did not need the cytoskeleton and glucose-dependent motor protein that are essential for some types of protein trafficking, such as an axonal flow or vesicle transport (Bloom, 1992; Cheney et al., 1993). In addition, based on the findings that the C2 deletion mutant of γ-PKC (BS 239) could be translocated by TPA, phorbol ester–induced translocation of γ-PKC from cytosol to plasma membrane is probably not necessary for the association of RACK because RACK was reported to bind the C2 region of PKC (Ron and Mochly-Rosen, 1995).

In conclusion, a GFP fusion protein with γ-PKC is a useful tool for investigating the mechanism and significance of γ-PKC translocation in living cells.

We thank Dr. Ushio Kikkawa for many useful discussions.

This work was supported by grants from the Ministry of Education, Science, Sports and Culture in Japan, the Yamanouchi Foundation for Research on Metabolic Disorders, and the Kato Memorial Bioscience Foundation.

Received for publication 4 August 1997 and in revised form 30 September 1997.

References

Abeliovich, A., C. Chen, Y. Goda, A.J. Silva, C.F. Stevens, and S. Tonegawa. 1993*a*. Modified hippocampal long-term potentiation in PKC γ-mutant mice. *Cell.* 75:1253–1262.

Abeliovich, A., R. Paylor, C. Chen, J.J. Kim, J.M. Wehner, and S. Tonegawa. 1993*b*. PKCγ mutant mice exhibit mild deficits in spatial and contextual learning. *Cell.* 75:1263–1271.

Atlas, D., and M. Adler. 1981. α-Adrenergic antagonist as possible calcium channel inhibitors. *Proc. Natl. Acad. Sci. USA.* 78:1237–1241.

Bloom, G.S. 1992. Motor proteins for cytoplasmic microtubules. *Curr. Opin. Cell. Biol.* 4:66–73.

Chen, C.S., and M. Poenie. 1993. New fluorescent probes for protein kinase C. Synthesis, characterization, and application. *J. Biol. Chem.* 268:15812–15822.

Cheney, R.E., M.A. Rieley, and M.S. Mooseker. 1993. Phylogenetic analysis of the myosin superfamily. *Cell Motil. Cytoskel.* 24:215–223.

Cubitt, A.B., R. Heim, S.R. Adams, A.E. Boyd, L.A. Gross, and R.Y. Tsien. 1995. Understanding, improving and using green fluorescent proteins. *Trends Biochem. Sci.* 20:448–455.

Disatnik, M.H., G. Buraggi, and D. Mochly-Rosen. 1994. Localization of protein kinase C isozymes in cardiac myocytes. *Exp. Cell. Res.* 210:287–297.

Goodnight, J.A., H. Mischak, W. Kolch, and J.F. Mushinski. 1995. Immunocytochemical localization of eight protein kinase C isozymes overexpressed in NIH 3T3 fibroblasts. Isoform-specific association with microfilaments, Golgi, endoplasmic reticulum, and nuclear and cell membranes. *J. Biol. Chem.* 270:9991–10001.

Hashimoto, T., K. Ase, S. Sawamura, U. Kikkawa, N. Saito, C. Tanaka, and Y. Nishizuka. 1988. Postnatal development of a brain-specific subspecies of protein kinase C in rat. *J. Neurosci.* 8:1678–1683.

Ikeda, K., M. Nagasawa, H. Mori, K. Araki, K. Sakimura, M. Watanabe, Y. Inoue, and M. Mishina. 1992. Cloning and expression of the epsilon 4 subunit of the NMDA receptor channel. *FEBS Lett.* 313:34–38.

Jaken, S., K. Leach, and T. Klauck. 1989. Association of type 3 protein kinase C with focal contacts in rat embryo fibroblasts. *J. Cell Biol.* 109:697–704.

Kikkawa, U., R. Minakuchi, Y. Takai, and Y. Nishizuka. 1983. Calcium-activated, phospholipid-dependent protein kinase (protein kinase C) from rat brain. *Methods Enzymol.* 99:288–298.

Kiley, S.C., and S. Jaken. 1990. Activation of α-protein kinase C leads to association with detergent-insoluble components of GH4C1 cells. *Mol. Endocrinol.* 4:59–68.

Kishimoto, A., N. Kajikawa, M. Shiota, and Y. Nishizuka, 1983. Proteolytic activation of calcium-activated, phospholipid-dependent protein kinase by calcium-dependent neutral protease. *J. Biol. Chem.* 258:1156–1164.

Kraft, A.S., W.B. Anderson, H.L. Cooper, and J.J. Sando, 1982. Decrease in cytosolic calcium/phospholipid-dependent protein kinase activity following phorbol ester treatment of ELA4 thymoma cells. *J. Biol. Chem.* 257:13193–13196.

Meguro, H., H. Mori, K. Araki, E. Kushiya, T. Kutsuwada, M. Yamazaki, T. Kumanishi, M. Arakawa, K. Sakimura, and M. Mishina. 1992. Functional characterization of a heteromeric NMDA receptor channel expressed from cloned cDNAs. *Nature.* 357:70–74.

Mochly-Rosen, D., C.J. Henrich, L. Cheever, H. Khaner, and P.C. Simpson. 1990. A protein kinase C isozyme is translocated to cytoskeletal elements on activation. *Cell Regul.* 1:693–706.

Mochly-Rosen, D., H. Khaner, and J. Lopez. 1991. Identification of intracellular receptor proteins for activated protein kinase C. *Proc. Natl. Acad. Sci. USA.* 88:3997–4000.

Nishizuka, Y. 1984. The role of protein kinase C in cell surface signal transduction and tumour promotion. *Nature.* 308:693–698.

Nishizuka, Y. 1986. Studies and perspectives of protein kinase C. *Science.* 233: 305–312.

Nishizuka, Y., 1988. The molecular heterogeneity of protein kinase C and implications for cellular regulation. *Nature.* 334:661–665.

Nishizuka, Y. 1992. Intracellular signaling by hydrolysis of phospholipids and activation of protein kinase C. *Science.* 258:607–614.

Ono, Y., T. Fujii, K. Igarashi, U. Kikkawa, K. Ogita, and Y. Nishizuka. 1988*a*. Nucleotide sequences of cDNAs for α and γ subspecies of rat brain protein kinase C. *Nucleic Acids Res.* 16:5199–5200.

Ono, Y., T. Fujii, K. Ogia, U. Kikkawa, K. Igarashi, and Y. Nishizuka. 1988*b*. The structure, expression, and properties of additional members of the protein kinase C family. *J. Biol. Chem.* 263:6927–6932.

Ono, Y., T. Fujii, K. Igarashi, T. Kuno, C. Tanaka, U. Kikkawa, and Y. Nishizuka. 1989. Phorbol ester binding to protein kinase C requires a cysteine-rich zinc-finger-like sequence. *Proc. Natl. Acad. Sci. USA.* 86:4868–4871.

Papadopoulos, V., and P.F. Hall. 1989. Isolation and characterization of protein kinase C from Y-1 adrenal cell cytoskeleton. *J. Cell. Biol.* 108:553–567.

Parker, P.J., and L.V. Dekker. 1997. Introduction. *In* Protein Kinase C. P.J. Parker and L.V. Dekkers, editors. R.G. Landes Co., Austin, TX. 1–9.

Prasher, D.C., V.K. Eckenrode, W.W. Ward, F.G. Prendergast, and M.J. Cormier. 1992. Primary structure of the *Aequorea victoria* green-fluorescent protein. *Gene.* 111:229–233.

Ron, D., and D. Mochly-Rosen. 1995. An autoregulatory region in protein kinase C: the pseudoanchoring site. *Proc. Natl. Acad. Sci. USA.* 92:492–496.

Tanabe, Y., M. Masu, T. Ishii, R. Shigemoto, and S. Nakanishi. 1992. A family of metabotropic glutamate receptors. *Neuron.* 8:169–179.

Tanaka, C., and Y. Nishizuka. 1994. The protein kinase C family for neuronal signaling. *Annu. Rev. Neurosci.* 17:551–567.

Tsutakawa, S.E., K.F. Medzihradszky, A.J. Flint, A.L. Burlingame, and D.J. Koshland. 1995. Determination of in vivo phosphorylation sites in protein kinase C. *J. Biol. Chem.* 270:26807–26812.

Yamazaki, M., H. Mori, K. Araki, K.J. Mori, and M. Mishina. 1992. Cloning, expression and modulation of a mouse NMDA receptor subunit. *FEBS Lett.* 300:39–45.

Zalewski, P.D., I.J. Forbes, L. Valente, S. Apostolou, and N.P. Hurst. 1988. Translocation of protein kinase C to a Triton-insoluble sub-cellular compartment induced by the lipophilic gold compound auranofin. *Biochem. Pharmacol.* 37:1415–1417.

THE JOURNAL OF BIOLOGICAL CHEMISTRY

Vol. 273, No. 17, Issue of April 24, pp. 10755–10762, 1998
Printed in U.S.A.

Visualization of Dynamic Trafficking of a Protein Kinase C βII/Green Fluorescent Protein Conjugate Reveals Differences in G Protein-coupled Receptor Activation and Desensitization*

(Received for publication, December 4, 1997, and in revised form, February 4, 1998)

Xiao Feng‡, Jie Zhang‡§, Larry S. Barak‡§, Tobias Meyer‡, Marc G. Caron‡§¶, and Yusuf A. Hannun‡¶

From the Departments of ‡Cell Biology and ¶Medicine, §Howard Hughes Medical Institute Laboratories, Duke University Medical Center, Durham, North Carolina 27710

PD 24-04-98 P 10755-7622 (C)

Protein kinase C (PKC) links various extracellular signals to intracellular responses and is activated by diverse intracellular factors including diacylglycerol, Ca^{2+}, and arachidonic acid. In this study, using a fully functional green fluorescent protein conjugated PKCβII (GFP-PKCβII), we demonstrate a novel approach to study the dynamic redistribution of PKC in live cells in response to G protein-coupled receptor activation. Agonist-induced PKC translocation was rapid, transient, and selectively mediated by the activation of $G_q\alpha$- but not $G_s\alpha$- or $G_i\alpha$-coupled receptors. Interestingly, although the stimuli were continuously present, only one brief peak of PKC membrane translocation was observed, consistent with rapid desensitization of the signaling pathway. Moreover, when GFP-PKCβII was used to examine cross-talk between two $G_q\alpha$-coupled receptors, angiotensin II type 1A receptor ($AT_{1A}R$) and endothelin A receptor (ET_AR), activation of ET_ARs resulted in a subsequent loss of $AT_{1A}R$ responsiveness, whereas stimulation of $AT_{1A}R$s did not cause desensitization of the ET_AR signaling. The development of GFP-PKCβII has allowed not only the real time visualization of the dynamic PKC trafficking in live cells in response to physiological stimuli but has also provided a direct and sensitive means in the assessment of activation and desensitization of receptors implicated in the phospholipase C signaling pathway.

The protein kinase C (PKC)[1] family of phospholipid-dependent serine/threonine kinases plays key roles in the transduction and regulation of many cellular signaling processes by catalyzing specific substrate phosphorylation (1, 2). Activation of protein kinase C can be triggered by stimulating a wide variety of plasma membrane hormone, neurotransmitter, and growth factor receptors, among which seven-transmembrane G protein-coupled receptors (GPCRs) relay extracellular signals to PKC by activating heterotrimeric guanine nucleotide-binding regulatory proteins (G proteins) (3). G proteins are composed of α- and βγ-subunits, both of which serve as signal moieties and mediate cellular responses by modulating the activity of different effector systems and levels of various second messengers (4). $G_q\alpha$ is one of the major G protein α-subunits and is coupled to a large number of receptors including angiotensin receptors and endothelin receptors. The activation of $G_q\alpha$ by these receptors triggers the hydrolysis of membrane inositol phospholipids by phospholipase Cβ to form two important second messengers, inositol 1,4,5-triphosphate (IP_3) and diacylglycerol (DAG) (1, 5, 6). The binding of IP_3 to its intracellular receptor results in a rise in intracellular Ca^{2+} (7). The increased membrane DAG and intracellular Ca^{2+} lead to the mobilization of PKC to the plasma membrane and its subsequent activation (1). The activation of PKC by DAG, Ca^{2+}, and many other lipid mediators such as arachidonic acid has been associated with many important biological functions including cell proliferation, differentiation, and gene expression (1, 2, 8).

In $G_q\alpha$-coupled receptor signal transduction, PKC activation not only serves to relay the signal from effector phospholipase Cβ to various PKC substrates for initiating downstream cellular responses, but it also exerts feedback effects on the system and is involved in the turning off of signaling from the receptors, an important regulatory process termed desensitization (9, 10). The ability of PKC to phosphorylate and desensitize a receptor relies on the existence of consensus PKC phosphorylation site(s) at the intracellular domains of the receptors (11–14). Since PKC does not discriminate between agonist-occupied and -unoccupied receptors (15), activation of PKC is believed to be associated with both homologous and heterologous desensitization of G protein-coupled receptors. Consequently, exposure of cells to a $G_q\alpha$-coupled receptor agonist that causes PKC activation potentially results not only in the loss of cellular response to that specific agonist but also the diminution of cellular responses to various other agonists.

The current methods of assessing $G_q\alpha$-coupled receptor signaling and desensitization are based mainly on the generation of IP_3 or the increase of intracellular Ca^{2+} as a result of IP_3 generation (16–18). However, neither approach assesses the equally important and independent branch of phospholipase Cβ signaling reflected by the production of DAG and the subsequent membrane translocation and activation of PKC. Although as important as IP_3, DAG is rarely used as a measurement in assessing $G_q\alpha$ activation because of its quick turnover (1) and the lack of techniques to follow its real time cellular distribution or behavior. Moreover, biochemical studies have indicated that the activation of PKC by DAG is also transient and is mainly associated with many cellular events mediated by short term activation of PKC such as hormone secretion and

* This work was supported in part by National Institutes of Health Grant HL-43707. The costs of publication of this article were defrayed in part by the payment of page charges. This article must therefore be hereby marked "*advertisement*" in accordance with 18 U.S.C. Section 1734 solely to indicate this fact.

‖ To whom correspondence should be addressed: Dept. of Biochemistry, Medical University of South Carolina, 171 Ashley Ave., Charleston, SC 29425.

[1] The abbreviations used are: PKC, protein kinase C; PKA, cAMP-dependent protein kinase; GFP, green fluorescent protein; EGFP, enhanced GFP; $AT_{1A}R$, angiotensin II type 1A receptor; ET_AR, endothelin A receptor; β_2AR, β_2-adrenergic receptor; D_2R, dopamine D_2 receptor; HEK-293 cells, human embryonic kidney 293 cells; PMA, phorbol 12-myristoyl 13-acetate; IP_3, inositol 1,4,5-triphosphate; DAG, diacylglycerol; PBS, phosphate-buffered saline; CMV, cytomegalovirus; GPCR, G protein-coupled receptor.

muscle contraction (1, 2). Phorbol esters mimic the action of DAG, but they are more potent, and their effects last longer in cells due to their persistence in the cell membrane (1). This has made feasible the study of PKC subcellular localizations before and after activation by phorbol esters by immunofluorescent microscopy in fixed cells (19, 20). However, the same method is not applicable in following the more physiologically relevant redistribution of PKC in response to receptor activation in live cells. Furthermore, it is not clear whether the short term of PKC activation in response to receptor activation is related to the signaling desensitization at the level of receptors.

In the present study, we report the development of a green fluorescent protein conjugated PKCβII (GFP-PKCβII) to study PKC mobilization in response to agonist stimulation of G protein-coupled receptors and to assess the activation and desensitization of these receptors. GFP, originally identified in the jellyfish *Aequorea victoria*, displays an inherent green bioluminescence and has been used as a fluorescent reporter molecule in the localization of membrane receptors, cytoplasmic proteins, and secretory proteins (21–28). When fused to the amino terminus of PKCβII, the resulting fusion protein, GFP-PKCβII, was found to be fully functional in terms of its phospholipid-dependent kinase activity and its ability to translocate from cytoplasm to the plasma membrane in response to phorbol ester (PMA) stimulation, similar to that reported for a PKCγ-GFP conjugate (28). Interestingly, while in PMA-treated cells GFP-PKCβII remained on the plasma membrane, in cells stimulated with physiological signals that activate $G_q\alpha$-coupled receptors, the translocation of GFP-PKCβII to the plasma membrane was found to be transient, reaching a peak and being reversed within minutes. This provided a real time visual demonstration of the cellular trafficking of a PKC isoenzyme in live cells, revealing a dynamic nature of the interaction of PKCβII with lipid and/or protein molecules on the plasma membrane. Furthermore, since GFP-PKCβII selectively responded to only signals activating $G_q\alpha$- but not $G_s\alpha$- and $G_i\alpha$-coupled receptors and such responses were transitory, our results also demonstrate an important analytical role of GFP-PKCβII as a reporter in the study of $G_q\alpha$-coupled receptor activation and desensitization.

EXPERIMENTAL PROCEDURES

Materials—[γ-^{32}P]ATP was purchased from NEN Life Science Products. Monoclonal antibody against GFP was from CLONTECH. Polyclonal rabbit antibody against PKCβII was prepared and extensively characterized as described previously (29). Mammalian expression vector pBK-CMV and GFP plasmid pEGFP-N1 was from Stratagene and CLONTECH, respectively. Restriction enzymes were from Promega or New England Biolabs. Ampli-*Taq* DNA polymerase was obtained from Perkin-Elmer. Protein A-Sepharose CL-4B was from Amersham Pharmacia Biotech. Phosphatidylserine and *sn*-dioctanoyl-glycerol were purchased from Avanti Polar Lipids Inc. Eagle's minimum essential medium, phosphate-buffered saline (PBS), and 1 M HEPES buffer were from Life Technologies, Inc. Fetal bovine serum was obtained from Summit Biotechnology Inc. Fluorescein isothiocyanate-conjugated donkey anti-rabbit IgG was from Jackson ImmunoResearch Laboratories, Inc. All other chemicals were from Sigma.

Plasmid Constructs—The human PKCβII cDNA was inserted between *Bam*HI and *Kpn*I sites of pBK-CMV. A unique *Bss*HII restriction site was located three base pairs prior to the start codon (ATG) of PKCβII cDNA. To construct GFP-PKCβII, EGFP cDNA without the stop codon was first amplified from plasmid pEGFP-N1 by polymerase chain reaction using 5′-oligonucleotide primer 5′-GTGAACCGTCAGATCCGCTAG-3′ (based on the sequence of pEGFP-N1 from 575 to 595) and 3′-primer 5′-CCATCTTGCGCGCCTTGTACAGCTCGTCCATGC-3′ (with the native sequence of pEGFP-N1 from 1376 to 1396 underlined). The polymerase chain reaction fragment containing EGFP cassette was gel-purified, digested with *Bam*HI and *Bss*HII, and directly inserted between the *Bam*HI and *Bss*HII sites of plasmid pBK-CMV-PKCβII prior to the 5′-end of the PKCβII cDNA (Fig. 1). The sequence of the construct was confirmed by DNA sequencing. The cDNAs of AT$_1$R, ET$_A$R, α$_{1B}$AR, and D$_1$R were subcloned in pcDNA I or pcDNA I/amp mammalian expression vectors (Invitrogen).

Cell Culture and Transfection—HEK 293 cells from the American Type Culture Collection (ATCC) were maintained in Eagle's minimum essential medium supplemented with 10% (v/v) fetal bovine serum in a 5% CO$_2$ incubator at 37 °C. Cells were seeded at a density of 2.0×10^6 cells/100-mm dish and transfected using a modified calcium phosphate method with 1–10 μg of plasmid (30).

Immunoprecipitation—HEK 293 cells were transfected with EGFP-PKCβII or GFP-PKCβII. Immunoprecipitation was performed 48 h after transfection as follows. The cells were washed with cold PBS and solubilized in 0.5 ml of lysis buffer with protease inhibitors (50 mM Tris-HCl, pH 8.0, 150 mM NaCl, 0.5% Nonidet P-40, 10 mM NaF, 1 mM sodium orthovanadate, 1 mM dithiothreitol, 10 μg/ml leupeptin, 10 μg/ml aprotinin, 10 μg/ml trypsin/chymotrypsin inhibitor, 5 μg/ml pepstatin A, 1 mM phenylmethylsulfonyl fluoride) for 1 h, and the lysates of EGFP-PKCβII or GFP-PKCβII transfected cells were immunoprecipitated with PKCβII antibody. Protein A-Sepharose beads were used to absorb immunoprecipitates and were then washed four times with lysis buffer followed by one wash with kinase buffer (50 mM Tris-HCl, pH 7.4, 10 mM NaF, 1 mM Na_3VO_4, 0.5 mM EDTA, 0.5 mM EGTA, 2 mM MgCl$_2$). The kinase activity of immunoprecipitated proteins was analyzed by protein kinase C assay (see below).

Immunoblot—Cell lysates from HEK 293 cells transfected with EGFP-PKCβII or GFP-PKCβII were separated by SDS-polyacrylamide gel electrophoresis and electrophoretically transferred onto nitrocellulose membranes (31). The membranes were blocked in PBS with 0.1% Tween 20 and 5% dried milk, probed with anti-GFP antibody (1:2500 dilution) or rabbit anti-PKCβII antibody (1:2000 dilution), and exposed using the enhanced chemiluminescence (ECL) Western blotting detection system (Amersham Pharmacia Biotech).

Protein Kinase C Assay—PKC activity was measured using the vesicle assay for PKC as described previously (32). Standard assay conditions were as follows: 20 mM Tris-HCl, pH 7.4, 100 μM MgCl$_2$, 1 mM CaCl$_2$, 10 μM ATP, 10–15 μCi/ml [γ-^{32}P]ATP, 40 μg/ml phosphatidylserine/*sn*-dioctanoyl-glycerol vesicles, and 200 μg/ml histone IIIS as substrate in a final volume of 250 μl at 30 °C for 10 min. 10 mM EGTA was used in determining basal kinase activity. The phosphorylated proteins were analyzed by SDS-polyacrylamide gel electrophoresis followed by autoradiography.

Indirect Immunofluorescence—Transfected cells were seeded on glass coverslips placed in six-well culture dishes at a density of 5×10^5 cells/well. For experiments involving phorbol ester treatment, cells were treated with 100 nM PMA for 5 min. The cells were then rinsed briefly in PBS and fixed in 3.7% paraformaldehyde for 10 min. The fixed cells were permeabilized in PBS containing 0.2% Triton X-100 for 10 min and blocked in PBS containing 0.2% bovine serum albumin for 10 min. After 1 h of incubation with anti-PKCβII polyclonal antibody (1:100 dilution), the cells were washed and incubated with fluorescein isothiocyanate-conjugated donkey anti-rabbit IgG (1:100 dilution) for 1 h. The coverslips were mounted onto the slides, and PKCβII immunofluorescence was observed with a Zeiss LSM-410 laser scanning microscope at 488-nm excitation.

Confocal Microscopy—HEK 293 cells were transfected with GFP-PKCβII and one or two of the G protein-coupled receptors as described in figure legends. 24 h after transfection, the cells were plated onto 35-mm glass-bottomed culture dishes (MatTek) at a density of 1×10^5 and incubated for another 24 h for the cells to attach to glass. The cells expressing GFP-PKCβII (25–40% of the total cell population) were observed under confocal microscopy. Confocal microscopy was performed on a Zeiss LSM-410 laser scanning microscope using a Zeiss 40 × 1.3 NA oil immersion lens. The cells were kept warm during microscopy at 30 °C in culture medium containing 20 mM HEPES on a heated microscope stage. GFP-PKCβII fluorescent signals were collected sequentially using the Zeiss LSM software time series function with single line excitation (488 nm) with a time interval of 20 s between two scannings. Various drugs were applied to the cells during the scanning of GFP-PKCβII transfected cells.

RESULTS

Comparison of Wild-type PKCβII and GFP-PKCβII—Due to its inherent fluorescence and unique compact structure, GFP has been reported in many studies to serve as a valuable reporter molecule in the localization of various proteins without interfering with their biological activity (21, 33). GFP-PKCβII was constructed by fusing EGFP to the 5′-end of PKCβII (Fig. 1). When examined using SDS-polyacrylamide gel

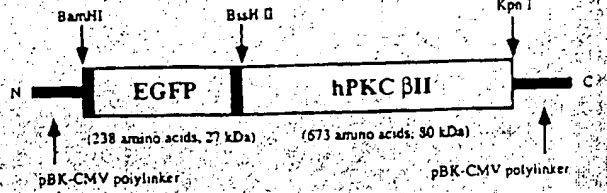

FIG. 1. **Architecture of GFP-PKCβII fusion protein in pBK-CMV vector.** As described under "Experimental Procedures," the EGFP fragment without the stop codon was inserted at the 5′ end of human PKCβII (hPKCβII) cDNA with *Bam*HI and *Bss*HII sites. Also indicated are the numbers of amino acids and expected sizes of EGFP and human PKCβII.

electrophoresis followed by immunoblotting. GFP-PKCβII was found to express to the same extent in HEK 293 cells as wild-type PKCβII but migrated more slowly due to the added mass of GFP (Fig. 2*A*). To compare the biological activity of GFP-PKCβII with that of wild-type PKCβII, both proteins were immunoprecipitated from HEK 293 cells transiently expressing GFP-PKCβII or PKCβII with an antibody against PKCβII and analyzed for their relative kinase activity using a recently developed PKC assay with histone IIIS as the substrate (32). As shown in Fig. 2*B*, the cells transfected with EGFP contained very low kinase activity, but transfection of either GFP-PKCβII or PKCβII significantly increased the phosphorylation of histone IIIS. The ability of GFP-PKCβII to phosphorylate histone IIIS in a Ca^{2+}- and phospholipid-dependent manner was comparable with that of wild-type PKCβII, indicating that the fusion of the GFP molecule to the N terminus of PKCβII has no significant effect on PKC activity.

Phorbol esters such as PMA are well known to mimic the action of diacylglycerol in inducing PKC to translocate from cytosol to the plasma membrane (1, 34). Thus, the ability of GFP-PKCβII to respond to PMA was also examined (Fig. 2*C*, *top*). Under normal unstimulated conditions, GFP-PKCβII was evenly distributed in the cytoplasm and excluded from the nuclei, a distribution exactly reflecting the cellular localization of wild-type PKCβII detected with indirect immunofluorescence microscopy (Fig. 2*C*, *middle*). Stimulation with 1 μM PMA triggered redistribution of GFP-PKCβII to the plasma membrane. This membrane translocation was completed within 5 min, and about 90% of GFP-PKCβII fluorescence was mobilized to the plasma membrane, similar to that observed with transfected wild-type PKCβII in fixed HEK 293 cells (Fig. 2*C*, *top* and *middle*). The distribution of wild-type PKCβII and GFP-PKCβII observed in HEK 293 cells corresponded to the reported distribution of endogenous PKCβII in U937, a cell line expressing endogenous PKCβII (35). In contrast to GFP-PKCβII, unconjugated GFP molecules were distributed throughout the cell body, and their distribution was not affected by PMA (Fig. 2*C*, *bottom*). These results indicate that GFP-PKCβII fusion protein retains the biological activity of wild-type PKCβII with respect to kinase activity as well as cellular localization.

Dynamic and Selective Trafficking of GFP-PKCβII in Response to G Protein-coupled Receptor Activation—Although the redistribution of PKC upon phorbol ester stimulation has been extensively studied with indirect immunofluorescence microscopy (19, 20), the kinetics of PKC membrane translocation in response to physiological signals have not been well characterized. One such physiological signal that activates PKC is through activation of G protein-coupled receptors. Therefore, initial studies using confocal microscopy examined the real time cellular distribution of GFP-PKCβII in response to the activation of the $G_q\alpha$-coupled $AT_{1A}R$ by its physiological ligand angiotensin II (Fig. 3*A*). This was done at 30 °C in live HEK 293 cells which had been transiently transfected to overexpress the $AT_{1A}R$ and GFP-PKCβII. In the absence of receptor activation, confocal microscopy revealed that GFP-PKCβII was evenly distributed throughout the cytoplasm. However, upon agonist activation of the $AT_{1A}R$, a redistribution of GFP-PKCβII to the plasma membrane and clearance of cytosolic fluorescence occurred and peaked within 40 s. This angiotensin II-induced GFP-PKCβII membrane trafficking was rapid compared with the translocation caused by PMA stimulation, which did not peak until after 2–5 min. More interestingly, unlike PMA-induced translocation in which PKC remained persistently localized on the plasma membrane, the mobilization of GFP-PKCβII to the plasma membrane following $AT_{1A}R$ activation was transient, and the redistributed GFP-PKCβII rapidly returned to the cytoplasm within 1 min after translocation. The time frame for GFP-PKCβII recovery in the cytoplasm in the majority of the cells observed ranged from 20 s to 1 min after GFP-PKCβII membrane translocation. Moreover, even in the continuous presence of angiotensin II for 30 min, only an initial brief peak of PKC membrane translocation was observed (data not shown). These visual results are consistent with biochemical studies indicating a dynamic nature of PKCβII in interacting with molecules on the plasma membrane (1, 34).

Among major groups of G protein-coupled receptors, those coupled to $G_q\alpha$ are directly associated with the activation of phospholipase C, resulting in the generation of diacylglycerol and a rise of intracellular Ca^{2+}, whereas the effector for receptors coupled to $G_s\alpha$ and $G_i\alpha$ is mainly adenylyl cyclase associated with the production of cyclic AMP. To examine the specificity and selectivity of agonist-induced PKC trafficking, three additional G protein-coupled receptors were tested for their ability to trigger GFP-PKCβII translocation, including ET_AR (coupled to $G_q\alpha$), β_2AR (coupled to $G_s\alpha$), and D_2R (coupled to $G_i\alpha$). In HEK 293 cells, transiently transfected with GFP-PKCβII and ET_AR, a rapid PKC membrane translocation was observed in response to the ET_AR endogenous agonist endothelin (Fig. 3*B*). Similar to that caused by the activation of the $AT_{1A}R$, this ET_AR-promoted redistribution of GFP-PKCβII was transient and readily reversible. In contrast, when cells were transfected to coexpress GFP-PKCβII with either β_2AR or D_2R, the activation of neither receptor by its cognate ligand affected the distribution of GFP-PKCβII fluorescence (Fig. 3, *C* and *D*). These results indicate that the mobilization of GFP-PKCβII in live cells are selectively mediated by receptors activating the phospholipase C signaling pathway including GPCRs coupled to $G_q\alpha$ but not $G_s\alpha$ and $G_i\alpha$.

Desensitization of $G_q\alpha$-coupled Receptor Signaling Revealed by GFP-PKCβII Trafficking—The observation that there was only one brief peak of PKC membrane translocation even in the continuous presence of angiotensin II or endothelin suggests that the transitory nature of PKC trafficking in response to these receptor agonists might be associated with the rapid desensitization of $AT_{1A}R$ or ET_AR signaling. To further investigate this phenomenon, HEK 293 cells transfected with GFP-PKCβII and $AT_{1A}R$ were sequentially exposed to two pulses of stimulation by angiotensin II separated by 10 min (Fig. 4*A*). Whereas the first exposure resulted in a transient GFP-PKCβII trafficking between the cytoplasm and plasma membrane and GFP-PKCβII returned to the cytoplasm within 1 min following its membrane translocation, there was no apparent PKC mobilization in response to the second angiotensin II stimulation, indicating the $AT_{1A}R$ signaling was turned off as a result of initial receptor activation at a step prior to PKC translocation or at the level of PKC. The possibility that PKC itself might be desensitized and loses its ability to respond to further receptor activation was examined by exposing $AT_{1A}R$

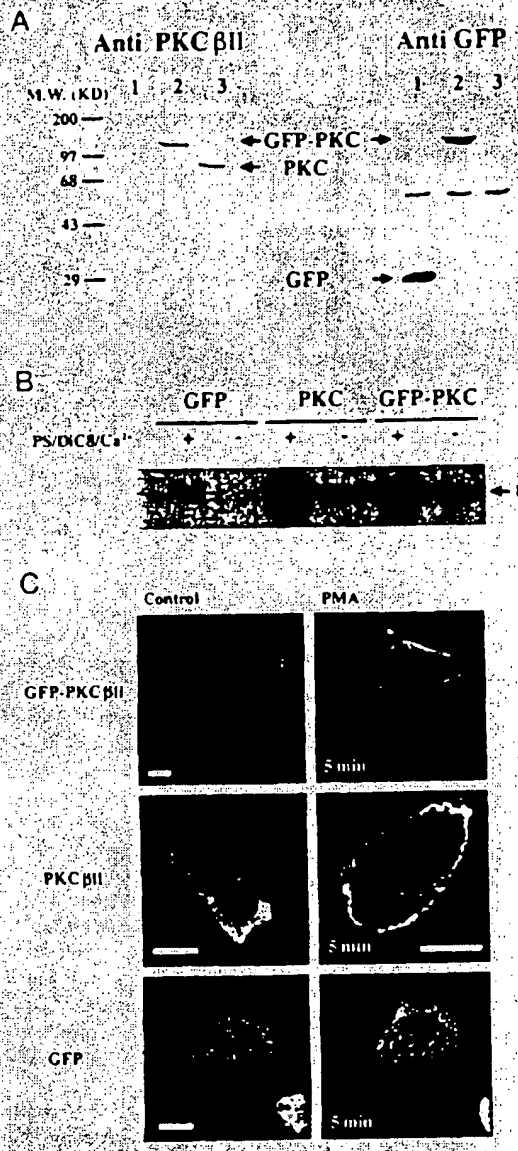

FIG. 2. **Characterization of GFP-PKCβII fusion protein expressed in HEK 293 cells by immunoblotting analysis, protein kinase C assay, and confocal microscopy.** *A*: shown are immunoblots of homogenates from HEK 293 cells transfected with 1 μg of pEGFP-N1 (*lane 1*), pBK-CMV-GFP-PKCβII (*lane 2*), and pBK-CMV-PKCβII (*lane 3*) probed with polyclonal antibody against PKCβII (*left*) and monoclonal antibody against GFP (*right*). 20 μg of homogenate was loaded in each lane. As expected, the homogenate from cells transfected with pBK-CMV-GFP-PKCβII showed strong immunoreactivity to both the PKCβII antibody and GFP antibody. The band seen at approximate 50 kDa in each lane with anti-GFP represents nonspecific immunoreactivity. *B*: the above described HEK 293 cell homogenates (100 μg) were immunoprecipitated with PKCβII antibody, and kinase activity of the immunocomplexes was assayed. Protein kinase C assay was performed under standard conditions in the presence (+) and absence (−) of PKC activator *sn*-dioctanoyl-glycerol (*DiC8*), and cofactors Ca^{2+} and phosphatidylserine. Shown is a representative autoradiograph indicating GFP-PKCβII and wild-type PKCβII comparably phosphorylated substrate histone IIIS. *C*: shown are the confocal micrographs of HEK 293 cells transfected with 1 μg of pBK-CMV-GFP-PKCβII (*top*) or pEGFP-N1 (*bottom*) before (control) and after 5 min of PMA treatment (*PMA*). The transfected cells were stimulated with 1 μM PMA at 30 °C to activate PKC. The redistribution of GFP-PKCβII started within 1 min, and almost 90% of fluorescence was located at the plasma membrane after 5 min of stimulation. In contrast, there was no change of the PMA stimulation. Shown

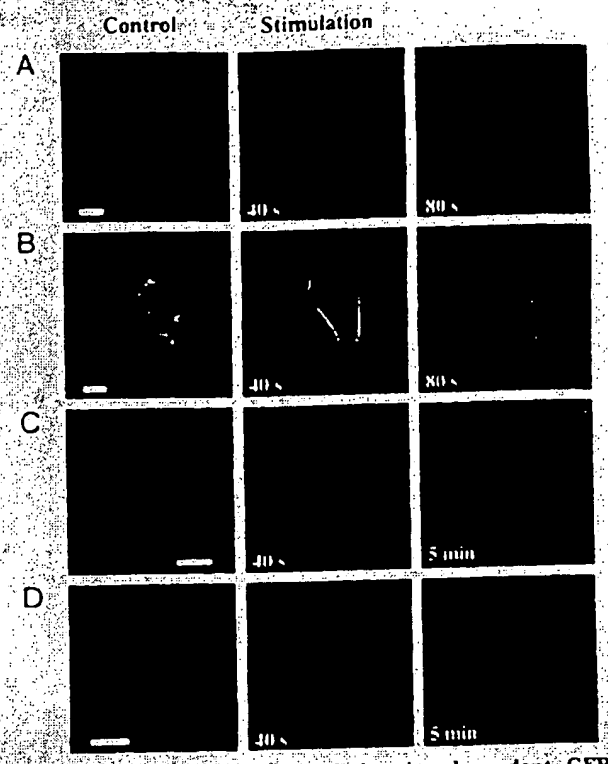

FIG. 3. **Confocal microscopy of the time-dependent GFP-PKCβII redistribution in response to G protein-coupled receptor activation.** HEK 293 cells were transfected with 1 μg of pBK-CMV-GFP-PKCβII as well as 10 μg of one of the following G protein-coupled receptor constructs: $AT_{1A}R$, ET_AR, β_2AR, or D_2R. All cells were visualized at 30 °C with a confocal microscope. Before receptor activation (control), GFP-PKCβII was evenly distributed in the cytoplasm. When cells transfected with $AT_{1A}Rs$ or ET_ARs were stimulated with corresponding receptor agonists, 0.5 μM angiotensin II (*A*) or 0.1 μM endothelin (*B*), GFP-PKCβII underwent a transient redistribution between the cytoplasm and plasma membrane. In contrast, no GFP-PKCβII mobilization was observed in cells transfected with either β_2AR (*C*) stimulated with 10 μM isoproterenol or D_2R (*D*) stimulated with 10 μM dopamine. Also indicated in the micrographs are the time points following agonist stimulation for each receptor. The experiments were performed independently on three different occasions, and each time 3–5 cells from independent stimulation by each agonist were recorded. All of the micrographs are representative of more than 70% of the cells observed. *Bar*, 10 μm.

and GFP-PKCβII-containing cells to PMA following agonist activation of the $AT_{1A}R$. As shown in Fig. 4*B*, PMA triggered a second peak of stable GFP-PKCβII redistribution to the plasma membrane in cells preexposed to angiotensin II. The time profile and extent of this PKC translocation were indistinguishable from PMA-induced PKC redistribution in cells untreated with receptor agonist. Similar results were obtained when cells were transfected with GFP-PKCβII and ET_AR and pretreated with endothelin (Fig. 4, *C* and *D*). These results strongly suggest that the transient nature of PKC trafficking in response to $G_q\alpha$-coupled receptor activation is a direct consequence of the rapid desensitization of receptor signaling at a step prior to PKC translocation.

Cross-talk of $G_q\alpha$-coupled Receptor Signaling Revealed by GFP-PKCβII Trafficking—The $AT_{1A}R$ and ET_AR share the

with 1 μg of pBK-PKCβII before (control) and after 5 min of treatment with 100 nM PMA (*PMA*) at 37 °C. The cells were fixed and stained for wild-type PKCβII as described under "Experimental Procedures." The experiments were performed independently on 5–10 cells on two or

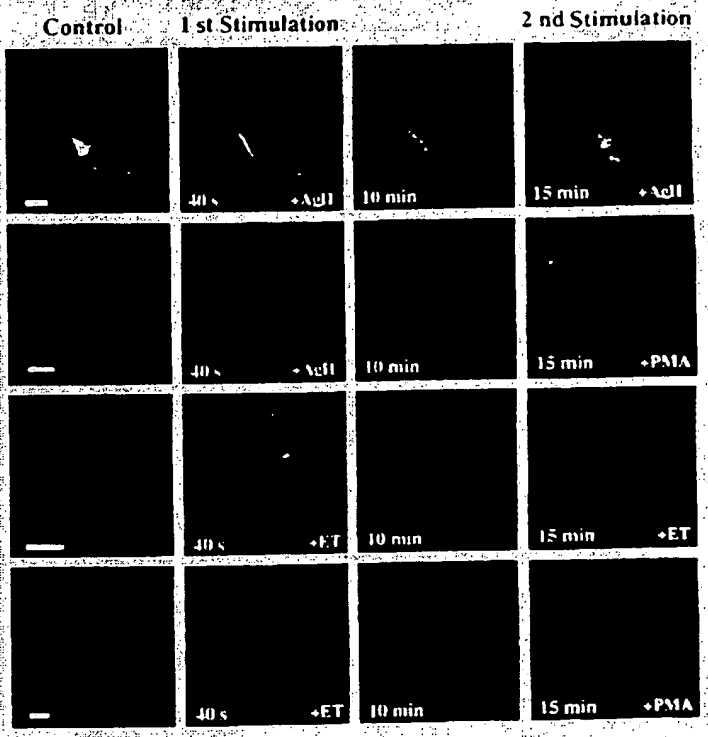

FIG. 4. **Effects of angiotensin II (*AgII*), endothelin (*ET*), and PMA on the redistribution of GFP-PKCβII in cells preexposed to angiotensin II or endothelin.** HEK 293 cells were cotransfected with 1 μg of pBK-CMV-GFP-PKCβII and 10 μg of pcDNA I/amp-$AT_{1A}R$ and stimulated with either 0.5 μM angiotensin II (*A* and *B*) or cotransfected with 1 μg of pBK-CMV-GFP-PKCβII and 10 μg of pcDNA I/ET_AR and stimulated with 0.1 μM endothelin (*C* and *D*) to induce GFP-PKCβII transient trafficking between the cytoplasm and plasma membrane. 10 min after the first stimulation, the cells were restimulated with additional 1.5 μM angiotensin II (*A*), 0.5 μM endothelin (*C*), or 1 μM PMA (*B* and *D*). Indicated in the micrographs are the time points following the first agonist stimulation. All cells were visualized at 30 °C by confocal microscope. The experiments were performed independently on three different occasions, and each time 3–5 cells from independent stimulation by each drug were recorded. The confocal micrographs are representative of more than 70% of the cells observed. *Bar*, 10 μm.

same $G_q\alpha$-mediated signaling pathway in which $G_q\alpha$ activates phospholipase Cβ and results in the hydrolysis of phosphoinositol lipid to generate IP_3 and DAG, the latter serving as a second messenger for activation of PKC. To further study the rapid receptor desensitization as well as the relationship between signaling pathways of different receptors, $AT_{1A}R$ and ET_AR were cotransfected with GFP-PKCβII into HEK 293 cells, and the effect of their potential cross-talk on the trafficking of GFP-PKCβII was examined and visualized by confocal microscopy. In initial experiments, the cells were prestimulated with angiotensin II to activate the $AT_{1A}R$ and induce PKC response. As described above, the resulting GFP-PKCβII trafficking was transient and GFP-PKCβII returned to the cytoplasm within 1 min following its membrane translocation. No second peak of PKC translocation was observed in the continuous presence of agonist for as long as 30 min. However, when endothelin was subsequently added to the angiotensin II-pretreated cells to activate the ET_AR, a second peak of GFP-PKCβII translocation was apparent within 1 min, the time profile and extent of which were indistinguishable from the first peak (Fig. 5*A*). As both $AT_{1A}R$ and ET_AR induce PKC response by activating $G_q\alpha$, which increases the activity of phospholipase C, the ability of endothelin to mobilize PKC in cells prestimulated with $AT_{1A}R$ agonist further indicates that the activation of $AT_{1A}R$ did not desensitize $G_q\alpha$-mediated signaling pathways, but instead the desensitization occurred at the level of the $AT_{1A}R$ receptor itself. Moreover, these results also demonstrate that the activation of $AT_{1A}Rs$ does not contribute to the desensitization of the ET_AR.

To further investigate the effect of ET_AR activation on $AT_{1A}R$ signaling, we reversed the order of introducing agonists and sequentially added endothelin and then angiotensin II to the cells cotransfected with both receptors. Surprisingly, when the cells were preexposed to endothelin for 5 min, no additional peak of GFP-PKCβII cellular movement was detected by confocal microscopy in response to a subsequent stimulation with angiotensin II (Fig. 5*B*). This result indicates that in contrast to the inability of $AT_{1A}R$ to cause ET_AR desensitization in HEK 293 cells, the activation of ET_ARs indeed led to the heterologous desensitization of the $AT_{1A}R$ in the same cells, possibly mediated by the activation of PKC and subsequent phosphorylation of the receptor by PKC. This is consistent with the observation that inhibition of activation of PKC by 0.5 μM staurosporine, a potent protein kinase inhibitor, resulted in a 42% lose of total agonist-stimulated phosphorylation of the $AT_{1A}R$ but had no effect on that of the ET_AR (16, 36). The specificity of the heterologous desensitization was further assessed by examining the effect of activation of another second messenger-dependent kinase, cyclic AMP dependent protein kinase (PKA) on $AT_{1A}R$ signaling in cells cotransfected with the β_2AR and $AT_{1A}R$ (Fig. 5*C*). The activation of the β_2AR by isoproterenol is easily detectable by measuring the membrane translocation of a β-arrestin 2/GFP conjugate (26) and is known to stimulate $G_s\alpha$, which eventually leads to the accumulation of cyclic AMP and activation of PKA (3). As expected, stimulation of β_2AR by isoproterenol did not have a visible effect on the distribution of GFP-PKCβII. However, this preexposure of the cells to isoproterenol did not prevent the rapid cellular redistribution of GFP-PKCβII between the cytoplasm and plasma membrane triggered by subsequently added angiotensin II, indicating that activation of PKA did not result in the heterologous desensitization of the $AT_{1A}R$.

DISCUSSION

In the present work, the development of a fully functional green fluorescent protein conjugated PKCβII has allowed visualization in live cells of the real time interaction of PKC with the plasma membrane in response to extracellular signals. Whereas stimulation by phorbol esters (*e.g.* PMA) causes a persistent localization of PKC to the plasma membrane, our results reveal a dynamic nature of PKCβII trafficking between the cytoplasm and plasma membrane in response to physiological signals such as those activating G protein-coupled receptors. PKCβII responds selectively only to specific signals that

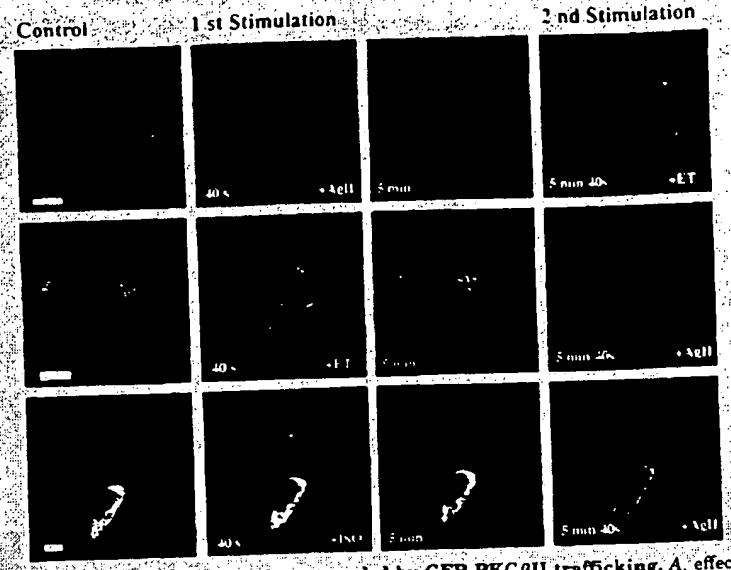

FIG. 5. **Cross-talk of G protein-coupled receptor signaling revealed by GFP-PKCβII trafficking.** *A*, effect of $AT_{1A}R$ activation on the subsequent stimulation of ET_ARs by endothelin. HEK 293 cells were transfected to coexpress GFP-PKCβII, $AT_{1A}R$, and ET_AR. The cells were stimulated with 0.5 μM angiotensin II (*AgII*), which induced GFP-PKCβII redistribution between the cytoplasm and plasma membrane. This was followed by a second stimulation with 0.1 μM endothelin (*ET*) 5 min after the first stimulation. A second peak of GFP-PKCβII redistribution was observed in response to ET_AR activation. *B*, effect of ET_AR activation on the subsequent stimulation of $AT_{1A}R$s by angiotensin II. The cells were transfected as described in *A* and stimulated with 0.1 μM endothelin, which induced GFP-PKCβII redistribution between the cytoplasm and plasma membrane. This was followed by a second stimulation with 0.5 μM angiotensin II 5 min after the first stimulation. The preexposure of cells to endothelin blocked the subsequent activation of $AT_{1A}R$s, as revealed by the lack of GFP-PKCβII redistribution. *C*, effect of β_2AR activation on the subsequent stimulation of $AT_{1A}R$s by angiotensin II. HEK 293 cells were transfected to coexpress GFP-PKCβII, $AT_{1A}R$, and β_2AR. The cells were stimulated with 10 μM isoproterenol to activate β_2ARs, and this was followed by a second stimulation by angiotensin II, indicating activation of the $AT_{1A}R$. Also first stimulation, GFP-PKCβII redistribution was observed following stimulation by angiotensin II 5 min after the indicated in the micrographs are the time points following the first agonist stimulation. All cells were visualized at 30 °C by confocal microscope. The experiments were performed independently on three or four different occasions, and each time 10–15 cells from independent stimulation by different agonists were recorded. All of the confocal micrographs are representative of more than 60% of the cells observed. *Bar*, 10 μm.

activate receptors coupled to $G_q\alpha$ but not $G_s\alpha$ and $G_i\alpha$ proteins. The membrane translocation of PKCβII triggered by the activation of $G_q\alpha$-coupled receptors is rapid and transient and is followed immediately by the returning of PKC to the cytoplasm within minutes, indicating a desensitization of the signaling pathway. Moreover, when GFP-PKCβII trafficking in response to the sequential activation of two distinct $G_q\alpha$-coupled receptors (*i.e.* $AT_{1A}R$ and ET_AR) was studied, the results indicated that the signaling desensitization occurs at the level of receptors and that there is cross-talk between the two receptors. Thus, GFP conjugated PKC fusion proteins serve as a novel useful tool not only for studying the dynamic localization of PKCs in signal transduction in live cells but also for detecting the activation and desensitization of receptors coupled to phospholipase C such as $G_q\alpha$-coupled receptors.

PKC cellular localization has been extensively studied in culture cells using antibody staining and immunofluorescent microscopy (19, 20). However, many signal transduction events involving PKC are rapid, transient, and difficult to follow in fixed cells. Green fluorescent protein, because of its inherent bioluminescence and stoichiometric labeling, represents a sensitive optical reporter to follow the real time localization of many proteins in live cells and is thus well suited for the study of transitory and dynamic distribution of molecules in the process of signal transduction (26). Recently, the GFP technique has been used in the study of cellular distribution of PKCγ (28). In our study, when EGFP was fused to the N terminus of PKCβII, GFP-PKCβII conjugate displayed Ca^{2+}- and phospholipid-dependent kinase activity comparable with that of wild-type PKCβII and was localized mainly in the cytoplasm and excluded from the nuclei. Moreover, in cells stimulated with PMA, like wild-type PKCβII, GFP-PKCβII redistributed to the plasma membrane. The stable association of GFP-PKCβII with the plasma membrane is a true reflection of the persistence of PMA in the plasma membrane as well as the stable interaction of PKCβII to PMA. Therefore, although GFP is about one-third the size of PKCβII (Fig. 1), as reported for many other proteins, our data demonstrate that GFP-PKCβII conjugate retains the function of native PKCβII in terms of biochemical behavior and cellular localization, although the possibility cannot be ruled out that the coupling of GFP to PKCβII may alter the affinity of the enzyme to its interacting molecules.

The activation of PKC is triggered by a large number of extracellular signals including hormones, neurotransmitters, and growth factors that act through cell surface receptors. The activation of these receptors regulates the intracellular level of various PKC activators including DAG, Ca^{2+}, and many other lipid mediators. G protein-coupled receptors were used in this work as an example to address PKC cellular trafficking and distribution in response to various physiological stimuli. Four receptors were examined for their ability to stimulate GFP-PKCβII redistribution, including $G_s\alpha$-coupled β_2AR, $G_i\alpha$-coupled D_2R, and $G_q\alpha$-coupled $AT_{1A}R$ and ET_AR. The physiological relevance of PKC activation mediated by these receptors is apparent since PKC responded selectively only to signals activating $G_q\alpha$-coupled receptors (*i.e.* $AT_{1A}R$ and ET_AR) but not $G_s\alpha$- and $G_i\alpha$-coupled receptors, corresponding to the fact that among the three major G proteins only $G_q\alpha$ mediates the production of DAG at the plasma membrane and a rise of intracellular Ca^{2+}. More importantly, unlike PMA-stimulated PKC translocation, physiological signals activating $AT_{1A}R$s and ET_ARs induce a redistribution of GFP-PKCβII to the plasma membrane, which appears to be transient, consistent with the

biochemical studies indicating that DAG is one of the plasma membrane stimuli for PKC and that the interaction between DAG and PKC is rapid and reversible (1, 34).

However, it is somewhat unexpected that only one rapid cycle of PKC translocation from the cytoplasm to plasma membrane and back was observed although receptor agonists were present continuously. This lack of further PKC responsiveness is probably the result of a rapid desensitization of the agonist-mediated signaling pathway upstream of PKC, since PKC itself still retains the ability to respond normally when subsequently exposed to PMA. In addition, sequential stimulation of the $AT_{1A}R$ and then the ET_AR with their corresponding agonists induced consecutive transient cycles of PKC translocation, one after each stimulation. As the $AT_{1A}R$ and ET_ARs presumably share the same signaling components downstream of the receptors, this suggests that the desensitization of $AT_{1A}R$ signaling occur at the level of the receptor itself. More interestingly, although activation of the $AT_{1A}R$ does not affect the activity of the ET_AR, activation of the ET_AR not only shuts off its own signaling but also causes the desensitization of the $AT_{1A}R$, indicating differential regulation of the two receptors.

The rapid desensitization of G protein-coupled receptors is achieved mainly through phosphorylation of the receptors by two classes of serine/threonine protein kinases: the second messenger activated protein kinases, PKA and PKC; and the G protein-coupled receptor kinases that specifically phosphorylate agonist-activated receptors (15). Although the role of PKC in regulating $AT_{1A}R$ desensitization in different tissues is still variable depending on experimental conditions, recently it was reported that the $AT_{1A}R$ was phosphorylated by both G protein-coupled receptor kinases and PKC in response to short term angiotensin II stimulation in HEK 293, a cell line widely used in the study of receptor desensitization (16). In contrast, in the same cell line, the ET_AR was mainly phosphorylated by G protein-coupled receptor kinases but not by activated PKC in response to agonist (36). These studies suggest that while both receptors serve as substrates for G protein-coupled receptor kinases, only the $AT_{1A}R$ (but not ET_AR) has the unique biochemical property to undergo agonist-dependent phosphorylation by PKC. The homologous desensitization of both receptors probably involves G protein-coupled receptor kinase or possibly PKC in the case of the $AT_{1A}R$. However, our results suggest that cross-talk (*i.e.* heterologous desensitization) between the two receptors is mainly mediated by PKC, and the distinct ability to be phosphorylated by PKC might underlie the observed differential desensitization properties of the two receptors. For instance, the inability of the ET_AR to be phosphorylated by PKC might account for its lack of heterologous desensitization by activation of the $AT_{1A}R$. In addition, despite the finding that the $AT_{1A}R$ was phosphorylated by PKA in intact aortic vascular smooth muscle cells (RASM) (37), we demonstrate that activation of PKA by stimulating the β_2AR does not lead to desensitization of the $AT_{1A}R$, consistent with the lack of PKA phosphorylation of the $AT_{1A}R$ found in HEK 293 cells (16).

A large variety of signaling pathways are known to culminate in the activation of PKC, including those mediated by $G_q\alpha$ protein-coupled receptors (1, 34). The numbers of such receptors are expected to expand rapidly with the progress of genomic sequencing and challenge the conventional biochemical measurements that assess individual receptor-specific properties for defining their corresponding ligands, detecting signaling activation and measuring change of second messenger levels. In this study, by combining the inherent fluorescence of GFP with the translocation property of PKC, we have developed a potential live cell biosensor that may provide simple, sensitive, and rapid assessment of the involvement of PKC activation in the signaling pathways of these receptors. In addition, since GFP-PKC redistribution can serve as a sensitive indicator for receptor activation, it may provide a simple and universal tool for screening new ligands for receptors coupled to PKC as well as for associating newly discovered receptors with their cognate ligands and physiological functions. Moreover, by monitoring inhibition of PKC translocation, it may be potentially also applicable to the identification of the inhibitors of PKC itself as well as inhibitors that block the signaling components leading to activation of PKC. In the case of GPCRs, GFP-PKC translocation has been shown in this study to be a specific measure of $G_q\alpha$-coupled receptor activation. The transitory nature of the translocation makes GFP-PKC a useful tool for studying $G_q\alpha$-coupled receptor desensitization. Compared with detecting Ca^{2+} signals, measuring PKC trafficking represents a more direct and accurate assessment of the properties of the plasma membrane receptors without concerns from the permeability, solubility, and compartmentalization of Ca^{2+} indicators and interference from plasma membrane and intracellular Ca^{2+} channels (*e.g.* the IP_3 receptor) (7, 18, 38). Furthermore, with the discovery of numerous novel G protein-coupled receptors by genomic sequencing, GFP-PKC should also be extremely useful in quickly identifying those receptors coupled to $G_q\alpha$ and their ligands and functions.

The visualization of GFP-PKCβII dynamic translocation in this study provides a direct real time assessment of the distribution of a PKC in live cells in response to changes of intracellular PKC activators triggered by physiological stimuli. To date, 12 members are identified as belonging to the PKC superfamily, associated with a wide variety of cellular signaling events, such as mitogenesis and tumorigenesis (2, 8). The use of GFP conjugates as optical reporters should provide valuable information concerning not only the specific cellular distribution of different PKC isoenzymes but also their dynamic trafficking in response to various physiological stimuli. Therefore, GFP-PKC conjugates may represent ideal optical tools in the study of specific functions and kinetics of each PKC isoenzyme in different signal transduction systems. Furthermore, when employed as a biosensor, GFP-PKC fusion proteins may also provide a unique and sensitive means for studying the kinetics and components of signal transduction pathways in which PKCs are involved.

REFERENCES

1. Nishizuka, Y. (1992) *Science* 258, 607–614
2. Blobe, G. C., Stribling, S., Obeid, L. M., and Hannun, Y. A. (1996) *Cancer Surv.* 27, 213–248
3. Watson, S., and Arkinstall, S. (1994) *The G-protein Linked Receptor Facts Book*, pp. 296–314, Academic Press, Inc., San Diego, CA
4. Neer, E. J. (1995) *Cell* 80, 249–257
5. Taylor, S. J., Chae, H. Z., Rhee, S. G., and Exton, J. H. (1991) *Nature* 350, 516–518
6. Smrcka, A. V., Hepler, J. R., Brown, K. O., and Sternweis, P. C. (1991) *Science* 251, 804–807
7. Berridge, M. J. (1993) *Nature* 361, 315–325
8. Nishizuka, Y. (1984) *Nature* 308, 693–698
9. Lefkowitz, R. J. (1993) *Cell* 74, 409–412
10. Ferguson, S. S., Barak, L. S., Zhang, J., and Caron, M. G. (1996) *Can. J. Physiol. Pharmacol.* 74, 1095–1110
11. Greene, N. M., Williams, D. S., and Newton, A. C. (1997) *J. Biol. Chem.* 272, 10341–10344
12. Widmann, C., Dolci, W., and Thorens, B. (1996) *J. Biol. Chem.* 271, 19957–19963
13. Yuan, N., Friedman, J., Whaley, B. S., and Clark, R. B. (1994) *J. Biol. Chem.* 269, 23032–23038
14. Diviani, D., Lattion, A.-L., and Cotecchia, S. (1997) *J. Biol. Chem.* 272, 28712–28719
15. Grady, E. F., Bohm, S. K., and Bunnett, N. W. (1997) *Am. J. Physiol.* 273, G586–G601
16. Oppermann, M., Freedman, N. J., Alexander, R. W., and Lefkowitz, R. J. (1996) *J. Biol. Chem.* 271, 13266–13272
17. Zhang, M., Turnbaugh, D., Cofie, D., Dogan, S., Koshida, H., Fugate, R., and Kem, D. C. (1996) *Hypertension* 27, 269–275
18. Kao, J. P. Y. (1994) *Methods Cell Biol.* 40, 155–181
19. Mochly-Rosen, D. (1995) *Science* 268, 247–251

20. Jaken, S. (1997) *Protein Kinase C*, pp. 179–188, R. G. Landes Company, Austin, TX
21. Cubitt, A. B., Heim, R., Adams, S. R., Boyd, A. E., Gross, L. A., and Tsien, R. Y. (1995) *Trends Biochem. Sci.* 20, 448–455
22. Naray-Fejes-Toth, A., and Fejes-Toth, G. (1996) *J. Biol. Chem.* 271, 15436–15442
23. Moores, S. L., Sabry, J. H., and Spudich, J. A. (1996) *Proc. Natl. Acad. Sci. U. S. A.* 93, 443–446
24. Gerisch, G., Albrecht, R., Heizer, C., Hodgkinson, S., and Maniak, M. (1995) *Curr. Biol.* 5, 1280–1285
25. Kaether, C., and Gerdes, H. H. (1995) *FEBS Lett.* 369, 267–271
26. Barak, L. S., Ferguson, S. S. G., Zhang, J., and Caron, M. G. (1997) *J. Biol. Chem.* 272, 27497–27500
27. Barak, L. S., Ferguson, S. S., Zhang, J., Martenson, C., Meyer, T., and Caron, M. G. (1997) *Mol. Pharmacol.* 51, 177–184
28. Sakai, N., Sasaki, K., Ikegaki, N., Shirai, Y., Ono, Y., and Saito, N. (1997) *J. Cell Biol.* 139, 1465–1476
29. Wetsel, W. C., Khan, W. A., Merchenthaler, I., Rivera, H., Halpern, A. E., Phung, H. M., Negro-Vilar, A., and Hannun, Y. A. (1992) *J. Cell Biol.* 117, 121–133
30. Cullen, B. R. (1987) *Methods Enzymol.* 152, 684–704
31. Towbin, H., Staehelin, T., and Gordon, J. (1979) *Proc. Natl. Acad. Sci. U. S. A.* 76, 4350–4354
32. Lee, J. Y., Hannun, Y. A., and Obeid, L. M. (1996) *J. Biol. Chem.* 271, 13169–13174
33. Yang, F., Moss, L. G., and Phillips, G. N. (1996) *Nat. Biotechnol.* 14, 1246–1251
34. Newton, A. C. (1995) *J. Biol. Chem.* 270, 28495–28498
35. Kiley, S. C., and Parker, P. J. (1995) *J. Cell Sci.* 108, 1003–1016
36. Freedman, N. J., Ament, A. S., Oppermann, M., Stoffel, R. H., Exum, S. T., and Lefkowitz, R. J. (1997) *J. Biol. Chem.* 272, 17734–17743
37. Kai, H., Griendling, K. K., Lassegue, B., Ollerenshaw, J. D., Runge, M. S., and Alexander, R. W. (1994) *Hypertension* 24, 523–527
38. Mikoshiba, K. (1997) *Curr. Opin. Neurobiol.* 7, 339–345

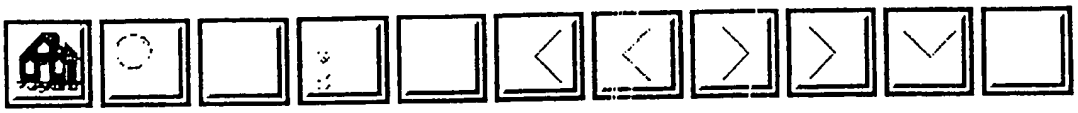

Current Contents, weeks 9301-9812

LibOrder: 980059081 Week 9805 ISSN: 0021-9525

Title:

Direct visualization of the translocation of the gamma-subspecies of **protein**-kinase-c in living cells using fusion proteins with **green fluorescent protein**.

Author(s):

Sakai, N ; Sasaki, K; Ikegaki, N; Shirai, Y; Ono, Y; Saito, N

Corporate Source:

KOBE UNIV, BIOSIGNAL RES CTR, MOL PHARMACOL LAB, NADA KU, 1-1 ROKKODAI CHO; KOBE; HYOGO 657; JAPAN; KOBE UNIV, BIOSIGNAL RES CTR, MOL PHARMACOL LAB, NADA KU; KOBE; HYOGO 657; JAPAN; KOBE UNIV, FAC SCI, DEPT BIOL; KOBE; HYOGO 657; JAPAN;

Source:

JOURNAL OF CELL BIOLOGY Vol. 139 , No. 6 pp. 1465-1476 (1997) DEC 15 (0021-9525

Abstract:

We expressed the gamma-subspecies of **protein** kinase C (gamma-PKC) fused with **green fluorescent protein** (GFP) in various cell lines and observed the movement of this fusion **protein** in living cells under a confocal laser scanning **fluorescent** microscope. gamma-PKC-GFP fusion **protein** had enzymological properties very similar to that of native gamma-PKC. The fluorescence of gamma-PKC-GFP was observed throughout the cytoplasm in transiently transfected COS-7 cells. Stimulation by an active phorbol ester (12-O-tetradecanoylphorbol 13-acetate [TPA]) but not by an inactive phorbol ester (4 alpha-phorbol 12, 13-didecanoate) induced a significant translocation of gamma-PKC-GFP from cytoplasm to the plasma membrane, A23187, a Ca2+ ionophore, induced a more rapid translocation of gamma-PKC-GFP than TPA. The A23187-induced translocation was abolished by elimination of extracellular and intracellular Ca2+., TPA-induced translocation of gamma-PKC-GFP was unidirected, while Ca2+ ionophore-induced translocation was reversible; that is, gamma-PKC-GFP translocated to the membrane returned to the cytosol and finally accumulated as patchy dots on the plasma membrane. To investigate the significance of C1 and C2 domains of gamma-PKC in translocation, we expressed mutant gamma-PKC-GFP fusion **protein** in which the two cysteine rich regions in the C1 region were disrupted (designated as BS 238) or the C2 region was deleted (BS 239). BS 238 mutant was translocated by Ca2+ ionophore but not by TPA. In contrast, BS 239 mutant was translocated by TPA but not by Ca2+ ionophore, To examine the translocation of gamma-PKC-GFP under physiological conditions, we expressed it in NG-108 cells, N-methyl-D-aspartate (NMDA) receptor-transfected COS-7 cells, or CHO cells expressing metabotropic glutamate receptor 1 (CHO/mGluR1 cells). In NG-108 cells,K+ depolarization induced rapid translocation of gamma-PKC-GFP., In NMDA receptor-transfecte COS-7 cells, application of NMDA plus glycine also translocated gamma-PKC-GFP., Furthermore, rapi translocation and sequential retranslocation of gamma-PKC-GFP were observed in CHO/mGluR1 cells stimulation with the receptor, Neither cytochalasin D nor colchicine affected the translocation of gamma-PKC-GFP, indicating that translocation of gamma-PKC was independent of actin and microtut gamma-PKC-GFP fusion **protein** is a useful tool for investigating the molecular mechanism of gamma-PKC translocation and the role of gamma-PKC in the central nervous system.